A NOVEL FUNCTIONALIZED COMPOSITE COATING FOR CONTROLLNG BIO-CORROSION IN WASTEWATER CONCRETE PIPES

by

Negar Roghanian

A THESIS SUBMITTED IN PARTIAL FULFILLMENT OF
THE REQUIREMENTS FOR THE DEGREE OF

DOCTOR OF PHILOSOPHY
in

The Faculty of Graduate and Postdoctoral Studies
(Civil Engineering)
THE UNIVERSITY OF BRITISH COLUMBIA
(Vancouver)

April 2018

Abstract

Bio-corrosion in sewage pipes is mainly caused by the diffusion of aggressive solutions and in-situ production of sulfuric acid by sulphur-oxidizing microorganisms which affect the physicochemical properties of concrete pipes. In this study an accelerated pilot-scale experimental setup is designed and built to replicate conditions in sewage transport systems as well as the bacterial induced corrosion processes in pipes. The reliability of the accelerated set-up is evaluated by conducting different tests on corroded samples over a 6 months period. In addition to the parameters such as weight loss and pH measurements that have been investigated by previous authors, variations in corrosion depth, flexural strength and absorption were also studied.

Prevention of concrete bio-corrosion usually requires modification of concrete mix or application of antimicrobial coatings on the inner surface of the pipe. The composition of the coating is a key factor in controlling resistance to bio-corrosion which is dependent on the neutralization capacity of the material or its ability to prevent the growth of bacteria. The most common method for controlling the growth of bacteria is using bioactive chemicals (biocides) which are essentially toxic compounds. Undesired leaching of biocides to the surrounding environment as well as their short bio-resistance lifetime have increased the need for more efficient, environmental friendly and long-lasting alternatives.

In this study, multiphase composite coatings are developed and tested. Controled-release mechanism was implemented inside the coating by mixing the binder matrix with functionalized sodium bentonite clay impregnated with zinc oxide and solidifying the antibacterial agent in 3D framework of coating material. Tensile strength, chemical resistance, leaching stability, microstructure and resistance to bio-corrosion in the accelerated chamber were investigated. Results show that the developed antibacterial coating can create a corrosion-resistant and effective physical/chemical barrier on concrete wastewater pipes and protects the concrete from bio-acid. Moreover, coatings successfully immobilized antibacterial agents inside the matrix and increased bio-resistant lifespan and durability of the repair material. This would likely lead to an increase in the service life of aged/corroded concrete pipelines.

Lay Summary

Thousands of kilometers sewage pipelines suffer from severe bio-corrosion caused by prolonged exposure to highly aggressive environments. Over the past several decades, many approaches have been developed to reduce the risk of concrete bio-corrosion with variable degrees of success.

In this study, a novel cement-free corrosion-resistant coating material was developed to enhance pipes durability and service-life. The antibacterial particles were encapsulated within the coating network which extended the bio-resistance lifespan of the coating material.

A novel close-to-reality accelerated chamber was designed to simulate the bio-corrosion process and predict the actual behavior of different coating materials in sewage pipes. The proposed methodology and the results will contribute to a better understanding of the bio-corrosion process and provide quantitative information on the performance, effectiveness and durability of developed coating materials compared to conventional coatings.

Preface

Hereby, I declare that this thesis is an original work by Negar Roghanian under the primary supervision of Prof. Nemy Banthia. Identification and design of the research program, tests, data collection, analysis, result presentations and the writings were done by Negar Roghanian.

The objective of this research project was to develop a sustainable long-lasting antibacterial coating material not only to prevent concrete bio-corrosion but also extend the pipe lifetime and efficiency of antibacterial activity. The experimental work including the design and manufacturing of the accelerated bio-corrosion chamber as well as the material testing was performed at Sustainable Infrastructure Research Group (SIERA) laboratory at UBC under the supervision of Prof. Banthia. The experimental work is presented in chapter 2, 3, 4 and 5. The work in chapters 2-5 are in the publishing process. The results of work done in Chapter 4 is patented (US provisional patent application No. 62/642,883 on 14th of March 2018).

Table of Contents

List of Tables

List of Figures

Acknowledgements

I owe particular thanks to Professor Banthia who has modelled what it is to be a great supervisor and mentor. I want to thank him for his continuous support, guidance and encouragement. Also, I would like to acknowledge the guidance and help of my thesis supervisory committee members, Prof. Frank Ko and Dr. Patricia Keen. This work would have not been possible without their support and cooperation.

I offer my enduring gratitude to the faculty, staff and my fellow students at UBC, who have helped and inspired me to continue my work in this field. Specially the kind support of Mr. Harald Schrempp, Mr. Russell Scott Jackson, Mr. Bill Leung and Mr. John Wong who helped me with building the experimental set-up, instrumentation and data acquisition. Also sincere thanks to Mrs. Jane Wu who assisted me with SEM images and Masoud Namini for helping me with the microbiological part. In addition, I would like to thank my friends and colleagues at SEIRA Obinna Onuaguluchi, Aamer Bhutta, Salman Soleimani-Dashtaki, Cristina Zanotti, Brigitte Goffin, Ricky Ratu, Tahmineh Teymourian, Mohammed Farooq and Sasan Soleimani-Dashtaki.

I owe an enormous debt of gratitude to my best friend and companion, Mahda for his unconditional love and support. I am always grateful for his technical and non-technical support and understanding.

Special thanks are owed to my family (Mohammad, Elahe and Navid), who have supported and encouraged me throughout my years of education. I am very grateful for their everlasting love and the inspiration they have been to me throughout my life. Without their support and encouragement, I would not be where I am today.

I would like to dedicate this work to my son, Davin who has been a constant source of joy through the struggles and trials of this thesis.

The work was supported by India-Canada Centre for Innovative Multidisciplinary Partnerships to Accelerate Community Transformation and Sustainability (IC-IMPACT).

Dedication

To my parents Elahe and Mohammad

Chapter 1: Introduction

1.1 Statement of the problem

Concrete is the most widely used construction material in large water and wastewater treatment plants, pipelines and conduits because of its low cost and ability to take forms. In North America, more than 75 percent of the population is served by wastewater collection systems and treatment plants for which concrete is a key construction material because of its longevity, ease of installation and local availability [USEPA, 2004]. Although concrete has been long-established construction material, as with any structural component, it has its limitations. The durability of concrete should always be considered and monitored to ensure safe and serviceable infrastructures.

Significant amounts of concrete pipe are used to develop the main sanitary sewer system throughout the lower mainland of the Greater Vancouver beginning in 1914 and are in growing need of repair, rehabilitation or rebuild. Some of the larger interceptors, which service significant areas of the surrounding municipalities, were cast-in-place in the late 1950s and 70s to move sewage to newly constructed treatment plants. As can be seen in Table 1.1, around 380 km of sewage pipeline in greater Vancouver is made of Concrete which is about 78% of the total pipeline. Around 71% of concrete pipes in greater Vancouver are between 25 and 50 and 20% is older than 50 years old. It should be noted that network designers often use 50 years as the average life expectancy for most pipe types.

According to the Canadian Society of Civil Engineers report card released 2016, most of Canada's infrastructure has now reached the end of its useful service life with 28% of assets between 80 and 100 years old. This problem does not belong exclusively to the infrastructure built in the 19^{th} and early 20^{th} centuries. Even with current durability guidelines, there is evidence to suggest that the trend in construction for faster setting concrete creates a parallel growth-trend in deterioration problems even when "state of the art" construction practices are in use [Mirza, 2006].

Table 1-1: Metro Vancouver sewer line [Metro Vancouver sewer services report, 2008]

	0-24 yrs (1980-2006)	**25 - 49 yrs (1979-1955)**	**50 – 74 yrs (1930-1954)**	**75 – 99 yrs (1905-1929)**	**>100 yrs (1904 or less)**	**Total (km)**
Total (km)	92.50	319.61	22.88	50.53	0.00	485.52
PVC (km)	21.14	2.01	---	---	---	23.14
HDPE (km)	---	0.03	---	---	---	0.03
Steel (km)	33.80	23.21	0.18	---	---	57.19
DI (km)	1.52	0.00	---	---	---	1.52
Concrete (km)	34.17	272.26	22.70	50.53	---	379.66
AC (km)	0.39	6.16	---	---	---	6.55
Fibreglass (km)	---	8.79	---	---	---	8.79
Polyethylene (km)	1.25	5.73	---	---	---	6.99
Other (km)	0.23	1.43	---	---	---	1.66

Apart from the problem of aged infrastructure, underground concrete pipes deteriorate over time due to soil condition and aggressive environment. Thousands of kilometers of lines must be removed each year for replacement suffering from severe bacterial induced corrosion (bio-corrosion) which caused by prolonged exposure of concrete surface to highly aggressive environments. Concrete corrosion in these environments is mainly caused by the diffusion of aggressive solutions and in-situ production of sulfuric acid by sulphur oxidizing bacteria (SOB) which affects the physicochemical properties of concrete. During microbial attack, microorganisms colonize the material surface, its pores, capillaries and microcracks, and form colonies of bacteria within a protective film. The produced bio-film allows bacteria to grow, producing acidic and corrosive conditions. Hydrated Portland cement has limited ability to resist acid attack over time due to its chemical composition and calcium content which cause damage resulting in aesthetic, functional and structural problems, biocorrosion, water quality deterioration, service interruptions, and in extreme cases, catastrophic structural failures that may affect the

general population. These problems are ever present in underground sewage pipes and are costly and health threatening.

The problem of biodeterioration of sewer pipelines in North America is facing a critical phase and several buried infrastructures are in need of repair. According to the inaugural Canadian Infrastructure Report Card that was released in September 11, 2016 by the Canadian Society for Civil Engineering (CSCE), the Canadian Public Works Association (CPWA), the Canadian Construction Association (CCA) and the Federation of Canadian Municipalities (FCM), 40.3% of plants, pumping stations and storage tanks and 30.1% of pipes are in fair to very poor condition. The rehabilitation/replacement cost is estimated to be around $39 billion. Regarding drinking water infrastructures, 15.4% of drinking water pipes are in fair to poor condition with replacement cost of around $25.9 billion. 12.5% of the storm water installations surveyed fall below good condition, 23.4% of the storm water pipes fall below good condition and replacement cost for storm water infrastructures is estimated to be more than $15.8 billion. So, the total replacement cost to upgrade all of these linear assets is $80.7 billion which is around $6,488 per Canadian household. Moreover, advanced corrosion can lead to unexpected premature catastrophic failure resulting in significant system interruption and extensive damage to surrounding roads and pavements.

In the U.S., the repair and maintenance cost of every 800,000 miles of wastewater collection infrastructure is estimated to be $4.5 billion per year [Gomez-Alvarez et al., 2012]. In Germany, the annual costs associated with maintenance, repair, and exchanging corroded wastewater pipes are over $50 billion [Wells et al., 2009]. Table 1.2 and Figure 1.1 shows some of the examples of recent collapses and replacement/repair costs in U.S. and Canada [Perrin et al., 2004].

In addition to wastewater systems, marine structures can also have problems related to microbiologically induced concrete deterioration. Marine environments have high concentrations of chloride ions and other salts in which microorganisms thrive. Oil and water storage systems are also affected by bacterial corrosion as the stagnant water around these structures can produce large

amounts of hydrogen sulfide. As infrastructure are aging, biocorrosion will become more often a risk factor which leads to faster pipe failure.

Table 1-2: Examples of recent pipeline collapses and replacement/repair cost (American Concrete Pipe Association Report, 2008)

Pipeline Location	Age (yrs), Diameter (inches)	Total replacement/repair Cost
US, Michigan, Prudenville	30, 73	$ 3,140,000
US, New Hampshire, Route 101A	25, 108	$ 889,500 (after two repairs)
US, Colorado, Vail	Unknown, 66	$ 8,200,000
US, Georgia, Gwinnett County	10-12, 60	$ 475,000
US, North Carolina, Charlotte	20, 126	$ 300,000
US, North Carolina, Hickory	30, 96	$ 1,500,000
US, South Dakota, Sioux Falls	20, 84	$ 500,000
Canada, Ontario, Toronto	25, 30	Not Reported
US, Tennessee, Knoxville	24, 84	$ 1,300,000

Maryland, Owings Mills , US

North Carolina, Hickory, US

Figure 1-1: Examples of pipeline collapses in U.S.

It is very challenging for municipalities to maintain and repair aged and deteriorated concrete infrastructures and sewage lines. This is complicated by the fact that older pipes often run under crowded, well-developed, sometimes historic neighborhoods, necessitating careful planning for assessment, repairs and replacement.

1.2 Sustainable infrastructure

Infrastructures of various categories have become an indispensable part of people's everyday lives. So it is crucial to design and develop comprehensive infrastructure systems and monitor and improve them consistently without having a negative impact on economic, environmental and social aspects.

In recent years, sustainability has become even more critical in infrastructure projects because the demand of infrastructure development in the foreseeable future is enormous. Furthermore, concerns about environmental protection and climate change have raised awareness for sustainability in infrastructure. So, innovations that enhance sustainability should be given priority in research and development. In this regard, government regulations and interventions can play a crucial role in incentivizing and encouraging public and private sectors to make more sustainable choices and adopt new technological solutions and products. This is achievable by implementing policies that improve old processes or substitute them by newer and more environmental friendly techniques and materials. The rapid rise in demand for infrastructure services offer an opportunity and a challenge to correct past wrongs and develop sustainable future.

Although sustainable infrastructure has a short history within the construction industry, the construction methods to make them much more efficient, effective and environmentally friendly have significantly transformed over this short interval. Sustainable infrastructure has not only benefited the environment, it improves resiliency and livability in the social and economic dimensions of the society.

In a statement from the Canadian Society for Civil engineering (CSCE) vision 2020, sustainability in infrastructures was stated as a core element for the civil engineering profession. Among many possible ways, using sustainable materials is the most pivotal part of sustainable infrastructure. Sustainable infrastructure design is a modern solution that will greatly reduce the life cycle cost of an infrastructure and lessen negative effects on the environment. Sustainability can be achieved through green, energy efficient infrastructures. Green infrastructures are not only great energy reducers but can actually have considerable economic advantages and increased productivity and durability. Alongside the benefits of improving carbon emission targets, life cycle costs are reduced by increasing productivity, durability, health and natural resources usage.

Portland cement production is a major contributor to greenhouse gas emissions and raw material depletion. Production of one tone of Portland cement requires about 2.8 ton raw materials and is responsible for about 0.9 ton of greenhouse gas CO_2 emission. The emission of the CO_2 from de-carbonation of lime in the kiln in cement manufacturing process is about 7% of the total CO_2 emission in all the human activities. So, with the growing awareness of our finite resources, there is a need for replacing cement-based repair materials with durable, economic, effective and also sustainable and environmental friendly alternatives. Innovations through extensive research have brought sustainable materials into new light while increasing the recyclable potential of the existing materials used in construction. These new advances along with future research will make the future of construction more sustainable, efficient and productive thus being advantageous to all sections of society. Infrastructures built today will bridge the way for future generations and if ecological steps are not taken now, it will become too late to reverse the harm we have done.

1.3 Mechanisms of bio-corrosion in concrete pipes

Many different terms have been used to describe corrosion caused by bacteria in sewage pipes, including bacteria induced corrosion, bio-corrosion, bio-deterioration and microbiologically influenced/induced corrosion (MIC). Parker in 1945 published a paper on concrete bio-deterioration and examined the role of microorganisms on the corrosion of concrete pipes. Then in the early 1980s, National Pollution Discharge Elimination System (NPDES) suggested to use

toxic compounds to stop bacteria growth in sewage systems. In 1983, Milde et al. reported that H_2S gas is a key element in production of biogenic acid and subsequent review by Boon in 1995 showed that supplying oxygen to the sewer system can mitigate H_2S gas formation and reduce bio-deterioration rate [Milde et al., 1983; Boon, 1995]. The mechanisms of sewage pipe bio-deterioration are described in the following sections.

1.3.1 Diffusion of sulfate compounds

High sulfate and dissolved sulfide concentration in wastewater is one of the most important factors in deterioration of concrete pipes [O'Connell et al., 2010]. Wastewater naturally contains sulfur as inorganic sulfate or organic sulfur compounds. The sulfate originally comes from the mineral content of the municipal water supply or from saline groundwater infiltration and is reduced biologically under anaerobic condition to sulfide [Metcalf and Eddy, 2003]. Organic sulfur compounds are present in detergents, and in certain industrial effluents such as those derived from leather, brewing, and paper industries.

Sulfate (SO_4^{2-}) compounds have the ability to be absorbed and diffuse into concrete pore structure and react with hydrated compounds in hardened cement paste. Sulfate compounds such as calcium sulfate react with calcium hydroxide (CH) and calcium aluminate hydrates and generate expansive products such as Ettringite (see Equation 1.7) which causes cracking, spalling and loss of paste cohesion and strength. The concentration of sulfate up to 1000mg/L is considered moderately severe and up to 2000 mg/L is severe [Zhao et al., 1998]. Sodium sulfate solutions (Na_2SO_4) decompose calcium hydroxide and produce gypsum and finally Ettringite which has expansive effects described above. Depleting CH will result in alkalinity reduction which will put rebar in danger of corrosion. When there is insufficient source of CH for the reaction to continue, then the sodium sulfate compound is able to start attacking CSH (decalcination reaction). Calcium silicate hydrate (CSH) is the most important cement hydration product that contributes to concrete strength. Magnesium sulfate solutions (e.g. $MgSO_4$) attack all phases simultaneously, preferring CH first followed by CSH. The product of the reaction includes gypsum, Ettringite and magnesium-silicate-hydrate and the mineral form of magnesium hydroxide [O'Connell et al.

2010]. In addition, crystallization and precipitation of salts in capillary pores in case of alkali sulfate existence (such as sodium sulfate) at locations where the concrete is exposed to wetting and drying cycles will apply pressure that could leads to cracks and spalling.

1.3.2 Sulfate reducing bacteria (SRB) and H_2S production

As reported by several authors [Zhao et al., 1998; Monteny et al., 2000; Sanchez-Silva & Rosowsky, 2008; O'Connell et al., 2010; Hudon et al., 2010; Alexander et al., 2013], in the wastewater stream colonies of anaerobic sulphate reducing bacteria (SRB) such as members of genus Desulfovibrio are active (Figure 1.2). They colonize in biofilm layers on submerged sewer walls and are highly dependent on pH, carbon and sulfate concentration in the wastewater. When the flow is inactive and there is no oxygen available, SRB bacteria break down the organic matter and use sulfates present in wastewater to obtain the oxygen and energy they require and, in turn, release sulfur ions. The sulfur ions released by bacteria react with dissolved hydrogen in the wastewater and form H_2S.

$$\text{Organic matter} + SO4^{2-} \text{ (in the presence of SRB)} \rightarrow S^{2-} + H_2O + CO_2 \qquad \textbf{(Equation 1.1)}$$

$$S^{2-} + 2H^{+} \rightarrow H_2S \qquad \textbf{(Equation 1.2)}$$

The produced H_2S initially is in dissolved liquid form but finally leaves the wastewater and enters the gas phase. At low pH (in conjunction with turbulent flow), the H_2S and CO_2 escape and accumulate in the atmosphere above the water line and in the sewer headspace. Later the gas dissolves into the moist film that forms on the crown and walls of the sewer and contributes to reducing the concrete pH from 12-13 to about 7.5.

When H_2S diffuses into the concrete surface, it reacts with calcium hydroxide in the concrete (CH) and transforms to calcium sulfide. In addition, diffused CO_2 react with H_2O and H_2S and forms calcium sulfide. Carbonation reactions also helps reduce the pH of the concrete surface.

$$H_2S + Ca(OH)_2\ _{(Calcium\ hydroxide)} \rightarrow CaS\ _{(calcium\ sulfide)} + 2H_2O \qquad \textbf{(Equation 1.3)}$$

CO_2 reactions

$$CO_2 + H_2O \rightarrow H_2CO_3$$
$$H_2CO_3 + Ca(OH)_2 \rightarrow CaCO_3 + H_2O \text{ (Carbonation)} \qquad \textbf{(Equation 1.4)}$$
$$2CaCO_3 + H_2S \rightarrow Ca(HCO_3)_2 + CaS$$

Diffused H_2S can also react with oxygen and produce sulfuric acid which is known as the most corrosive agent in sewers and wastewater treatment plants. Sulfuric acid reacts with the CH constituents of the concrete and produces expansive products such as gypsum and Ettringite. The produced gypsum is a white, mushy substance which has no cohesive properties and Ettringite is a very expansive product which causes cracks.

$$H_2S + 2O_2 \rightarrow H_2SO_4 \text{ (auto-oxidation)} \qquad \textbf{(Equation 1.5)}$$

1.3.3 Bacteria-induced sulfuric acid production

The effect of biologically formed sulfuric acid on cement hydration products have been reported by several authors [Zhao et al., 1998; Monteny et al., 2000; Sanchez-Silva & Rosowsky, 2008; O'Connell et al., 2010; Hudon et al., 2010; Alexander et al., 2013]. If sufficient moisture, hydrogen, sulfide, carbon dioxide, nitrogen and oxygen are present aerobic sulfur oxidizing bacteria (SOB) such as members of genus "Thiobacillus" can colonize the concrete surface, walls and crown of the sewer above the water line (Figure 1.2). The first bacterial colonization is dominated by the SOB groups able to survive at high pH since the concrete surface is a very alkaline environment. As the pH drops below 9 (due to carbonation and hydrogen sulfide fixation), these bacteria multiply, and reduce the pH to as low as 1.

Sulfur oxidizing bacteria (SOB) are capable of using the diffused H_2S (produced by SRB) as a food source and oxidize sulfur compounds to sulfuric acid. Generated sulfuric acid first reacts with CH in concrete to form gypsum, followed by reaction of gypsum with tri-calcium aluminate (cement hydration product) to form Ettringite. Both products involve volume expansion and result

in cracking. However, formation of Ettringite is mainly responsible for the large volume expansion and crack propagation. Corroded parts can be removed from concrete walls by the flowing sewage over time.

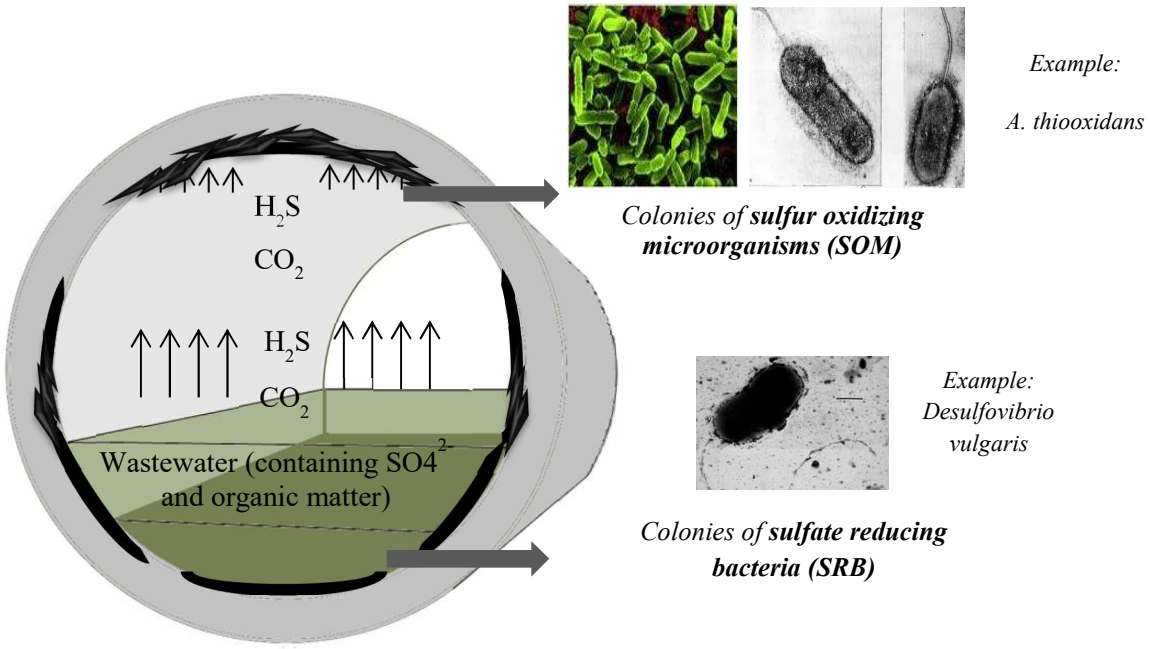

Figure 1-2: Schematic pattern of bio-corrosion in sewer pipes

$$Ca(OH)_2 + H_2SO_4 \rightarrow CaSO_4.2H_2O \text{ (gypsum)} \qquad \textbf{(Equation 1.6)}$$

$$C_3A + 3CaSO4\ (aq.) + H_2O \rightarrow C_3A.3CaSO_4 \cdot 32\ H_2O\ (Ettringite) \qquad \textbf{(Equation 1.7)}$$

If all CH is consumed, decalcification of CSH (Calcium silicate hydrate) takes place according to the following reaction:

$$CSH + H_2SO_4 \rightarrow CaSO_4.2H_2O_{\ (gypsum)} + SiO_{2\ (aq.)}\ (Hydrous\ silica\ residue) \qquad \textbf{(Equation 1.8)}$$

The steel rebar in reinforced concrete pipes are protected by a passive oxide film generated on rebar surfaces due to the high pH of the environment and the oxidation reaction between alkaline

ions and steel. When the cracks form due to the creation of expansive products; microorganisms, corrosive chemical ions and gases diffuse faster into the concrete. Consequently, the pH drops due to carbonation process, H_2S diffusion or biological acid generation. The passive film on the rebar surface starts dissolving at low pH which accelerates aggressive ions reaction and rebar corrosion [Kosmatka et al., 2002]. As it was well illustrated by Sanchez-Silva in Figure 1.3, the combined action of crack propagation due to sulfate attack and biological corrosion process together with expansive pressures caused from steel oxidation increase concrete cracking rate and spalling [Sanchez-Silva & Rosowsky, 2008].

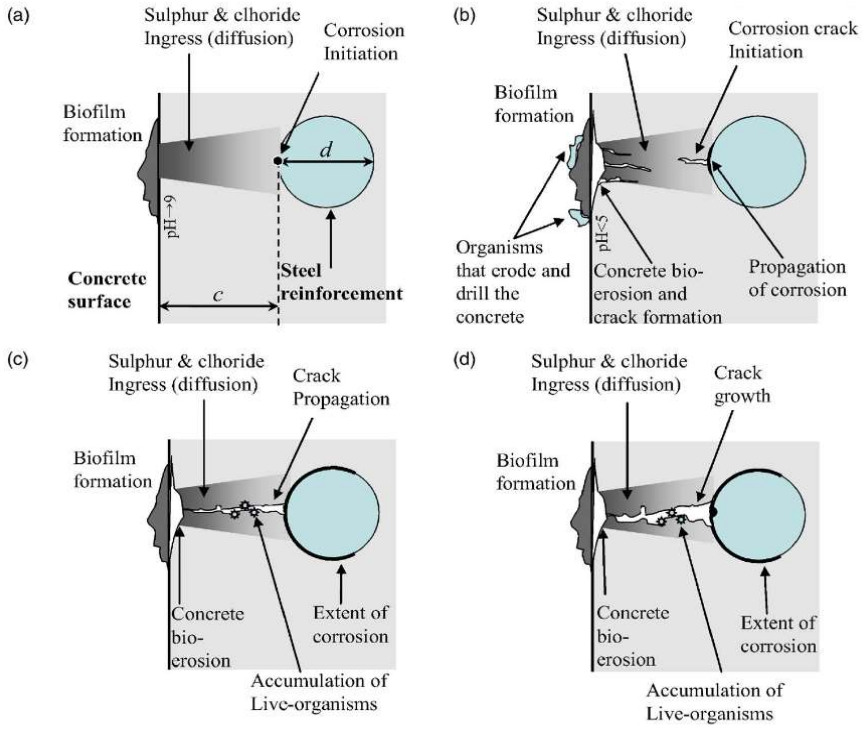

Figure 1-3: Schematic diagram of wastewater concrete pipe deterioration process adapted from Sanchez-Silva and Rosowsky, 2008

1.4 Deteriorated concrete pipes rehabilitation methods and challenges

When the pipes deteriorate, the replacement by means of traditional open-cut methods is very costly and complicated. Over the past several decades many approaches were attempted to protect

structures exposed to aggressive environments from bio-corrosion. However, few methods have shown acceptable long term performance. Mitigation methods consist of using bioactive chemicals (biocides) that disrupt bacteria growth on the surface of the concrete which often lose effectiveness over time due to leaching and chemical degradation. So often they require reapplication to remain effective. Other methods include using prevention techniques that apply physical changes on the surface of the pipe or use corrosion-resistant materials that make growth less likely to occur. Some of the most common techniques that are being used in wastewater concrete pipes include: physical cleaning of pipe surface, modification of concrete mix, application of chemical or antimicrobial thin layer of coating on the inner surface of concrete pipe or provide protective layer between concrete surface and corrosive solution, introduction of bactericides to the wastewater, chlorination, injection of compressed air and addition of lime which were attempted with limited success [Berndt, 2011; Montes & Allouche, 2012].

According to the literature, modification of concrete mixes by adding supplementary cementitious materials such as silica fume, fly ash and slag or using advanced cementitious materials with different chemical compositions and low calcium contents are reported to enhance the resistance of the pipes to some acceptable limits in acidic environments [Berndt, 2011; Montes & Allouche, 2012].

Another category of prevention methods are via the introduction of coating materials. In 1931, the U.S. Bureau of Reclamation established one of the largest and longest running concrete technology laboratories in Denver, Colorado. It was established, originally to support the construction of the Hoover dam. Bureau of reclamation also performed research on concrete repair technology. The techniques and standards developed at the U.S. Bureau of Reclamation are still in use to this day [US engineering and Research Center, 1981]. The general approach to repair (as it was well described in the guide published by U.S. Bureau of Reclamation) is to remove the existing damaged material, perform a cut around the damaged area and patch the concrete with a suitable repair material. Suitable materials include Portland cement mortars, dry pack concrete, polymer concrete (polymer in place of Portland cement, such as epoxy resins) and polymer-modified concretes (polymers as an admixture to Portland cement concrete). Each material has its

advantages and disadvantages and their selection is based on the context and required performance. [Guide to concrete Repair, 1997 and 2015]. Regardless of the type of repair material used, the U.S. Bureau of Reclamation's guide emphasizes that proper substrate preparation is required in order to get a suitable bond between the coating material and the substrate. Pressurized water blasting or wet sand-blasting (between 8000 psi and 40000 psi) is required in order to prepare the surface properly. Mechanical methods such as bush-hammering and jack-hammering are also effective but leave micro-fractures on the surface that prevent proper bonding.

Concrete infrastructure repair requires using coating materials that fit naturally within existing structure but also within the environment in larger context. Current coating technologies are divided into four main groups. One of the most common repair options includes coating the pipe with cured-in-place cement-based or polymer-based coating materials and liners such as epoxy, polyesters, high alumina cement, asphalt and PVC sheets [Montes & Allouche, 2012]. However, there are common issues associated with this type of coatings such as cost, tendency to the propagation of cracks, pinholes or rips, delamination, corrosion, compatibility with the host material, short bio-resistance lifetime, poor adhesion to the substrate material and toxicity. Furthermore, coatings are prone to acid and/or bacteria penetrate the layer, corrode the host pipe substrate material behind the liner and destroy the bond. Also, in some cases it is difficult to monitor pipe's condition over time with conventional methods when it is coated with a thick layer of polymer-based coating. Success with protective coating materials has been variable.

The second type of repair technologies is introducing a coating which minimizes the adhesion of bacteria on the surface without involving chemical reactions. Generally, bacterial biofilm formation starts with initial attachment and adhesion of bacteria to surfaces. Microbial cells aggregate on the surface and produce insoluble polymeric substance called exopolysacharides (EPS) proteins that encase the adherent bacteria in a three-dimensional matrix. EPS help the cell to adhere to a surface, trap nutrients and protect them from antibacterial. With accumulation of EPS and reproduction of bacteria, colonies develop into mature biofilm and exhibit increased resistance to removal. The chance of initial microbial attachment to the surface is dependent on coating material chemistry, surface topography, mechanical properties, surface

hydrophobicity/surface energy, environmental conditions as well as bacterial surface structure [Graham & Cady 2014]. Anti-adhesive layers basically reduce the chance of microbial attachment to concrete surface, such as polydimethylsiloxane (PDMS) and polyethyleneglycol (PEG). These types of coatings are divided into two main categories, fouling release coatings including silicone- and fluoropolymer-based binders and engineered micro-topographical surfaces.

The third group are coatings integrated with antimicrobial agents or bioactive chemicals (biocides) that act on bacteria and limit or prevent their settlement. Biocides are considered to be the most commonly used materials to prevent the growth of undesirable microorganisms on concrete surfaces. Biocides were introduced in 1967 by the Penarth Research Center to inhibit microorganism growth on stonework with applications extended to ancient masonry buildings and cement-based substrates [Richardson, 1988]. Currently more than 18 chemicals are used as biofilm inhibitor agents throughout the world. However, several challenges exist with respect to adding biocides to construction materials, such as the degradation of biocides into inactive compounds due to environmental conditions, fast dissipation due to leaching and/or volatilization from the surface film, short bio-resistance lifetime, high required concentrations and large dosage requirements in order to have a sustained long-term effect. Moreover, since most of the effective biocides are essentially toxic chemical compounds, such as mercury-based biocides and tin-based biocides, the environmental impact of their release to the soil and water and the surrounding environment at such increased levels has led to stricter environmental legislations over the last decade and requires careful monitoring [Edge et al., 2001; Whitekettle et al., 2010].

In addition to biocides, various antibacterial micro/nano agents and heavy metals also have toxic effect on sulfate-reducing microorganisms. Heavy metals ions such as zinc or silver impregnate the microbe surface and are absorbed by the cells through active transfer. The heavy metal ions react with metabolic enzymes within the metabolic system of the microbes. Ultimately, the activity of these enzymes is hindered, and the growth of microbes is inhibited.

Coating the pipe's internal wall by cuprous oxide or silver oxide in epoxy is reported to reduce the bacterial corrosion [Hewayde et al., 2005]. Maeda et al. (1996) suggested the possibility of using

nickel to prevent concrete corrosion [Maeda et al., 1996]. It is also been reported that sodium tungstate completely inhibits the growth of A. Thiooxidans cells [Negishi et al., 2005]. However, the use of metal salts in repair coatings is limited because of leachability into the surrounding environment, safety concerns and regulations that restrict levels of certain metals in sewer systems. Due to these challenges involved in using biocides, increasing attention is being paid to implementation of slow release mechanisms inside a material coating by integrating the biocide into a carrier or a mechanism which is able to release the antibacterial agent or biocide slowly to the environment. Slow release systems have the potential to extend the duration and efficiency of biocidal activity, modulate its release and reduce environmental pollution risks. In addition to the fact that antibacterial agents are protected from leaching out into the ecosystem, handling threats associated with skin sensitization could be minimized [Edge et al., 2001; Erich et al., 2011].

Microencapsulation of chemical compounds is a well-known method in chemical literature and drug delivery systems to gain control over the release of active components. In this method, the molecule is retained inside a protective framework until a trigger affects its release [Edge et al., 2001]. Researchers demonstrated extended duration in biocidal activity with microencapsulated biocides [Gajanan et al., 2007; Nyden et al., 2010; Jamsa et al., 2012]. They also reported that the encapsulation is able to protect UV-sensitive biocides such as IPBC (iodopropynyl butyl carbamate) against premature degradation. In addition to extending the biocide effect, microencapsulation is able to reduce toxicity and cover odor of chemical compounds.

There are many studies looking at the synthesis of polymer-composite carriers impregnated with antimicrobial agents. These controlled release systems have attracted interest due to their potential of controlled-delivery of various active agents [Scarfato et al., 2011]. However, the overall performance of a coating containing polymer-composite carriers is highly dependent on its compatibility with other materials. Aldcroft et al. in 2005 tested different porous inorganic carrier particles such as amorphous silicate, amorphous alumina and zeolites having biocides adsorbed within the pore system in surface coatings [Aldcroft et al., 2005]. Botterhuis et al. and Sorensen et al. (2006) studied the effect of porous silica nano/micro particles loaded with biocide for controlled release applications. The studies showed that a controlled leaching of biocide is obtained which

protected the biocide from chemical degradation and extended the biocidal effect under accelerated weathering tests [Botterhuis et al., 2006; Sorensen et al., 2010].

In recent years, nanometer-scale hollow cylinders or nano-tubes have emerged as a good biocide-loading carrier option due to their large inner volumes. Lvov et al. (2008) studied two-layer alumino-silicate Halloysite clay nanotubes as an entrapment system for storage, loading and control release of anticorrosion agents. In the search for slow released systems, clay minerals are also widely used materials for modulating drug delivery. This is due to their high storing capacities as well as swelling and colloidal properties [Aguzzi et al., 2007].

Another method to gain control over the release of active components is to retain and solidify the antibacterial ions or heavy metal molecule in 3D framework of the coating material matrix. Antibacterial agents could be a combined as part of the material matrix or simply be embedded in the pores of the structure. Two examples are geopolymer and magnesium phosphate cement with the ability to immobilize and tightly lock heavy metals such Zn^{2+}, Cu^{2+}, Cr^{3+}, Cd^{2+}, Pb^{2+}, TiO_2 and MnO into their 3D network with minimum losses in compressive strength and mechanical properties [Terzano et al., 2005; Wang et al., 2007; Xu et al., 2006; Van Jaarsfeld et al., 1997]. The microstructure of these materials is similar to zeolites or feldspathoids which are known for their excellence ability in absorbing and solidifying chemicals/heavy metal and thus they have been used as a potential matrix for waste stabilization during the last decade. Kriven et al. reported that Geopolymer-based material containing silver/copper particles is a possible coating with a combination of antibacterial activity and good adhesion to majority of inorganic surfaces [Kriven et al. ,2010]. However, geopolymer has limited potential to solidify and encapsulate the antibacterial agent. In addition, depending on the antibacterial agent used, the encapsulation process of heavy metals in the geopolymer matrix may affect geopolymerization reaction and mechanical properties.

In this research project, different types of coating materials including cement-based, geopolymer-based and novel multiphase composite were evaluated. Two different systems were considered to gain control over the release of heavy metals embedded in the coating. The first mechanism was

to keep the heavy metal molecule in the 3D framework of the coating binder. The second approach was to use sodium bentonite clay impregnated with zinc ions to functionalize it as an antimicrobial agent and then mix it with the coating material. Sodium bentonite clay is an abundant, durable and economically viable clay material. It has high strength and biocompatibility and can be integrated as a carrier loaded with the biocide into protective coatings. While there are studies on the antimicrobial characteristics of clay functionalized with heavy metals, the feasibility and properties of geopolymer-based and multiphase composite coatings integrated with zinc doped bentonite clay have not been investigated to date.

The ultimate goal of this research was to overcome the current rehabilitation challenges by developing a sustainable repair coating to prevent concrete bio-corrosion, yield a prolonged exposure of the biocide and extend the durability and service life of the concrete pipes.

1.5 Test methods for evaluation of concrete bio-corrosion

Methodologies of evaluating concrete biogenic acid corrosion that have been studied since 1945 could be divided into three main categories: chemical tests, microbiological simulation tests and tests in-situ. Some of the difficulties of in-situ investigations include great diversity in sampled sites, different used concrete mixes and large amount of parameters involved in-situ corrosion tests which makes it difficult to compare the results of different studies.

Regarding using chemical tests, most studies revealed that resistance to chemical sulfuric acid does not always indicate resistance against biogenic acid corrosion [O'Connell et al., 2010; Wei et al., 2013; Zhao et al., 1998]. Another disadvantage of chemical tests is that the formation of corroded layer on the surface of concrete pipe creates an extra barrier for future acid attack, while the corroded layer is an excellent platform for the penetration and growth of bacteria near un-attacked concrete in microbiological simulation tests.

The third category of investigation was carrying out a close-to-reality accelerated experiment to simulate wastewater environment as well as bio-corrosion process. While accelerated tests have

the advantages of simulating bio-corrosion as it occurs in-situ in a more rapid way, there is a need for standardization of methods and acceleration procedures.

The theory of concrete bio-corrosion that is presented in the literature does not provide researchers with enough information to develop an accurate test to predict the life cycle of concrete pipes with and without repair materials. Moreover, there is no standard quantitative test method for evaluating the resistance of coating materials to biogenic acid attack. It is very beneficial to the industry if obtained information from the simulation chamber could be used to estimate the corrosion rate and residual safe life of corroded pipes. Also, it is very valuable to predict and quantify the effectiveness of the coating material in protecting the corroded pipe from further corrosion and/or extending pipe's service life. Such prediction helps develop rational decisions on maintenance and repair of corroded pipes and so unexpected failures could be prevented.

Different laboratory test experiments have been developed and conducted to simulate the biogenic corrosion and various parameters are modified to evaluate the resistance of different materials [Mori et al., 1992; Sand et al., 1994; Hormann et al., 1997; Ehrich et al., 1999, Wei et al., 2010]. In most of the cases, researchers used concrete or cement-based mortar specimens and accelerated the test by applying unreal conditions such as submerging small cubic/cylindrical samples in aggressive solutions of different concentrations and/or applying very high concentrations of H_2S to the system, which affects the mechanism of bio-corrosion compare to what occurs in the field and leads to different or even contradictory results. In addition, in order to compare the relative performance of different materials and coatings, it is necessary to use a combination of multiple evaluation test methods and indicators. In general most of the researchers have focused on parameters such as mass loss, residual compressive strength of the corroded specimens and surface pH variations during the bio-corrosion process and monitored microbial characterization, bacteria growth and corrosion products as an indicator of bi-corrosion activity.

However, it is difficult to evaluate corrosion rate and residual life time of the pipes through these tests. Moreover, it should be considered that some of these parameters are not applicable when comparing the performance of different coating materials. For example, it has been reported that

it is difficult to monitor bio-corrosion rate through surface pH measurements since pH may remain constant on the surface due to the acid neutralization by alkalinity released from concrete or wastewater spray [Mori et al., 1992]. Microbial analysis is time consuming and quantitative microbial population analysis has not been successfully correlated with bio-corrosion rates [Satoh et al., 2009]. Also, most of these methods are not very good for predicting the remaining serviceability and strength of pipe's material which are the matter of concern in corroded pipes. The failure of buried pipes (Figure 1.4) is either serviceability failure (cracking and loss of concrete thickness) or ultimate strength failure (flexural failure and shear failure).

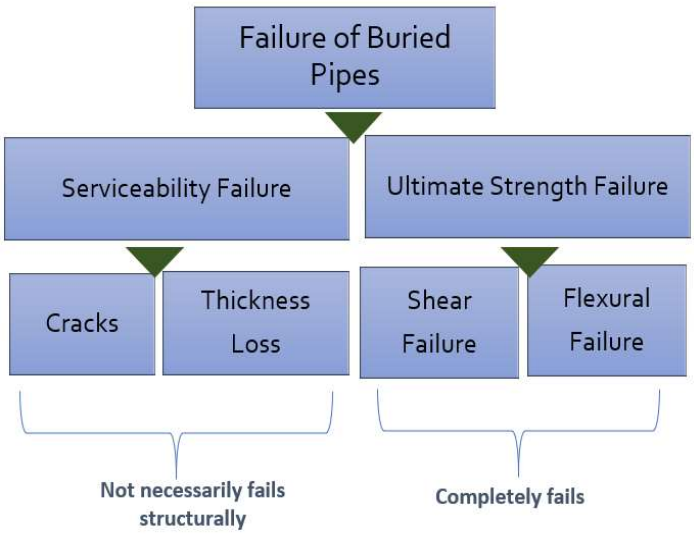

Figure 1-4: Failure of buried pipes

If the pipe loses its flexural strength and/or shear strength, it will completely fail but if it cracks or loses the thickness it will not necessarily fail structurally [Mahmoodian and Alani, 2013]. Consequently, cracking and loss of wall thickness affects pipe's durability and serviceability and flexural failure is a representative of pipe's ultimate strength failure. The combination of these factors is able to evaluate the performance of corroded concrete pipes as well as the effectiveness of coating material in extending pipe's structural lifetime.

In this research study, a novel accelerated experimental setup was designed to replicate conditions in sewage systems as well as the bio-corrosion process in concrete pipes. In addition to the parameters such as weight loss, pH measurements and microbiological activity on corroded surfaces that has been investigated by previous authors, variations in material's microstructure and flexural strength were also studied to evaluate the performance of corroded samples over the 6 months period. Also, the accelerated chamber was used to compare the performance of different coating materials.

The proposed methodology and the results contribute to a better understanding of the bio-corrosion process and provide quantitative information on the performance and effectiveness of different coating materials which is necessary in evaluating concrete pipe's serviceability and predicting the remaining service life of rehabilitated pipes.

1.6 Research objectives and key contributions of the project

The objective of this research project was to develop a sustainable long-lasting antibacterial coating material not only to prevent concrete bio-corrosion but also extend the bio-resistance life time and efficiency of biocidal activity. This general objective was developed in various stages by:

- Designing and building a novel close-to-reality pilot-scale experimental apparatus to replicate conditions in sewage systems as well as the bio-corrosion process in concrete pipes
- Developing a novel corrosion-resistant coating alternative with antibacterial properties to increases the durability and serviceability of aged and deteriorated concrete pipes
- Evaluating an alternative coating material with possible antibacterial properties as a solution to bio-corrosion of sewer systems. And also attempting to extend the bio-resistance lifetime of the coating by encapsulating the antibacterial agent in the coating matrix as well as clay particles

- Studying bio-corrosion process from an engineering perspective rather than a pure microbiological and/or chemical perspective. Although there are several researches on the mechanism of bio-corrosion, few efforts have been conducted to incorporate novel products as a solution for the construction industry.

- Using a quantitative methodology to evaluate the operational condition of the rehabilitated pipes. It is necessary to develop test methods to evaluate capability of the rehabilitated concrete pipes to meet service requirements

- Attempting to use the developed quantitative methodology to evaluate the effectiveness and performance of different coating materials in protecting pipes from further corrosion or extending pipe's structural lifetime

Chapter 2: An innovative approach to simulate bio-corrosion in wastewater concrete pipes

2.1 Previous laboratory experiments conducted to simulate bio-corrosion

Bio-corrosion is a very complex and slow process, usually in the magnitude of 1 to 5 mm per year. The bacteria species colonize in the 1-5 mm layer of concrete surfaces and produce sulfuric acid that penetrates into deeper layers over time. In other words, the bio-corrosion process starts at the concrete surface and attacks one layer after the other. Therefore, it would require many years to evaluate the bio-corrosion resistance of different materials.

The laboratory research investigating the bio-corrosion resistance of concrete could be divided into chemical tests and microbiological simulation tests. As described in the introduction chapter, studies have shown that the resistance of concrete to only chemical sulfuric acid is not always a good indicator of resistance to microbial-produced sulfuric acid [Monteny et al., 2000]. Thus, researchers simulate bio-corrosion as it happens in the site by carrying out microbiological tests in laboratories.

Microbiological experimental tests can be conducted in different ways, (1) realistic concentrations of biogenic acids can be used in combination with a sensitive method to detect deterioration and estimate the future degradation with an extrapolation method; or (2) design accelerated tests and increase the bio-deterioration rate by increasing medium concentration, creating optimum environment for the bacterial growth and altering parameters such as humidity and temperature in the chamber. It is possible to simulate the entire life of the specimen in accelerated chambers.

Mori et al. (1992) designed a simulation chamber (see Figure 2.1), for investigating the effect of nutrients, moisture and pH on the microbial corrosion of concrete samples. Three media were tested including wastewater, water and a special nutrient solution. They worked with very high concentration of H_2S (400 ppm) and temperature between 12 and 30°C which would be intended

to mimic heavy corrosion in wastewater concrete pipes. The test specimens were cement mortar samples of size 4×4×16 cm that were placed in sewage containing nutrients and minerals and were inoculated with A. Thiooxidans spices every 2 weeks for 2 months. The corroded samples were investigated by SEM- EDS (Energy Dispersive Spectroscopy fitted to Scanning Electron Microscope system) and the corrosion rate was determined by measuring the reduction in cross-section of the specimens. The experiment was conducted for 6 months and a corrosion rate of 6.1mm/year was found for specimens submerged in sewage [Mori et al. 1992]. So, it could be concluded that nutrients and oxygen must be present to cause maximum sample corrosion. Also, bacteria require a supply of moisture and nutrients to initiate the corrosion process.

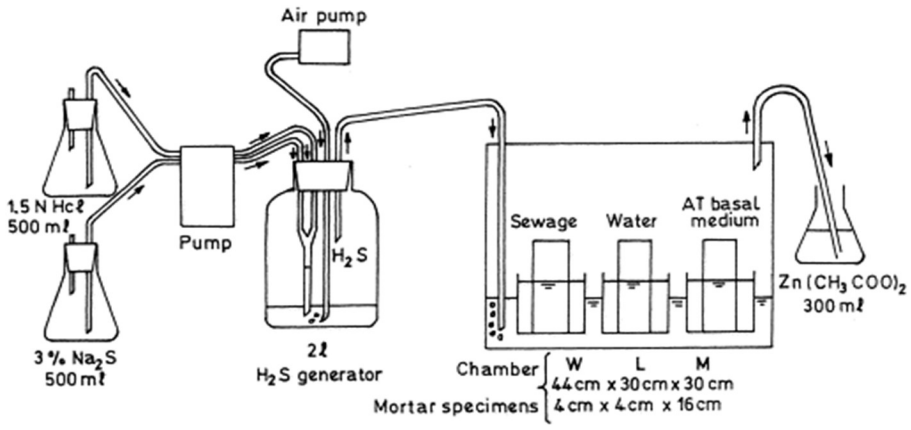

Figure 2-1: Simulation chamber, adapted from Mori et al., 1992

In 1994, Sand et al. investigated the effect of different types of bacteria, nutrients and sulfur source (hydrogen sulfide, methylmercaptan and sodiumthiosulfate) on bio-corrosion rate in a similar accelerated chamber shown in Figure 2.2. In this test, concrete samples of size 60×11×7 cm were placed in water (pH 7, 30°C) and were periodically sprayed with different Thiobacilli cultures. The cell density on the surface of corroded samples, weight loss and pH variations of the specimens was determined as a measure for evaluating the bio-corrosion rate. The authors reported that the corrosion in the case of using H_2S gas (10 ppm) and A. Thiooxidans species were higher than the corrosion measured when other bacteria and sulfur sources were used. Corrosion was just observed above the waterline [Sand et al., 1994].

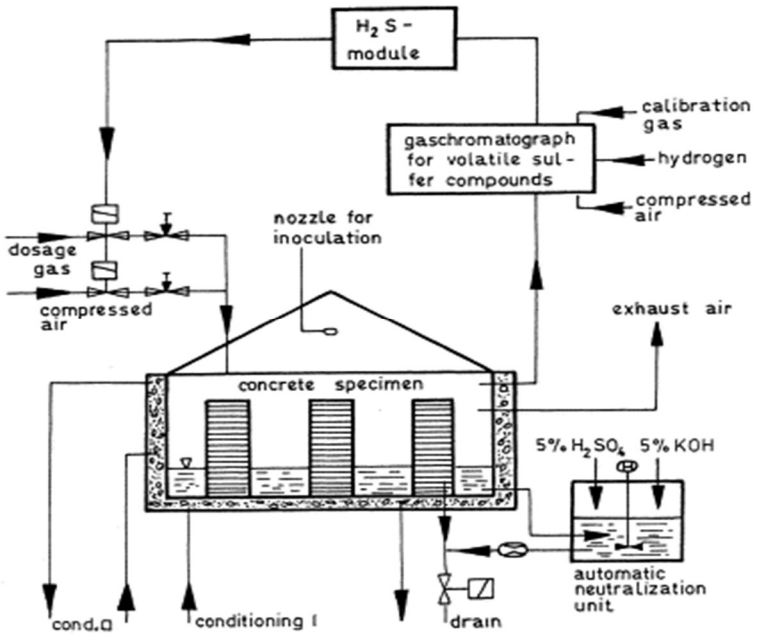

Figure 2-2: Simulation chamber, adapted from Sand et al., 1994

Another simulation chamber was designed by Hormann et al. (1997) which consisted of two separate parts: growth chamber and reaction chamber (see Figure 2.3). The authors kept the temperature to 30°C in a glass bioreactor with the pH around 3.5. In this experimental set-up, the corrosion resistant properties (weight loss and cell density measurements) of high alumina cement and ordinary Portland cement samples (10×10×60 mm) as well as the influence of the type of aggregates on the corrosion were investigated. According to the results, the specimens with high alumina (3-4% weight loss) showed less corrosion compare to ordinary Portland cement specimens (18-31% weight loss) after 5 months of testing. It is reported that the influence of different types of aggregates on the corrosion resistant properties was very small [Hormann et al., 1997].

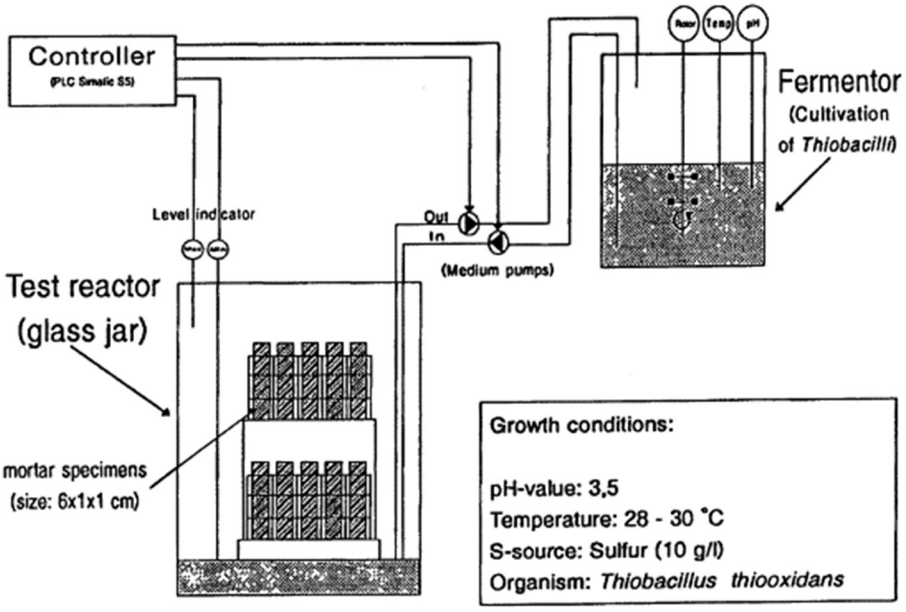

Figure 2-3: Simulation chamber, adapted from Hormann et al., 1997

Ehrich et al. (1999) simulated the bio-corrosion process in a controlled chamber (30°C temperature, humidity above 98% and 15 ppm H_2S) as shown in Figure 2.4. The authors tested different samples made of calcium aluminate cement, Portland cement and blended Portland cement mortars. The samples were sprayed with different strains of Thiobacillus bacteria during a period of 3 months. Cubic samples were immersed and shaken in bottles containing mineral solution for 2 hrs before measurements. Comparison of weight lose, surface pH variations and sulfate content of corroded samples after 350 days showed that calcium aluminate cement bio-corrosion rate was lower than other cement types which is related to higher neutralization capacity due to their chemical composition [Ehrich et al. 1999].

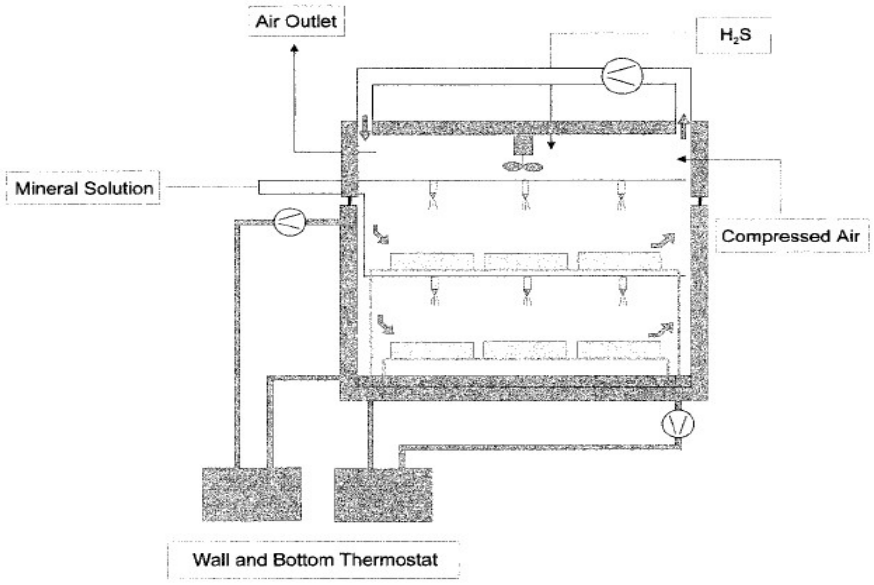

Figure 2-4: Simulation chamber, adapted from Ehrich et al., 1999

Vincke et al. (1999) exposed 5×2×2 cm samples of Portland cement concrete and blended concrete containing slag and styrene-acrylic polymer to biogenic acid containing Thiobacili bacteria (Figure 2.5). The initial gas concentration in the chamber was around 250 ppm, temperature around 28°C and the duration of the experiment was 51 days. The samples were analyzed in terms of weight loss, and the authors reported that polymer-based material performed better than cement-based material against biogenic acid attack.

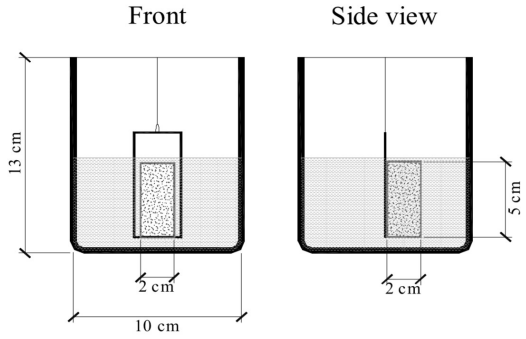

Figure 2-5: Simulation chamber, adapted from Vincke et al., 1999

De Belie et al. (2004) designed a similar experimental set-up to Vincke et al. and tested cylindrical samples (80 mm diameter and 15 mm deep). The corrosion progress was simulated in four cycles of 17 days performed at 28 C. Microbiological tests with biogenic sulfuric acid included measurements of variations in pH, sulfate and calcium concentration of the solution, weight loss, thickness and surface roughness. The bio-corrosion simulation test resulted in a maximum corroded depth of 0.8 mm after 4 cycles of 10 days in biogenic acid suspension. The authors concluded that Portland cement performed better than slag cement [Vincke et al., 1999].

Gutiérrez-Padilla et al., simulated degradation of low and high-quality concrete pipe samples (5×2×2 cm) in a chamber containing 300-600 ppmv H_2S, bacteria and artificial wastewater (pH between 7-8) as a cyclic process where batches of wastewater were changed when the system reached stable condition (Figure 2.6). As could be seen in the Figure, small concrete samples are fully immersed in biogenic acid. The measured corrosion rate after 227 days indicated that low strength, low-w/c concrete corrosion is lower than high-w/c concrete [Gutiérrez-Padilla et al. 2010].

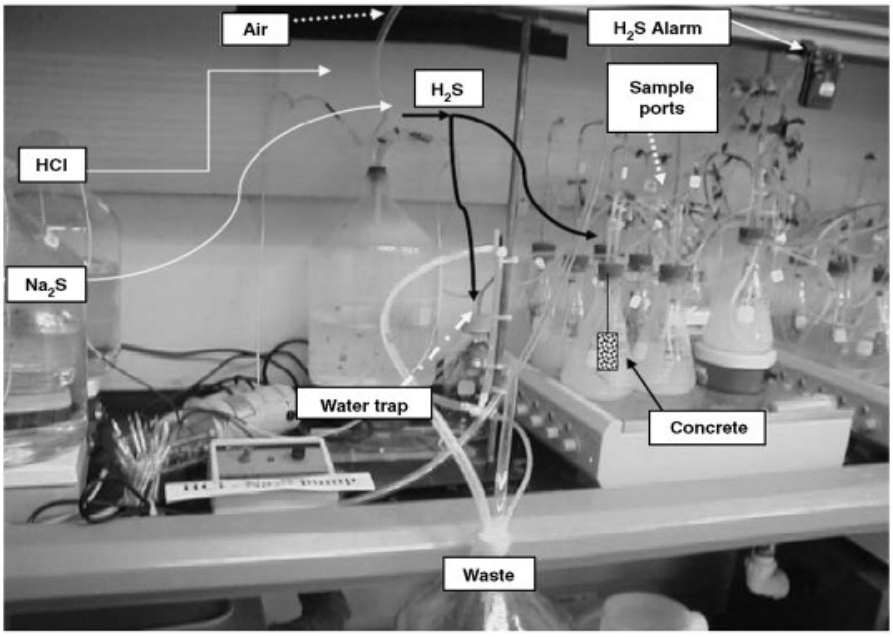

Figure 2-6: Simulation chamber, adapted from Gutiérrez-Padilla et al., 2010

The components of the simulation chamber designed by Magniont et al. (2011) are presented in Figure 2.7. In this study, small samples were immersed in the overflow from the bacteria culture reactor (solid liquid ratio of approximatly 0.15) for 30 days. One tube feed with raw culture medium containing growth medium, bacteria cells and their metabolism, the second tube filled with filtered Sertolon 0.2 polyamin membrane to remove bacteria cells. The study was conducted on Portland cement paste using water cement ratio of 0.27 [Magniont et al. 2011].

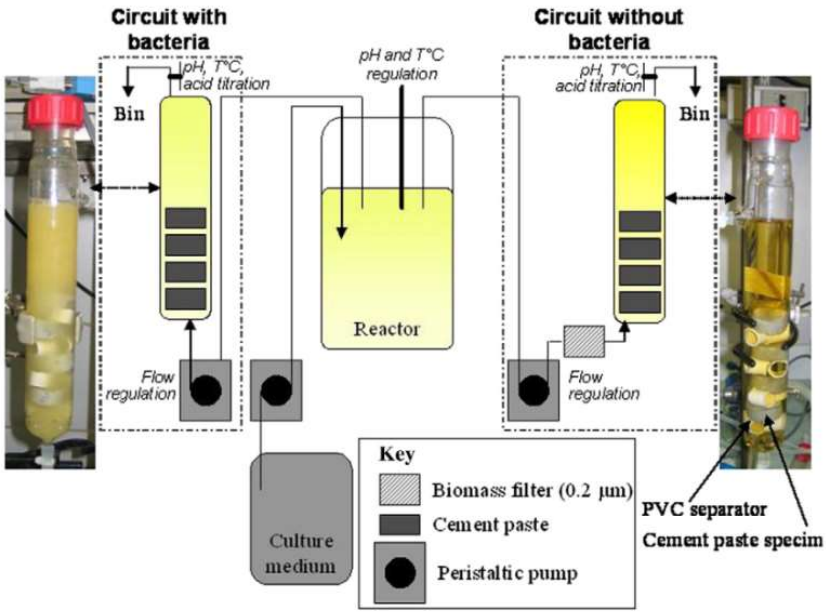

Figure 2-7: Simulation chamber, adapted from Magniont et al., 2011

In the study conducted by Yousefi et al. (2014), strength, mass loss and microstructure of small cement paste specimens (2×2×2 cm) were measured in an acceleration chamber (Figure 2.8). The surface pH of the samples was reduced to a more favorable level for bacteria growth by exposing the specimens to biogenic sulfuric acid for 6 days in advance. The samples were then tested in 1% inoculum of bacteria (pH less than 2, temperature around 30 C, acid/cement ratio of 5) in slow and accelerated test conditions. Mass loss, dimensions of specimen, pH surface variations and compressive strength of the samples were measured to evaluate bio-corrosion rate up to maximum 90 days. The authors reported that the compressive strength of the cement paste specimens was reduced by 96% [Yousefi et al., 2014].

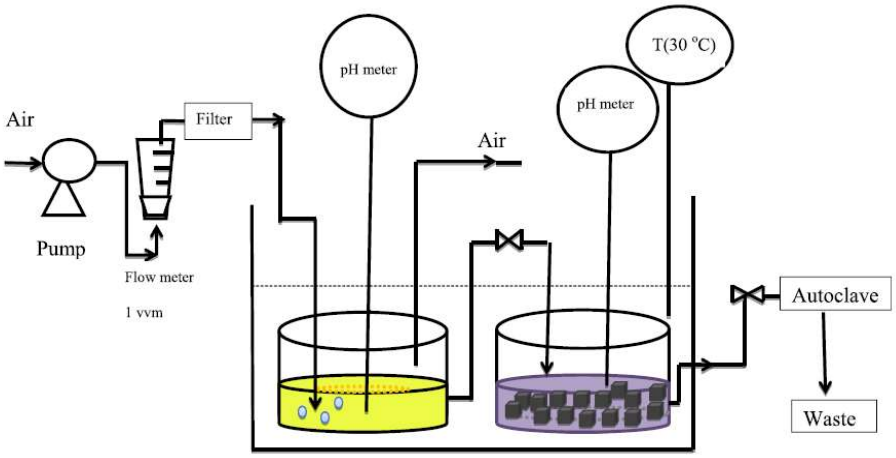

Figure 2-8: Simulation chamber adapted from Yousefi et al., 2014

2.2 Proposed accelerated test chamber

2.2.1 Methodology and novelty

As described in the previous section, carrying out an accelerated test in the laboratory is one of the most common ways of investigating the bio-corrosion resistance of different materials and systems. As it was described in section 2.1, bio-corrosion mechanism of sewage concrete pipes were simulated by several authors in various accelerated test chambers. However, there are some parameters that were not considered in the previous studies and were included in this research to improve the realistic applicability of the test. Core reasons for developing such a test include:

- The theory of concrete bio-corrosion that is presented in the literature does not provide researchers with enough information to develop an accurate test for prediction of the life cycle of repair materials. There is a need for standardization of methods and procedures in developing accelerated tests.

- The scale of the test method has a significant effect on the corrosion results. Accelerated test specimens with larger surface-to-volume ratio, not fully immersed in the aggressive solution better represent of the bio-corrosion process.

- In most of the experimental set-ups as described in the previous section, researchers used concrete or cement-based mortar specimens and accelerated the test by applying unrealistic conditions such as submerging small cubic/cylindrical samples in aggressive solutions of different concentrations, which affects the mechanism of bio-corrosion compare to what is happening in the field and leads to different or even contradictory results. In addition, the growth of acid producing bacteria on the surface of submerged samples is harder since it is very much dependent on the amount of available oxygen.

- It has been observed by different researchers that bacteria cause more intense deterioration compare to a medium without bacteria or synthetic acid solution. It has been also reported that concrete degradation mechanism with chemical sulfuric acid and sulfate salts are different from biogenic sulfuric acid that is bacterially produced.

- Novel concrete compositions and non-cement-based coating materials such as geopolymers were investigated in previous studies based on chemical tests; however the bio-corrosion resistant properties are not confirmed in simulation chambers.

- Advanced coating materials impregnated with different biocides showed enhanced resistance in acidic environment and ability to extend bio-resistant lifetime of the coatings, but no research has yet been performed using biogenic sulfuric acid.

- A combination of multiple evaluation methods and indicators is necessary to compare the relative performance of different concrete types and coating materials. According to the literature, in most of the simulation chambers, parameters such as pH variations, weight loss, reduction in compressive strength, microbial characterization, bacteria growth and corrosion products were measured as an indicator of bio-corrosion activity.

However, it is difficult to evaluate corrosion rate and residual life time of the pipes through these tests. For example, it has been reported that it was difficult to monitor bio-corrosion rate through surface pH measurements since pH may remain constant on the surface due to the acid neutralization by alkalinity released from concrete or wastewater [Mori et al., 1992]. Microbial analysis is time consuming and quantitative microbial population analysis has not been successfully correlated with bio-corrosion rates [Satoh et al., 2009].

- Some of the evaluation parameters and methods are not applicable when comparing the performance of different coating materials. Also, most of these methods are not very good for quantifying and predicting the remaining serviceability and strength of rehabilitated pipes which are the matter of concern in corroded pipes. It is very beneficial to the industry if obtained information from the simulation chamber could be used to estimate the residual safe life of rehabilitated pipes. Such prediction helps to develop rational decisions on maintenance and repair of corroded pipes and so unexpected failures could be prevented.

2.2.2 Principle

To meet the needs summarized in section 2.2.1, an accelerated test chamber was designed and a test procedure was developed. In the developed accelerated test, the degradation rate is increased by means of higher concentrations of the aggressive medium, higher temperature and humidity, greater contact surfaces and alternate wetting drying cycles.

As previously described, bio-corrosion in sewage pipes is mainly caused by the diffusion of aggressive solutions and in-situ production of sulfuric acid by microorganisms. First, anaerobic sulphate reducing bacteria (SRB) break down the organic matter and use sulfates present in wastewater to obtain the oxygen and energy they require, and in turn, release sulfur ions. The released sulfur ions react with dissolved hydrogen in the wastewater and forms H_2S. Ultimately, produced H_2S gas escapes and accumulates in the atmosphere above the water line and dissolves

into the concrete surface [Zhao et al, 1998; Monteny et al., 2000; Sanchez-Silva et al., 2008; O'Connell et al., 2010; Hudon et al., 2010; Alexander et al., 2013].

Diffused H_2S degrades in concrete pore solution and releases H^+ and HS^-. Both CS and CSH (Calcium silicate hydrate) constituents of the concrete are able to react with H_2S and produce CaS (Calcium sulfide) which is not stable in acidic solution and turns into calcium hydrogen sulfide ($Ca(HS)_2$) when H_2S is available. Dissociation reactions are summarized in Fig 2.9. During the neutralization process, the pH of the concrete surfaces is reduced due to the carbonation and H_2S acidification and so the concrete surface changes to a more favorable environment for bacteria to grow on.

Jiang et al. (2016) reported that relative humidity, temperature and H_2S concentration are the most important three factors that have significant role in neutralization rate of concrete samples. Highest pH reduction after 6 months was reported for the specimens located in the chamber with more than 15 ppm H_2S concentration, 25 to 30°C temperature and more than 90% humidity [Jiang et al., 2016].

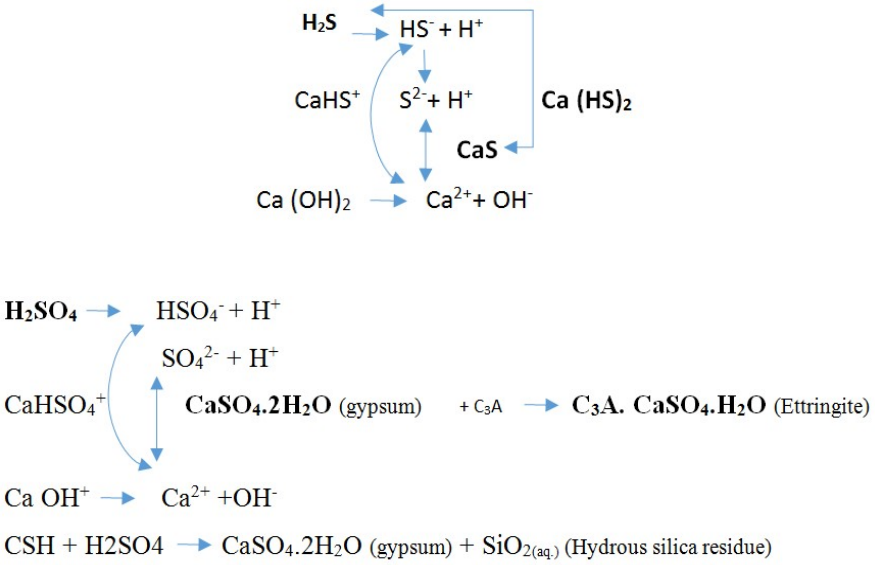

Figure 2-9: Reactions on concrete surface

The first bacteria colonization occurs by the neutrophilic sulfur oxidizing bacteria (NSOB) able to survive at high pH, around 9 [Tazawa et al., 1994]. NSOB converts H_2S to sulfuric acid and decrease the pH. When the pH drops below 4, more sulfuric acid is produced by acidophilic sulfur oxidizing bacteria (ASOB) and reduce the PH to as low as 1-2.

It is reported by several authors that the production rate of biogenic sulfuric acid is related to the biological activity and amount of SOB (which is determined by pH), sulfur source content, temperature, relative humidity and oxygen [Islander et al., 1991; Yongsiri et al., 2004; Nielsen et al., 2005; Jiang et al., 2014]. Therefore, by keeping humidity, temperature, oxygen and H_2S level constant, the production rate of biogenic acid is only dependent on pH. Yuan et al (2015), showed that it is possible to model biogenic acid production rate by fitting the SOB pH evolution curve. They reported that the amount of produced acid is as low as 2.5e-9 (mol/L) until pH reaches 4 and around $7e^{-7}$ (mol/L) when the pH reaches 1.5. The acid production rate drops rapidly when the pH decreases to lower than 1.5. So, the maximum activity of microorganism and acid production rate is happening when the surface pH of the samples are between 4 and 1.5. The oxidation kinetics at 25°C was reported by Nielsen et al. (2005) to be on average 15% faster than at 20°C [Nielsen et al., 2005]. Jiang et al. also observed a more rapid and higher corrosion rate in increasing humidity and temperature (around 100% RH and 30°C) [Jiang et al., 2014].

Generated sulfuric acid penetrates into the pores, reduces concrete alkalinity and dissolves calcium hydroxide. H_2SO_4 reacts with CH and CSH (Calcium silicate hydrate) to form gypsum, followed by reaction of gypsum with tri-calcium aluminate to form Ettringite (Figure 2.9). Corroded parts can be removed from concrete wall by the flowing sewage during time.

It is very complicated to determine the bio-corrosion rate of concrete as the rate is highly dependent on several parameters including the quantity of sulfur compounds, moisture, exposure time and temperature. The best-known formula for calculation and estimation of corrosion rate in sewer pipes was developed (Equation 2.1) [Pomeroy, 1976]:

$$Z = BOD_5 \times \frac{P/_b}{(35.314\, Q^{0.33})\, S^{0.5}} \times 1.07^{(T-20)} \qquad \textbf{(Equation 2.1)}$$

Where BOD_5 is biological oxygen demand during five days (gm^{-3} of Oxygen), P is wetted pipe-wall perimeter (m), B is pipe width at sewage surface (m), T is temperature °C , S is slope (mm^{-1}) and Q is the flow ($m^3\ s^{-1}$).

Wells et al. (2015) proposed a simpler and more practical model for predicting the rate of corrosion in concrete pipes in which C is the rate of corrosion (mm/year), [H_2S] is the concentration of the H_2S gas in ppm, H is the relative humidity of the sewer atmosphere, R is the universal gas constant equal to 8.314 $Jmol^{-1}K^{-1}$ and T is the temperature of the sewage atmosphere in Kelvin. The authors determined the scaling constant (A) equal to 207750 $mmyr^{-1}\ ppm^{-1/2}$ [Wells et al., 2015]:

$$C = A \times [H_2S]^{0.5} \times \frac{(0.1602\, H - 0.1355)}{1 - 0.9770\, H} \times e^{\left(-\frac{45000}{RT}\right)} \qquad \textbf{(Equation 2.2)}$$

According to equation 2.2, corrosion rate is a function of temperature, relative humidity and gas concentration. The corrosion rate increases if the H_2S concentration increases, however, even with high gas concentration (100 ppm), low humidity (lower than 82%) results in very low or no corrosion. In the range of temperature between 25-30°C (ideal conditions for the growth of the bacteria) and humidity between 83% and 89%, with only 2% increase in humidity, corrosion rate increases by 50%. Above 90% humidity, 1% increase in the humidity doubles the corrosion activity.

Jiang et al. (2014) used Pomeroy's formula that estimates rate of deterioration of concrete in millimeters per year according to the alkalinity of the pipe material and sulfide flux, Equation 2.3 [Jiang et al., 2014]:

$$Cr = 11.5 \times \frac{\varphi sw}{alk} \qquad \textbf{(Equation 2.3)}$$

In which C_r is the rate of deterioration of concrete in mm per year, alk is the alkalinity of the pipe material measured in gr of calcium carbonate per gr of concrete. The variable φsw is known as sulfide flux and it is measured in grams of hydrogen sulfide per m^2 per hr.

The average rate of the corrosion can also be calculated according to the acid penetration rate, rate of H_2S release from the surface of the sewage and geometry and hydraulic properties of the pipe [Pomeroy, 1976; Mahmoodian et al., 2013]:

$$C = 8.05\ k \times b \times j\ [DS] \times (su)^{3/8}\ P \times A \qquad \textbf{(Equation 2.4)}$$

In which C is corrosion rate (mm/yr), k is a coefficient for acid reaction ranging from 100% (slow acid formation) to 30% (acid forms rapidly), A is the acid consuming capacity of the pipe material, j is related to H_2S release rate, P is the perimeter of the exposed pipe wall (m), u is the stream velocity (m/s), b is the surface width of the stream (m), DS is the dissolved sulfide concentration (mg/l) and s is the slope of the pipeline. According to Equation 2.4, increasing the perimeter of the exposed sample and surface width of the stream increases the corrosion rate. In addition, decreasing the stream velocity and slope of the pipeline also have significant role in increasing the corrosion rate.

Other important factors affecting corrosion rate include material properties of the concrete, water/cement ratio, and concrete permeability. The amount of concrete deterioration in sewage pipes is also a function of oxygen concentration which is necessary for sulfuric acid production. This is the main reason that retains SOB on pipe surfaces (1 to 5 mm layer of the surface). At thickness deeper than this, there is insufficient oxygen to produce the corrosive sulfuric acid [Yousefi et al., 2014].

Building on the information obtained from literature, a novel laboratory test method was designed in this study to observe and measure the bio-corrosion. Stages of the corrosion in actual concrete pipe and simulated conditions in the accelerated test chamber are summarized in Table

2.1. Arch-shaped samples were used to create a close-to-reality situation and increase exposed surface area of the samples.

Table 2-1: Stages of bio-corrosion in concrete pipe and simulated conditions in the accelerated test chamber

Stages of Bio-corrosion	Real-life situation in pipes	Simulated condition in the accelerated test chamber
Neutralization process of concrete	H_2S production by SRB and escape into the atmosphere	For simplicity H_2S gas was injected directly to the chamber
	H_2S gas absorption into concrete and surface pH reduction	The samples were immersed in biogenic acid for two weeks then the reactor operated with pulse injection of 100 ppm $H_2S(g)$ into the system over 45 hr for two weeks period in order to reduce concrete pH to a point at which sulfur oxidizing bacteria can grow.
Biogenic sulfuric acid attack	NSOB colonization on concrete pipe surface followed by ASOB	First Thioparus was injected into the wastewater and sprayed on samples followed by injecting and spraying A. Thiooxidans when the pH of the samples reached 4.
	Favorable condition for bacterial growth and biogenic acid production is available in sewage pipes	Ideal condition was provided for the bacteria to grow. Level of Oxygen, Nitrogen, H_2S, temperature, humidity and pH were monitored and controlled during the test. Wastewater in the system periodically renewed by fresh wastewater Fresh Microorganisms were re-cultivated periodically and sprayed on samples
	Optimal condition for corrosion process is available in sewage pipes	Based on literature review, the following conditions were kept constant to accelerate the corrosion process: H_2S level (50± 5%ppm) Oxygen level (15% ± 5%) Temperature (29° C ± 1° C) Relative humidity (90% ± 5%)
Abrasion	High flow rates in sewage pipes	The corrosion materials were brushed and removed periodically
Wetting-drying cycle	Wetting/drying by fluctuation of the wastewater flow is happening in sewage pipes	Specimens were flooded periodically in the chamber

2.2.3 Description of the apparatus

According to Table 2.1, a chamber was designed to obtain controlled environment simulating that of real sewage pipes (Figure 2.10). The reactor (90 ×20×10cm) was constructed of PVC panels of 10 mm thickness with a free water surface to replicate gravity sewer conditions. As can be seen in Figure 2.10, the reactor consisted of an intermediate container, main reaction chamber containing different concrete samples, an air circulation system, a wastewater circulation system, H_2S, nitrogen and oxygen gas tanks.

Figure 2-10: Developed chamber for simulating bio-corrosion in the laboratory

The H_2S gas system (Figure 2.11) was comprised of an intermediate container (1000 ppm, 1-5 psi, 3.8 L), tubing with an inner diameter of 0.8 cm, H_2S tank (200000 ppm), nitrogen and oxygen feeding tanks, gas monitoring systems, controller and a pump. The resulting gas velocity was around 0.06 m/min. During all the bio-corrosion test cycles, H_2S and nitrogen were injected from the tanks containing compressed gas (through separate tubes) into the intermediate container. Oxygen was injected directly to the chamber through separate tubing system and was monitored by a portable oxygen monitor and data logger model HHAQ-104 (accuracy ± 1%). The frequency

of gas injections into the system was adapted to the rate of consumption and adsorption. When the pressure in the intermediate tank dropped (from 5psi to approximatly 1 psi) it was refilled manually. The H_2S concentration was controlled inside the chamber using H_2S gas monitor Detronics UD-10 with NTMOS detector which was connected to the intermediate container through a solenoid valve. When the H_2S concentration in the main chamber dropped to lower than 50ppm, the solenoid valve automatically let more gas into the main chamber. The final goal was to keep the concentration of H_2S around 50 ppm and oxygen around 15%.

The pressure capacity of the main chamber was around 4 inches of water that was monitored and controlled by a pressure guage, valves as well as the height of scrubber solution (NaOH solution). There were two H_2S neutralizing systems connected to the chamber (Figure 2.11). Scrubber neutralizing systems, containing steel wool and 10 cm NaOH solution, calculated to last about 182 days.

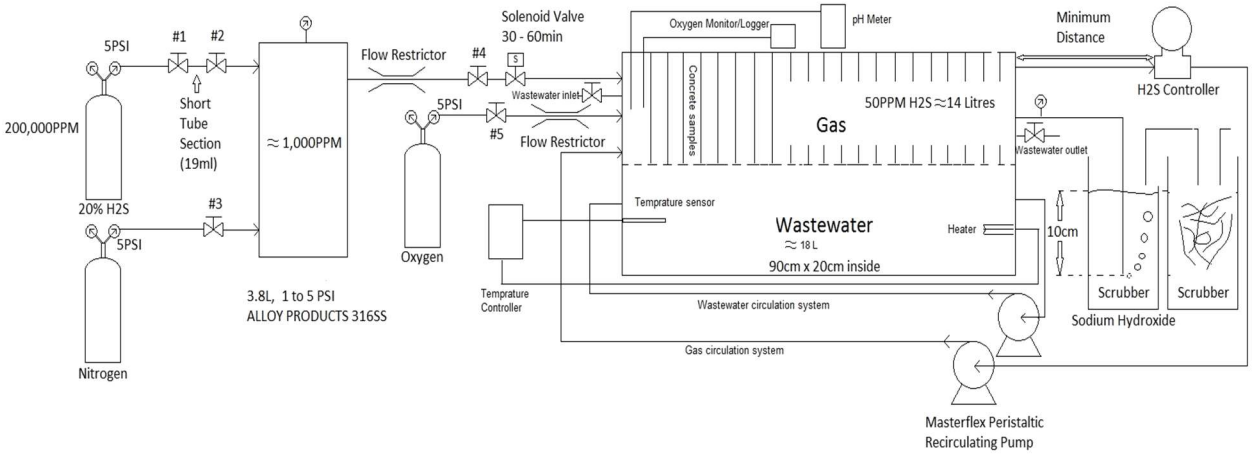

Figure 2-11: Schematic diagram of the proposed chamber for simulating concrete bio-corrosion

The wastewater circulation system was comprised of a liquid heater (OMEGA stainless steel self-regulating immersion heater) with digital controller (to keep the temperature at around 30°C for optimum bacterial growth) and a peristaltic pump. Every 2-3 weeks, when stable pH was reached, approximately 2/3 of the wastewater was replaced by fresh wastewater. Surplus wastewater was discharged out of the reactor through 32 mm out let pipe. Environmental parameters including

wastewater pH (measured by Omega PHH-SD1 pH meter), oxygen level (15% ± 5%) and the temperature (28° C ± 1° C) and relative humidity (85% ± 5%) (Omega HHAQ-104) were monitored and kept constant during the test. The chamber was planned to run for approximately 6 months for each set of the samples. Variation of oxygen, wastewater pH and temperature is plotted in Fig 2.12.

During each cycle, the chamber's condition (pressure, humidity, gases concentrations, sewage pH and temperature) was monitored continuously. Samples surface pH was measured, and test specimens were sprayed with cultures of Thiooxidans and Thioparus every two weeks. After the first cycle, the samples were removed from the chamber for some tests including weight loss, thickness loss and remaining strength. Then returned to the chamber for cycle 2 and 3 respectively. The ultimate strength loss of the samples was measured after the last cycle (cycle 3) that happens after 180 days.

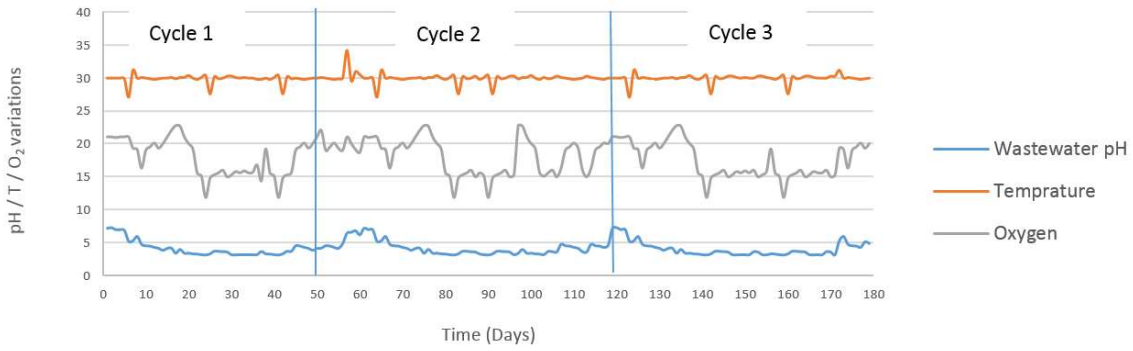

Figure 2-12: Variation of oxygen, wastewater pH and temperature in the experimental chamber

2.3 Microorganisms and cultivation media

2.3.1 Microorganisms

As it was described in chapter one, moisture forms on the concrete surface by condensation and fluctuation of the wastewater flow. This process will transfer microorganisms, nutrients and water

to the concrete surface. When the environmental conditions and surface pH are suitable, aerobic sulfur oxidizing bacteria (SOB) can inoculate on the concrete surface and produce acid. According to the literature, the production rate of biogenic acid is related to the biological activity and amount of SOB (which is determined by pH), sulfur source content, temperature, relative humidity, oxygen and concentration of Al^{3+} [Islander et al., 1991; Yongsiri et al., 2004]. When the surface pH of pipes drop below 9, the first bacteria colonization happens by the neutrophilic sulfur oxidizing bacteria (NSOB) able to survive at higher pH. During this time, H_2S gas absorbed into the concrete surface degrades into S^{2-} which could be oxidized into elemental sulfur by a combination of chemical and biological process [Hudon et al., 2011]. Then colonized NSOB on the pipe surface converts produced H_2S to sulfuric acid and decreases concrete surface's pH further. When the pH drops below 4, more sulfuric acid is produced by acidophilic sulfur oxidizing bacteria (ASOB). ASOB is able to reduce the surface pH to as low as 1 (see Figure 2.13). Table 2.2 summarized the most important types of microorganisms that are responsible in the bio-corrosion process of wastewater concrete pipes. Santo Domingo et al. (2011) studied concrete sewer microbial communities and examined different sewage concrete surfaces. The authors stated that biofilms are more diverse than previously reported. Some of the species may be directly associated with bio-corrosion while others may just facilitate formation and activity of other bacterias involved in bio-corrosion process by reducing pH or increasing attachment surface area. According to their findings, mature biofilms are dominated by Acidithiobacillus Thiooxidans [Santo Domingo et al. 2011].

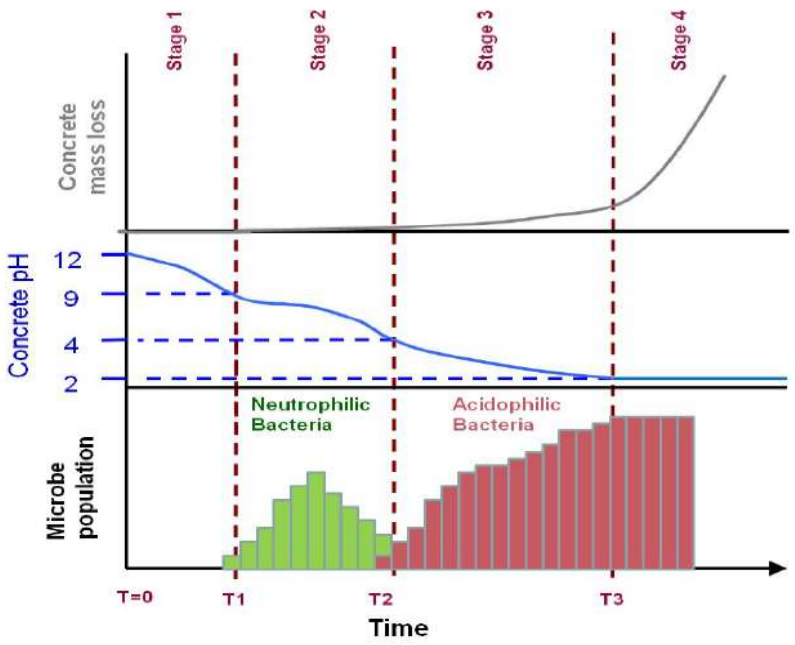

Figure 2-13: Progression of microbial corrosion of sewer pipe adapted from Alexander et al., 2008

Table 2-2: Some of the most important types of bacteria responsible for bio-corrosion of concrete pipes

	Bacteria type	Role		Examples
Bio-corrosion	Anaerobic	H_2S producing bacteria		Xanthomonas sp.
	Aerobic	Sulfur Oxidizing Bacteria (SOB)	Neutrophilic sulfur oxidizing bacteria (NSOB)	Halothiobacillus (H.) neopolitanus Starkeya (S.) novella Thiomonas (T.) intermedia Thiobacillus thioparus
			Acidophilic sulfur oxidizing bacteria (ASOB)	Acidithiobacillus (A.) Thiooxidans Tiobacillus(T.) ferrooxidans T. intermedius

Table 2.3 summarized the most important microorganisms that were used by other researchers in microbiological accelerated test chambers.

The microorganisms used throughout this study were sulfur-oxidizing bacteria species, T. Thioparus and A. Thiooxidans strains that were purchased from American type culture collection (ATCC). In order to focus on the last stage of the biocorrosion process, H_2S gas was injected

directly to the chamber instead of using anaerobic bacteria to produce H_2S. Also instead of using NSOB species to reduce surface pH of the concrete to a point at which ASOB can grow, the samples were immersed in biogenic acid for two weeks and the reactor operated with pulse injection of 100 ppm H_2S for two weeks.

Table 2-3: Summary of the most important microorganisms that were used by other researchers in microbiological accelerated test chambers

Reference	Bacteria type	Testing condition
Yousefi et al., 2014	T. thioparus A. Thiooxidans	• Samples were immersed in produced biogenic acid • Shaker incubator at 30°C and 150 rpm was used • Specimens were also exposed to 1% inoculum of bacteria
Gutiérrez-Padilla et al., 2010	Cryptum A. Thiooxidans H. neopolitanus T. thioparus	• Species isolated from sewer collection system • Grow in LHET2 medium at room temp (reported rapid growth) • Grow in S6 at room temp (reported slow growth)
Ehrich et al., 1999	T. Thiooxidans T. intermedius S. novellus H. neapolitanus	• Cultures were sprayed onto test specimens • Nozzles installed in chamber to spray salt solution containing nitrogen and phosphorus
Hormann, 1997	A. Thiooxidans	• Growth condition: pH 3.5, temp 28-30°C, sulfur content 10 gr/l • The specimens flooded periodically for 5 min Followed by 1 hr interruption
Sand et al., 1994	T. Thiooxidans	Test blocks periodically sprayed with cultures
Tazawa et al., 1994	Xanthomonas sp. T. intermedius	The specimens were immersed in culture bottles
Mori et al., 1992	T. Thiooxidans	The specimens were inoculated with bacteria every 2 weeks up to 2 months

T. Thioparus is a strict aerobe that grows at the pH between 4.5 and 7.5 that was initially isolated from sea water. These organisms are able to grow on the surface of uncorroded concrete and sequentially reduce the surface pH. A. Thiooxidans bacteria has a key role in bio-corrosion process and oxidizing sulfur compounds that has been isolated originally from soil and corroded concrete. These species are colorless and obtain energy from the oxidation of reduced sulfur compounds and CO_2. The pH range for their growth is between 4 to less than 0.5.

2.3.2 Culture media

Culture media composition that were used to grow microorganisms used throughout this study was obtained from ATCC medium 125 and 290 S6 (Table 2.4).

Table 2-4: Composition of the culture medium, Acidithiobacillus Thiooxidans (ATCC Medium 125) and Thiobacillus Thioparus (ATCC Medium 290 S6)

	ATCC 125	**ATCC 290 S6**
$(NH_4)_2SO_4$	0.2 g	1.2 g
$MgSO_4 \times 7H_2O$	0.5 g	0.1 g
$CaCl_2$	0.25 g	0.03 g
KH_2PO_4	3.0 g	1.8 g
$FeSO_4$	5 mg	---
$(NH_4)_2SO_4$	---	0.1 g
$FeCl_3$	---	0.02 g
$MnSO_4$	---	0.02g
$Na_2S_2O_3$	---	10.0 g

The culture media were used as liquid medium. Each component of the medium was individually prepared and sterilized, and the pH adjusted to the recommended values after mixing the sterile components. The growth of bacteria was studied in a 200 ml flask in a shaker incubator at 30°C and 150 rpm (see Figure 2.14) with 1% v/v inoculum which was also recommended by Yousefi et

al. [Yousefi et al., 2013]. Afterwards, the samples were kept in a refrigerator at 4°C in a liquid medium and re-inoculated every 2 weeks for 6 months.

Figure 2-14: Bacteria cultivation process

2.3.3 Growth curve experiment

The bacterial growth profile was studied using the conditions described in 2.3.2. According to the growth studies illustrated in Figure 2.15, the middle log phase time for A. Thiooxidans (Figure 2.15 b) was less than two days. T. Thioparus (Figure 2.15 a) culture's pH decreased slightly during the early time, however a sharp reduction of pH was observed after around 8 days.

(a)

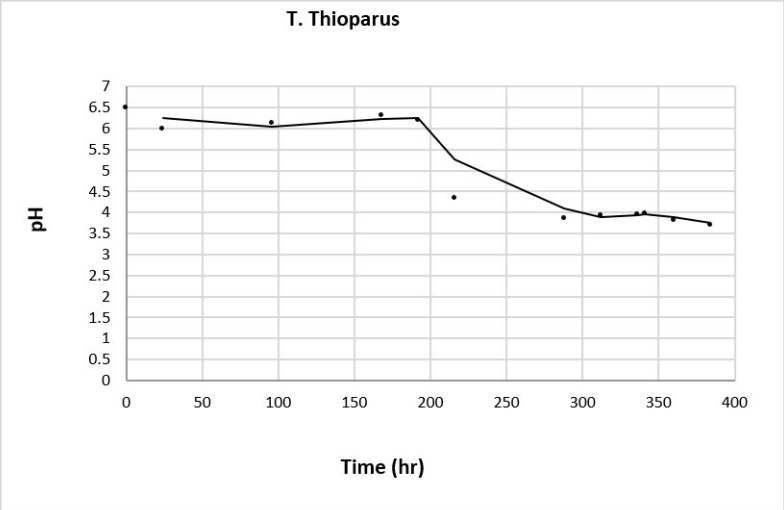

(b)

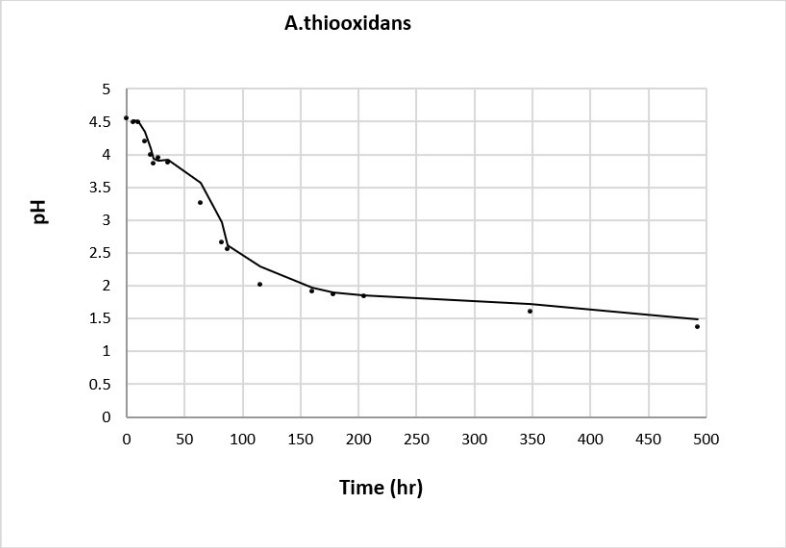

Figure 2-15: Growth studies for A. Thiooxidans and T. Thioparus species (moving average is used to highlight longer-term trends)

Flow cytometry was used to enumerate cells within the medium before injecting it into the chamber. The number of cells was around 45000 cells per 50µL of the sample with the average Thiobacillus cell size of about 0.5× 2µm (details are provided in Appendix A). Turbidity of the microbial culture was also measured to correlate with the rate of bacterial growth. UV-Visible spectrophotometer (OD600) was used at a wavelength of 600 nm for measuring cell optical density. The only problem with using OD600 was that the elemental sulfur should be removed from the culture medium because it is insoluble in medium solution. An alternative was to use thiosulfate rather than elemental sulfur. The cultures were sprayed on samples during their log phase.

In the accelerated test experimental set-up, the samples were immersed in biogenic acid for two weeks at the beginning of each cycle, then the reactor was operated with pulse injection of 100 ppm H_2S(g) into the system over 45 hr for two more weeks period to lower down the pH to around 7-8 which is a more favorable pH for Thioparus to grow. Then Thioparus was sprayed on samples followed by injecting and spraying Thiooxidans when the pH of the samples reached around 5 (after 14 days). Then test specimens were sprayed with Thiooxidans and Thioparus every 2 weeks for 6 months.

2.4 Test specimens

According to the literature, bio-corrosion around the circumference of the pipe does not occur evenly. Research indicates that the region of highest deterioration occurs near the sewage level and pipe crown. Moreover, the section of the sewer pipe underneath the water level (submerged part) does not corrode. At the sewage level, three key components are readily available that makes the environment ideal for the microorganisms to grow which includes, moisture, oxygen and nutrients. In this experimental set-up, arch-shaped mortar samples were cast to represent the top half of the concrete pipe and near the water level (Fig 2.16). Prepared cement mortar samples, having a w/c of 0.5 were de-molded at 24 hours, and stored in curing room with 95% humidity and temperature (22 ±3°C) for 28 days. The average dry weights of the samples were 1.57 kg.

Figure 2.17 shows how the specimens were positioned in the accelerated test chamber after 28 days.

Figure 2-16: Preparation of arch-shaped test specimens

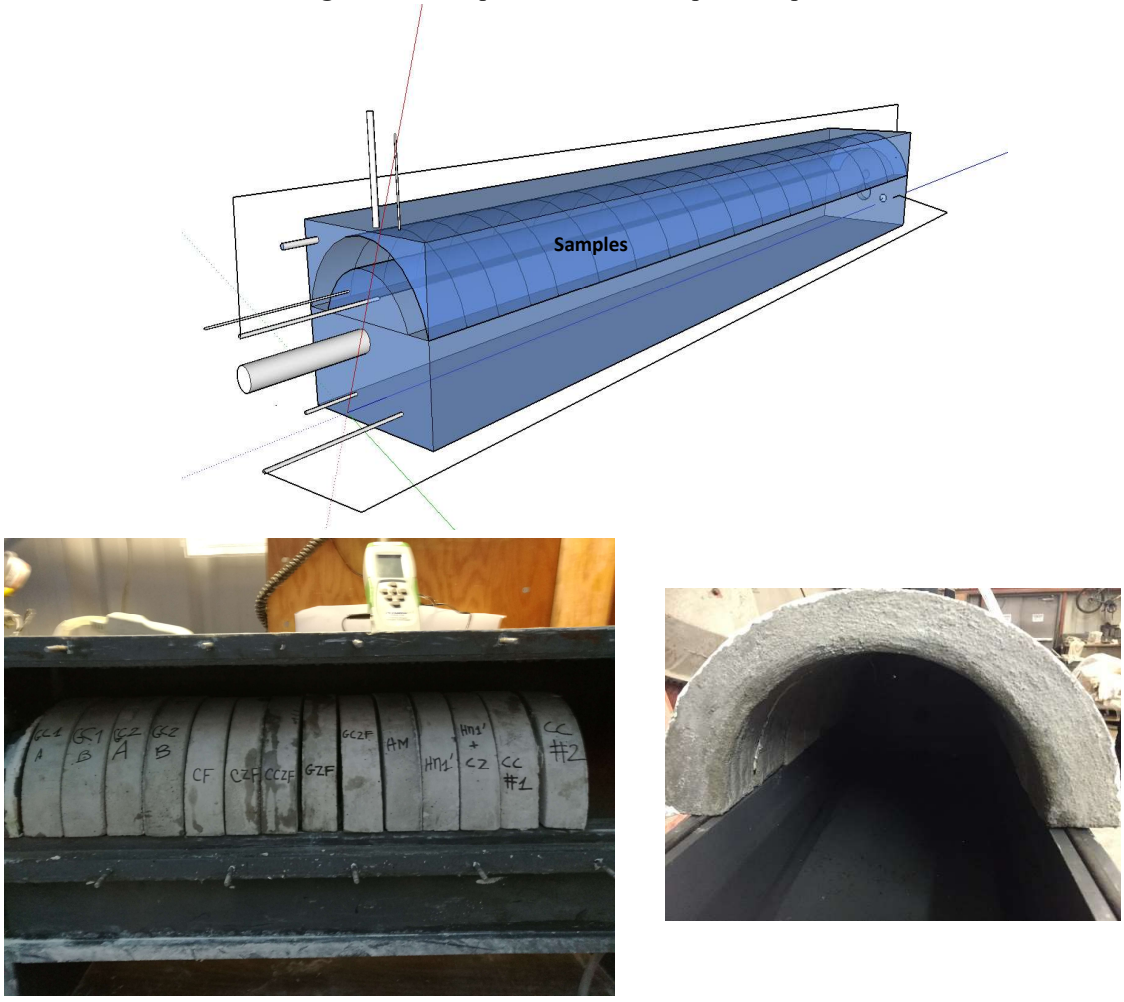

Figure 2-17: Allocating arch-shaped samples (age 28 days) in the accelerated test chamber

2.5 Discussion of developing an accelerated test chamber to simulate bio-corrosion in wastewater concrete pipes

As it was discussed at the beginning of the chapter, carrying out an accelerated test in the laboratory is one of the most common ways of investigating the bio-corrosion resistance of different materials. In the accelerated test, the degradation rate increased by means of higher concentrations of the aggressive medium, higher temperature and humidity, greater contact surfaces and alternate wetting drying cycles.

In this study, an accelerated test chamber was designed and built to simulate bio-corrosion in wastewater concrete pipes. Stages of the bio-corrosion in actual concrete pipe and simulated conditions in the accelerated test chamber are summarized in Table 2.1. In order to be able to focus on the last stage of the biocorrosion process, H_2S gas was injected directly to the chamber instead of using anaerobic bacteria to produce H_2S. Also, instead of using NSOB species to reduce concrete surface's pH to a point at which ASOB can grow, the samples were immersed in biogenic acid and the reactor operated with pulse injection of 100 ppm H_2S. The culture media were used as liquid medium and the growth of bacteria was studied in a 200 ml flask in a shaker incubator at 30℃ and 150 rpm with 1% v/v inoculum.

Arch-shaped mortar samples were cast to represent the top half of the concrete pipe and near the water level. The microorganisms used throughout this study were sulfur-oxidizing bacteria species, T. Thioparus and A. Thiooxidans strains that were purchased from American type culture collection (ATCC). After the pH of the samples was reduced to around 7-8 which is more favorable pH for Thioparus to grow. Then Thioparus was sprayed on samples followed by injecting and spraying Thiooxidans when the pH of the samples reached around 5. Then test specimens were sprayed with Thiooxidans and Thioparus every 2 weeks for 6 months. Environmental parameters including wastewater pH (measured by Omega PHH-SD1 pH meter), oxygen level (15% ± 5%) and the temperature (28° C ± 1° C) and relative humidity (85% ± 5%) (Omega HHAQ-104) were monitored and kept constant during the test. The chamber ran for approximately 6 months for each set of the samples.

Chapter 3: Reliability assessment of the test chamber

As described in chapter 2, an accelerated test was carried out in the laboratory to investigate the bio-corrosion resistance of different coating materials. This chapter describes a validation/test phase to evaluate the performance of the accelerated test chamber.

Fifteen arch-shaped mortar samples were cast to represent the top half of the concrete pipe and near the water level and tested over the 6 months period. Prepared cement mortar samples, having a w/c ratio of 0.5 were de-molded at 24 hours, and stored in a curing room with 95% humidity and 22 ±3°C for 28 days. Six samples were kept in the bio-corrosion chamber for the second round of the test which was conducted to evaluate the performance of coating materials on corroded samples.

A combination of multiple evaluation tests and indicators was conducted to compare the relative performance of bio-deteriorated samples. The corrosion rate was determined by measuring surface pH (for all 15 samples), absorption (6 samples) and mass loss (15 samples) as well as the reduction in thickness (same 6 samples that were used for absorption measurements) and flexural strength (3 samples were used) which are the most important factors in durability and serviceability of concrete pipes. Also, the corrosion products were investigated by SEM.

At the beginning of the bio-corrosion test, H_2S gas absorption rate was determined in order to have an estimation of how H_2S is consumed in the system. Then, as was described in Chapter 2, the samples were exposed to biogenic acid and high concentration of H_2S gas to reduce surface pH to around 7-8 which is more favorable for bacterial growth. During the test, the chamber's condition (pressure, humidity, gas concentrations, sewage pH and temperature) was monitored continuously. Samples surface pH is measured, and test specimens were sprayed with cultures of A. Thiooxidans and T. Thioparus every two weeks for 6 months. After the first cycle (approximately 60 days), the samples were removed from the chamber for other tests including weight loss, thickness loss and

remaining strength. Then returned to the chamber for cycle 2 and 3 respectively. The ultimate strength loss of the samples was measured after the last cycle (cycle 3) that occurs after 180 days.

3.1 Gas absorption rate

Feeding gas system of the accelerated test chamber comprised of H_2S, nitrogen and oxygen tanks. H_2S and nitrogen was injected from the tanks into the intermediate container first and then main chamber. The H_2S concentration was controlled inside the chamber by H_2S gas monitoring system. When the H_2S concentration in the main chamber dropped to lower than 50 ppm, the solenoid valve automatically let more gas from the intermediate container into the main chamber. When the pressure in the intermediate tank dropped from 5 psi to around 1 psi it was refilled manually.

Oxygen was injected directly in to the chamber through separate tubing system. The frequency of gas injections into the system was adapted to the rate of consumption and adsorption. The final goal was to keep the concentration of oxygen around 15%. The pressure capacity of the main chamber was around 4 inches of water that was monitored and controlled by a pressure guage, valves as well as the height of scrubber solution (NaOH solution).

Gas absorption rate in the chamber was determined in order to have an estimation of how H_2S was consumed in the system. For this purpose, the reactor was operated with pulse injections of 100 ppm $H_2S_{(g)}$ over around 45 hr period, while wastewater circulation was off in order to minimize the gas absorption to the wastewater. It should be noted that a portion of hydrogen sulfide was lost in the system by wastewater absorption, PVC surfaces and sensors. But for simplicity, the gas absorption by other processes rather than oxidation and samples absorption was considered negligible [Vollersten et al., 2008]. The absorption rate of the H_2S is plotted in Fig 3.1.

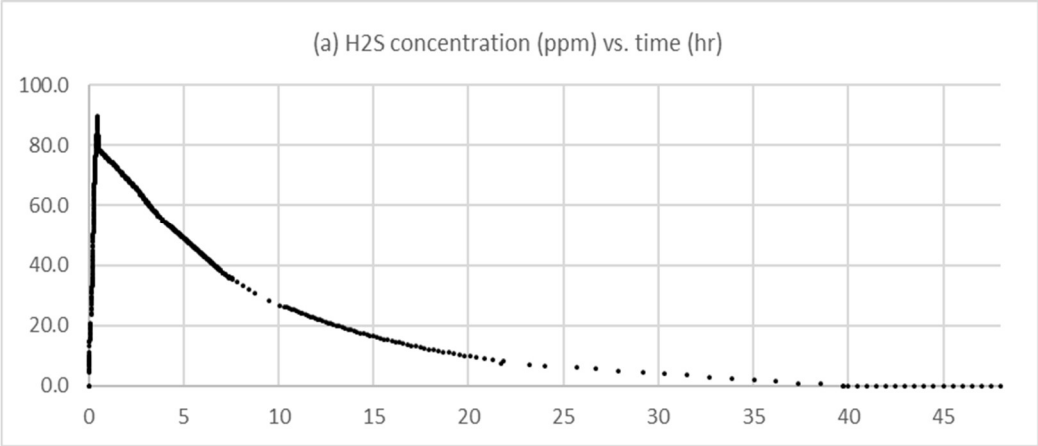

Figure 3-1: Gas absorption over time

The hydrogen sulfide absorption rate is determined by calculating the slope of the hydrogen sulfide concentration vs. time, see equation 3.1:

$$\frac{dp_{H_2S}}{dt} = k_p \; p_{H_2S}^n \qquad \textbf{(Equation 3.1)}$$

Where p_{H_2S} is the gas concentration in ppm, n is reaction order and k_p is the process rate constant ($ppm^{1-n}\,s^{-1}$). Vollersten et al. (2008) observed and quantified the absorption rate of hydrogen sulfide to peak concentration of around 1000 ppm in a test ring consisting of 6 samples operated under sewer conditions. The authors simulated the absorption rate by an exponential function for three cases representing low (10 ppm), medium (100 ppm) and high (1000 ppm) hydrogen sulfide concentrations, see Figure 3.2.

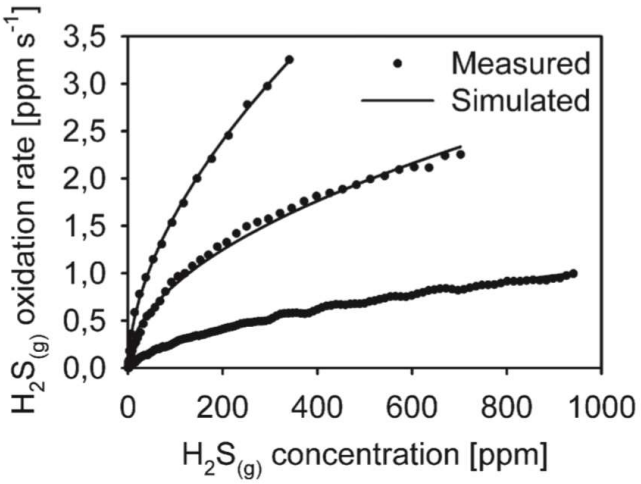

Figure 3-2: Simulation examples of hydrogen sulfide gas, adapted from Vollersten et al., 2008

According to the simulation examples, authors reported k_p =0.019 and n=0.58 for low absorption rate, k_p =0.094 and n=0.5 for medium and k_p =0.177, n=0.52 for high absorption rates. Figure 3.3 shows the absorption rate vs the gas concentration data measured in this study and is compared with the Vollersten et al. (2008) simulation models. Results obtained from this experiment are comparable with an exponential function in which k_p is 0.094 and n is 0.5 (medium rate).

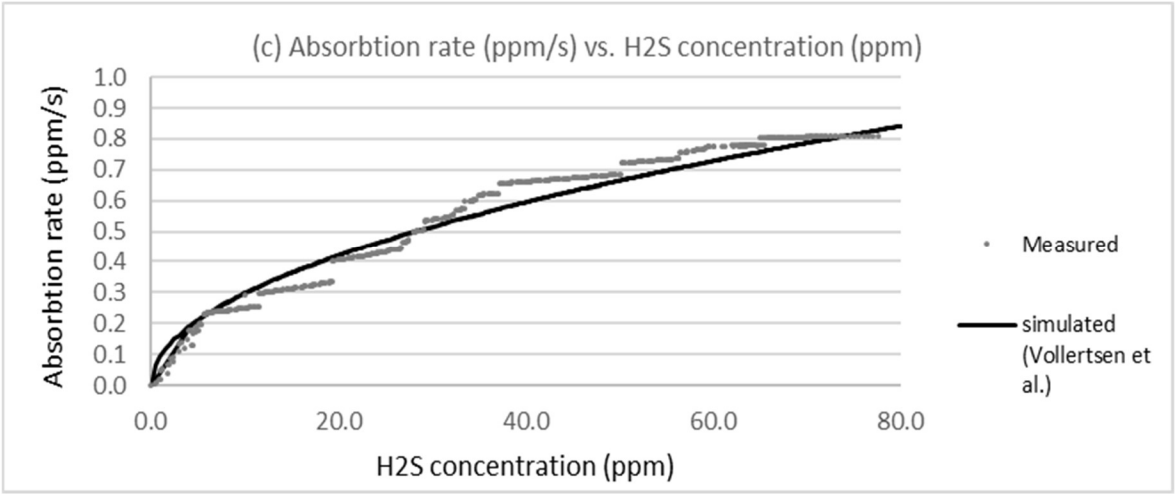

Figure 3-3: Gas absorption rate for the present experiment

3.2 Surface pH

Samples surface pH was measured every two weeks for 6 months. A flat surface pH electrode (Extech 601100) was used to measure surface pH over time, Fig 3.4. For each measurement, the surface of the samples were wetted with about 1 ml of water. Five readings were made to determine the average value. Results were plotted in Fig 3.5, 3.6 and 3.7.

Figure 3-4: Flat surface pH electrode (Extech 601100) used to measure surface pH of the samples

At the beginning of the biocorrosion process, Figure 3.5, pH dropped very quickly by 50% to around 7-8. This occurred while the samples were exposed to high gas concentration and biogenic acid to make the surface more favorable for bacterial growth. Afterwards the rate of pH variations slowed down.

Initially the calcium hydroxide compounds in cement neutralized the produced acid and prevented the growth of bacteria. For this reason, the rate of pH variations in cycle 1 was slower compare to cycle 2 and 3. Gradually, the neutralizing capacity of the samples was reduced, and the bacteria started to grow and lowered down the pH faster on the surface. In addition, due to an increase in the porosity of the samples, pH dropped quicker in cycle 2 and 3 compare to cycle 1. It was observed that the pH drop in cycle 3 was much faster compare to cycle 1 and 2. It should be noted that since the corroded parts were brushed and removed at the end of each cycle, there was a slight increase in the surface pH at the beginning of cycle 2 and 3. Overall the pH dropped by an average 50% at the end of cycle 1, by around 30% at the end of cycle 2 and by more than 50% at the end of cycle 3.

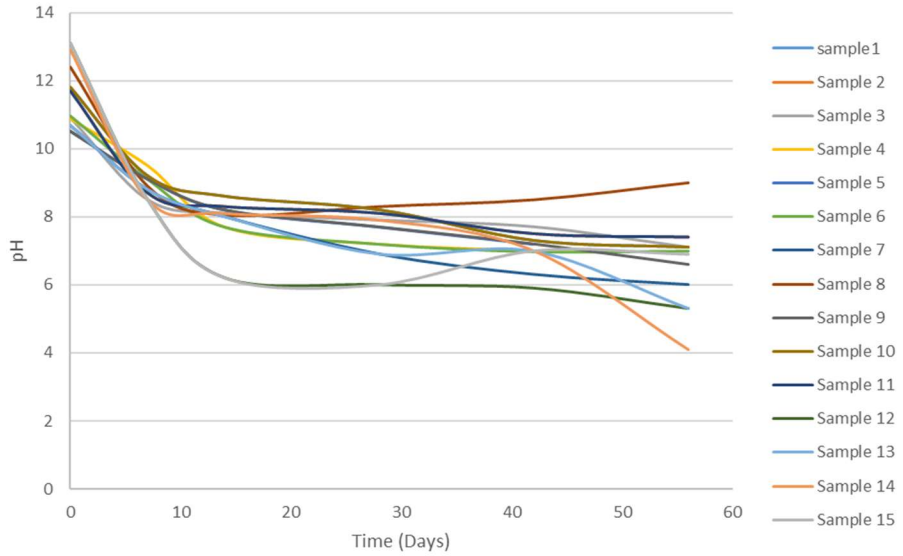

Figure 3-5: Sample's surface pH variations during cycle1 (0-56 days)

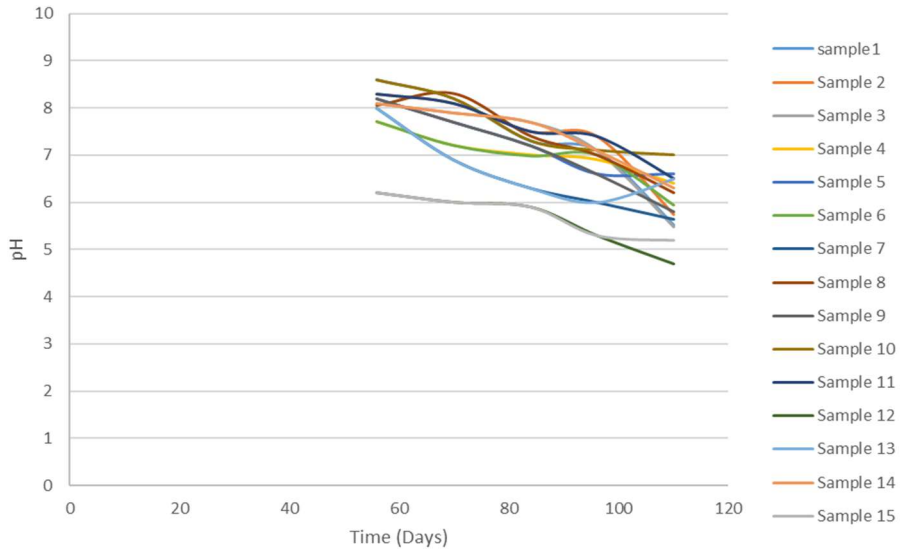

Figure 3-6: Sample's surface pH variations during cycle 2 (60-112 days)

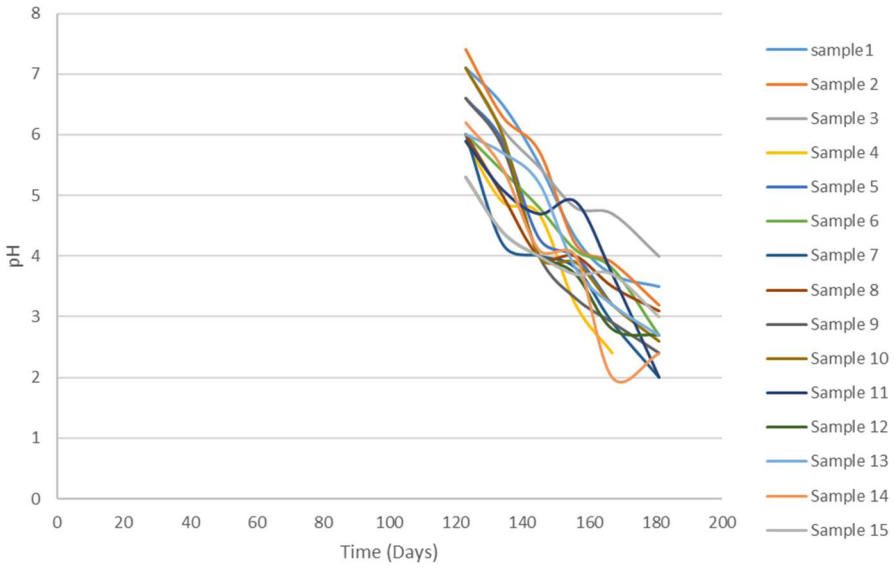

Figure 3-7: Sample's surface pH variations during cycle 3 (120-180 days)

3.3 Weight loss and absorption

At the end of each corrosion cycle, the degraded layers of concrete surface were brushed (w) similar to what is happening in the field because of sewage flow. Then the samples were washed, and oven dried in 110±5°C for 24 hours and weighted (w_A). For determination of absorption, samples were immersed in water at approximately 21°C for 72 hours, then dried in air (w_B).

The absorption and weight loss vs time (Fig 3.8 and 3.9) at the end of each cycle was calculated according to the following equations in which w_0 is the initial weight of the specimens and ΔW is the weight loss rate at the end of each cycle:

$$Absorption\% = \frac{(wB - wA)}{wA} \times 100 \quad , \quad \Delta W\% = \frac{(w0 - w)}{w0} \times 100 \qquad \textbf{(Equation 3.2)}$$

According to Figure 3.8, maximum 13% weight loss observed in the samples at the end of the test. Similar to pH variation, in most of the specimens, the corrosion degree and therefore the weight loss was slower in cycle 1 compare to cycle 2 and 3. After cycle 2, small holes appeared on the surface and surface material was discolored.

Formation of corrosion products is responsible for the volume expansion and crack propagation on the surface of cement mortar samples. Cracks provide flow channels for more water and gases to penetrate and absorb into the microstructure. The water absorption plot, Figure 3.9 shows that the absorption of the specimens increased by around 4% after 6 months. Variability in curves are explained by the sensitive nature of bacteria growth on different samples.

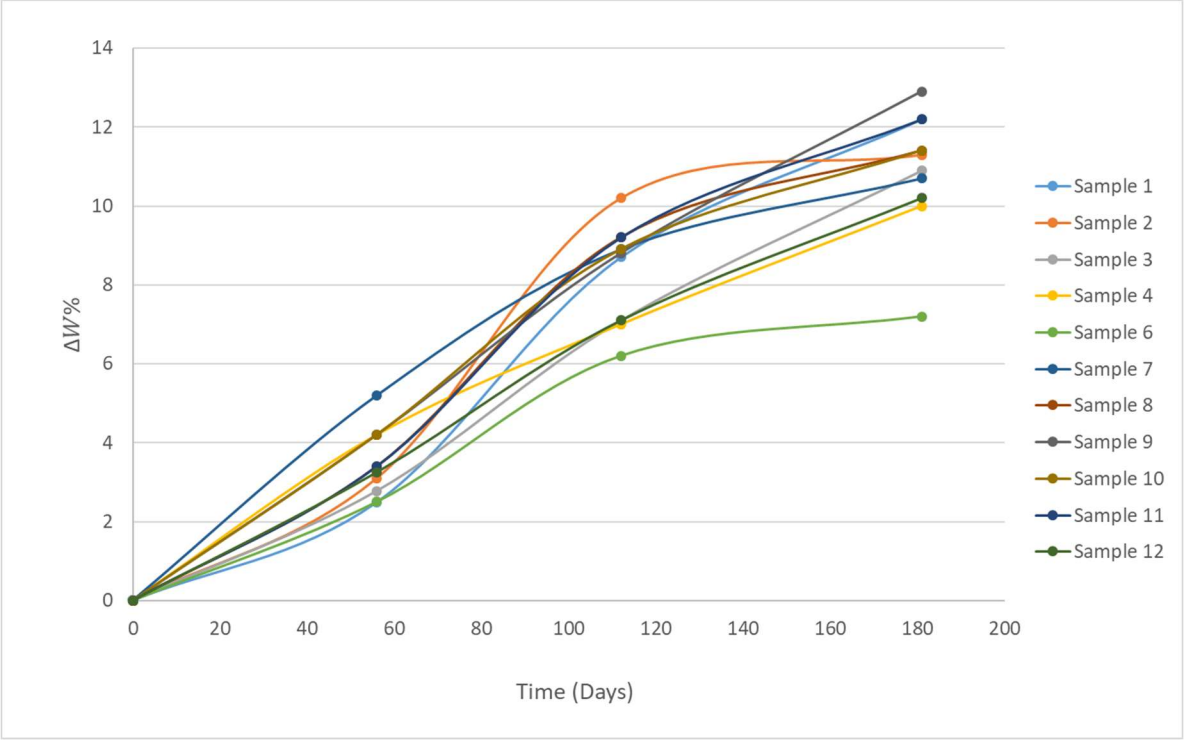

Figure 3-8: Sample's weight loss variation of samples during the bio-corrosion process

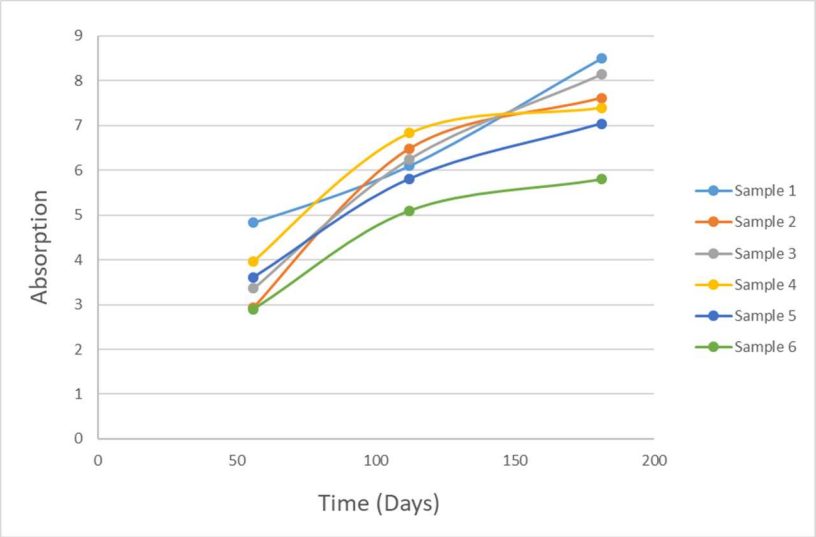

Figure 3-9: Sample's absorption variations (%) of samples during the bio-corrosion process (Days)

3.4 Corrosion depth and thickness loss

The change in dimension of the samples is an important factor for measuring corrosion intensity. The surface profile of 6 specimens before corrosion and after corrosion was plotted by scanning the surface with laser sensors. The laser sensor used in this study generated and used 670 nm-wavelenght laser beams to measure distance between the concrete surface and the sensor via triangulation principle. The principal of the laser measurements was based on the study done by De Belie et al., 2002.

During the measurements, the laser sensor was mounted on a designed set-up which rotates in a semicircular lane with a speed of around 1 mm/s and was able to record around 1900 measurements on each row. The mechanical device allowed adjustment of the height of the sensor. Two parallel profiles in steps of 2 cm was plotted for each specimen at the end of the test. The thickness loss was calculated by subtracting the surface profile plots. Summary of the results (profile depth in mm vs. measured point location along the sample) was plotted in Figures 3.10 to 3.15.

Figure 3-10: Cement mortar sample 1 profile depth after corrosion

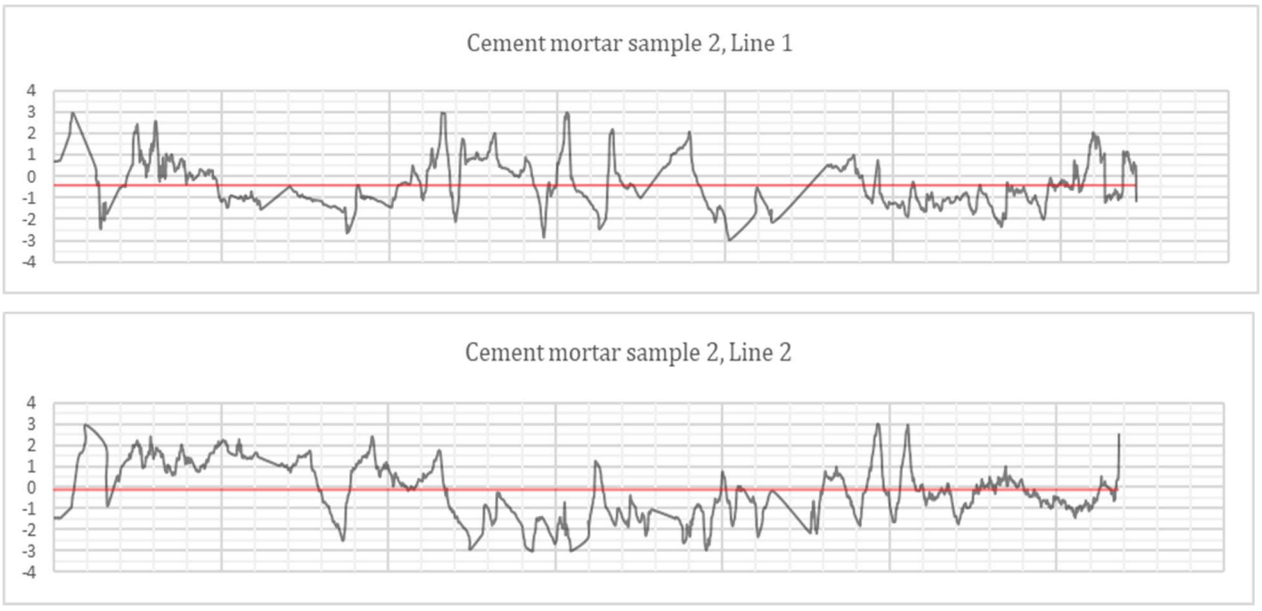

Figure 3-11: Cement mortar sample 2 profile depth after corrosion

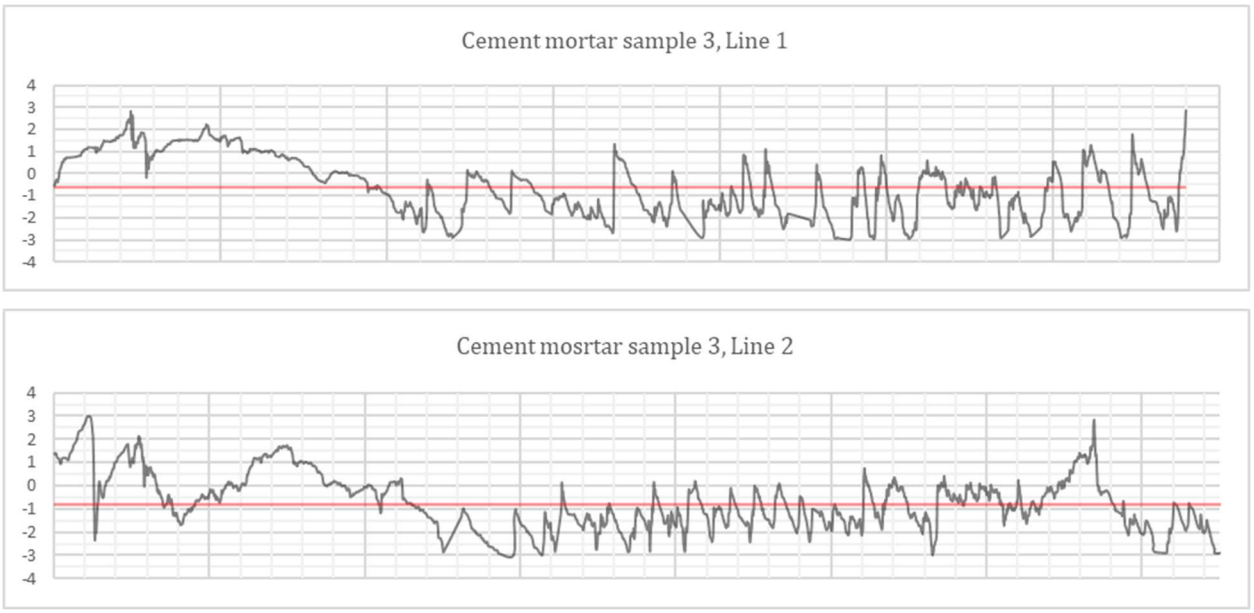

Figure 3-12: Cement mortar sample 3 profile depth after corrosion

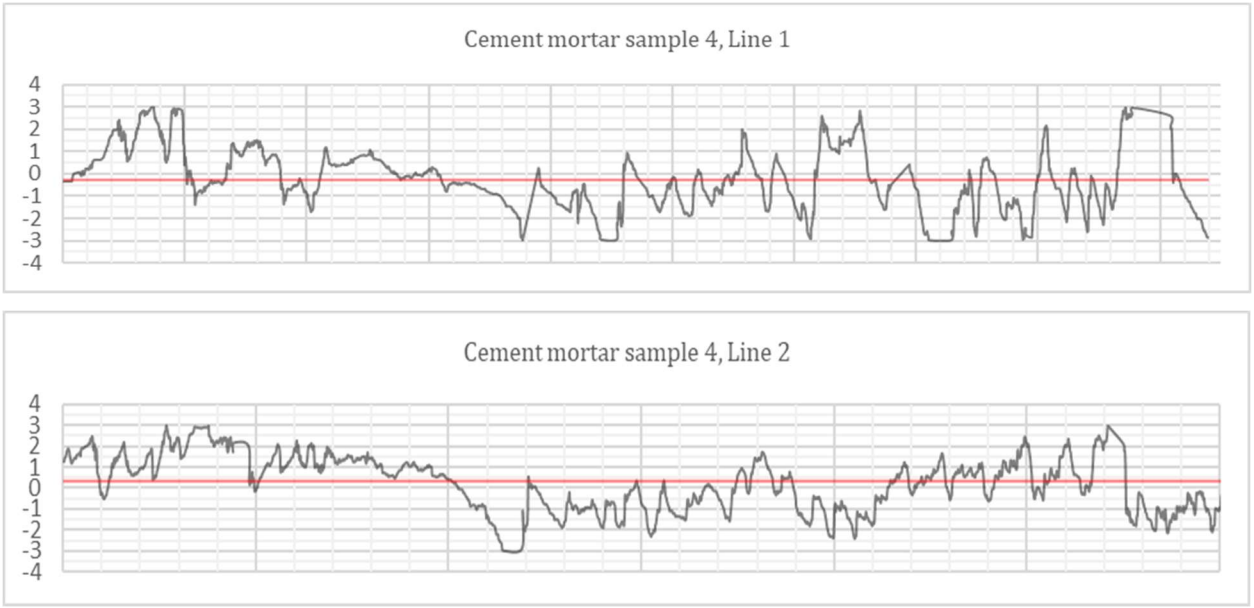

Figure 3-13: Cement mortar sample 4 profile depth after corrosion

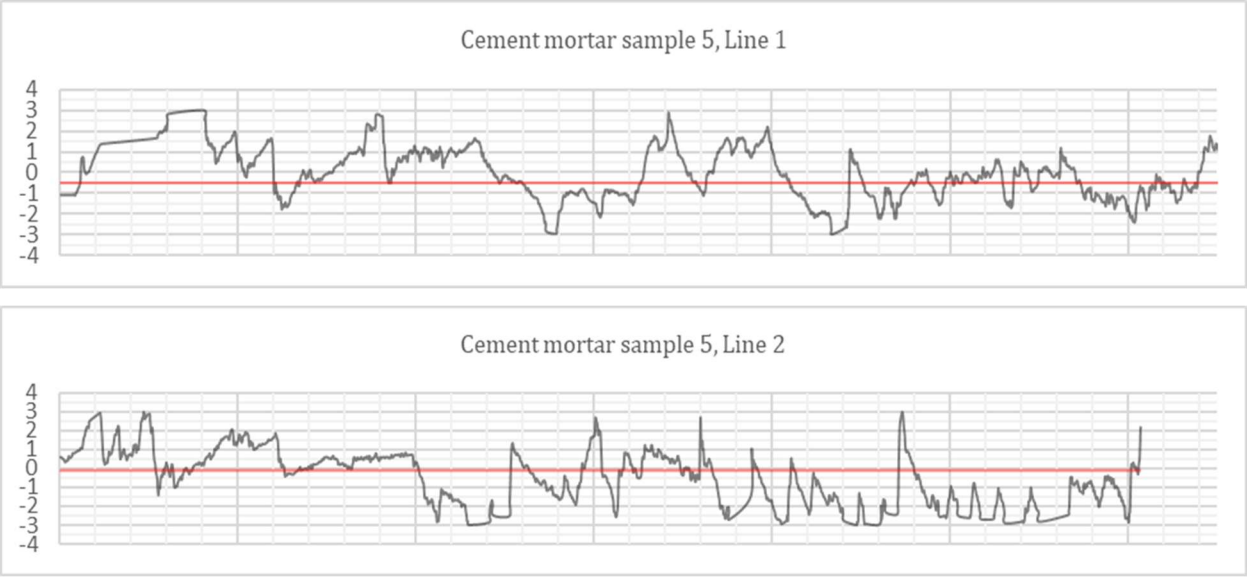

Figure 3-14: Cement mortar sample 5 profile depth after corrosion

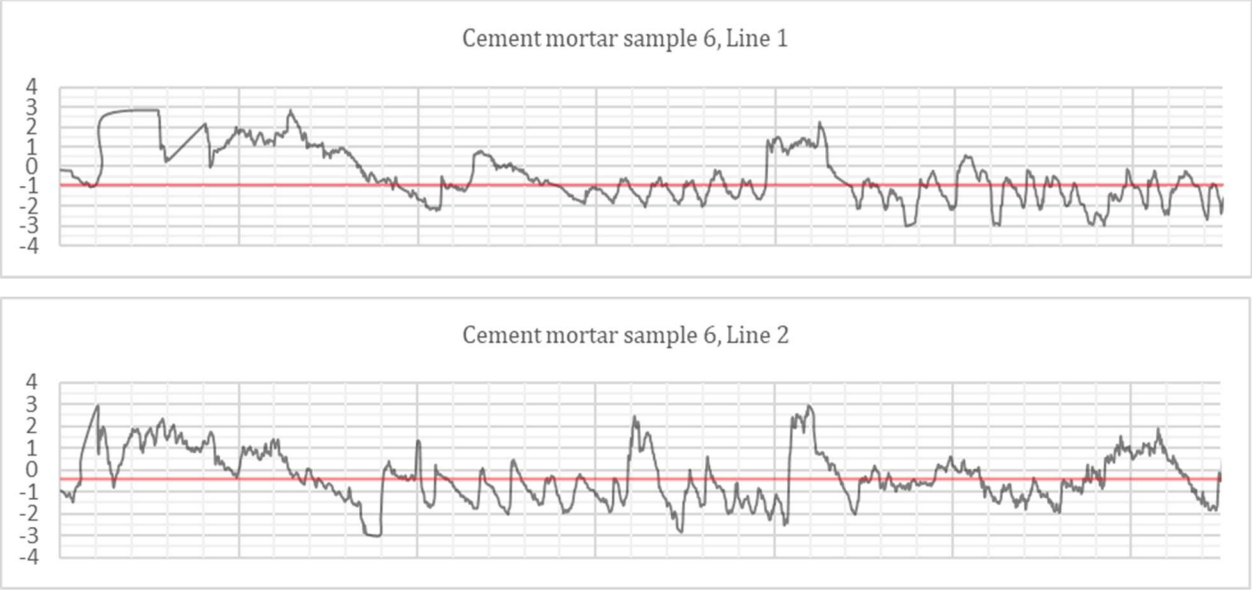

Figure 3-15: Cement mortar sample 6 profile depth after corrosion

Figure 3.15 show the average thickness loss caused by the bio-acid attack along the circumference of the samples. The bio-corrosion process caused an average thickness loss of around 2 mm and maximum thickness loss of around 4 mm on mortar samples. According to the results, the surface

of the specimens at the crown and close to the water line were corroded more severely which confirms findings of other studies [Mori et al., 1992].

The measurements with the laser scan were also used to calculate surface roughness change after 180 days corrosion period, see Figure 3.17. The R-values (as a measure of roughness) were calculated by drawing the center line (Y) and making the sum of all surfaces between the line and surface profile, Figure 3.18. Dividing this sum by the sample length, the R value could be calculated [De Belie, 2002].

In this study the surface roughness of the samples before and after corrosion were measured. The average initial surface roughness of 0.82 mm increased after corrosion to 0.9737 on line 1 and from 0.93 to 1.43 on line 2. The surface roughness of the sample is an important factor since the bacteria colonizes on rougher surfaces better. Bacteria on rough surfaces are more protected against external forces and have more time in direct contact with the surface. Therefore, the attachment maybe more strongly established.

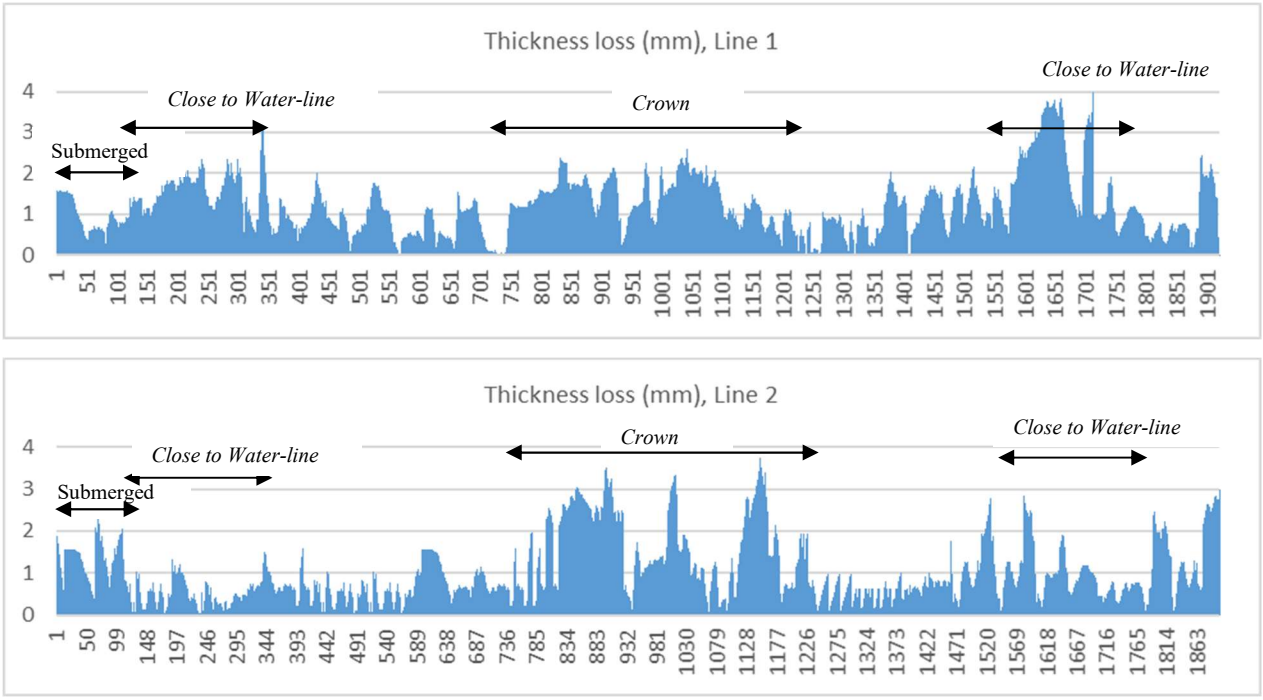

Figure 3-16: Average cement mortar sample's thickness loss (Thickness loss vs. Time)

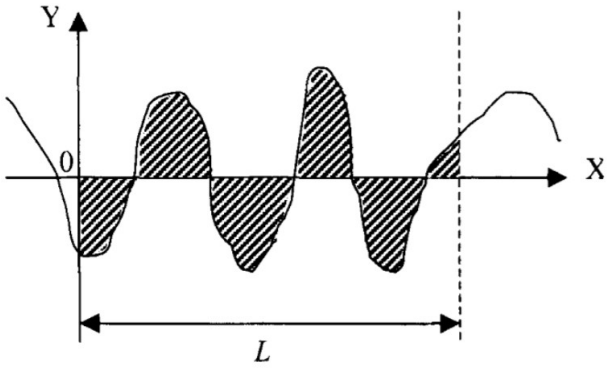

Figure 3-17: Calculation of roughness value, R [De Belie, 2002]

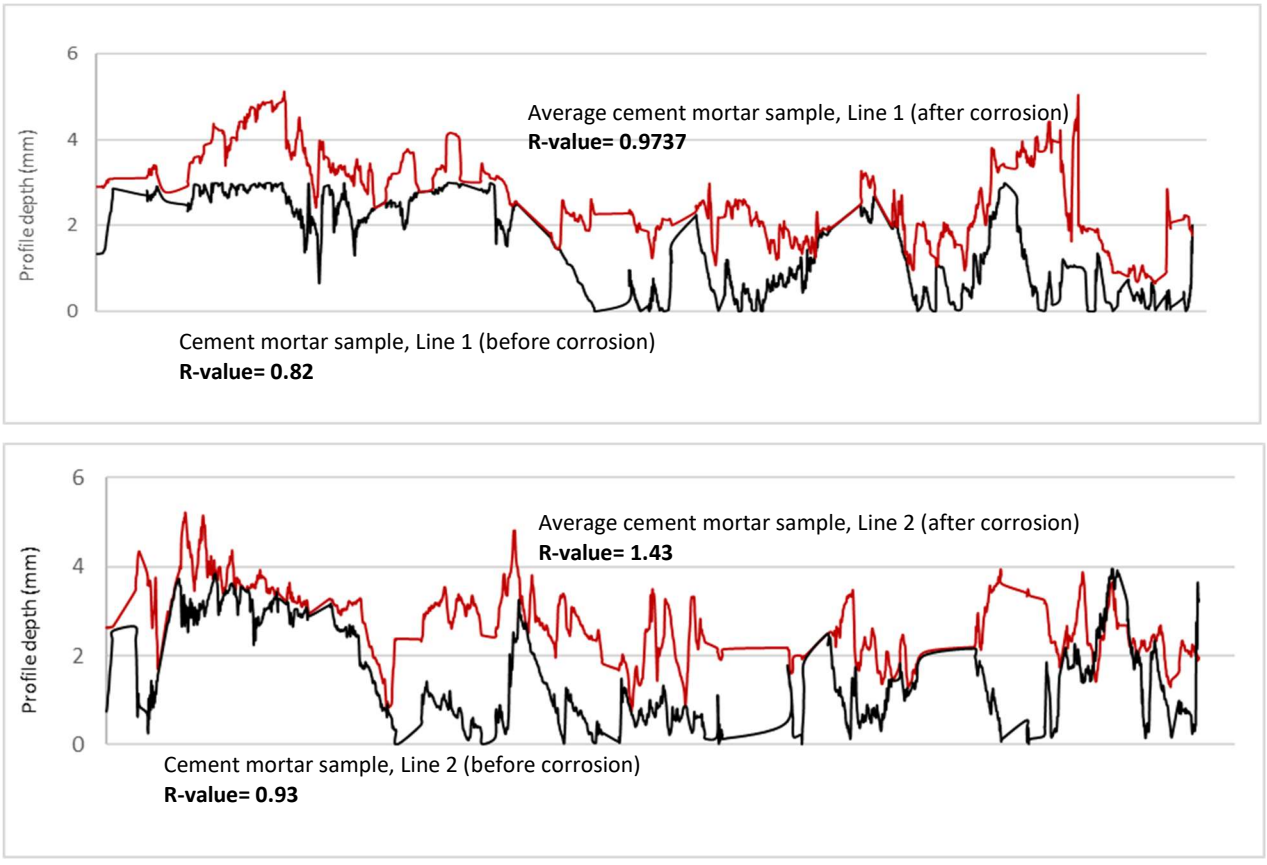

Figure 3-18: Average cement mortar sample's profile depth after and before corrosion

3.5 Surface morphology analysis

SEM-EDS (Energy Dispersive Spectroscopy fitted to Scanning Electron Microscope system) was used to investigate the microstructure and composition of the corrosion products. Proper sample preparation is very important in obtaining the required information when using SEM. For this purpose, samples of non-corroded and corroded cement-mortar were taken and impregnated using epoxy-based resin. Then epoxy impregnated samples were cut with a saw and polished with diamond grit. Ultimately, samples were cleaned in a desktop UV cleaner chamber and dried at 50℃. Figure 3.19 is SEM images of cement mortar sample before and after deterioration in the accelerated test chamber.

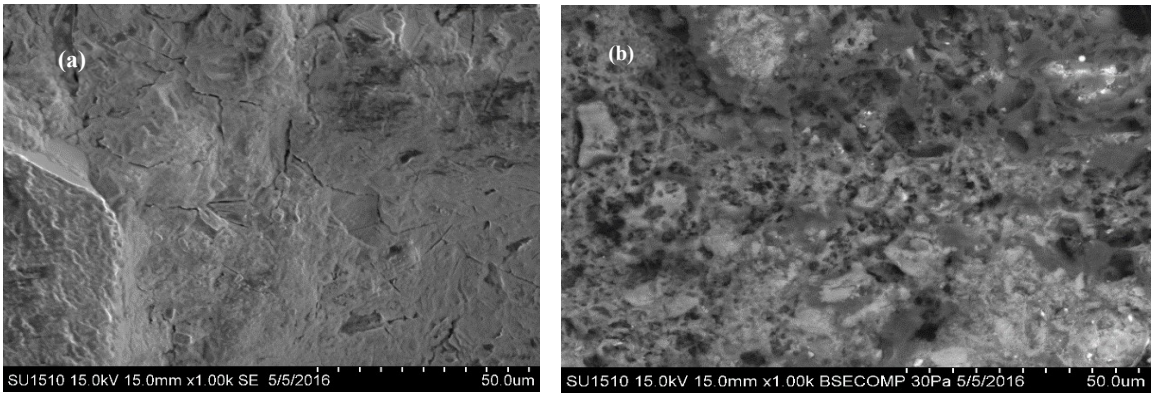

Figure 3-19: SEM images of (a) non-corroded and (b) corroded samples

SEM-EDS analysis of non-corroded samples were shown in Figure 3.20. Non-deteriorated samples had a condensed structure and mainly composed of these elements: O, Ca, Si, Mg, Fe and Al. Major elements of Si, O and Ca indicate high contents of SiO_2, CaO, Ca_2SiO_4 (C_2S) and Ca_3SiO_5 (C_3S). After the bio-corrosion process, there were loosely bound materials covering the interior surface of the samples but not evenly distributed along the perimeter. Figure 3.21 is a SEM image of the same sample after bio-corrosion. The elemental distribution pattern shows that the voids contain a high level of C and low levels of Ca and Si.

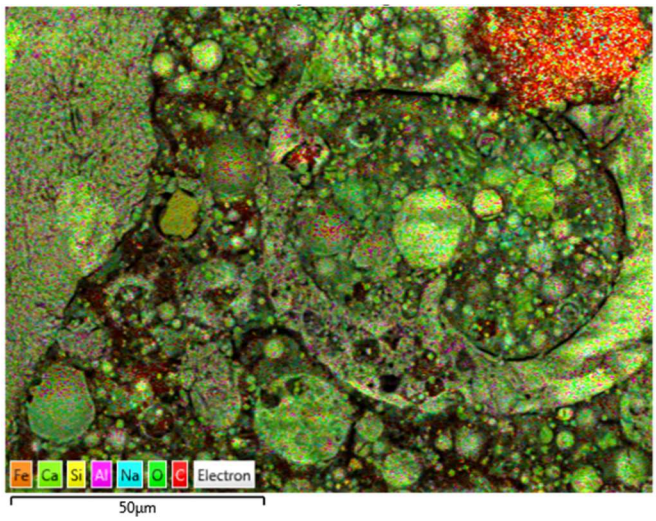

Figure 3-20: SEM image and elemental composition of non-corroded sample

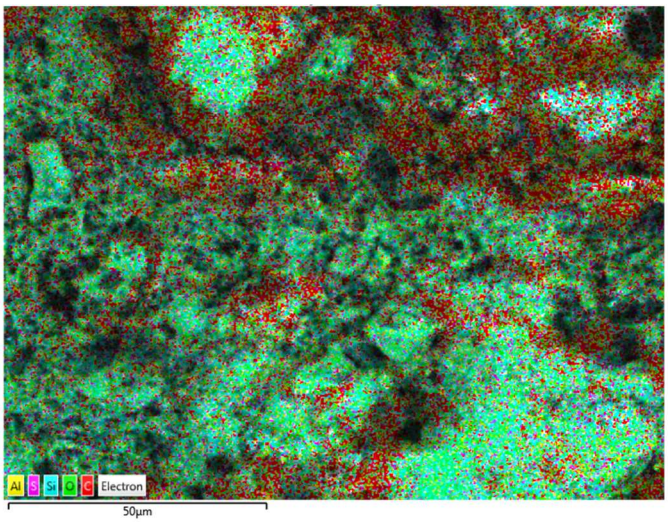

Figure 3-21: SEM image and elemental composition of sample after corrosion

By comparing the composition of cement mortar samples before and after bio-corrosion, it is clear that the amount of Ca, Si and Al reduced (see Figure 3.22). Reduction in Fe must be due to leaching or bacteria consumption as nutrient elements. Figure 3.23 shows the Ca/ S variation in corroded sample vs. non-corroded sample.

As it was described in Chapter 2, biological activity and the reaction of diffused H_2S on sample's surface produce sulfuric acid. Creation of localized acidic conditions in pores and cracks cause

dissolution of CH and CHS. Sulfuric acid reaction with the CH (calcium hydroxide) and CSH (Calcium silicate hydrate) of the hydrated cement produce expansive products such as gypsum. The produced gypsum was a white, mushy substance which has no cohesive properties, causes cracks and has a highly porous structure. So, dissolved and ionized calcium moves easily through connected network of pores in corroded cement matrix and leaches out of the system. Leached calcium can react with CO_2 in the air above the sewage and form calcite (calcium carbonate). As the pH value of the surface reduced due to carbonation and bacterial activity, calcite became soluble and left the matrix.

Figure 3.24 is scattered plots of atomic ratios of Al/Ca vs. Si/Ca and S/Ca vs. Si/Ca of both corroded and non-corroded samples. According to the data points corresponding CH, CSH and gupsum, the amount of CSH reduced and gypsum/CH increased after corrosion.

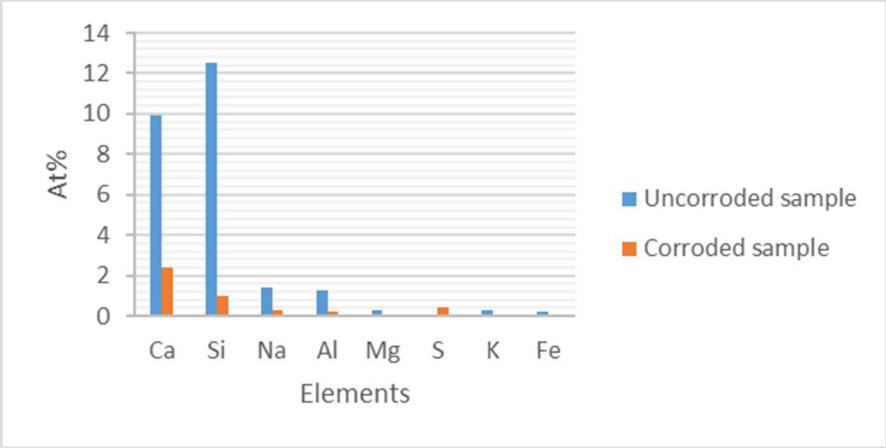

Figure 3-22: Composition of cement mortar samples before and after bio-corrosion

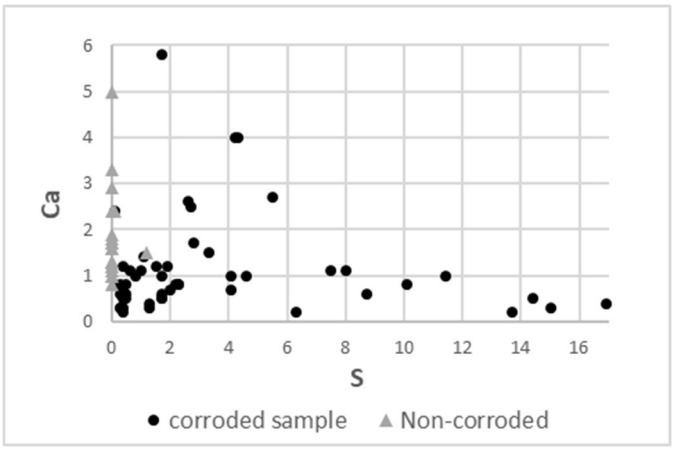

Figure 3-23: Scatter plots of Ca/S variation in corroded and non-corroded samples

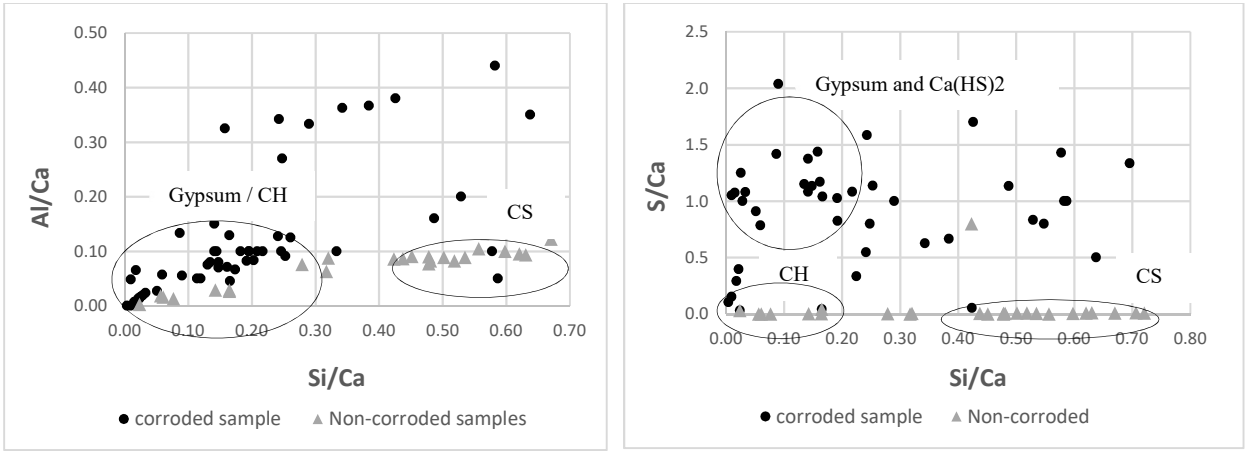

Figure 3-24: Atomic ratio plot of (a) Al/Ca v Si/Ca, and (b) S/Ca vs. Si/Ca

(CH: calcium hydroxide, Ca: Calcium, Si: Silicate, Al: Aluminum, CS: Calcium sulfate, S: Sulfur)

3.6 Flexural strength loss

Corrosion products on the surface of the concrete pipes were eroded over time and new surface was exposed to acid attack. This process will continue until the pipeline fails. In this study, resistance (capacity) of arch-shaped concrete samples were tested subjected to three-point bending. The test set-up is illustrated in Figure 3.25 and 3.26.

Figure 3-25: Test set-up for measuring flexural strength of the samples after and before corrosion

Figure 3-26: Measurements of the effect of corrosion on the ultimate load bearing capacity of the samples

After 112 days three samples were removed from the chamber for strength loss measurements, and then returned to the chamber. Samples' final strength loss was measured after 180 days.

The maximum load applied on samples (F) at the end of each corrosion cycle (t_1, t_2, t_3), was around 500 N. The amount of the applied load was kept to a minimum in order to avoid damage and microcracking as much as possible. The normalized load-deflection curves obtained (see Fig 3.27,

3.28 and 3.29) enables each sample to be characterized by the deflection capacity (δ_0, δ_{112}, δ_{180}) corresponding to the applied load (F) and flexure stiffness (k_1, k_2, k_3).

(a)

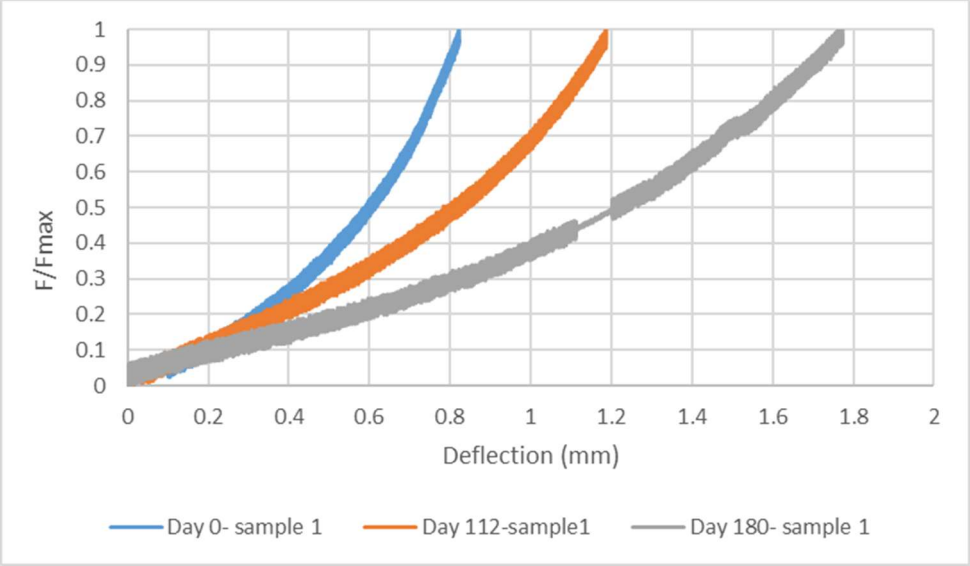

(b)

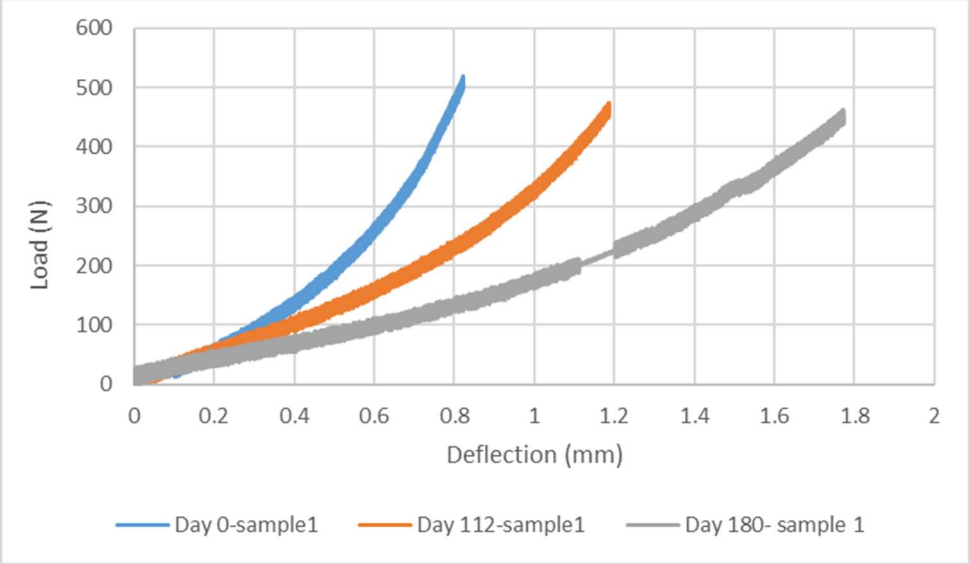

Figure 3-27: Effect of corrosion on deflection capacity of sample 1

(a) Normalized load-deflection curve for sample 1, (b) Load-deflection curve for sample 1

(a)

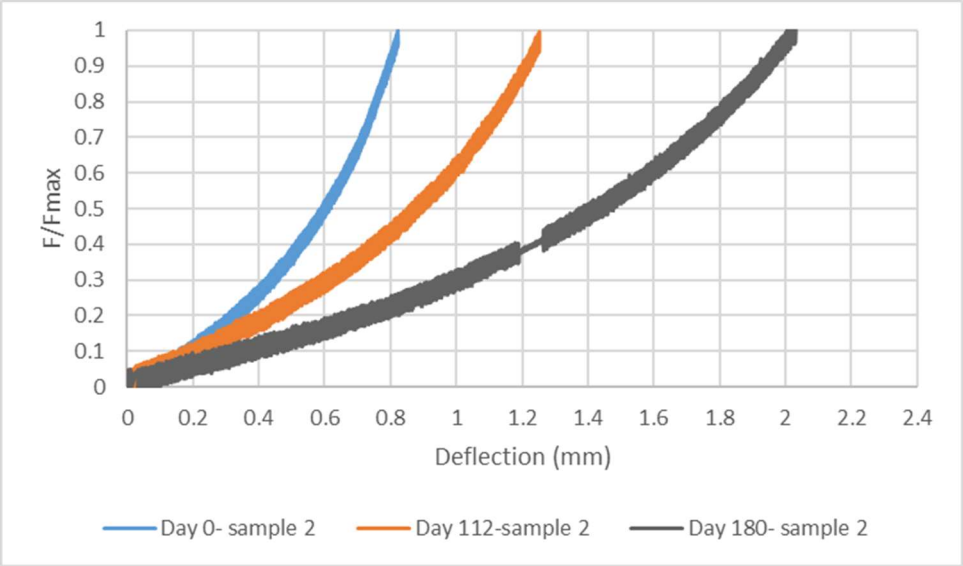

(b)

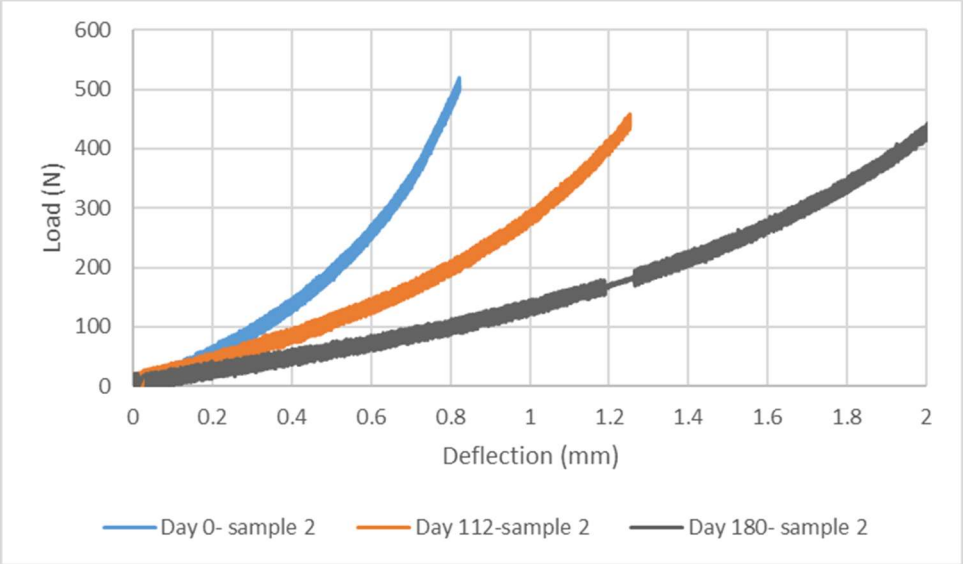

Figure 3-28: Effect of corrosion on deflection capacity of the sample 2

(a) Normalized load-deflection curve for sample 2, (b) Load-deflection curve for sample 2

(a)

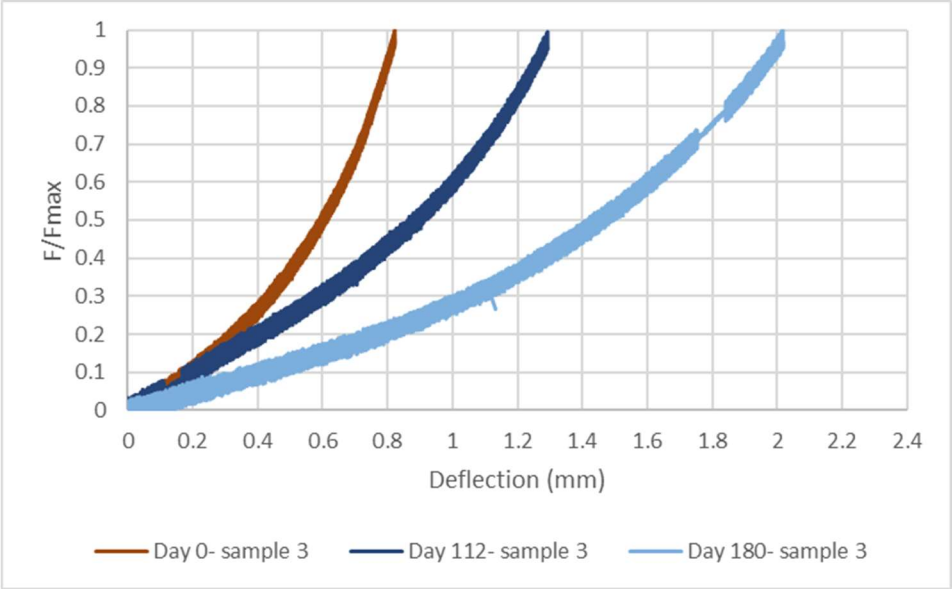

(b)

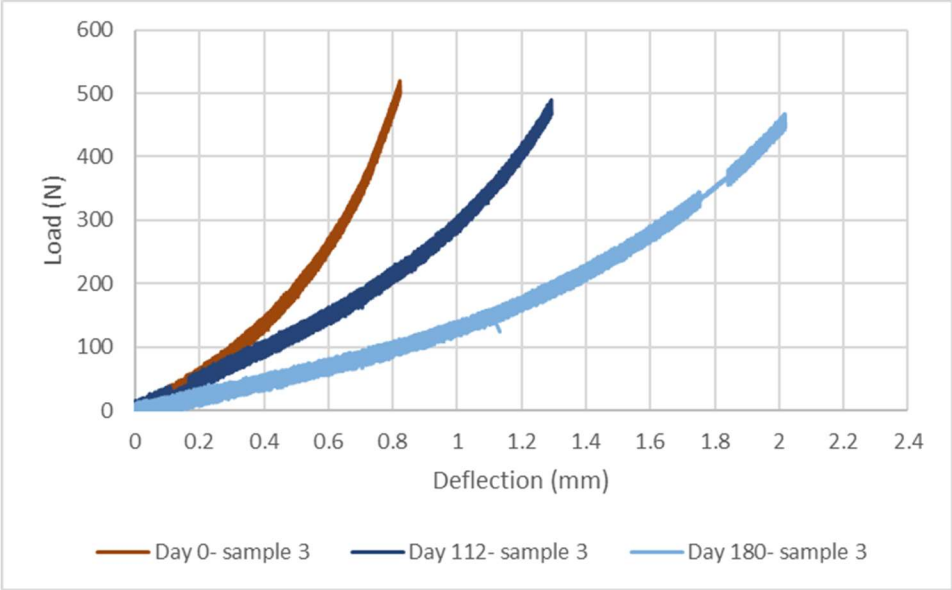

Figure 3-29: Effect of corrosion on deflection capacity of the sample 3

(a) Normalized load-deflection curve for sample 3, (b) Load-deflection curve for sample 3

The effect of corrosion on the ultimate load bearing capacity (F_{max}) and corresponding deflection capacity of the samples (δ_{max}) was measured at the end of the test (after 6 months). Average results of the samples are summarized in Table 3.1. ΔS is the strength loss rate which is calculated according to the following equation (Eq. 3.2):

$$\Delta S\% = \frac{(F_{max(t=0)} - F_{max(t=180)})}{F_{max(t=0)}} \times 100 \qquad \textbf{(Equation 3.2)}$$

Table 3-1: Results of the flexural strength test
(a) Results of the compliance tests (b) Results of the ultimate strength tests

(a)

t_i (days)	0	112	180
δ_i (mm)	0.8	1.2	1.8
$k_i = \Delta F/\Delta \delta$	357.4	87.6	173.5

(b)

t_i (days)	0	180
F_{max} (N)	4306.7	1120.6
δ_{max} (mm)	1.9	2.5

δ_i is an indicator showing that the deflection capacity of the corroded samples increased by 51% after 112 days and by 113% after 180 days. The k values show that the average resistance of the samples against bending deformation was reduced after 112 days in the bio-corrosion chamber. Although slight increase was observed after 180 days, Ultimately the stiffness of the samples was reduced by 48.5%. Figure 3.30 and 3.31 shows the test conducted on samples after 180 days. According to the results the peak load decreased by 73% and the corresponding deflection increased by 25.5% after 180 days in corrosion chamber. The sharp drop in the flexural strength of the samples was related to higher porosity, mass loss and size reduction. The reaction products were structurally weak and easily leached out of the hydrated matrix.

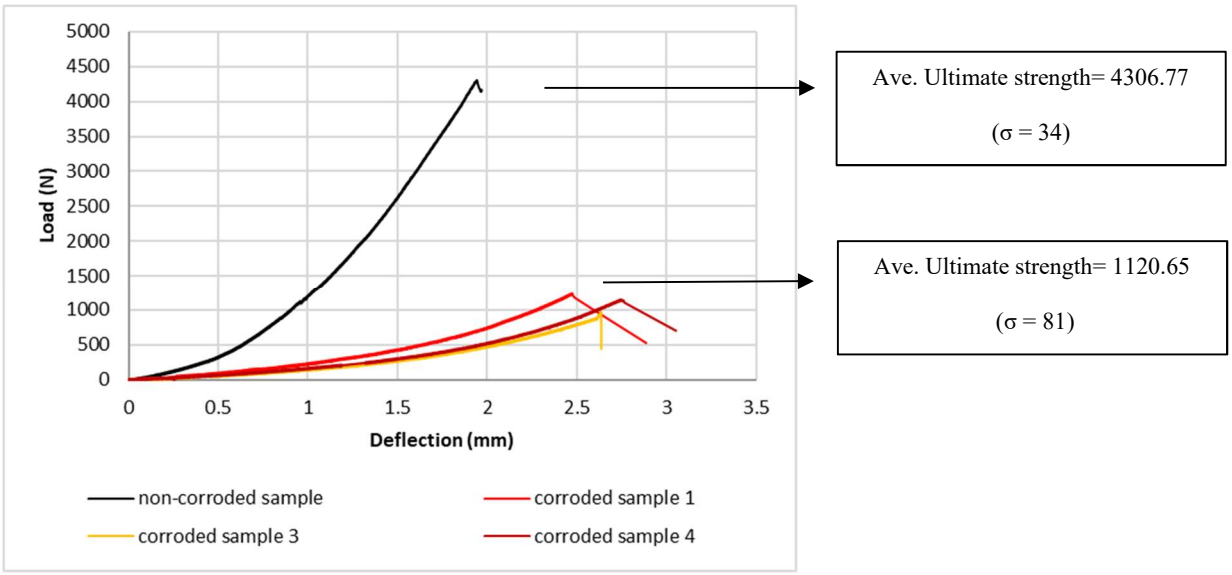

Figure 3-30: Load-deflection curves: effect of corrosion on the ultimate load bearing capacity of the samples

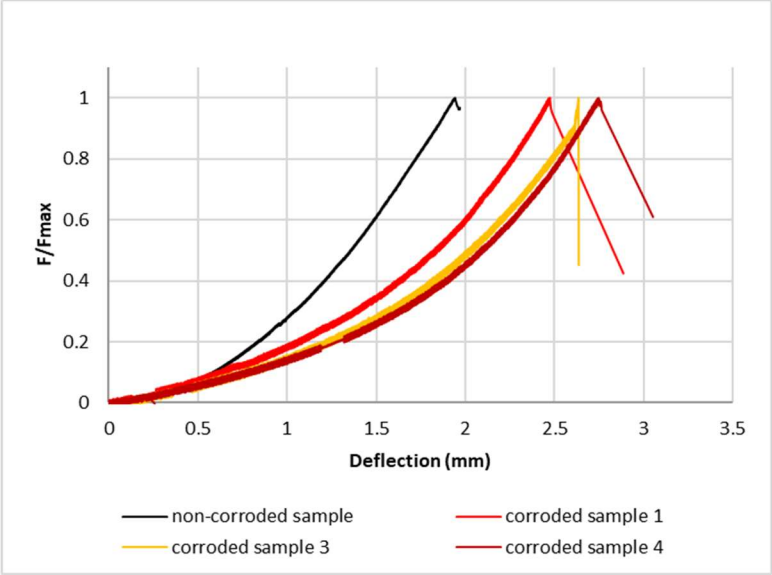

Figure 3-31: Normalized load-deflection curves

3.7 Corrosion rate

As discussed in Chapter 2, many methods of forecasting the corrosion rate are available. However, the actual corrosion rate in concrete pipes is different from the values calculated in accordance with available methods. Wells et al. (2015) proposed a simple model for predicting the rate of corrosion in concrete pipes in which C is the rate of corrosion (mm/year), [H_2S] is the concentration of the H_2S gas in ppm, H is the relative humidity of the sewer atmosphere, R is universal gas constant equal to 8.314 $Jmol^{-1}K^{-1}$ and T is the temperature of the sewage atmosphere in Kelvin. The authors determined the scaling constant (A) equal to 207750 $mmyr^{-1}$ $ppm^{-1/2}$ [Wells 2015]:

$$C = A \times [H_2S]^{0.5} \times \frac{(0.1602\,H - 0.1355)}{1 - 0.9770\,H} \times e^{\left(-\frac{45000}{RT}\right)} \qquad \textbf{(Equation 3.3)}$$

According to the Eq. 3.3, corrosion rate is a function of temperature, relative humidity and gas concentration. The corrosion rate increases if the H_2S concentration increase, however, even with high gas concentration, low humidity results in very low corrosion which is the reason that the H_2S level kept at 50 ppm but the humidity increased to the maximum possible humidity in the chamber. Although the corrosion rate increases with higher temperature, the ideal temperature in this experimental test was chosen according to the ideal conditions for the growth of the bacteria.

By using this equation and considering the average field observations of Metro Vancouver's sewage system in Canada, with an average temperature of around 23°C, humidity 0.91, and average gaseous levels of 15 ppm (H_2S_{ave}), 0.74 mm per year corrosion is predicted by the Eq. 3.3. By replacing the conditions in Eq. 3.3 with the amounts that were used in this study, (T=30°C, H=0.9, and H_2S_{ave}= 50 ppm), the corrosion rate is predicted to around 1.86 mm per year which likely reflects the accelerated bio-corrosion process by 2.4 times. Also, this experiment demonstrated that the corrosion rate increased additionally by spraying bacteria cultures on cement mortar samples and removing corroded parts manually at the end of each cycle. Ultimately, the average corrosion rate obtained from the accelerated test experiment in this study (thickness loss results in section 3.4) was around 2 mm after 6 months. The developed experimental test

accelerates the bio-corrosion process by 5 to 6 times compared to what appears to occur in sewage pipes.

3.8 Discussion of the performance of the accelerated test chamber

A novel experimental apparatus was designed and manufactured to simulate bio-corrosion in concrete pipes and measure the deterioration rate of cement mortar samples. This chapter summarized the validation/test phase to estimate performance of the designed accelerated test chamber.

A combination of multiple evaluation tests and indicators compared the relative performance of bio-deteriorated samples. The corrosion rate was determined by measuring pH, absorption and mass loss as well as the reduction in thickness and flexural strength which are the most important factors in durability and serviceability of concrete pipes. Also, the corrosion products were investigated by SEM. The results showed a very large variability in weight and absorption loss which is due to the nature of working with live microorganisms. So, it could be concluded that weight and absorption loss are not good indicators for evaluating the performance of the samples.

According to the results of pH measurements, the rate of variations was slower at the beginning. Gradually, the neutralizing capacity of the samples was reduced, and the bacteria started to grow and reduced the pH faster on the surface. In addition, due to an increase in the porosity of the samples, pH dropped quicker after 60 days. Approximately 14% weight loss was observed in the samples at the end of the test. Similar to pH variation, in most of the specimens, the corrosion degree and so the weight loss was slower at the beginning. After around 100 days, small holes appeared on the surface and surface material was discolored.

Formation of corrosion products is responsible for the volume expansion and crack propagation on the surface of cement mortar samples during the test. Cracks provide flow channels for more water and gases to penetrate and be absorbed into the microstructure. Results show that the absorption of the specimens increased by around 4% after 6 months in bio-corrosion chamber.

It could be seen that the bio-corrosion process caused an average thickness loss of around 2 mm and maximum thickness loss of around 4 mm on cement-mortar samples. The measurements with the laser scan were used to calculate surface roughness change after 180 days corrosion period. The average initial surface roughness of 0.82-0.93 mm increased after corrosion to 0.9737-1.43. The surface roughness of the sample is an important factor since the bacteria colonizes on rougher surfaces better. Bacteria on rough surfaces are more protected against shear forces and have more time to get the direct contact with the surface. So, the attachment maybe more strongly established.

SEM-EDS analysis is also conducted on corroded and non-corroded samples. Non-deteriorated samples had a condensed structure and mainly composed of O, Ca, Si, Mg, Fe and Al. After the bio-corrosion process, there were very loosely bound material covering the interior surface of the samples which was not evenly distributed along the perimeter. The elemental distribution pattern of corroded samples showed that the voids contain a high level of carbon and the amount of Ca, Si and Al reduced. This is due to the biological activity and the reaction of diffused H_2S on sample's surface. Creation of localized acidic conditions in pores and cracks cause dissolution of C2S and C3S. Sulfuric acid reaction with the CH (calcium hydroxide) and CSH (Calcium silicate hydrate) constituents of the hydrated cement produce expansive products such as gypsum.

The resistance of arch-shaped concrete samples was also tested before and after corrosion subjected to three-point bending. According to the results the peak load decreased by 73% and the corresponding deflection increased by 25.5% after 180 days in corrosion chamber. The sharp drop in the flexural strength of the samples is related to higher porosity, mass loss and size reduction. Also, the reaction products are structurally weak and easily leached out of the hydrated matrix.

The corrosion rate increased additionally by spraying bacteria cultures on cement mortar samples and removing corroded parts manually at the end of each cycle. Ultimately, the average corrosion rate obtained from the accelerated test experiment in this study was around 2 mm after 6 months. So, it could be concluded that developed experimental test accelerates the bio-corrosion process by 5 to 6 times compared to what is happening in sewage pipes.

Growth curves suggest that the improved accelerated test chamber design works. The proposed methodology and the results contribute to a better understanding of the bio-corrosion process and provide quantitative information on the performance and effectiveness of different coating materials which is necessary in evaluating concrete pipe's serviceability and predicting the remaining service life of rehabilitated pipes.

Chapter 4: Development of a sustainable composite coating integrated with zinc-doped clay

Over the past several decades many approaches have been undertaken to protect infrastructures exposed to aggressive environments from bio-deterioration. Prevention of bio-corrosion in concrete infrastructures usually requires modification of concrete mix, introduction of novel cementitious material or application of chemical/antimicrobial resistant thin coating layer on the inner surface of concrete pipe which inhibit biological activity or provide protective layer between concrete surface and corrosive solution. Other mitigation methods also include introduction of bactericides to the wastewater, chlorination, injection of compressed air and addition of lime which were attempted with limited success.

Major materials used to coat concrete pipes include cement mortar, epoxy mortar and polymer-based coatings with variable degrees of success. Most of the coating materials are not resistant to acid attack, have bonding issues with the concrete substrate and in many cases, bacteria are able to penetrate the coating material and grow on the concrete surface beneath the coating and destroy the bond. So, success with application of different types of linings and coating materials has been quite variable.

As it was discussed earlier, higher strength or lower porosity do not necessarily enhance the resistance of material to acid attack, but the chemical nature of the material is a key factor that determines the resistance of the coating material in acidic and corrosive environments.

Portland cement-based coating material has limited ability to resist acid attack over time in aggressive environments due to its chemical composition and calcium content. The hydrate phases CH (calcium hydroxide) and CSH (Calcium silicate hydrate) and their amount in the medium which is dependent on the proportion contributed by the binder, is a significant determinant of how stable chemically the matrix becomes. Water, which plays a key role in the hydration process, also

actively participates in the chemical reaction. So, examining materials that produce non-traditional hydration products to improve the resistance of pipes to acid attack has gained interest.

In addition, concrete production requires large quantities of Portland cement, production of which is a major contributor to greenhouse gas emissions and raw material. Production of one ton of Portland cement requires about 2.8 ton raw materials and is responsible for about 1 ton of greenhouse gas (CO_2) emission. The emission of the CO_2 from de-carbonation of lime in the kiln in cement manufacturing process is about 7% of the total CO_2 emission in all the human activities.

So, there is a need for replacing cement-based repair materials with durable, economic, effective and also sustainable and environmental friendly alternatives. Innovations through extensive research have brought sustainable materials into new light while increasing the recyclable potential of the existing materials used in construction. These new advances along with future research will make the future of infrastructures more sustainable, efficient and productive.

4.1 Concrete pipe coating strategies

4.1.1 Protective coatings

In the context of pipe rehabilitation, protective coatings are the most widely used means of preventing further corrosion. Most coating strategies rely on using a protective and corrosion-resistant material between concrete surface and corrosive solution such as cement-based mortars, epoxy, mortar epoxy, polyesters, high alumina cement, asphalt and PVC sheets.

Initially, the pipe must be prepared by being emptied and washed with water jet. Then, in the case of polymer-based coatings such as PVC membrane, the unformed PVC coating is entered into the pipe and brought through the entire length of the pipe. Once the coating has been put all the way through the pipe, the thermoplastic is heated to its designated temperature to make it workable. The PVC is then molded to the edge of the corroded pipe with a specialized molding device. After

it is molded, the thermoplastic is set and will no longer be pliable, so long as its temperature remains below the pliability temperature.

Similar to the polymer-based coatings, pipes must be washed out and prepared first before the application of mortar coatings. Then different methods such as trowel is used to apply the coating inside pipes which helps to repair corrosion damages and seal leaks. Also, the mortar or epoxy mixture can be sprayed on, by hand which is comparatively much cheaper and easier than the process of setting the PVC coating.

However, there are common issues associated with these types of coatings such as cost, tendency to the propagation of cracks, pinholes or rips, delamination, corrosion, compatibility with the host material, short bio-resistance lifetime, poor adhesion to the substrate material, long setting time, considerable thermal expansion and toxicity. Furthermore, most coatings are highly permeable and prone to acid and/or bacteria penetrate the layer, corrode the concrete substrate beneath the liner and destroy the bond. It is reported that conventional coatings often require reapplication after a year or more. In some cases, the coating material impair the breathability of the concrete that may cause blistering and coating failure. So, success with protective coating materials has been variable and it is uncertain if they could be used as long-term solutions.

The sanitation district of Los Angeles county is one of the regions that is affected by bio-corrosion severely and so rehabilitation and replacement of the corroded pipes costs millions of dollars every year. There is an extensive study conducted by the sanitation district of Los Angeles on using different coating systems for preventing corrosion in wastewater concrete pipes. The report is summarized in Table 4.1.

Table 4-1: Coating materials studied by Los Angeles Sanitation Districts

Coating material	Application	Corrosion resistance	Bond
Urethane (Senotex 3005)	2	1	3
Urethane (GS1490)	4	---	3
Epoxy Mortar (Fosroc)	3	3	1
Epoxy (Aquata-poxy)	2	1	1
PVC (Liner)	3	1	---
Acid Proof Cement (Liner)	2	2	---
Urethylene (Allied Liner)	1	2	3
Polyester (IET system 3)	2	1	1

Note: The performance of the coating materials is ranked as 1: Good, 2: Some problem (not significant), 3: Significant problems, 4: failure

4.1.2 Bactericide coatings

The second type of coating one that is integrated with antimicrobial bioactive chemicals (biocides) or heavy metals. Biocides were introduced in 1967 by the Penarth Research Center trying to inhibit bacteria growth on stonework with applications extended to ancient masonry buildings and cement-based substrates [Richardson, 1988]. Currently more than 18 different bioactive chemicals are used and classified according to their chemical structure and mode of antimicrobial action. Biocides attack bacteria through damaging or inhibiting the synthesis of cell wall or affecting bacterial DNA or RNA, proteins or metabolic pathways.

There are different methods of using biocides depending on the application. One method is fixing biocides on surfaces, such as when integrated in paints. However, the optimum method of using biocide is to include it in the material itself or incorporate it into a coating [Alum et al., 2008].

The most important concerns of using biocides in coating materials includes the range of microorganisms to be controlled, effectiveness of the biocide, compatibility of the chemical with

the host coating or pipe material, the toxicity of the biocide and requirements for its safe disposal, biodegradability and the cost of the product. Other challenges include capability of providing protection over the required time scale, degradation into inactive compounds, fast dissipation due to leaching and/or volatilization, short bio-resistance lifetime and high required concentrations to have long term effect. The last but not the least is that some of these chemical compounds are toxic (such as mercury-based and tin-based biocides) and undesirable leaching of them into the water and soil cause adverse environmental effect. Modifications techniques towards enhancing biocides activity include converting biocide into a slow-release or long-acting product.

The eco-toxicity and biodegradability of biocide have become very important recently as governments have become more concerned with environmental problems arising from the unregulated disposal of biocides. This has lead to stricter environmental legislations over the last decade and requires careful monitoring [Edge et al., 2001; Whitekettle et al., 2010]. Some of the toxic biocides that remain in use are formaldehyde (carcinogenic), copper compounds (persistence in environment) and chlorine (yield persistent secondary products).

Heavy metals such as copper, nickel, silver and zinc are also known for their antibacterial properties and have been used as an alternative for disinfection of wastewater in treatment plants. Coating the pipe's internal wall by cuprous oxide or silver oxide in epoxy is reported to reduce the bacterial corrosion. Hewayde et al. (2005) used two concrete pipes coated with the metals oxides. Then filled the pipes with nutrient and concentrated bacterial solutions (Desulfovibrio desulfricans strain). Results showed that the rate of corrosion for coated samples were less than uncoated samples. But silver oxide showed poor adhesion and metal ions leached out of the system easily [Hewayde et al., 2005]. The researchers found that the activity of SRB species in the presence of heavy metal ions such as Cu (20 mg/L), Zn (20 mg/L) and toxic chemical such as glutaraldehyde (10 mg/L) is reduced. Maeda et al. (1996) suggested the possibility of using nickel to prevent concrete corrosion [Maeda et al., 1996]. It has also been reported that sodium tungstate completely inhibits the growth of Thiooxidans cells [Negishi et al., 2005]. Zinc oxide is also reported to have good thermal quality and color stability. In addition, it has been used as an antibacterial agent in medicine and food packaging because of antibacterial effect and high safety.

The most important challenges of using heavy metals in coating materials include short bio-resistance life time and efficiency, leachability into the environment, safety concerns and regulations that restrict levels of certain metals in sewer systems, poor adhesion to concrete substrate and cost. Also, in high dosages they might affect the structural properties of the coating material. The last but not the least is that some of these heavy metals are toxic and undesirable leaching of them into the surrounding environment cause problems. Also, overuse and abandoned leaching of heavy metals could lead to the speedy development of bacteria that are immune to multiple drugs. Pollution of water and soil with toxic heavy metals and bioactive chemicals is of major concern for human health and environment.

Noeiaghaei et al. (2017) summarized some of the most common examples of coating systems applied to increase the resistance of concrete pipes in Table 4.2 [Noeiaghaei et al., 2017].

Table 4-2: Examples of common coating systems adapted from Noeiaghaei et al., 2017

Coating material	Remarks
Silane/siloxanes	Very low reduction of compressive strength due to sulphate attack in the concrete specimens coated with silane/ siloxane in conjunction with an acrylic topcoat
Polyester based polymers	Good bond strength with concrete surface and good ability to resist the penetration of acidic solution for wet-coated concrete samples
Epoxy	Excellent durability of epoxy-coated mortars after 60-day exposure to *T. ferrooxidans*
Glass fibre mat reinforced epoxy	No failure up to 20 months for reinforced epoxy-coated concrete in acidic environments (3% sulphuric acid solution)
Epoxy and polyurethane	Decreased absorption of water into concrete and excellent protection after 60-day immersion in 2.5% sulphuric acid solution for epoxy- and polyurethane-coated concrete and mortar samples
Polyurethane	Reduced solution penetration and mass gain (less than 2%) of polyurethane- and epoxy-coated concrete samples after three year exposure to 3% sulphuric acid solution
Epoxy mixed with cuprous oxide (Cu_2O) and silver oxide	Reduction of sulphide generation for cuprous and silver oxide coated concrete pipes by 92% and 99.9%, respectively after 26-day exposure to SRB (*Desulfovibrio*) suspension No formation of slime layer on the internal surface of silver oxide coated pipes
Epoxy containing silver-functionalised zeolites	Reduced number of microbial population (*Acidithiobacillus thiooxidans*) and lower rate of Ca^{2+} and Si^{4+} leaching from coated mortar specimens

4.1.3 Anti-adhesive layers

Another type of coatings is anti-adhesive layers that are able to reduce the chance of microbial attachment to concrete surface (such as polydimethylsiloxane (PDMS) and polyethyleneglycol (PEG)). Bacterial biofilm formation in concrete pipe starts with initial attachment and adhesion of bacteria to the concrete surface. Microbial cells aggregate on the surface and produce insoluble

polymeric substance (called exopolysacharides (EPS) proteins) that encase the adherent bacteria in a three-dimensional matrix, see Figure 4.1. EPS help the cell to adhere to a surface, trap nutrients and protect them from antibacterials. With accumulation of EPS and reproduction of bacteria colonies develop into mature biofilm and exhibit increased resistance to removal.

The chance of initial microbial attachment to the surface is dependent on coating material chemistry, surface topography, mechanical properties, surface hydrophobicity (surface energy), low intermolecular interaction with biomolecules, environmental conditions as well as bacterial surface structure. In addition, surface's physical and chemical properties could have the potential to kill the bacteria upon contact. For example, cationic polymers hold positive charge attract bacteria with negative charge and pull it into the pores causing cell rapture [Graham & Cady, 2014].

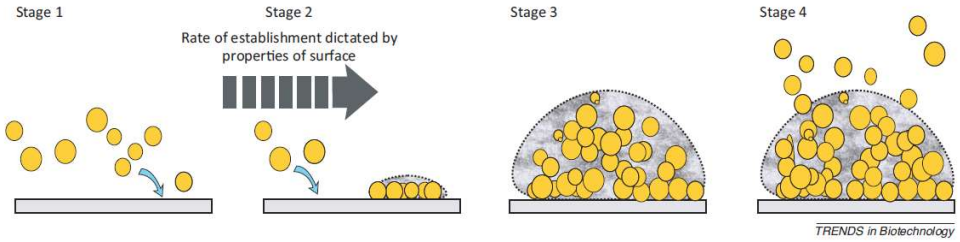

Figure 4-1: Biofilm formation stages [Salwiczek et al., 2014]

4.1.4 Long-acting biocide coatings- Techniques for immobilizing antibacterial agent

4.1.4.1 Biocide-loaded carrier

Due to the challenges involved in using biocides and their possible risks for the surrounding ecosystem (described in section 4.1.2), increasing attention is being paid to immobilize antibacterial agents inside the coating.

The first technique is integrating the antibacterial agent into a carrier which is able to release it slowly to the environment. The aim is to yield a prolonged exposure of the biocide and extend the

duration and efficiency of biocidal activity. In addition, they could get protected from leaching out into the ecosystem and so health and environmental pollution risks, as well as the handling threats associated with skin sensitization, could be minimized [Edge et al., 2001; Erich et al., 2011].

Microencapsulation of chemical compounds is a well-known method in chemical literature and drug delivery systems to gain control over the release of active components. In this method, the molecule is retained inside a protective framework until a trigger affects its release [Edge et al., 2001]. Researchers demonstrated extended duration in biocidal activity with microencapsulation of biocides [Gajanan et al., 2007; Nyden et al., 2010; Jamsa et al., 2012]. They also reported that the encapsulation is able to protect UV-sensitive biocides against premature degradation. Besides extending the biocide effect, microencapsulation is able to reduce toxicity and cover odor and taste of chemical compounds.

In the search for biocide immobilization techniques, there are many studies looking at the synthesis of polymer-nanocomposite hybrid carriers (e.g. polymers with inorganic clays or silica at nanometer scale). These inorganic-organic composites have attracted interest due to their capability of holding and controlled-delivery of various active agents [Scarfato et al., 2011].

Another potential technique is using porous inorganic carrier particles such as amorphous silicate, amorphous alumina and zeolites having biocides adsorbed within their pore system [Aldcroft et al., 2005]. Zeolites are highly porous crystalline aluminosilicate minerals with uniform pores and room for biological and chemical reactions. The ions such as calcium and sodium with the ability of easy exchange by silver, zinc or copper antibacterial heavy metals. Botterhuis et al. (2006) and Sorensen (2010) studied the effect of porous silica nano and micro particles loaded with biocide for similar applications. The studies show that a controlled leaching of biocide is obtained from microparticles. Also, microparticles keep the biocide from chemical degradation which increased the biocidal effect under accelerated weathering tests [Botterhuis et al., 2006; Sorensen et al., 2010].

In recent years, nano tubes (nanometer-scale hollow cylinders) have emerged as a good biocide-loading carrier option due to their accessible and large inner volumes and also the ability to effectively protect entrapped molecules against deterioration. Lvov et al. (2008) studied Halloysite clay nanotubes as a carrier for protective agents [Lvov et al. 2008]. Halloysite is an economically viable clay material. It is a two-layer alumino-silicate (chemically similar to kaoline) and has been developed as an entrapment system for the storage of antibacterial agents. Halloysite is cheap, abundant and durable with high strength properties [Lvov et al., 2008].

The most important challenges of using biocide carriers is that at high dosages they might affect the structural properties of the coating material (e.g. strength reduction). The overall performance of biocide-loading carriers are highly dependent on chemical and physical properties of the carrier and its compatibility with other materials. In addition, availability and cost are other important factors that should be considered.

4.1.4.2 Biocide solidification in coating matrix

Another method to gain control over the release of antimicrobials is to retain antibacterial ions or heavy metal molecule in the pores (3D framework) of the coating material or combine and solidify them in the coating structure. Immobilizing antibacterial agents with this technique can overcome the common biocide limitations, extend antibacterial activity, reduce health and environmental risks and modulate the release behavior.

An example of a matrix that is able to immobilize and lock heavy metals tightly in its 3D structure is Geopolymer. Alkali aluminosilicate polymers or “geopolymers” are a family of minerals with cementitious properties [Khale & Chaudhary, 2007]. Geopolymers are amorphous three-dimensional binder materials formed by mixing alumino-silicate minerals in an alkaline activator solution [Duxson et al., 2007].

The microstructure of geopolymers (similar to zeolites or feldspathoids) is known for an excellent ability to absorb and solidify chemicals/heavy metal, so they have been used as a potential matrix

for waste stabilization during the last decade. High Si/Al ratio in these materials creates low anionic field that gives good selectivity toward cations of lower charge such as Ag^{+}, Cu^{2+} and Zn^{2+} and poor selectivity towards cations of higher charge such as Ca^{2+}. Geopolymer's ability to encapsulate heavy metals such as Zn^{2+}, Cu^{2+} Cr^{3+}, Cd^{2+} ,Pb^{2+}, TiO_2 and MnO with minimum losses in strength is reported by many researchers [Terzano et al., 2005; Wang et al., 2007; Xu et al., 2006; Van Jaarsfeld et al., 1996]. Kriven et al. reported that Geopolymer-based silver/copper containing coating is a possible coating with a combination of antibacterial activity and high adhesion to majority of inorganic surfaces. Heavy metals have the potential to be a combined part of the geopolymerized structure or just being held among the porous network of the material. Leaching values of heavy metals from geopolymer matrix were reported to be much smaller compare to cement-based matrixes. However, the upper limit of the heavy metal content which can be encapsulated in the geopolymer matrix is low and limited. The system can tolerate limited amounts before it becomes chemically or physically unstable and leaching levels become inappropriate. The level of the metals that can be encapsulated in geopolymer matrix is in the order of 0.3-0.5%.

4.2 Coating modification strategies

The characteristics that are considered in developing composite coating integrated with zinc-doped clay are summarized in Table 4.3.

According to strategies summarized in Table 4.2, two types of corrosion resistant coating materials with encapsulating properties were evaluated and used. The first material is geopolymer and the second one is a blended mix of magnesium phosphate hydrates phase form in conjunction with geopolymer matrix. The aim of combining these two matrixes is to take advantage of each system's individual strengths, adding long-lasting anticorrosion properties, increasing the degree of encapsulation and creating a denser matrix. Combining magnesium phosphate matrix with fly ash could also reduce the cost which is very favorable to sustainable development and environmental protection.

Furthermore, the fineness of hydrated magnesium phosphate particles is much higher than ordinary Portland cement particles. Due to this fineness, magnesium phosphate reacts much faster with water. Un-hydrated magnesium particles are able to consume extra water produced during geopolymerization process and produce magnesium hydroxide which could react with sulfuric acid and produce $MgSO_4$ and increase the pH:

Acid-neutralization reaction of magnesium hydroxide

$$MgCO_3 + heat \rightarrow MgO + CO_2$$
$$MgO + H_2O \rightarrow Mg(OH)_2 \quad \textbf{(Equation 4.1)}$$
$$Mg(OH)_2 + H_2SO_4 \rightarrow MgSO_4 \text{ (Base, increase pH)} + H_2O$$

Two systems were also considered to gain control over the release of heavy metals embedded in the coating. The first mechanism is to keep the heavy metal molecule (zinc oxide) in the 3D framework of the coating binders. The second approach is to use sodium bentonite clay impregnated with zinc ions to functionalize it as an antimicrobial agent then combine it into the structure of the coating materials (blended geopolymer). Sodium bentonite clay is an abundant, durable and economically viable clay material. It has high strength and biocompatibility and can be combined into geopolymer structure. Loaded clay particles have the potential to get incorporated as a secondary binding material and act as a precursor in the geopolymerization reaction. Addition of fly ash as a first source is necessary for geopolymerization in order to attain certain mechanical properties and strength. This is due to the layered-like structure of clay particles which causes low reactivity and low strength.

Table 4-3: Characteristics considered in developing a new composite coating integrated with zinc-doped clay

Coating properties	Strategy
Bio-corrosion resistant	Using acid resistant materials (e.g. non-cement-based materials, Geopolymers, magnesium phosphate)
	Densify microscopic structure (e.g. using matrix densifiers)
	Adding antibacterial agents to inhibit bacterial growth (e.g. Heavy metals such as zinc-oxide)
	Increase pH
	Acid neutralizers (e.g. magnesium hydroxide)
Lifetime and Efficiency	Embedding antibacterial in a carrier (e.g. zinc-doped clay particle)
	Encapsulate antibacterial agents in 3D framework of coating material (e.g. encapsulate zinc-oxide in geopolymer matrix)
	Solidify biocide-loaded carrier in 3D framework of coating structure (e.g. solidify zinc-doped clay particles in blended geopolymer network)
	Increase degree of encapsulation (e.g. benefit from combining two networks with encapsulating potentials such as magnesium phosphate and geopolymer)
Durability and Sustainability	Increase corroded pipe's service life (e.g. restore structural integrity of corroded pipes, enhance remaining strength)
	Using non-toxic antibacterial agent
	Using energy efficient and green materials (e.g. supplementary cementitious materials such as fly ash)
	Contains no cement
	Good bonding and compatibility with concrete pipe surface

In this study, first different geopolymer mixes were prepared and the best mix was chosen according to chemical stability, compressive and tensile strength. Then blended mixes of magnesium phosphate hydrate-geopolymer were prepared and evaluated according to chemical stability and tensile strength properties. SEM-EDS (Energy Dispersive Spectroscopy fitted to Scanning Electron Microscope system) was used to investigate the microstructure and composition of developed materials.

Next, the best geopolymer and blended mixes were integrated with zinc-oxide particles and Zn-doped clay particles. Leaching and chemical stability, tensile strength, bonding and shrinkage properties were tested to evaluate the performance of the developed materials.

While there are studies on the antimicrobial characteristics of clay functionalized with heavy metals [Aguzzi et al., 2007], the properties and performance of blended geopolymer and multiphase composite coatings integrated with zinc doped bentonite clay has not been investigated. The ultimate goal was to overcome the current rehabilitation challenges by developing a repair coating to prevent concrete bio-corrosion, yield a prolonged exposure of the biocide and extend the durability and service life of the concrete pipes. The resistance of the zinc doped coatings to biogenic corrosion caused by bacteria is described in Chapter 5.

4.3 Sodium bentonite clay functionalized with zinc oxide

As it was discussed earlier in this chapter, in the search for biocide-loading carriers, clay minerals are widely used materials for biocide encapsulation. This is due to their high storing capacities as well as swelling and colloidal properties.

Clay minerals are inorganic cationic exchangers. So, ion exchange takes place by mixing clay particles with ionic drugs in a solution form. In this study, sodium bentonite clay was impregnated with zinc ions to functionalize it as an antimicrobial agent. Sodium bentonite clay is an abundant, durable and economically viable clay material. It has high strength and biocompatibility and can be integrated as a carrier loaded with the biocide into protective coatings.

4.3.1 Pretreatment methodology of clay minerals

In this study pure sodium bentonite clay, $Al_2H_2Na_2O_{13}Si_4$, was used as carrier material and loaded with Zn^{2+}-ions via an ion-exchange process. Metal ions such as sodium in clay are easily exchangeable by zinc ions to functionalize it as antimicrobial carrier.

Raw clay samples usually contain large amount of different minerals such as carbonates, quartz, illite and calcite. In order to increase the quality and ion exchange capacity of clay particles, samples are pretreated (also called clay enrichment). Several methods for clay enrichment are reported in the literature such as carbonate decomposition, dissolution of metal oxides/silica by acid and oxidation of organic materials [Aguzzi et al. 2007].

In this study, sodium chloride solution was prepared by stirring 10 gr sodium chloride in 100 ml water. Then 10 grams of clay was stirred in 1 M, 100 mL sodium chloride solution for 24 hours [Aguzzi et al. 2007]. After repeating the process three times, the samples were washed with distilled water and dried at 80°C for 1 hour.

SEM-EDS analysis was used to study the morphology as well as the chemical composition of the clay before and after treatment. For this purpose, samples of treated and non-treated clay taken and impregnated using epoxy-based resin. Then epoxy impregnated samples were cut with a saw and polished with diamond grit. Ultimately samples were cleaned in desktop UV cleaner chamber and dried at 50°C. Figure 4.3 and 4.4 are SEM images of clay samples before and after treatment. SEM images shows a typical layered structure with numerous nano-flakes of clay particles.

Results show significant reduction in the amount of matrix minerals after enrichment process, Table 4.4 and Figure 4.2. During the treatment process, clay is simultaneously activated interlayer calcium ions were replaced with sodium ions. So, Ca content is reduced, and Na content increased. Increase in Cl is due to samples immersion in sodium chloride solution.

Table 4-4: Chemical composition of clay before and after treatment

Element	WT%	
	Clay	Treated clay
Al	8.28	0.16
Ca	3.23	0.02
Cl	0.00	37.09
Fe	4.18	0.00
K	0.21	0.00
N	0.00	0.00
Mg	1.47	0.00
Na	0.95	24.80
O	51.90	3.28
S	2.02	0.00
Si	27.41	1.66
Zn	0.00	0.00

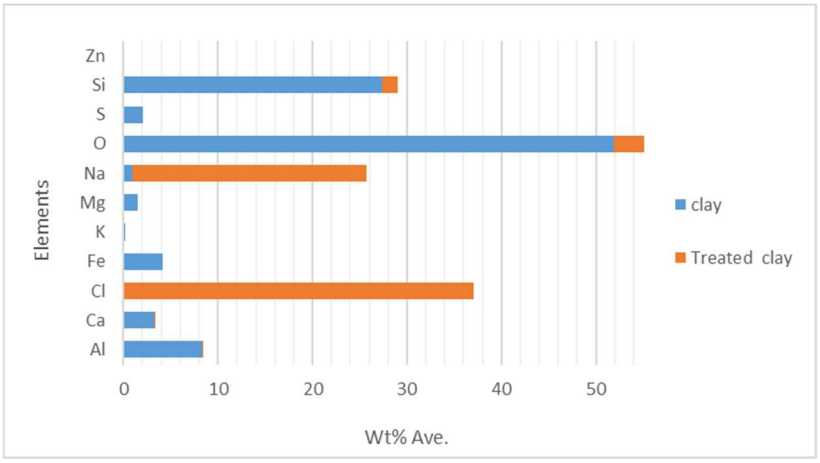

Figure 4-2: SEM-EDS results of treated and non-treated clay particles (average of 30 points were measured for each sample, CV: 2-5%)

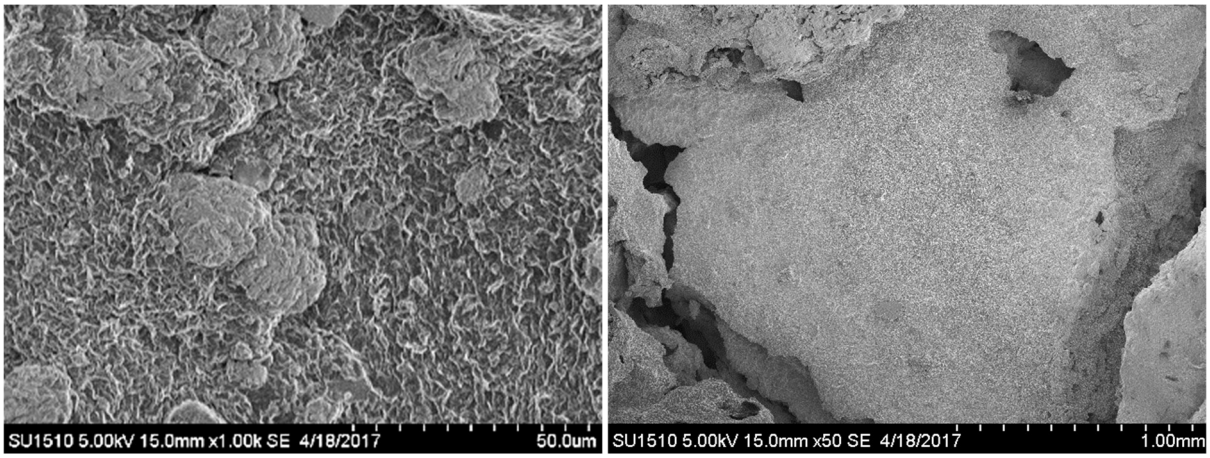

Figure 4-3: SEM images of sodium bentonite clay particles

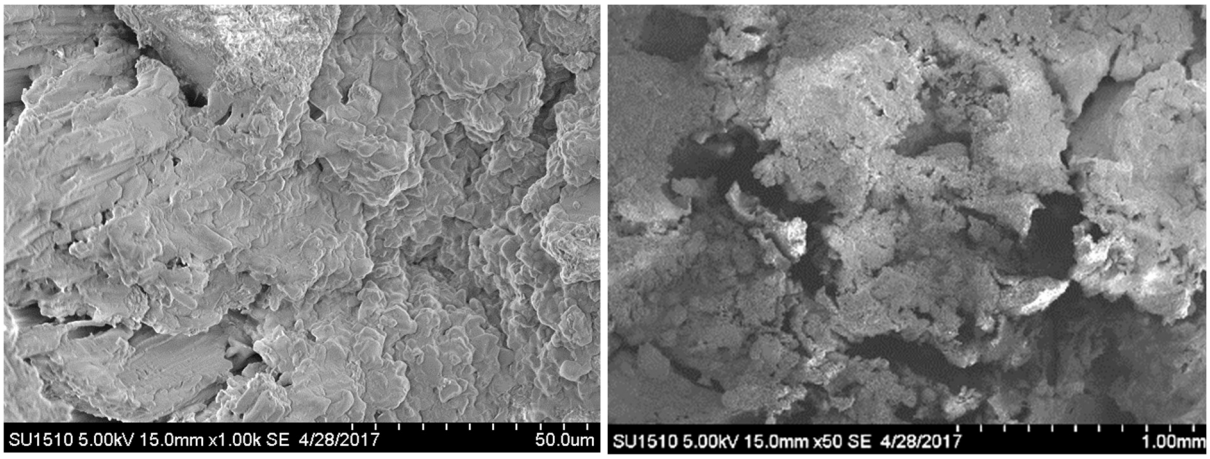

Figure 4-4: SEM images of sodium bentonite clay particles after treatment

4.3.2 Ion exchange with zinc

Ion exchange in clays and other minerals is highly dependent on the structure of the mineral and chemical composition of the solution in contact with the mineral. Ion exchange is a reversible chemical reaction that occurs between ions near mineral surface, unbalanced electrical charges in the mineral framework and ions in the solution. The common exchangeable cation in most clay minerals is Ca^{+2}.

Bentonite clay was subjected to an ion-exchange process by stirring 10 grams of sample in 100 mL of 0.35mol/L zinc oxide solution and stirred at 50 °C for 4 h at a dark environment with the pH value of the system maintained between 6 and 8 (it was possible by adding nitric acid to the solution). Then the slurry was separated into solid and liquid by vacuum filtration. The separated solid specimen was dispersed into 100 mL of distilled water for washing and then filtrated again. The washing and filtration were repeated until no Zn in washing solution was detected. After that, the modified clay was dried at 90 °C for 12 h.

SEM-EDS analysis was used to study the chemical composition of the zinc-doped clay. Figure 4.5 is SEM image of ion-exchanged clay sample. After ion exchange, the structure of clay particles was not changed much. However, impregnated zinc ions create more porous microstructure and texture.

Results show significant increase in the amount of Zn in the system, see Table 4.5 and Figure 4.6. Ion exchange occurred by replacement of Zn ions with sodium ions in the system. Na ions were replaced with Ca ions during treatment process (see section 4.3.1).

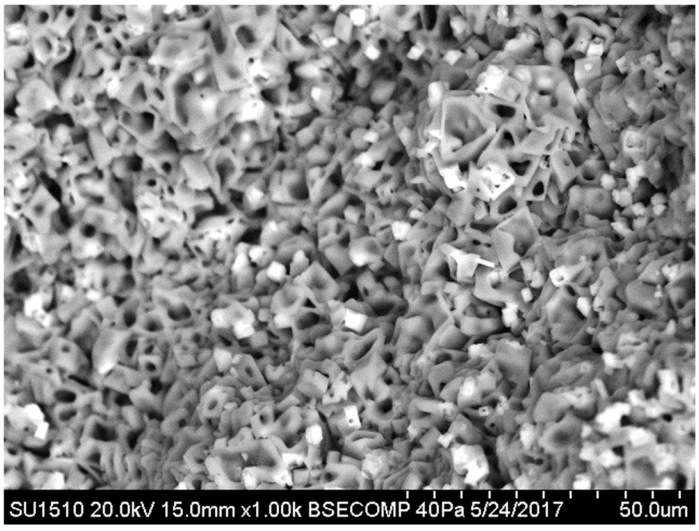

Figure 4-5: SEM images of ion-exchanged bentonite clay

Table 4-5: Chemical composition of ion-exchanged bentonite clay

Element	WT%	
	Clay	**zinc-doped clay**
Al	8.28	2.04
Ca	3.23	0.04
Cl	0.00	5.22
Fe	4.18	0.48
K	0.21	0.00
N	0.00	0.00
Mg	1.47	0.00
Na	0.95	2.37
O	51.90	28.83
S	2.02	0.00
Si	27.41	6.08
Zn	0.00	36.49

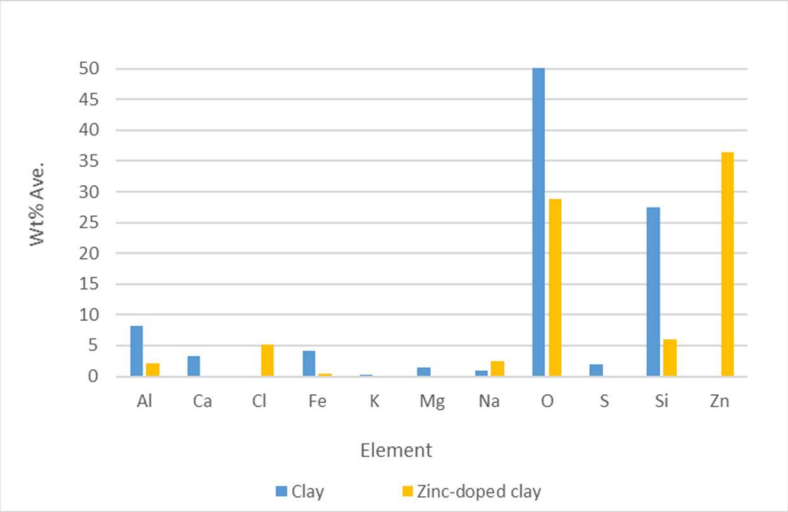

Figure 4-6: Comparison between the chemical composition of clay and zinc-doped clay

4.4 Geopolymer matrix

4.4.1 General properties

Alkali alumino-silicate polymers or "geopolymers" are a family of minerals with cementitious properties [Khale & Chaudhary, 2007]. Geopolymers are amorphous three-dimensional binder materials formed by mixing alumino-silicate minerals or industrial byproducts rich in SiO_2 and Al_2O_3 (e.g. fly ash) with an alkaline activator solution (e.g. NaOH) [Duxson et al., 2007]. Alkaline liquid is used to react with the silicon and aluminium and forms the geopolymer paste. The alkaline activation is a chemical process in which partially or totally amorphous structures changes into compact cemented frameworks.

When these two components, solids and the alkaline activation solution react, alumino-silicate materials rapidly dissolve into the strong alkaline solution to form free SiO_4 and AlO_4 units. These units are then polymerized together and form polymeric precursors (─SiO_4─AlO_4─ or ─SiO_4─AlO_4─SiO_4 or ─SiO_4─AlO_4─SiO_4─SiO_4─).

Geopolymers combine certain properties of ordinary cements, traditional ceramic materials. Geopolymerization can also be described in terms of a polymeric model similar to certain zeolites. Both Al and Si found in this product are tetrahedrally coordinated and the alkali (e.g. Na) is housed in the voids of the three-dimensional frame work [Shi et al., 2011].

Depending on the source of the alumino-silicate material, particle size and processing conditions, geopolymers can exhibit a wide variety of properties and characteristics including high early strength, low shrinkage, fast setting and high acid and fire resistance [Duxon et al., 2007]. Fly ash is the most favorable alumino-silicate source material for geopolymer production. Fernandez-Jimenez et al., 2005 investigated the suitability of various types of fly ash. The authors reported that in order to produce optimal binding properties, the fly ash should have LOI less than 5%, Fe_2O_3 less than 10% and silica content of 40-50%. Van Jaarsveld et al. (2003) reported that the

calcium content, amorphous content and morphology of the fly ash also affect the initial mix properties as well as final structure of fly ash-based geopolymers.

In addition to the source of alumino-silicate material, there are several other factors that have been reported as important parameters affecting geopolymer properties. Curing temperature, curing time and alkaline liquid concentrations are the most important factors that help geopolymerization reaction and significantly affect the mechanical strength [Wang et al., 2011; Yunfen et al., 2011]. Water to fly ash ratio, CaO content, Si/Al and Na_2SiO_3/NaOH ratios are also other important parameters that affect the properties of geopolymers [Wang et al., 2011; Al Bakri et al., 2012]. Some of the most important factors are summarized in Table 4.6.

An increase in fly ash content and alkaline activator concentration affect mechanical properties due to the increase in sodium oxide content that is required for geopolymerization reaction. However, Wallah et al. (2006) reported that by increasing the Na2SiO3/NaOH ratio to more than 3, excess OH- concentration produced in the mix which reduce the compressive strength of the geopolymer. Moreover, the excess sodium content forms sodium carbonate which disrupt geopolymerization process. The authors reported that the highest compressive strength was observed at fly ash/ alkaline solution ratio of 2 and Na_2SiO_3/NaOH ratio of 2.5. The ratio of sodium silicate to sodium hydroxide solution that were used by other researchers is between 0.4 to 2.5 (by mass). Wallah et al. recommended that the cost of alkaline liquid is also economical when the ratio of sodium silicate to sodium hydroxide solution is 2.5 and also the test results are reported to be remarkably consistent [Wallah et al., 2006].

The most used alkaline activators are a mixture of sodium silicate (Na_2SiO_3) or potassium silicate and sodium hydroxide (NaOH) or potassium hydroxide (KOH). Fernández-Jiménez et. al. (2005) also reported that the type of alkaline liquid is a significant factor affecting the mechanical strength of geopolymer. The authors reported that the combination of sodium silicate and sodium hydroxide gave the highest compressive strength in producing fly ash geopolymers [Fernández-Jiménez et al., 2005].

When the activator solution is NaOH, the produced sodium aluminosilicate gel has an Si/Al ratio of around 1.6-1.8 and Na/Al is equal to 0.46-0.68. By adding Na_2SiO_3, in the presence of silicate ions, the content of Si ions in the N-A-S-H bond increases. So, the ratio of Si/Al rises to around 2.7 and Na/Al to 1.5 which enhance condensation degree and mechanical strength of the product [Fernández-Jiménez et al., 2005]. It could be concluded form the literature that the increase of alkalinity resulted in shorter final setting time and higher strength [Ahmari & Zhang, 2012].

It was reported that the CaO content of fly ash to a certain amount played a significant role in enhancing the setting time, final hardening, strength development and mechanical properties of geopolymer products [Ahmari & Zhang, 2012; Van Jaarsveld et al., 2003]. According to the American Society for Testing and Materials, fly ash can be categorized into class F and C. Class F which is low calcium fly ash, characterized by $SiO_2 + Al_2O_3 + Fe_2O_3 > 70\%$ and $SO_3 < 5\%$. Class C fly ash is characterized by combination of $SiO_2 + Al_2O_3 + Fe_2O_3 < 70\%$ and high Ca and Mg contents which are around 27% and 3.8% respectively [American Society for Testing and Materials, ASTM Standards]. The Canadian Standards Association (CSA) classified fly ash as Type F, CI or CH based on the calcium oxide (CaO) content of the fly ash. Type F has CaO content of up to 15%, Type CI between 15% and 20%, and Type CH greater than 20% [The Canadian Standards Association A3000-08]. In order to obtain the optimal binding properties, reducing the risk of fast setting and increasing durability in acidic environments, low calcium fly ash is more preferable than high calcium fly ash. It has been recommended to have other characteristics such as unburned material lower than 5%, Fe_2O_3 not higher than 10% and reactive silica content 40-50% [Fernández-Jiménez et al., 2005]. In addition, since low-calcium Geopolymers chemistry is not based on calcium-aluminates which are subjected to sulfate attack, these materials have the potential to be an economic solution which enhance resistance to acidic environment compare to cement-based coatings.

Table 4-6: The most important factors affecting fly ash-based geopolymer mix design

Factor		Reference	Note
Activator Type	NaOH (Molarity 8-20)	[Bakharev, 2005] [Ahmari et al., 2012]	Crystalline geopolymer prepared with sodium hydroxide is very stable in acidic environment
			Compressive strengths at 28 days of 20–23 MPa is obtained with NaOH 9.5–14 M. NaOH concentration beyond this point reduce strength due to early precipitation of aluminosilicate products
	NaOH and Na_2SiO_3	[Wallah et al., 2006] [Fernández-Jiménez et al., 2005]	Na_2SiO_3/NaOH =2-2.5 is recommended Higher NaOH increase pH condition
Activator/fly ash	0.3-0.6	[Hardjito et al., 2004]	Activator/ fly ash ratio of 0.3-0.6 is recommended
Calcium content	CaO <5%	[Bakharev, 2005]	Low CaO content 3-4% is recommended
	CaO>5%	[Hardjito et al., 2004]	Higher CaO leads to lower acid resistance potential and higher strength
Fly ash type	F	[Hardjito et al., 2004]	Fly ash type F (CaO 2%) has 10% mass loss in pH less than 1, fly ash type C (CaO 20%) has around 25% mass loss.
	C		
	blend		
Cement additive	5%	[Pangdaeng et al., 2014]	Cement addition reduces setting time, porosity and enhances compresive strength, increase hydration products. Hydration liberated heat promote geopolymerization process
	10%		
	15%		
Curing condition (ambient temperature)	Wrapped in plastic	[Pangdaeng et al., 2014]	lower porosity
	Immersed in water		In case of having high CaO content or cement as additive, this curing condition gives higher strength but also higher porosity

Geopolymers are affected by sulfuric acid corrosion in different ways compare to Portland cement mortars. The first was by the formation of gypsum out of the CH present in the paste. The second way is by leaching of the alkaline elements (e.g. sodium or potassium) after diffusion of the SO^{-2} ions in the network. However, the alumino-silicate network remains unaffected and the

geopolymer can retain a great percentage of its structural strength after acid attack [Song et al., 2005].

Microorganisms and biogenic sulfuric acid attack is also controlled by diffusion mechanisms in geopolymers. Amount and connectivity of the capillary porosity affect the penetration of aggressive ions into the matrix. So, reducing the permeability could make the movement of the fluids and acid producing microorganisms harder through the system. Low permeability network is not immune to bio-corrosion, but it suffers from chemical attack only on the surface rather than on the surface and interior body and lasts longer.

As discussed before, geopolymers also have great potential of encapsulating heavy metals either physically (charge balancing of Al in framework) or chemically (covalent bonds) within the three-dimensional alumino-silicate network. Minarikova and Skvaria (2006) reported that geopolymers are able of storing Zn^{2+}, Cu^{2+}, Cr^{3+}, Cd^{2+} and Pb^{2+} with minimum losses in strength. Geopolymers can embed Cu ions among the pores of the structure in the uncombined forms such as $Cu(OH)_2$ and CuO. So, the ability of geopolymers to encapsulate anti-bacterials and heavy metals could have great opportunity for creating control-released antibacterial coatings.

4.4.2 Mix design and samples preparation

The fly ash used in this study was fly ash type F according to ASTM classification which originated from the Centralia power plant. Fly ash physical and chemical composition has been provided in Table 4.7. As could be seen, the silicon and aluminum constitute was about 60% of the total mass and the ratio of silicon to aluminum oxide is about 2.4.

Table 4-7: Physical and chemical composition of fly ash used in this study

Silicon Dioxide (SiO_2)	44.20%
Aluminium Oxide (Al_2O_3)	18.90%
Iron Oxide (Fe_2O_3)	7.20%
SiO_2+Al_2O_3+Fe_2O_3	70.2%
Sulphur Trioxide (SO_3)	1.40%
Calcium Oxide (CaO)	18%
Magnesium Oxide	4.80%
Moisture content	0.10%
Loss on Ignition (L.O.I)	0.26%
Available Alkali as Equiv. Na_2O	1.02%
Fineness retained on sieve no. 325	13.90%
Density	2.67 Mg/m^3

A combination of sodium silicate and sodium hydroxide was chosen as the activating alkaline. Sodium silicate solution contains (wt %) water = 55.9%, sodium silicate salt = 44.1%. The other characteristics of the sodium silicate solution are specified as SiO_2 / Na_2O = 2 and specific gravity of around 1.53 gr/cm^3.

The sodium hydroxide solutions were prepared in two concentrations by dissolving sodium hydroxide pellets in water. So, for example 12 Molar NaOH solution consisted of 12×40 (NaOH molecular weight) which is equal to 480 gr of NaOH solids per 1 liter of solution.

The alkali activator solution was prepared by mixing sodium hydroxide solution and sodium silicate according to the mix design provided in Table 4.8 one day before casting. A constant alkaline activator ratio of $NaSiO_2$ / NaOH = 2.5 and fly ash / alkaline activator = 2.8 was considered in most of the mixes for the ease of comparison.

At the beginning, numerous trial mixtures of geopolymer concretes were manufactured in cylinder moulds (100 × 200 mm). An eighty-litre capacity pan mixer available in the SIERA concrete laboratory for making ordinary Portland cement was used for producing the geopolymer paste. The main objectives of preliminary laboratory work were familiarizing with casting fly ash based geopolymer, understanding the effect of the sequence of adding alkaline solution to the solids constituents, understanding the basic mixtures proportions, observing the behaviour of the mix and developing a consistent process of mixing and curing. Details of different batches with different mixture proportions have been summarized in Table 4.8.

The casting and mixing procedure consisted of first mixing sodium silicate solution and the sodium hydroxide solution together at least one day prior to use. It was reported by Davidovits (2002), in order to assist the polymerization process and reducing the chance of bleeding and segregation of the paste, it was preferable to mix the sodium hydroxide and sodium silicate solution before mixing the alkaline activators with dry contents [Davidovits, 2002]. Then dry material was mixed for 3 minutes, and alkaline activator was slowly added and mixed for about 1 min, at last water was added and continue to mix for another 1 min. It was observed that geopolymerization is a fast reaction and initial setting is happenning in less than an hour. Adding water to the system after 1 min made the mix more workable and retarded the formation of alumino-silicate network.

After mixing, the samples were cast in cylinder plastic moulds (75 mm diameter by 150 mm high) and compacted by applying ten manual strokes per layer in three equal layers followed by compaction on a vibration table for ten seconds. Samples were also prepared for SEM-EDS, chemical stability and tensile strength test, see Figures 4.7 and 4.8.

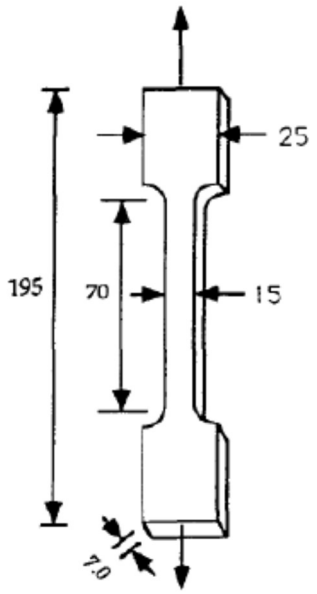

Figure 4-7: Tensile strength test samples used in this study (in mm)

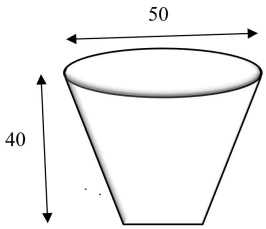

Figure 4-8: Chemical stability test samples used in this study (in mm)

After casting, all test samples were covered (using a plastic sheet) and left at ambient conditions. The specimens were demolded after 24 hours and stored at ambient temperature (18°C) until the date of testing. After evaluating the compressive and tensile properties of the 11 batches (Table 4.8), best mixes were selected for SEM-EDS and chemical stability tests.

Table 4-8: Geopolymer mix design used in this experiment

	G 1	G 2	G 3	G 4	G 5	G 6	G 7	G 8	G 9	G 10	G11
Activator / Fly ash (NaOH 14 M)	---	---	---	---	---	---	0.35	0.35	0.35	0.35	0.4
Activator / Fly ash (NaOH 12 M)	0.35	0.35	0.3	0.4	0.4	0.3	---	---	---	---	---
sodium silicate / sodium hydroxide	2.5	2.5	2.5	2.5	2.5	2.5	2.5	2.5	2.5	2.5	2.5
Slag / Fly ash	---	---	---	---	0.1	0.1	---	---	---	---	---
Silica fume / Fly ash	---	---	---	---	---	---	---	---	0.05	0.1	0.05
Water / Fly ash	0.25	0.09	0.25	0.09	0.09	0.09	0.1	0.09	0.09	0.09	0.1

4.4.3 Compressive strength

The compressive strength tests on hardened fly ash based geopolymer were performed on a Forney machine in accordance to ASTM C35 standards. From each batch of geopolymer at least three cylinders were tested.

At ambient temperature, the reaction of fly ash is extremely slow and also water evaporates slowly which led to lower compressive strength after 7 days. The higher the ambient temperature, the higher is the compressive strength. Based on the limited test results, geopolymer mortar develops sufficient strength even in ambient temperature conditions without any conventional curing which is an encouraging outcome for using geopolymer in some applications such pipe repairs. A maximum of 14-day compressive strength of 25-28 MPa was obtained in this study with NaOH concentration in a range of 8 and 14 M (see Figure 4.9).

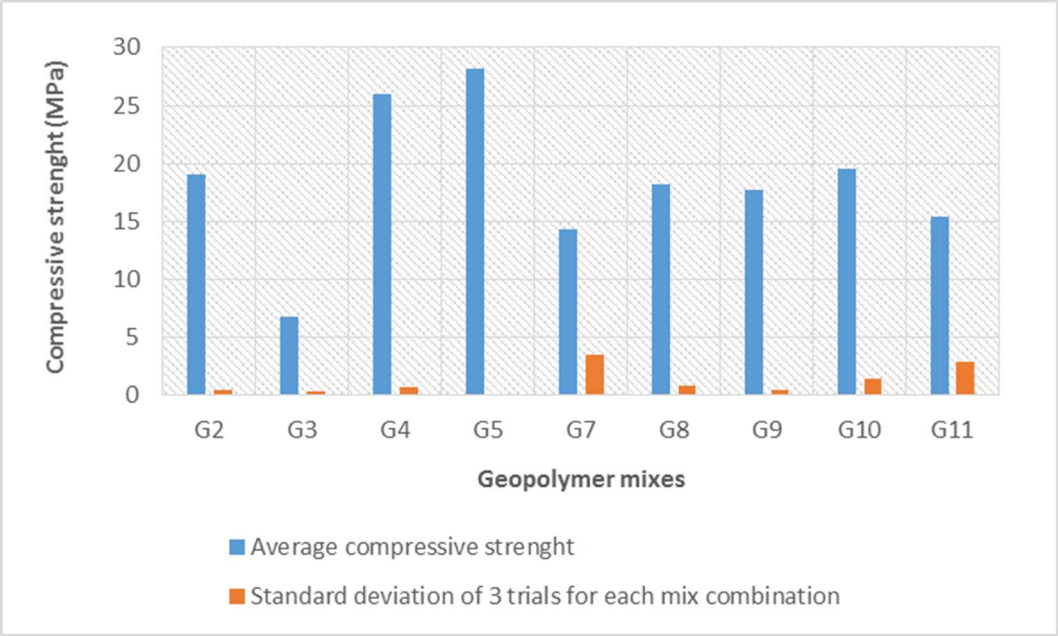

Figure 4-9: Variation of compressive strength for samples in this experiment

As reported by several authors and investigated in the lab experiments, the amount of water in the geopolymer mix plays an important role on behavior, workability and strength of fresh concrete and final product. The role of water in geopolymer is to improve the workability which leads to an increase in porosity due to the evaporation of water during the curing process. Ultimately, it reduces the strength of the geopolymer samples.

So, the mixes with higher amounts of water appear to be more workable. However, segregation occured when the mixing time was long in mixes with higher water content and the compressive strength was reduced, see Table 4.8 and Figure 4.9.

In Batches 5 and 6, 10% of the fly ash content was replaced with slag in order to investigate the effect of additional Ca source to the system. This induced very faster initial setting and drastically decreased the workability of the mix. The geopolymeric binder formed in the presence of slag is similar to the geopolymeric binder found in the absence of slag which could be explained by the coexistence of hydration and geopolymerization reaction. Faster setting time may also be due to the presence of calcium in solid material which will provide extra nucleation sites for precipitation of dissolved species and cause rapid hardening as suggested by Rattanasak et al., 2011.

According to the results, replacing 10% fly ash with slag increased the compressive strength slightly by around 5%. The calcium dissolved from the slag takes part in the formation of amorphous CSH (Calcium silicate hydrate) gel. However, because of the high concentration of NaOH, there is an excess amount of hydroxides present in the system and so the precipitation of calcium hydroxide in the form of $Ca(OH)_2$ will be encouraged. Consequently, the precipitation of calcium hydroxide will prevent any possible formation of CSH gel within a geopolymeric binder and so the compressive strength did not increase much.

Moreover, in low alkalinities the formation of CSH gel within a geopolymeric binder could work as a micro-aggregate, such that the resultant binder is more homogeneous and dense. Coexistence of both geopolymeric gel and CSH gel could also help to bridge the gaps between the different hydrated phases and unreacted particles. However, adding Ca source to the system affect the overall acid resistant properties. In higher alkalinities, the geopolymeric gel is a dominant product and calcium play less role in affecting the nature of the end product. Therefore, the dissolution of calcium species will not have major impact on the ultimate strength.

Depending upon the alkalinity of the system, it is also possible that as the calcium concentration increases, the formation of geopolymeric gel and CH gel start to compete against each other. Therefore, instead of having one phase acting as a micro-aggregate to fill voids and holes of the binder, the two reactions are competing for soluble silicates and available space for growth. Consequently, the resultant binder will be disordered with two phases of similar size, and more residual holes are produced resulting in strength reduction [Yip et al. 2008].

The effects of adding silica fume (5% and 10%) to the geopolymer mortars were investigated in batch 9, 10 and 11. This yielded a workable mix and strength enhanced in comparison to batch 7. As was described, alkali activating solution is important for dissolving of Si and Al atoms to form geopolymer precursors. The compressive strength increases with an increase in fly ash content and alkaline activator concentration which is because of the increase in sodium oxide content that is required for geopolymerization reaction.

In the synthesis of geopolymers, NaOH 12 Molar and 14 Molar have been used in batches 1- 6 and 7-11 respectively. Although Rattanasak et al. (2011) reported that NaOH 10 to 14 M produces geopolymer with highest compressive strength, experimental results did not show much improvement in the compressive strength of the specimens.

4.4.4 Uniaxial tensile test

Uniaxial tensile test was performed on 11 different batches of fiber reinforced geopolymer (0.1% PVA fiber was used), Table 4.8. A closed-loop controlled Instron testing system was used in displacement-controlled mode, see Figure 4.10. The testing gauge length was 60 mm and loading rate set at 0.001 mm/min. Typical load-deflection curves are presented in Figure 4.11 to 4.17.

Figure 4-10: Uniaxial tensile test set up

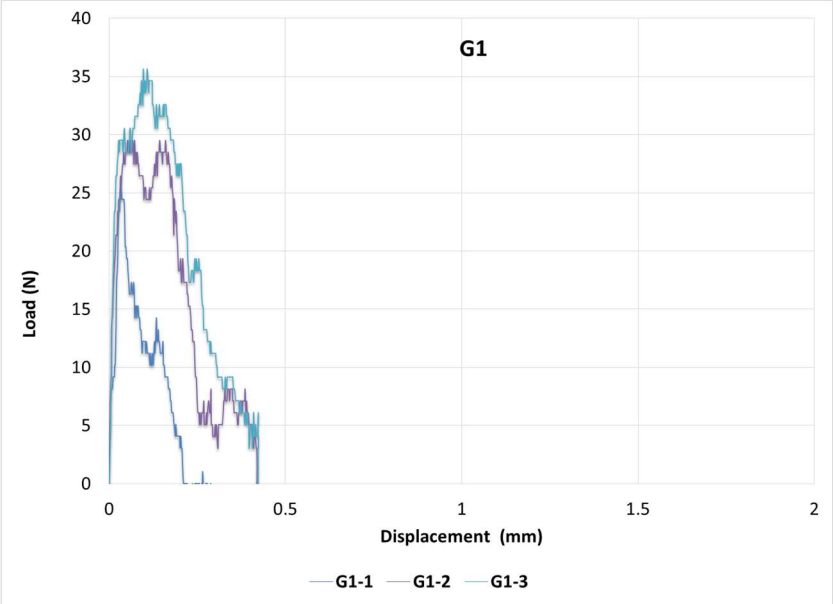

Figure 4-11: Load/displacement curve, G1 Mix

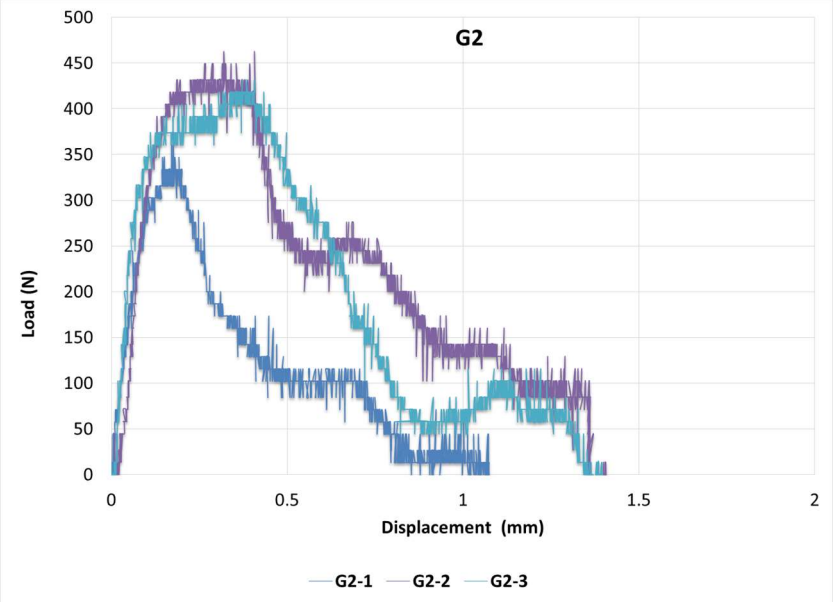

Figure 4-12: Load/displacement curve, G2 Mix

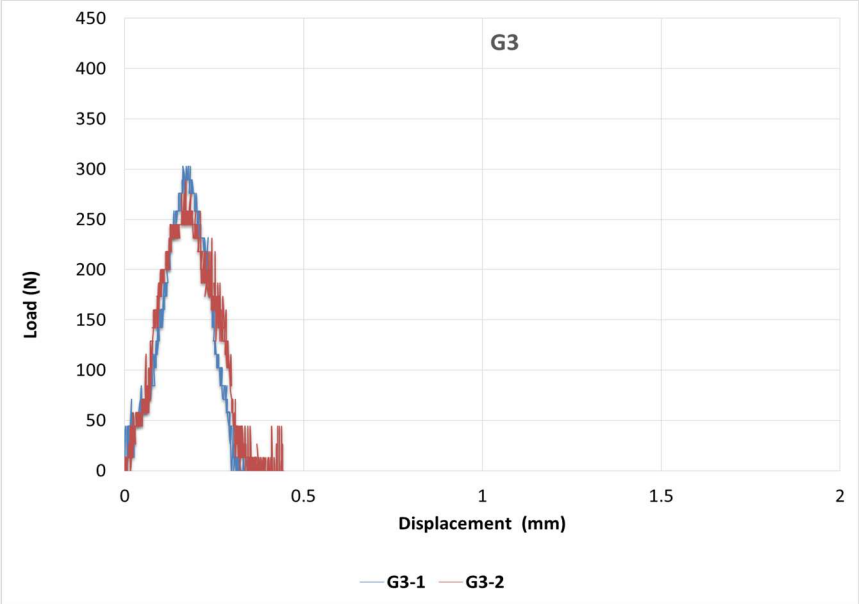

Figure 4-13: Load/displacement curve, G3 Mix

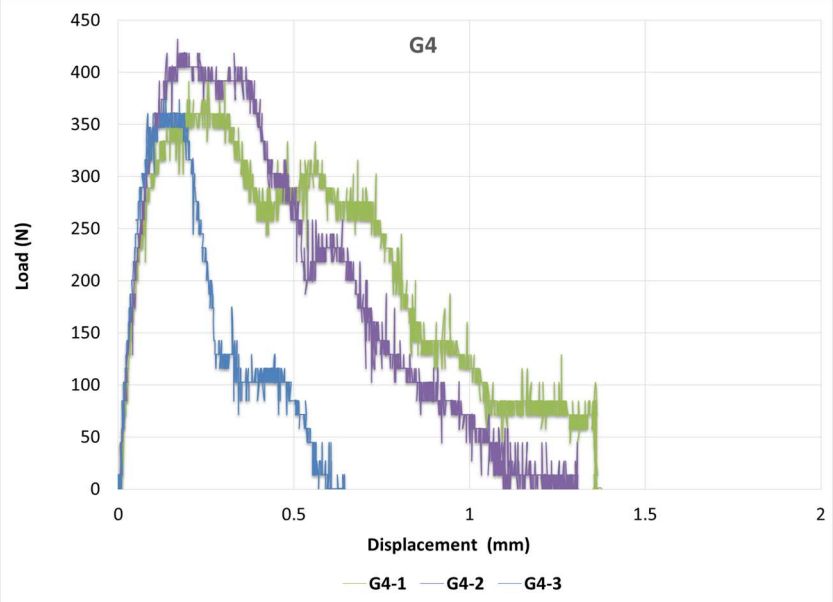

Figure 4-14: Load/displacement curve, G4 Mix

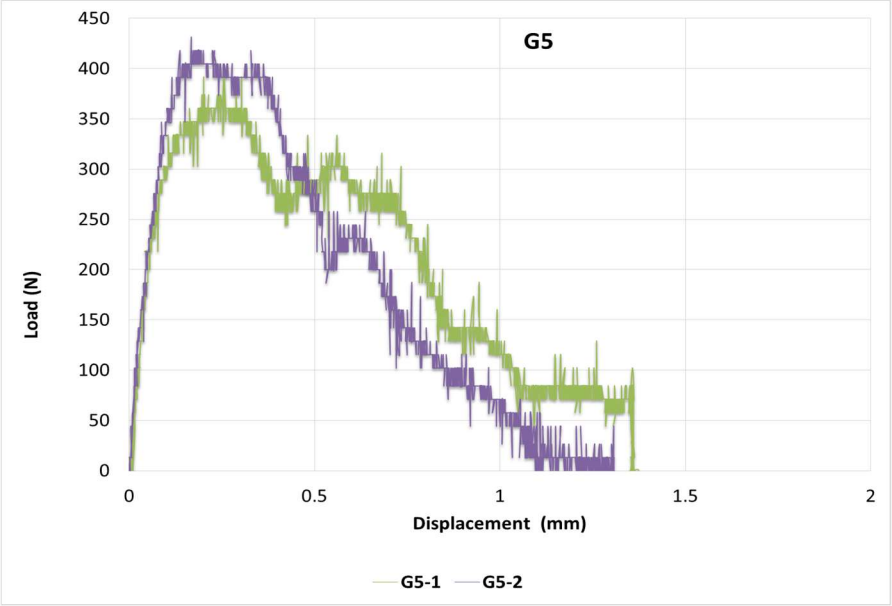

Figure 4-15: Load/displacement curve, G5 Mix

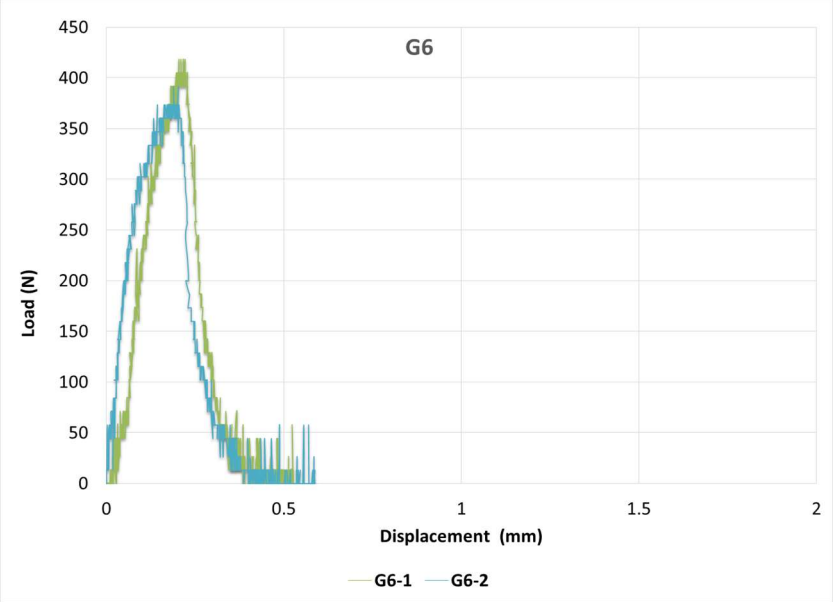

Figure 4-16: Load/displacement curve, G6 Mix

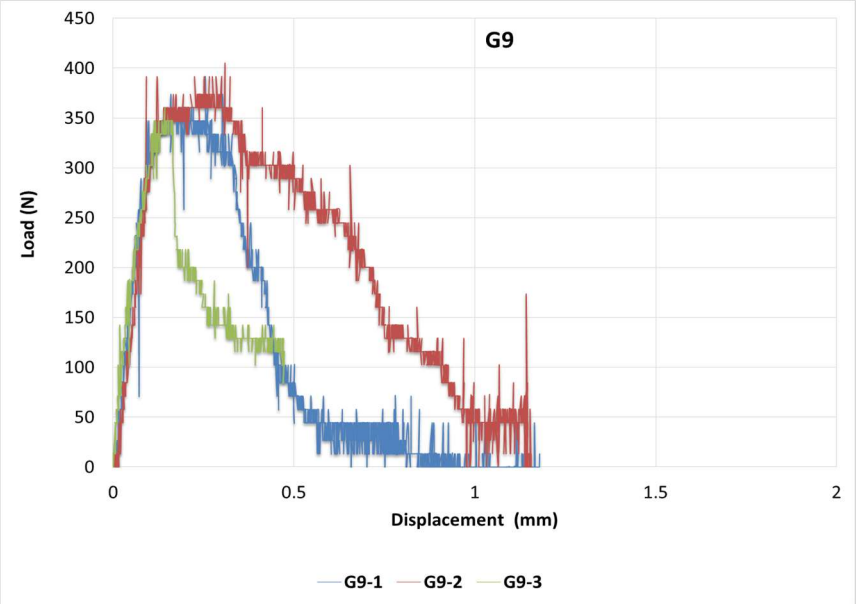

Figure 4-17: Load/displacement curve, G9 Mix

According to the results, it could be concluded that addition of extra source of Ca to the mix enhances tensile properties. According to the chemistry of geopolymerization, the reaction releases water and most of this water resides within the cavities in the system until evaporates. So if the samples are not cured in high temperature, the system may benefit from the hydration reaction of the Ca sources and CH production to enhance the tensile strength. Furthermore, the hydration process can provide heat for accelerating geopolymerization rate.

The incorporation of silica fume in geopolymer mortar has the potential to enhance the strength by decreasing the porosity which results in denser structure and absorb the extra water in the system. Some authors also reported that the mechanical properties of the geopolymer samples become increasingly elastic with increasing SiO_2 content, also the behavior is becoming more ductile rather than brittle [Manjunath and Giridhar, 2011]. Since the amount of the fiber used was very small, deflection hardening was not observed in any of the samples.

Based on the results on compressive and tensile properties of geopolymer samples, it could be concluded that there was not much improvement in compressive and tensile strength of the samples

with 10% slag. There was significant improvement in the strength when the amount of the water is reduced.

Samples with activator / fly ash ratio of 0.4 showed better flexibility and higher ultimate strength compare to other samples. Overall, batches G4, G2, G5 and G9 indicated better tensile performance compare to other geopolymer mixes. G2 and G9's compressive strength is lower than G4 and G5.

4.4.5 Microstructure

SEM-EDS was used to investigate the microstructure and composition of the geopolymer samples. For this purpose, samples were impregnated using epoxy-based resin. Then epoxy impregnated samples were cut with saw and polished with diamond grit. Ultimately samples were cleaned and dried at 50°C. Figure 4.18 and 4.19 are SEM images of geopolymer sample (Batch 4 and 5, Table 4.8). Analysis were conducted at magnifications of 500, 1000 and 2000 at 30 points.

SEM-EDS analysis of geopolymer samples is shown in Figure 4.20. Geopolymer samples have a condensed structure and are mainly composed O, Si, Na, Al but cement mortar samples are mainly composed of O, Ca, Si, Mg and S. The elemental distribution pattern also shows that the voids contain a high level of C that could be due to carbonation on the surface of the specimens.

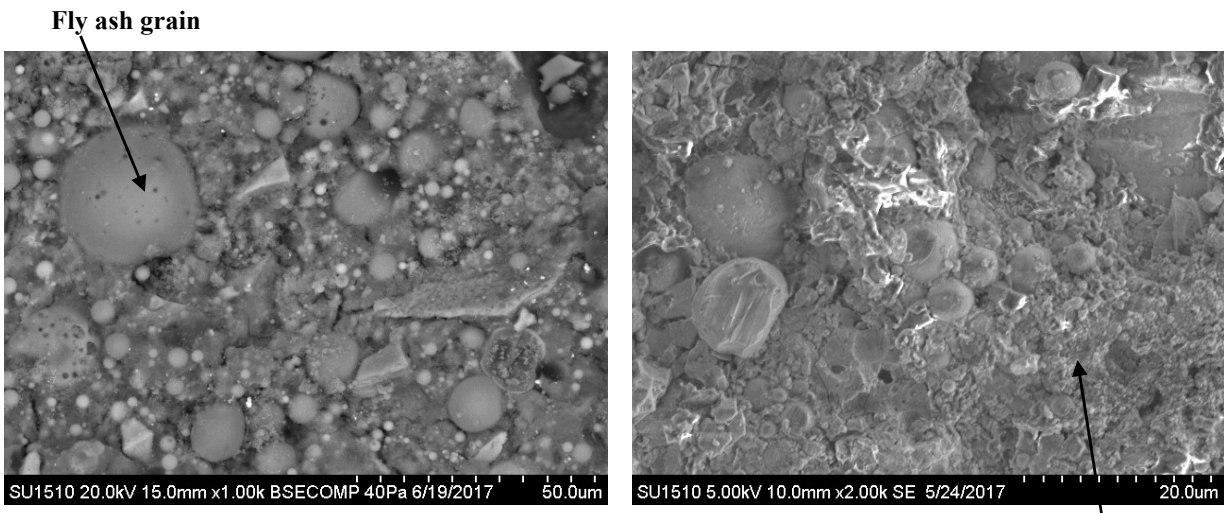

Figure 4-18: SEM image of geopolymer sample (Batch 5)

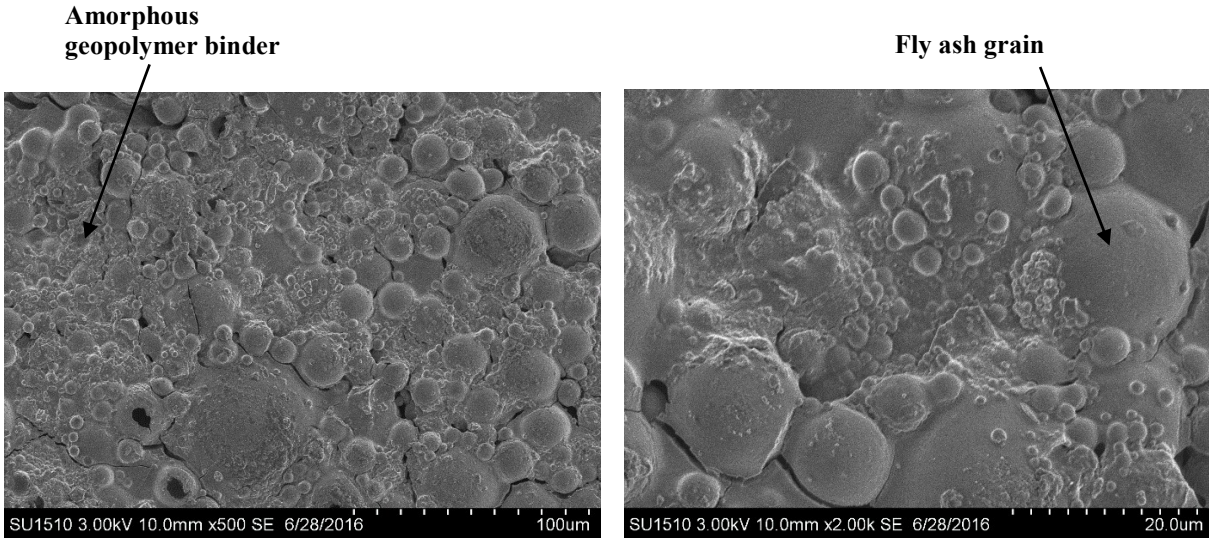

Figure 4-19: SEM image of geopolymer sample (Batch 4)

The biggest difference between geopolymer and cement mortar is in the wt% of Ca and Na. The presence of sodium cations in the geopolymer mix reduce the solubility of calcium ions but tends to promote the solubility of silicate and aluminate. In small concentrations the former effect is dominant and in large concentrations the latter effect becomes dominant. For this reason, KOH or NaOH are needed as alkaline solution and activator for geopolymerization process. So using large

concentration of NaOH has some benefits including promote solubility of silicate and aluminate ions. In addition, more OH^- ions increase alkalinity and acid resistant properties.

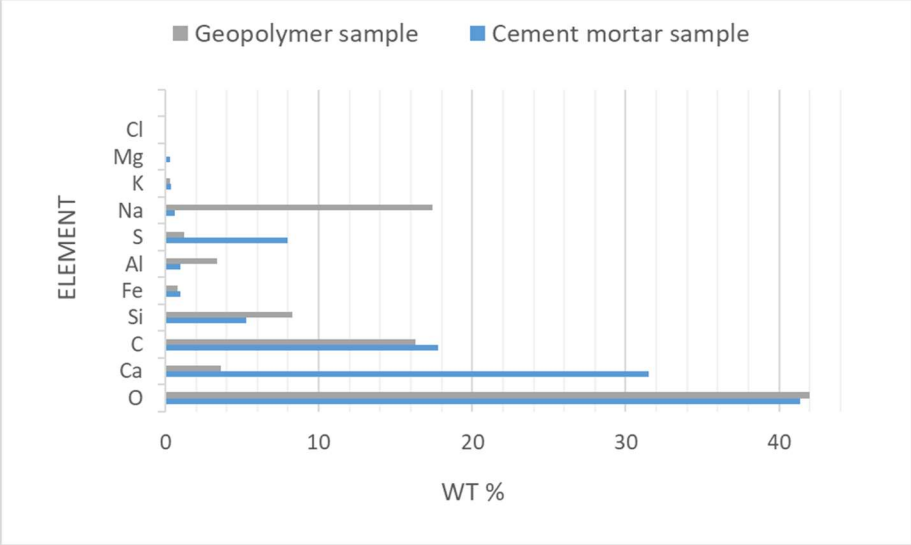

Figure 4-20: Chemical composition of geopolymer samples in comparison with cement mortar samples

4.4.6 Chemical stability

In order to study the resistance of geopolymers to acids, geopolymer specimens were immersed in acid solution with pH of 1.5. The changes in weight of the specimens, appearance was monitored after two months. Sulfuric acid solution was prepared by diluting 99% sulfuric acid with distilled water to form pH around 1.5. Small samples were cast (batches G2, G4, G5 and G9 according to Table 4.8) and immersed in sulfuric acid solution. Mass loss was recorded every 2 weeks for 2 months, the results are shown in Figure 4.21.

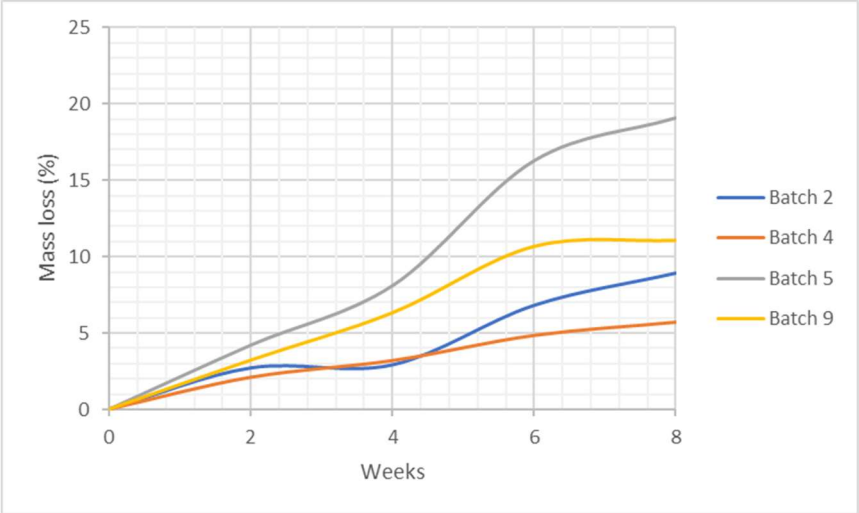

Figure 4-21: Mass loss vs. immersion time in acid sulfuric (pH=1.5) for Batch 2 (G2), Batch 4 (G4), Batch 5 (G5) and Batch 9 (G9)

It could be seen that G4 and G9 displayed almost similar trends over 2 months period with max mass loss of between 5 to 10%. However, G2 showed higher mass loss wich is explainable according to its higher calcium content compare to other specimens. So higher CaO content is a key reason for higher strength and lower corrosion resistant properties.

The visual appearance of geopolymer specimens following 6 weeks and 8 weeks immersion in acid is shown in figures 4.22 and 4.23. G5 exhibited severe erosion and significant dimensional change happened in the upper part of the sample. Leaching is clear on the surface of the samples after 6 weeks. G4 shows very small alteration in the visual appearance, color change and erosion. So, it could be concluded that geopolymers are a durable solution in acidic environments.

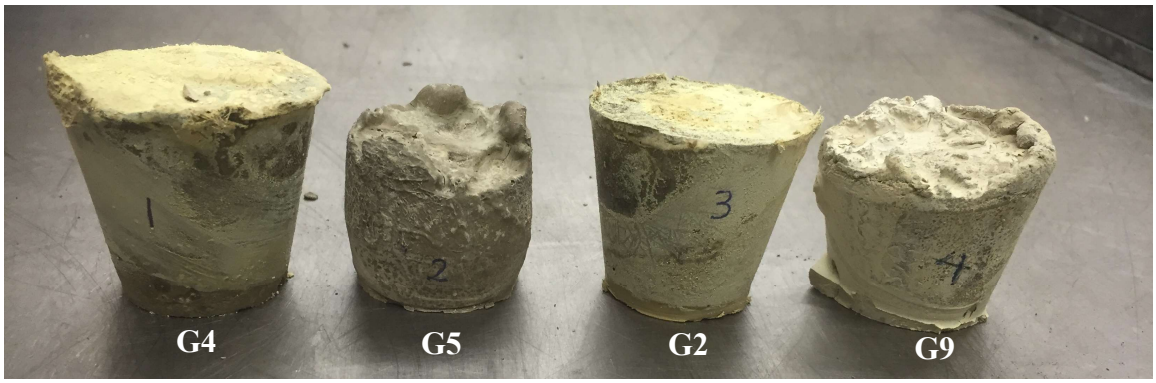

Figure 4-22: Chemical stability of geopolymer samples observed in this study after 6 weeks

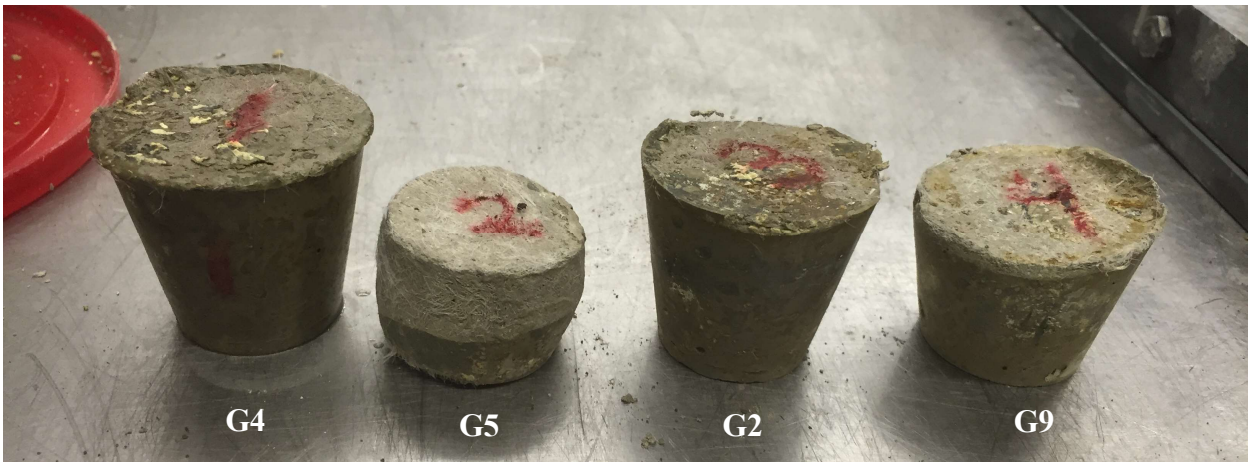

Figure 4-23: Chemical stability of geopolymer samples observed in this study after 8 weeks

4.5 Multiphase matrix integrated with Zn-doped clay

4.5.1 General properties

According to high chemical stability and acceptable mechanical properties, G4 described in section 4.4 was chosen as a base for the coating material. The base material was modified in this section in order to add antibacterial properties to the system and immobilizing the antibacterial agent in the coating.

For enhancing strength, adding neutralizing effect and densifying the microstructure, a blended mix of magnesium phosphate hydrates phase in conjunction with geopolymer matrix was prepared

and tested. The aim of combining these two matrixes was to take advantage of each system's individual strength and increasing the degree of encapsulation.

Magnesium phosphate binder consisted of a mixture of magnesium oxide and potasium phosphate. The reaction product was magnesium dihydrogen phosphate with high early strength, high adhesive properties and fast setting time. The fineness of hydrated magnesium phosphate particles is much higher than ordinary Portland cement particles and so magnesium phosphate reacts much faster with water. Un-hydrated magnesium oxide particles are able to consume extra water produced during geopolymerization process and produce magnesium hydroxide which could react with sulfuric acid and produce $MgSO_4$ and so increase the pH.

Zinc oxide was used to add antibacterial properties to the coating material. Two systems were considered to gain control over the release of heavy metals embedded in the coating. The first mechanism was to keep the heavy metal molecule (zinc oxide) in the 3D framework of the coating binders. The incorporation of metal in the matrix happens either physically through charge balancing of Al in the network or by creating covalent bonds between metal and silicate chain or hydroxide links [Van Jaarsveld et al., 1999].

The second approach was to use sodium bentonite clay impregnated with zinc ions to functionalize it as an antimicrobial agent then combine it into the structure of the coating materials (blended geopolymer), see section 4.3 for detailed information. Loaded clay particles have the potential to be incorporated as a secondary source of alumino-silicate in geopolymerization reaction. However, clay has lower surface area for geopolymmerization reaction compared to fly ash which has spherical-shaped particle [Liew et al., 2016]. So, using loaded clay particles alone produce weak structure.

Ten blended mixes of magnesium phosphate hydrate-geopolymer (Table 4.9) were prepared and evaluated according to chemical stability and tensile strength properties. SEM-EDS was used to investigate the microstructure and composition of developed materials. Then the best geopolymer and blended mixes were integrated with zinc-oxide particles and Zn-doped clay particles. Leaching

and chemical stability, bonding and shrinkage properties were tested to evaluate the performance of the developed materials.

4.5.2 Mix design and sample preparation

Ten blended mixes of zinc-doped magnesium phosphate hydrate-geopolymer (Table 4.9) were prepared and evaluated in this experiment.

The alkali activator solution was prepared by mixing sodium hydroxide solution and sodium silicate according to the mix design one day before casting. A constant alkaline activator ratio of $NaSiO_2$ / NaOH = 2.5 and fly ash / alkaline activator = 2.8 has been considered in all of the mixes according to the results described in section 4.4.

At the beginning, numerous trial mixtures were prepared. An eighty-litre capacity pan mixer available in the SIERA concrete laboratory for making ordinary Portland cement was used for producing the blended paste. The main objectives of preliminary laboratory work were familiarizing with casting the blended mix, understanding the effect of the sequence of adding alkaline solution to the solids constituents, understanding the basic mixtures proportions, observing the behaviour of the mix and workability and developing a consistent process of mixing and curing.

The casting and mixing procedure consisted of first mixing the alkaline solution, then dry material mixed for 3 minutes, and alkaline activator was slowly added to the mix. Ultimately water was added and mixing continued for another 1 min. Adding water to the system made the mix more workable and retarded the formation of alumino-silicate network. More water was needed for casting blended mix compare to geopolymer mixes. Also, more alkaline activator solution was needed when using zinc-doped clay particles. The setting time was observed to be much faster compare to cement paste and geopolymer mix.

Different ratios of Mg/potasium phosphate were also tested. Increasing magnesia content in the mix resulted in an accelerated setting reaction due to a higher pH and therefore a faster reaction between MgO and potasium phosphate. So, sodium borate (borax) was used to reduce the setting time. However, addition of more borax had adverse effect on the mix, so sodium borate / MgO ratio was kept constant at 0.08. After mixing, samples were prepared for bonding, shrinkage, SEM-EDS, chemical stability and tensile strength test.

Table 4-9: Mix design of composite coating in this experiment

	M1	**M 2**	**M3**	**M4**	**M5**	**M6**	**M7**	**M8**	**M9**	**M10**
Alkaline activator / Alumino-silictae source	0.45	0.45	0.45	0.45	0.45	0.45	0.45	0.45	0.7	0.7
sodium silicate / sodium hydroxide	2.5	2.5	2.5	2.5	2.5	2.5	2.5	2.5	2.5	2.5
water / binder	0.1	0.2	0.2	0.25	0.1	0.25	0.25	0.25	0.25	0.25
MgO + Potasium Phosphate / Fly ash	0	0.15	0.2	0.3	0	0.15	0.15	0.1	0	0.1
MgO / Potassium Phosphate	0	1.5	1.5	1.5	0	1.5	1.5	1.5	0	1.5
sodium borate / MgO	0	0.05	0.05	0.05	0	0.05	0.05	0.05	0	0.05
ZnO / Fly ash	0	0	0	0	0.15	0.15	0.2	0	0	0
zinc-doped clay / Fly ash	0	0	0	0	0	0	0	0.4	0.5	0.5

4.5.3 Tensile strength properties

Uniaxial tensile tests were performed on each mix design. A closed-loop controlled Instron testing system was used in displacement-controlled mode. The testing gauge length was 60 mm, loading rate set at 0.001 mm/min. Load-displacement curves are presented in Figures 4.24, 4.25 and 4.26. By comparing M2, M3 and M4 mixes, see Figure 4.24, it could be observed that replacing more than 15% geopolymer matrix with magnesium phosphate hydrate reduces tensile strength. When

magnesium oxide and potasium phosphate react, water soluble magnesium dihydrogen phosphate form as a reaction product which could act as a micro-aggregate in geopolymeric network. This will densify the ultimate product, increase encapsulation properties and strengthen the matrix. However, the geopolymeric gel could also act as a dominant product and MgO play less role in affecting the nature of the end product. In this case the dissolution of MgO species will not have major impact on the ultimate strength.

It is also possible that as the MgO concentration increases, the formation of geopolymeric gel and hydrated magnesium gel start to compete against each other. Therefore, instead of having one phase acting as a micro-aggregate to fill voids and holes of the binder, the two reactions compete for available space for growth. Consequently, the resultant product is a weak paste with two phases of similar size. Although the paste has high corrosion resistant and encapsulating properties, the strength reduction will be significant.

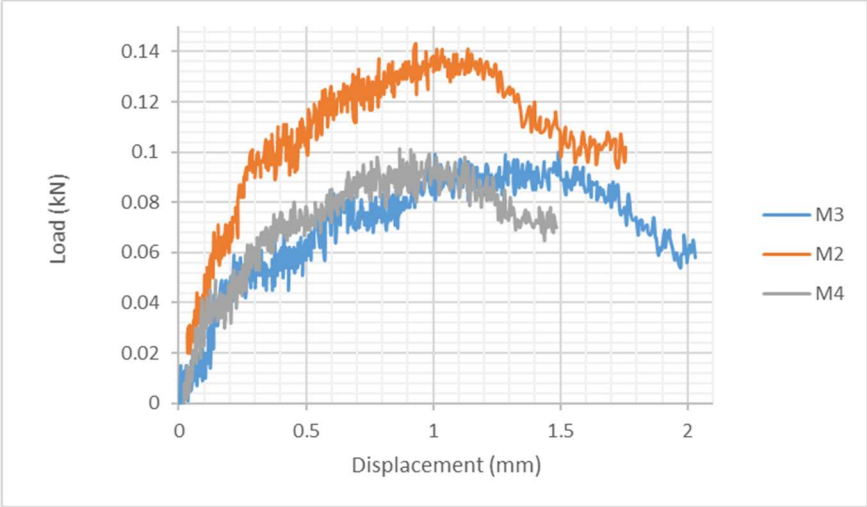

Figure 4-24: Uniaxial tensile test results for mix design M2, M3 and M4

According to the results obtained from comparing mixes M5, M6 and M7 (Figure 4.25) in this experiment, it could be concluded that adding heavy metal to the geopolymer and blended paste reduces ultimate tensile strength. The performance of blended mix with the addition of zinc oxide

powder is very poor compare to other mixes. Zinc oxide powder absorbed a significant amount of water and left the MgO particles un-hydrated in the system, Figure 4.25.

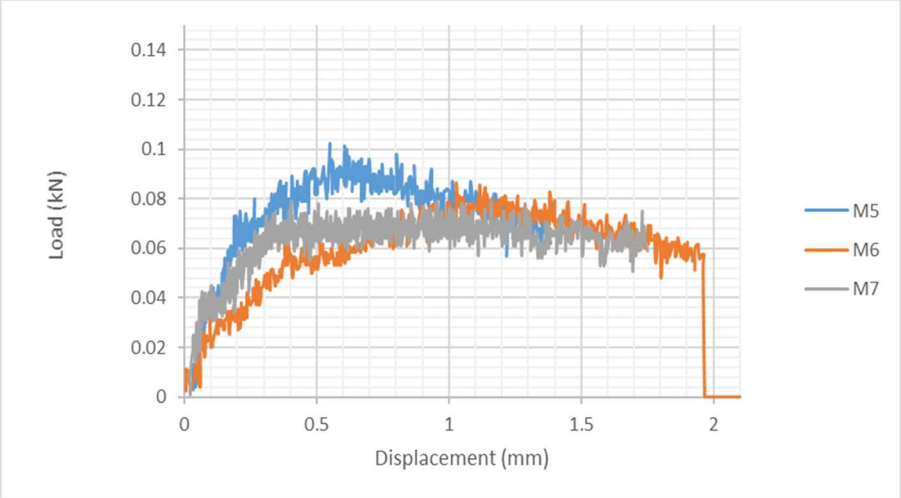

Figure 4-25: Uniaxial tensile test results for mix design M5, M6 and M7

Adding zinc-doped clay particles to the geopolymer and blended matrix and increasing the alkali activator to alumino-silicate ratio enhanced the tensile strength properties of the mix, see Figure 4.26. As it was discussed before, loaded clay particles have the potential to be incorporated as a secondary source of alumino-silicate in geopolymerization reaction. Increasing the alkali activator solution promoted the solubility and dissolution of clay particles and accelerated their geopolymerization reaction.

Ultimately, typical stress-strain curves were plotted for M1, M2, M5, M9 and M10 after 7 and 14 days in Figure 4.27. Toughness values (see Figure 4.28) were determined by calculating the area under the stress-strain curve in Figure 4.27.

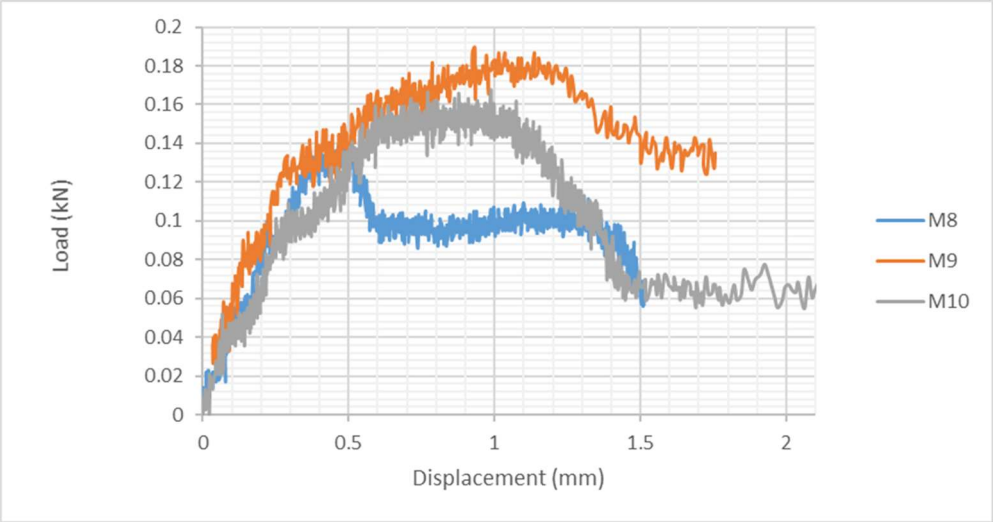

Figure 4-26: Uniaxial tensile test results for mix design M5, M6 and M7

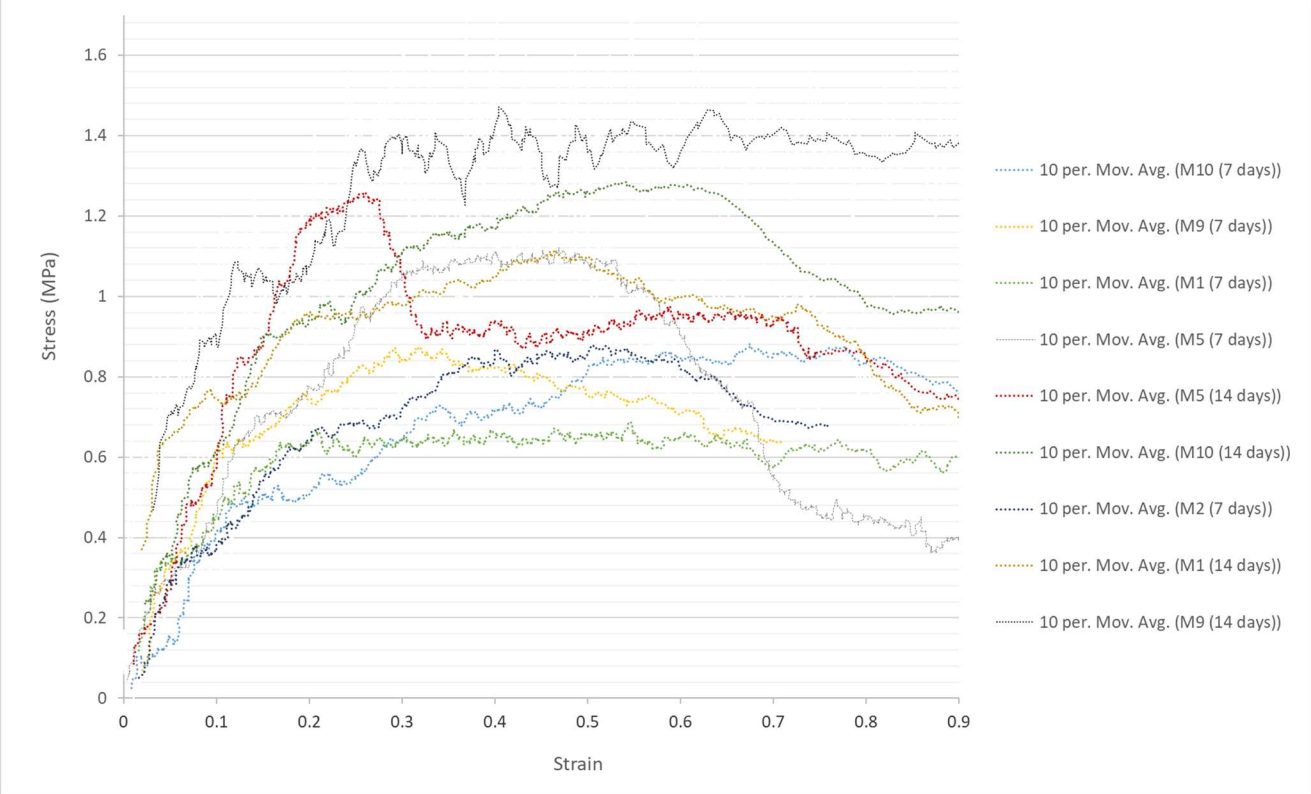

Figure 4-27: stress-strain curves for mix design M2, M5, M9 and M10 after 7 and 14 days

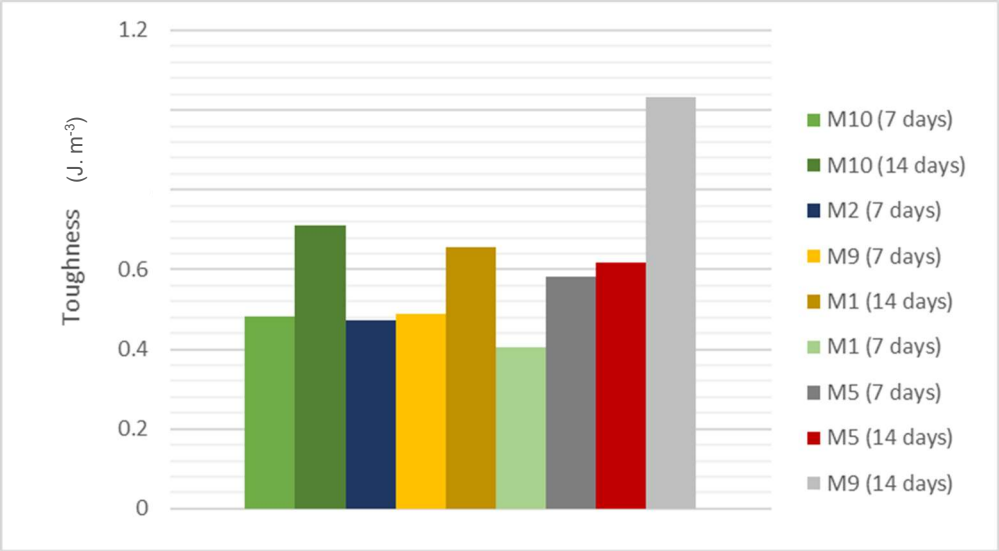

Figure 4-28: Toughness values for mix design M2, M6, M9 and M10 after 7 and 14 days

4.5.4 Bonding test

Bond pull-off test play a crucial role in determining bond strength between concrete surface and the repair coating material. Basically, the test determines the greatest perpendicular force (in tension) that a surface area can bear before a plug of material is detached. Failure will occur along the weakest plane within the system. This test was performed using the Delfesko Pull Off Adhesion Tester following the ASTM D4541, D7234.

M2, M5, M9 and M10 were applied onto a well-scrubbed and SSD concrete blocks (Figure 4.29). Then the samples were initially cured for 24 hours by plastic tenting to prevent moisture loss. After 24 hours, samples were placed in a closed container for a duration of 14 days (Figure 4.30).

Figure 4-29: Application of the mixes for the adhesion test

Figure 4-30: Curing of coated samples for the adhesion test

Once removed from curing, coated concrete blocks were cored and a metal fixture was glued using rapid setting epoxy. Samples were then left at room temperature for 2 days to ensure maximum adhesion of the dollies to the surface. Measurements of bonding strength (pull-off) between the concrete and the coating material were determined at 17 days of the application by applying load at a steady rate to the disc by the test equipment until failure occurs in the specimen. Samples were

tested following the ASTM D4541, D7234, as shown in Figure 4.31 . Three dollies were tested per sample.

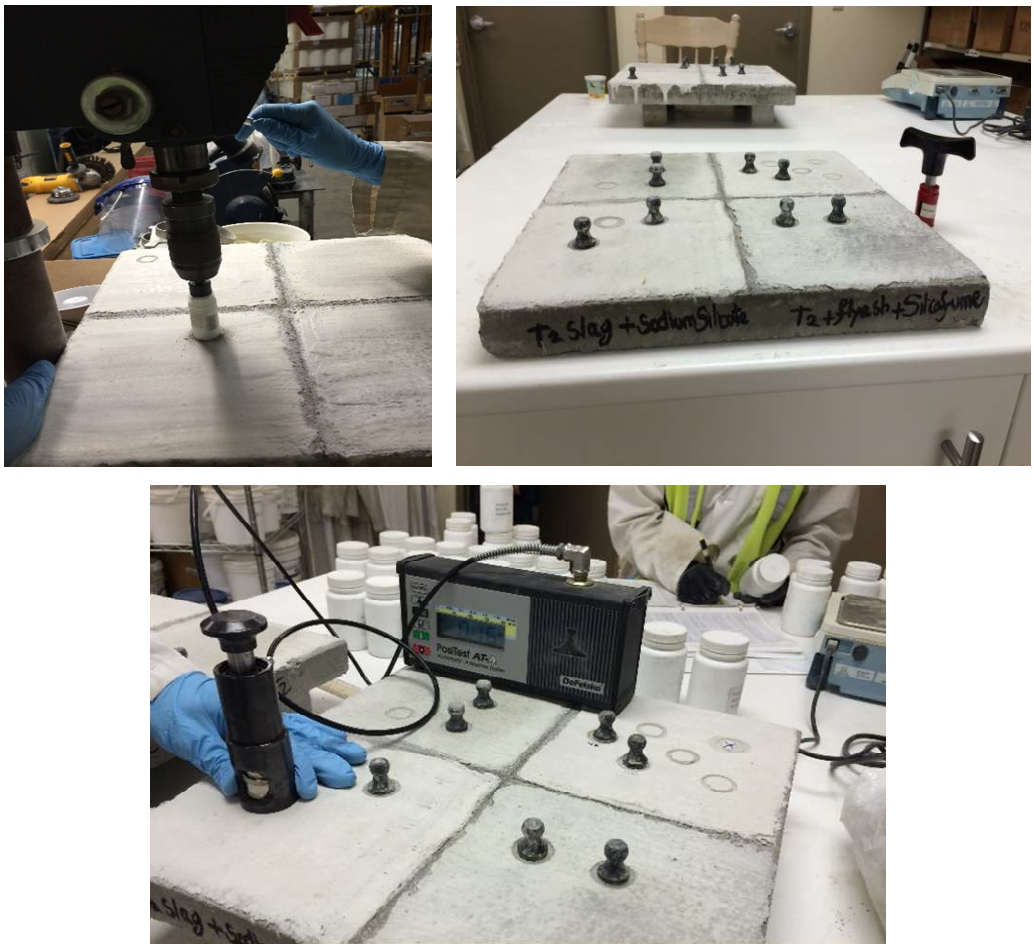

Figure 4-31: Installation of metal fixtures and pull-off testing procedure

The results were analyzed in terms of bonding strength and type of failure. When the test was performed, the measured strength is controlled by the failure mechanism requiring the least stress. Average bonding strength for each sample is presented in Table 4.10.

The nominal tensile strength or adhesion, E, between the overlay material and concrete substrate is given by:

$$E=F_{peak}/A \qquad \textbf{(Equation 4.2)}$$

in which f is the recorded failure tensile peak load (N) and A is the cross-sectional area of the test testing disc (mm^2).

The mode and location of the failure should be noted, since the failure can occur in the substrate, repair material or the bond or interface between the substrate and the repair material. The failure types including:

- Bonding failure: when the entire coating detaches from the concrete base
- Coating failure: when the weakest plane happens to be inside the coating, and the bonding between the coating and the base is unharmed
- Partial Failure: when the failure mechanism consists of a mixture of bonding and coating failure.
- Epoxy failure: when the detachment occurs between the test dolly and the coating surface, indicating the adhesive has failed.

Table 4-10: Average adhesion strength of coated samples

Mix	Average Bond Strength	Bond Strength Standard Deviation
M9	2.61	0.41
M1	2.83	0.17
M10	2.43	0.35
M5	1.98	0.17
M6	0.71	0.99
M2	2.24	0.34

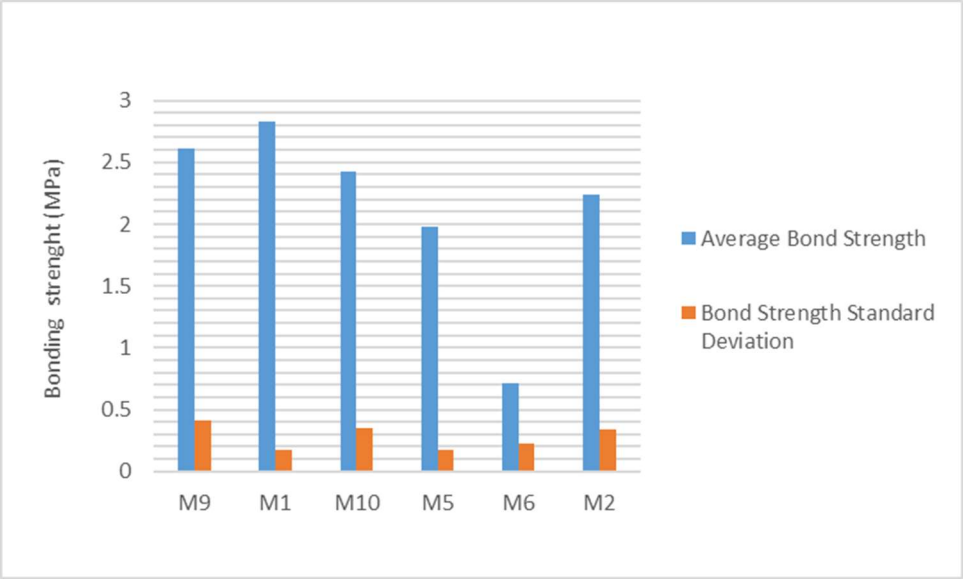

Figure 4-32: Bond strength summary graph for this experiment

It should be noted that the results of the pull-off test is dependent on the type of the equipment used, thickness of the repair material and the disc, geometry and dimension of the specimen, depth of cut drilling and loading rate. According to the literature, typical values of adhesion of repair materials or overlay to concrete substrate ranges from 0.41 to 3.44 MPa. EN1504-3 required bonding strength is at least 2 MPa.

According to the results, the average bond strength values (Table 4.10) are higher than the tensile strength results (Fig 4.27) which could be because of the shape, curing condition (which affects the matrix) and demolding procedure of tensile strength test samples. In addition, tensile strength test samples could be damaged slightly during demolding procedure. Specimens coated with zinc-doped multiphase composite materials exhibited comparable adhesion strength at early stages in comparison to the specimens coated with geopolymer.

4.5.5 Shrinkage

Shrinkage cracking at early ages have the potential to accelerate concrete deterioration and lead to leakage, reduced strength and failure. Surface cracks allow bacteria to penetrate the coating,

causing rapid delamination and corrosion. In this study, a test was conducted to study shrinkage induced cracking of developed materials.

To determine the plastic shrinkage behavior of different materials, a technique, developed by Banthia et al. (1996), was used to simulate realistic shrinkage conditions. To achieve this simulation, fresh samples of the material were applied on a hardened concrete base and placed in a chamber, capable of simulating aggressive drying conditions that encourage shrinkage induced cracking.

The environmental chamber used for this experiment was a semi-enclosed rectangular box, 1705×1705×380 mm, equipped with temperature and humidity probes, capable of regulating and monitoring the environment inside (Figure 4.33). Three heating fans (240 V, 4800 W with a 1/30 HP, 1550 RPM internal electrical fan) supplied the necessary heat to maintain a constant temperature of 50°C± 1°C, along with an approximate humidity of 5%. The heated air was allowed to escape through three 240×175 mm openings, creating a rate of surface evaporation of approximately 0.8 kg/m^2/h [Banthia et al. 1996].

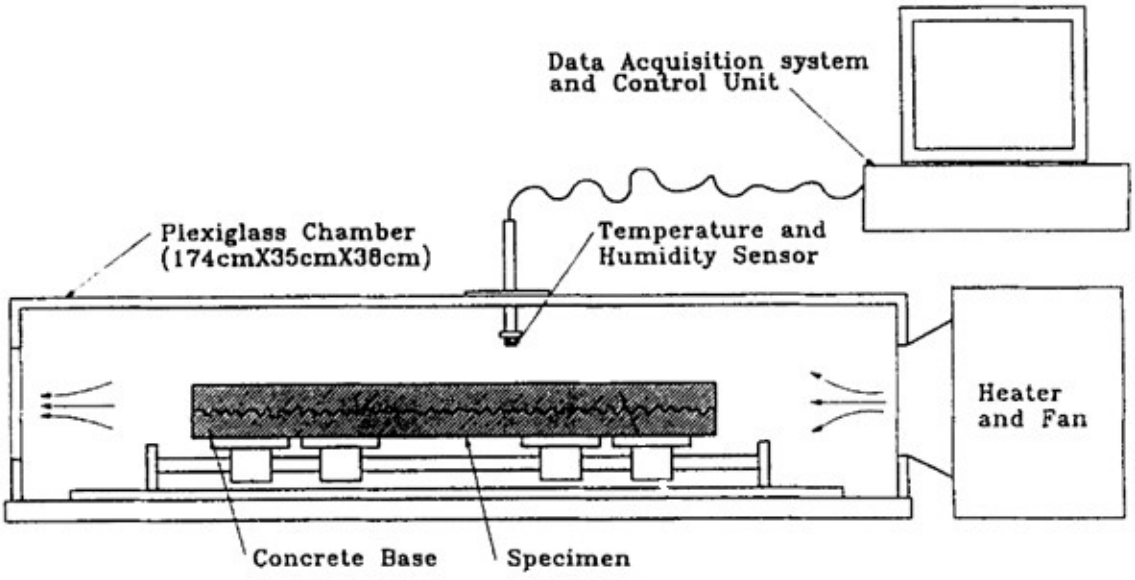

Figure 4-33: Schematic illustration of the plastic shrinkage inducing chamber used with permission from Banthia et al., 1996

In order to create a suitable base for our repair materials, square concrete slabs with dimensions of 50×400×400 mm were purchased and cut into 4 even pieces. Each smaller rectangular piece, 50x100x400 mm, was then thoroughly cleaned with water and a steel wire brush and kept in a saturated surface dry condition (SSD). Developed mixes M1, M2, M5, M6, M9 and M10 were brushed over each base and placed in the environmental chamber, Figure 4.34. A set of six samples were placed in the simulation chamber at a time. Each set of samples were removed after 72 hours and the crack patterns were characterized, Figure 4.35.

With two applicators applying the coating of the 6 samples, the first and last sample had a cast time difference of about 15 minutes. To minimize the potential error due to this cast time difference, each group of samples was tested multiple times, with different application orders.

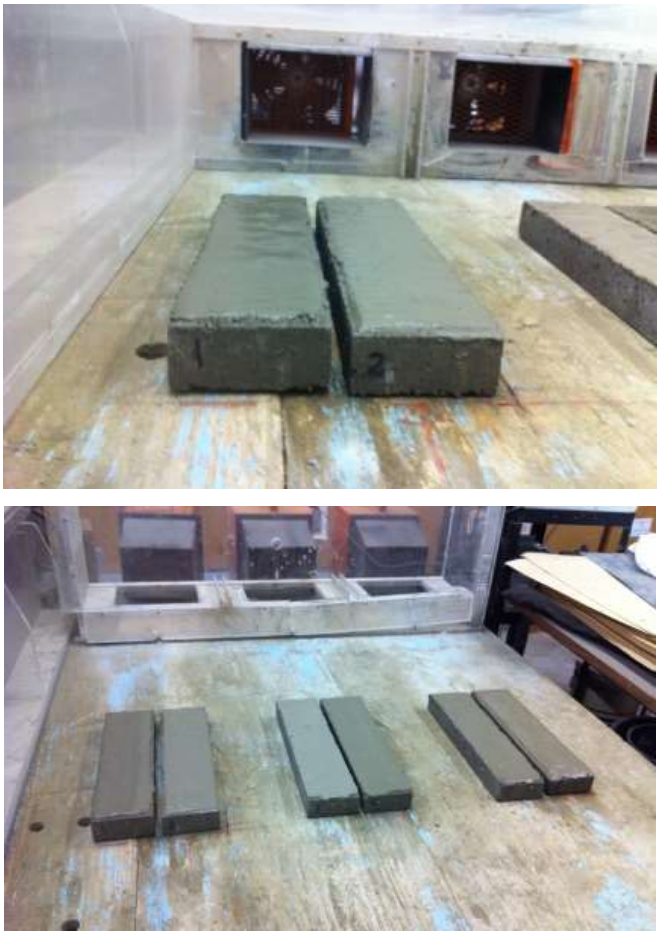

Figure 4-34: Application of coating on shrinkage samples for this experiment

After the first 24 hours, very few cracks were visible on the samples, suggesting that the samples were still hydrating. Within 48 hours, a larger quantity of cracks was visible, Figure 4.35. After 72 hours in the chamber, the samples seemed fully hydrated with visible cracks. A summary of the findings is presented in Table 4.11.

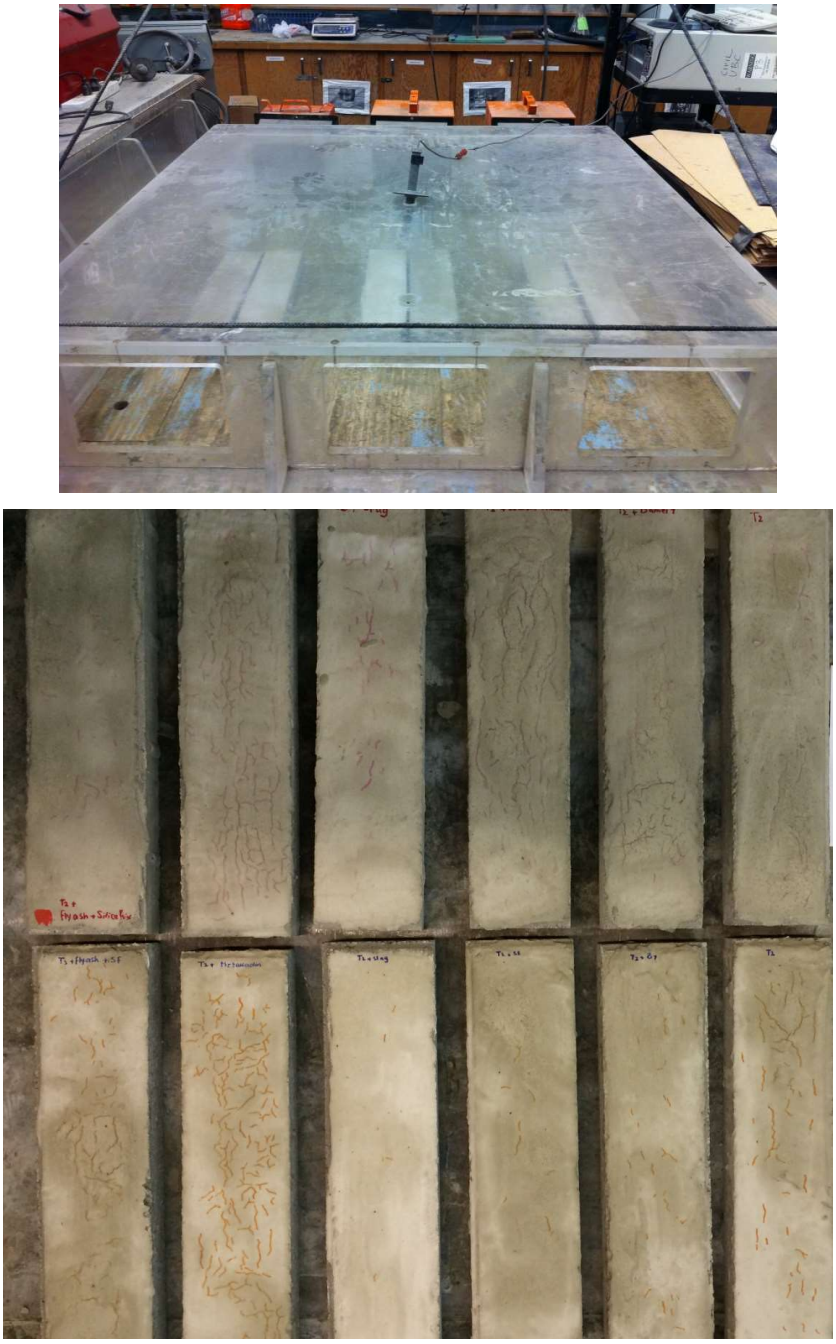

Figure 4-35: Plastic shrinkage crack inducing environmental chamber for this experiment

Table 4-11: Descriptive summary of plastic shrinkage test results for this experiment

	Set 1: Aug 14, 72 hours	**Set 2: Aug 17, 72 hours**	**Set 3: Aug 25, 72 hours**	**Set 4: Sept 1, 72 hours**
M2	Crack distribution was small Partial delamination noticed	Moderate cracks comparable to set 1 (almost same results)	Almost no cracks observed	Moderate cracks comparable to set 1 and 2 consistent workability
M6	Longer vertical cracks Few deep cracks compared to M1	Long cracks, poor performance Same results as set 1 Very poor performance		———
M9	Small micro cracks		Small cracks, performance similar to set 1	
M10	Long vertical cracks	Cracks were 20% less than set 1, needed to test another batch to verify the results Better performance compares to M6	Same results compare to set 2 and overall less cracks compare to M2	
M5	Smaller cracks compare to M9			Results very similar to set 1 More cracks observed compare to geopolymer
M1	Less crack compares to other samples	Crack were comparable to set 1		Almost no cracks observed

4.5.6 Surface morphology

SEM-EDS was used to investigate the microstructure and composition of different mixes including geopolymer, blended matrix and zinc-doped mixes. Proper sample preparation is very important in obtaining the required information when using SEM. For this purpose, samples were casted,

cured and impregnated using epoxy-based resin. Then epoxy impregnated samples were cut with a saw and polished with diamond grit. Ultimately samples were cleaned in desktop UV cleaner chamber and dried at 50°C, Figure 4.36.

Figure 4-36: Prepared samples for SEM-EDS test in this study

Figure 4.37-4.41 are SEM images of mixes, M2 (blended mix of geopolymer and magnesium phosphate), M5 (M1 integrated with zinc oxide particles), M6 (blended mix integrated with zinc oxide particles), M9 (M1 integrated with Zn-doped clay particles) and M10 (blended mix integrated with Zn-doped clay particles).

As seen in Figure 4.37, this geopolymer sample (M1) consisted of amorphous phase which could be responsible for its high strength and dense structure. Magnesium phosphate compound generally tend to yield crystalline structures, Figure 4.38 (M2).

However, when a source of amorphous silica such as fly ash was added to the crystalline structure, amorphous or glassy (structures with short range disordered) phases were formed within them, see Figure 4.39. Fly ash provides amorphous silica to the reaction which converts it into a dense geopolymer. So the network of crystaline magnesium phosphate minerals are connected by silicate geopolymeric amorphous materials.

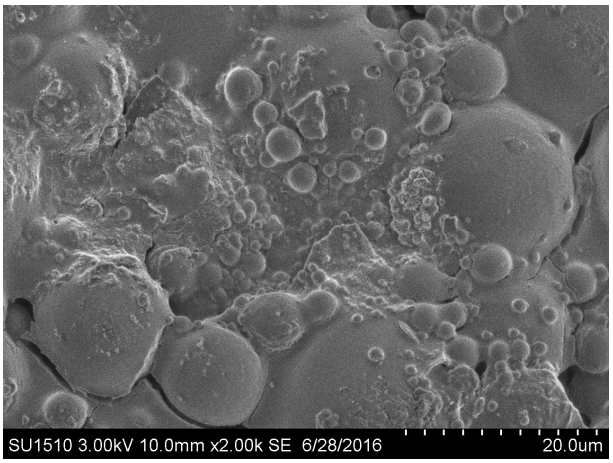

Figure 4-37: SEM images of M1

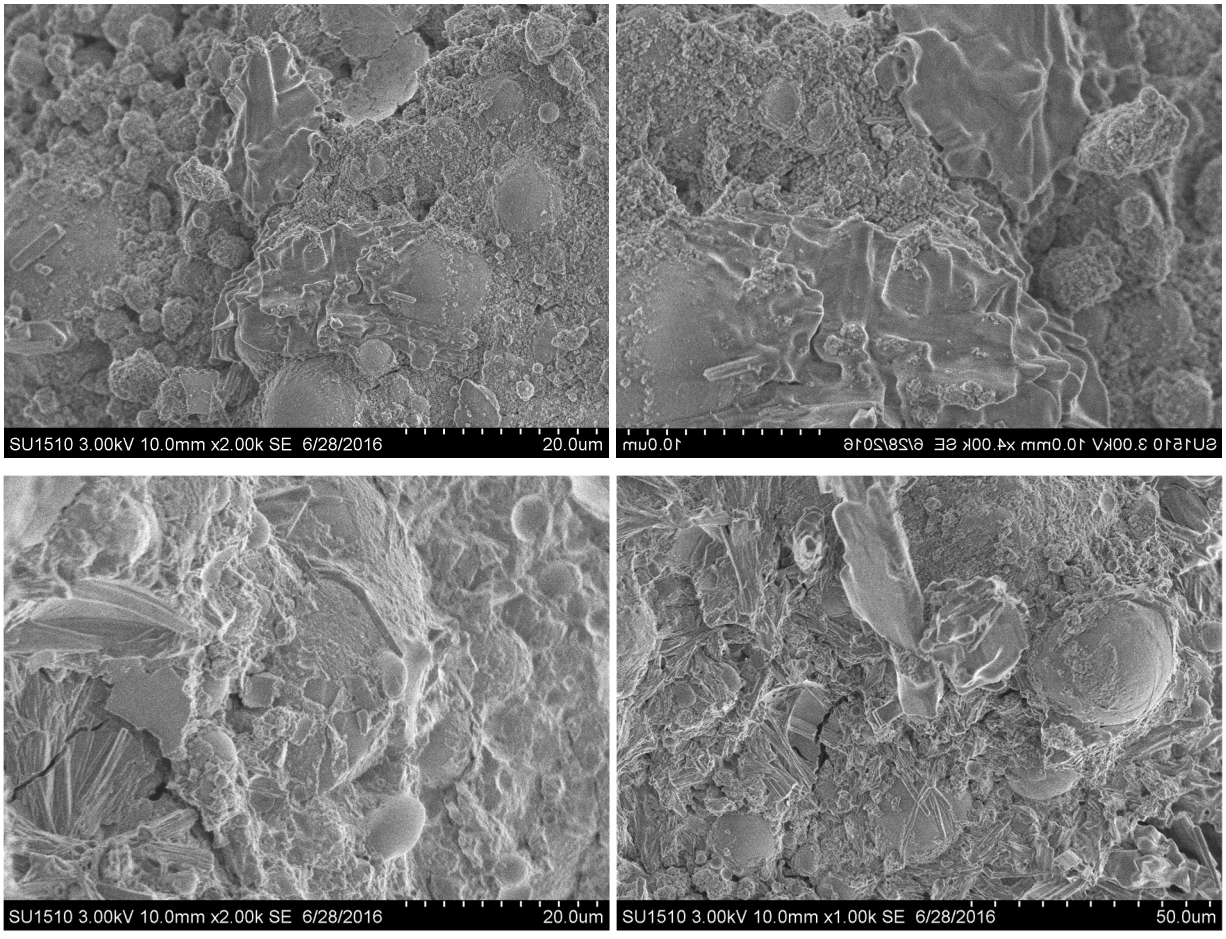

Figure 4-38: SEM images of M2

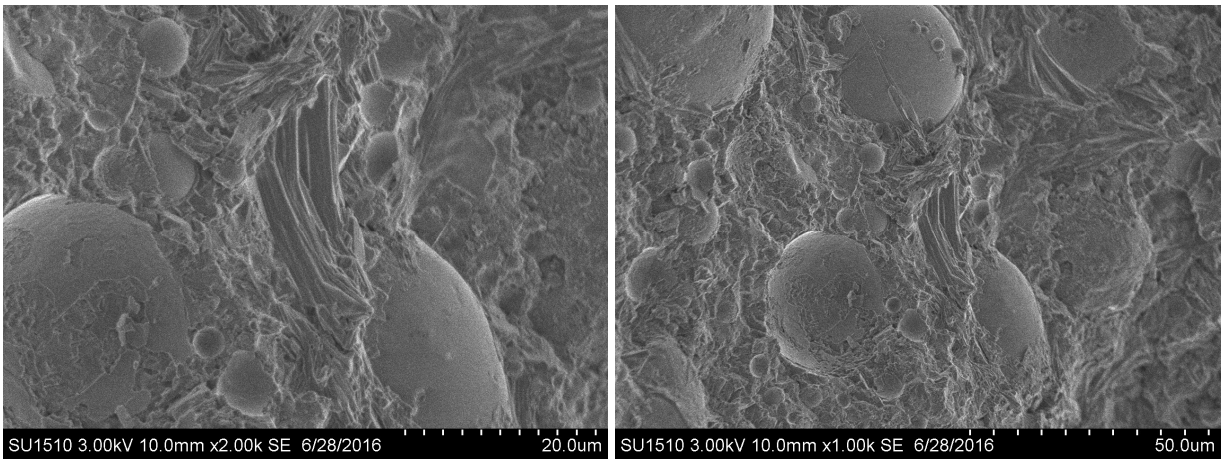

Figure 4-39: SEM images of M10

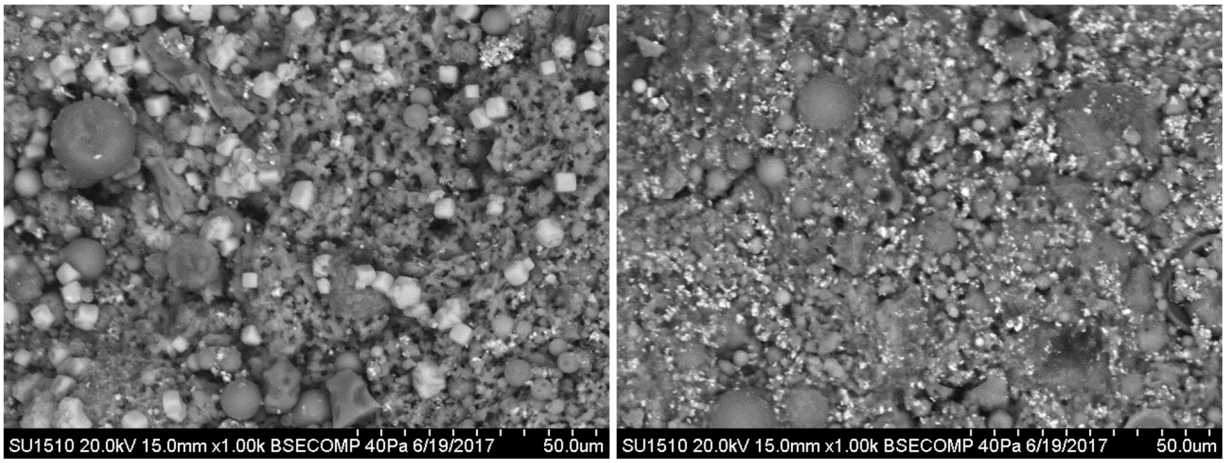

Figure 4-40: SEM images of M6

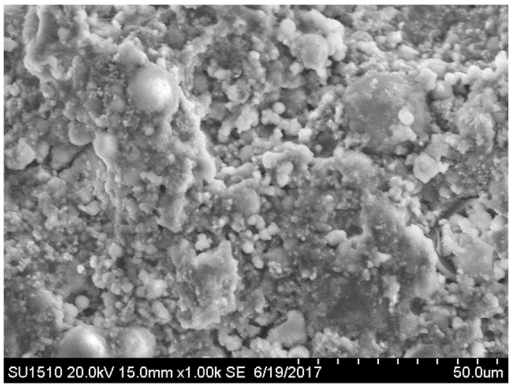

Figure 4-41: SEM images of M5

SEM-EDS analysis of the samples is shown in Figure 4.42. As described before, geopolymers are formed by polymerization of inorganic molecules containing mainly of aluminium, silicon, oxygen and other elements. As could be seen in Figure 4.42, Geopolymer matrix (M5) encapsulated Zinc particles physically (charge balancing of Al in framework) within the three-dimensional alumino-silicate network. According to Figure 4.44, Na and Ca amounts are reduced in M5 and M6 compare to M1 and M2 and may indicate that Zn particles were replaced by Na, Ca ions in the system.

Zn particles are also encapsulated in the 3D framework of the blended mix, (Figure 4.43). Comparing chemical composition of M6 with M2 suggests that Zn is replaced by Al, Na or Ca. The amount of the Zn particles encapsulated in the blended mix is higher than the geopolymer which indicates encapsulation degree in the blended mix increased compare to geopolymer mix, Figure 4.44.

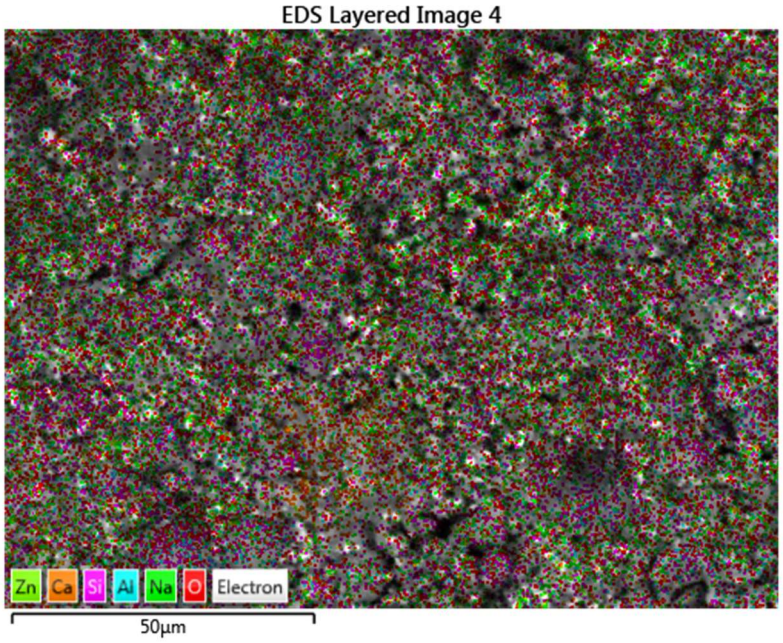

Figure 4-42: Chemical composition map of geopolymer (Mix M5)

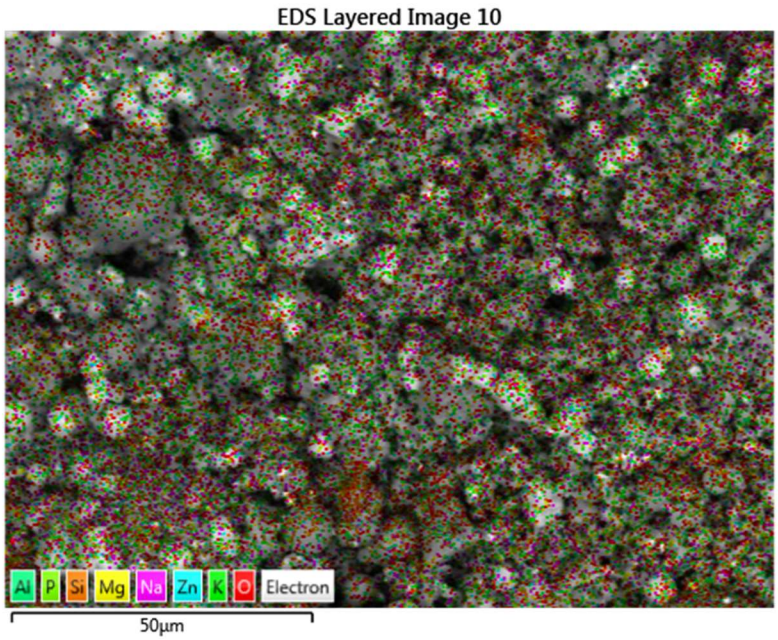

Figure 4-43: Chemical composition map of blended mix integrated with ZnO (Mix M6)

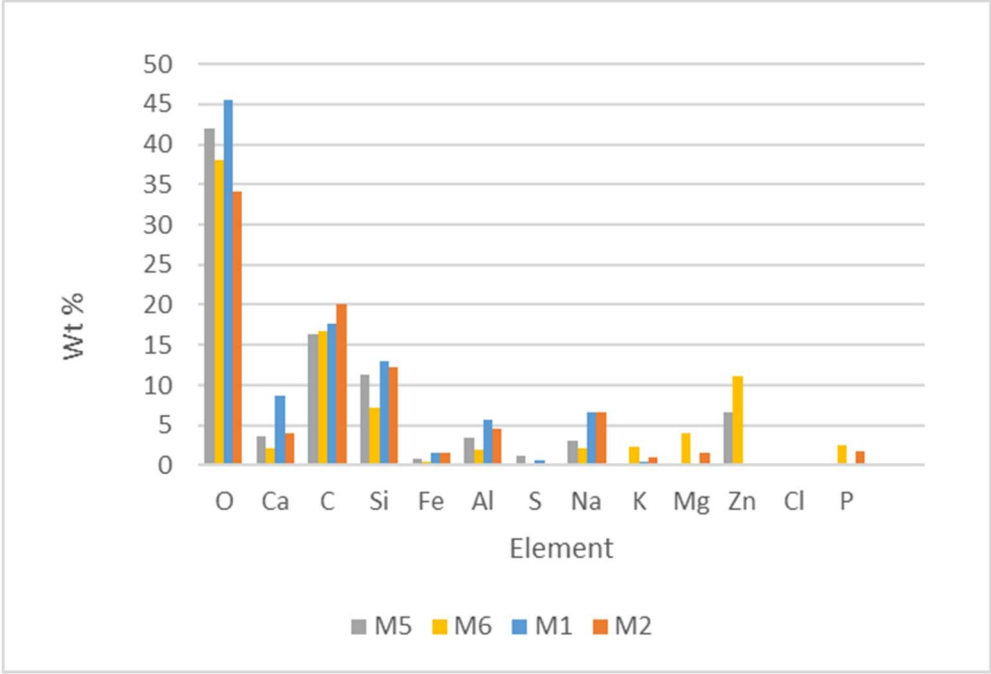

Figure 4-44: Comparison between the chemical compositions of mixes, M1 (Geopolymer mix), M2 (blended mix of geopolymer and magnesium phosphate), M5 (M1 integrated with zinc oxide particles), M6 (blended mix integrated with zinc oxide particles)

4.5.7 Leaching and chemical stability

In order to evaluate the stability of the antibacterial composites, leaching tests were conducted on the samples. Atomic absorption spectrometry was used to measure leaching of zinc ions. The leaching test was carried out on immersed cylindrical samples (D = 20 mm, h = 30 mm) in 20 ml of the leaching solution containing biogenic acid and distilled water (pH = 1.5) at 30°C for 120 days. The suspensions were continuously stirred during this period and samples were collected every 7 days. Each time the leachate samples were centrifuged, filtered and analyzed using atomic absorption spectrometer.

The leaching rate is measure by dividing the measured mass of Zn according to the time of exposure based on the work of Ikeda et al. in which Vd is leaching rate per unit area (micro grams /hr.cm2), Xd is the maximum amount of Zn leached out of of the sample during the experiment in micrograms, T is the period of the test (hr) and S is the area of exposure (cm^2)[Ikeda et al., 2004].

$$\boldsymbol{Vd = \frac{Xd}{T\,S}} \qquad \textbf{(Equation 4.3)}$$

Leaching of zinc was used as an expression of the efficiency of encapsulation of Zn ions in different mixes. Our findings that are given in Fig 4.45 demonstrate that multiphase composite coating is more chemically stable in aggressive environments and lower pH compare to other coatings. The percentage of leaching is significant in the first leaching and decreased as leaching is repeated.

According to Figure 4.45, the amount of leached Zn from cement mortar samples reduced when Zn was encapsulated in clay particles. However, slight difference was observed for geopolymer samples and composite coating mixed with zinc oxide and Zn-doped clay. This shows that geopolymer and composite coating matrixes were able of encapsulating Zn particles in their network. The high amount of leached zinc out of cement paste mixed with ZnO is due to large surface cracks that occur on the surface of the samples.

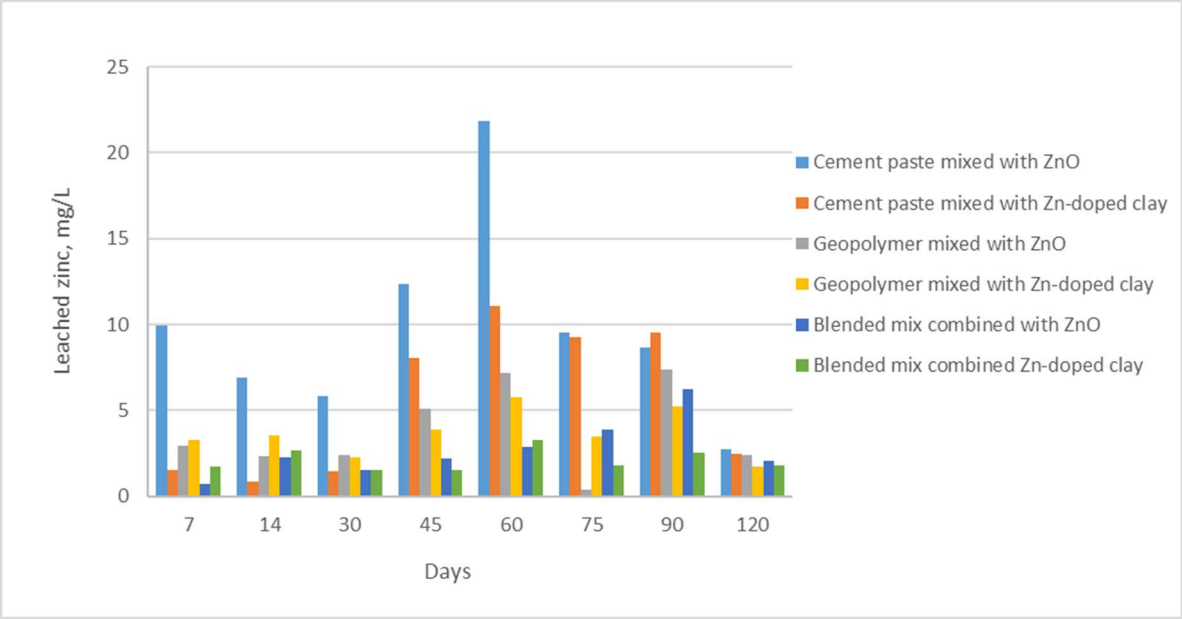

Figure 4-45: Leaching test performed on cement mortar, geopolymer and blended mix in this experiment

The leached concentration of Zn after 120 days is less than 3 mg/L for geopolymer and blended samples. Leaching rate for geopolymer and blended samples combined with Zn-doped clay particles was around 2.5 and 2 mg/L.hr which was the minimum compared to other mixes, Figure 4.46. This could be explained by the entrapment and attachment of Zn particles to the bentonite clay matrix. Also, the swelling properties of clay minerals has the blocking effect against the dissolved ions in the water inside the pores. Zn-doped clay particles also successfully reduced leaching rate in Portland cement mortar samples. Leaching rate of cement mortar samples mixed with ZnO was reduced by almost 50% compare to samples with Zn-doped clay.

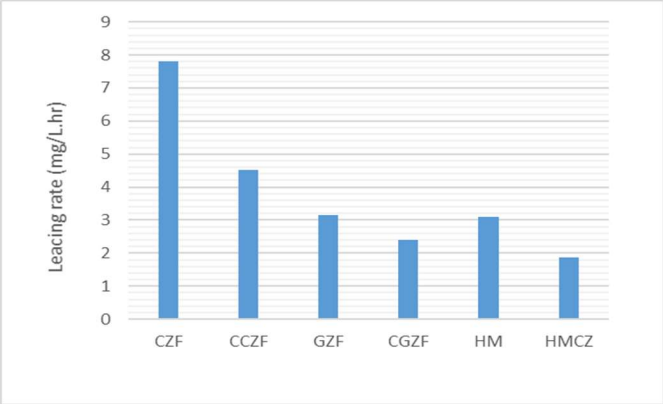

Figure 4-46 : Leaching rate of different mixes after 120 days, CZF: Cement mortar sample mixed with ZnO, CCZF: Cement paste combined with Zn-doped clay particles, GZF: Geopolymer sample mixed with ZnO, CGZF: Geopolymer sample combined with Zn-doped clay particles, HM: Blended sample mixed with ZnO, HMCZ: Blended sample of geopolymer and magnesium phosphate mixed with Zn-doped clay particles

In addition to acid leaching, according to Figure 4.47 and 4.48, CZF (cement mortar sample mixed with ZnO) and CF (cement mortar sample without zinc) had deformed and degraded completely in acid solution compared to other mixes which is explainable according to their higher calcium content compare to other specimens. CCZF (cement paste combined with Zn-doped clay particles) also exhibited severe erosion and significant dimensional change. Leaching was clear on the surface of the samples after 6 weeks. However, the amount of leached Zn in CCZF was 50% less than CZF.

The visual appearance of GZF (geopolymer sample mixed with ZnO) and HMCZ (blended sample of geopolymer and magnesium phosphate mixed with Zn-doped clay particles) and HMZ (blended sample mixed with ZnO) specimens following 16 weeks immersion in acid is shown in Figures 4.47. GZF shows very small alteration in the visual appearance, color change and erosion. Based on visual evaluation, it could be concluded that geopolymer and composite coatings appear to be durable solutions in acidic environments.

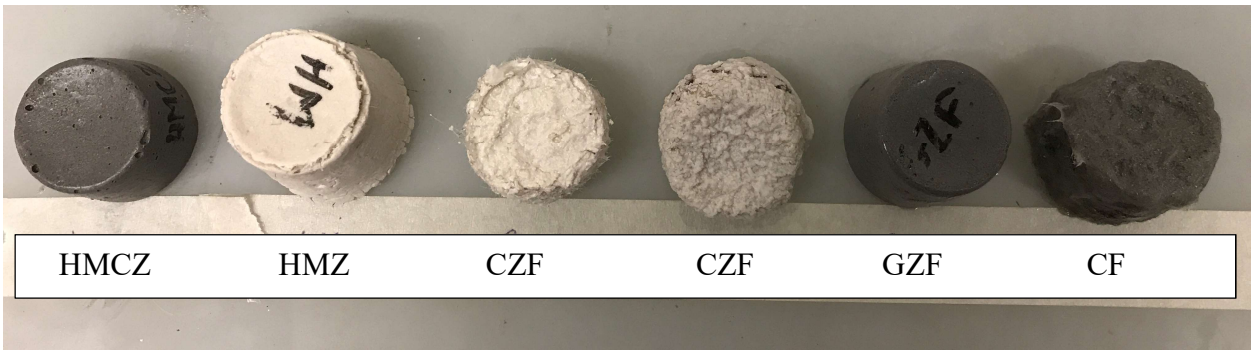

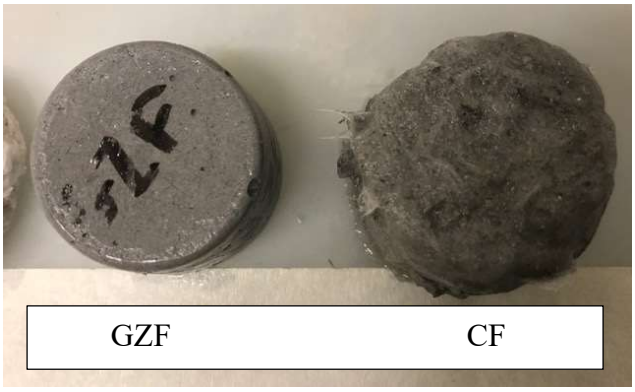

Figure 4-47: Deteriorated samples in acidic environment after 16 weeks of immersion

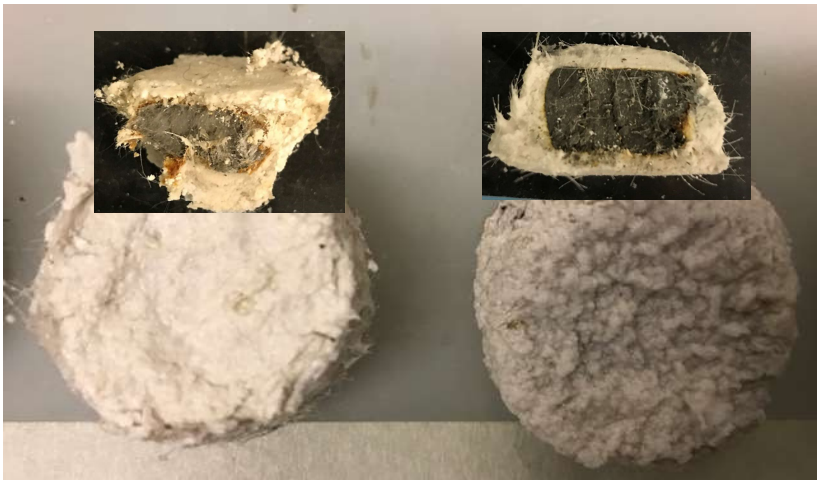

Figure 4-48: CZF samples deteriorated in acidic environment

4.6 Discussion of the development of composite coating integrated with Zn

Prevention of concrete bio-corrosion usually requires modification of concrete mix, introduction of novel cementitious material or application of chemical/antimicrobial resistant thin coating layer on the inner surface of concrete pipe which inhibit biological activity or provide protective layer between concrete surface and corrosive solution. Major materials used to coat concrete pipes include cement mortar, epoxy mortar and polymer-based coatings with variable degrees of success. Most of the coating materials are not resistant to acid attack, have bonding issues with the concrete substrate and in many cases, that bacteria are able of penetrating the coating material and grow on the concrete surface beneath the coating and destroy the bond. So, success with different types of linings and coating materials has been quite variable.

As it was discussed earlier, higher strength or lower porosity do not necessarily enhance the resistance of material to acid attack, but the chemical nature of the material is a key factor that determines the resistance of the coating material in acidic and corrosive environments. Cement-based materials have limited ability to resist acid attack over time in aggressive environments due to its chemical composition and calcium content. The hydrate phases CH (calcium hydroxide) and CSH (Calcium silicate hydrate) and their amount in the medium which is dependent on the proportion contributed by the binder, is a significant determinant of how stable chemically the matrix becomes. Water, which plays a key role in the cementitious process, also actively participates in the chemical reaction. So, examining materials that produce non-traditional hydration products to improve the resistance of pipes to acid attack has risen interest.

In addition, concrete production requires large quantities of Portland cement, production of which is a major contributor to greenhouse gas emissions and raw material. Production of one tone of Portland cement requires about 2.8 ton raw materials and is responsible for about 1 ton of greenhouse gas (CO_2) emission. So, there is a need for replacing cement-based repair materials with durable, economic, effective and also sustainable and environmental friendly alternatives.

In the context of pipe rehabilitation, protective antibacterial coatings are the most widely used means of preventing further corrosion. However, there are common issues associated with these types of coatings such as cost, tendency to the propagation of cracks, pinholes or rips, delamination, corrosion, compatibility with the host material, short bio-resistance lifetime, poor adhesion to the substrate material, long setting time, considerable thermal expansion and toxicity. The most important challenges of using antibacterial agents, bioactive chemicals (biocides) or heavy metals in coating materials include short bio-resistance life time and efficiency. Leachability into the environment, safety concerns and regulations restrict levels of certain metals in sewer systems, poor adhesion to concrete substrate and cost. Also, in high dosages they might affect the structural properties of the coating material. The last but not the least is that some of these heavy metals are toxic and undesirable leaching of them into the surrounding environment cause problems. Also, overuse and abandoned leaching of heavy metals could lead to the speedy development of bacteria that are immune to multiple drugs. Pollution of water and soil with toxic heavy metals and bioactive chemicals is of major concern for human health and environment.

Due to the challenges involved in using biocides and their possible risks for the surrounding ecosystem, increasing attention is being paid to immobilize antibacterial agents inside the coating. The first technique is integrating the antibacterial agent into a carrier which is able to release it slowly to the environment. The aim is to yield a prolonged exposure of the biocide and extend the duration and efficiency of biocidal activity. The most important challenges of using biocide-loading carriers is that in high dosages they might affect the structural properties of the coating material (e.g. strength reduction). The overall performance of biocide-loading carriers is highly dependent on chemical and physical properties of the carrier and its compatibility with other materials. In addition, availability and cost are other important factors that should be considered.

Another method to gain control over the release of antimicrobials is to retain antibacterial ions or heavy metal molecule in the pores (3D framework) of the coating material or combine and solidify them in the coating structure. Immobilizing antibacterial agents with this technique can overcome the common biocide limitations, extend antibacterial activity, reduce health and environmental risks and modulate the release behavior.

The microstructure of geopolymers (similar to zeolites or feldspathoids) is known for excellence ability in absorbing and solidifying chemicals/heavy metal and so they have been used as a potential matrix for waste stabilization during last decade. High Si/Al ratio in these materials creates low anionic field that gives good selectivity toward cations of lower charge such as Ag^{+}, Cu^{2+} and Zn^{2+} and poor selectivity towards cations of higher charge such as Ca^{2+}.

Geopolymer's ability to encapsulate heavy metals such as Zn^{2+}, Cu^{2+} Cr^{3+}, Cd^{2+}, Pb^{2+}, TiO_2 and MnO with minimum losses in strength is reported by many researchers. However, the ability of encapsulation of geopolymers is dependent on the pH of the leaching compounds. Also, the upper limit of the heavy metal content which can be encapsulated in the geopolymer matrix is very low and limited. The system can tolerate limited amounts before it becomes chemicaly or physically unstable and leaching levels become inappropriate.

Two types of corrosion resistant coating materials with encapsulating properties were evaluated in this chapter. The first material is geopolymer and the second one is a blended mix of magnesium phosphate hydrates phase form in conjunction with geopolymer matrix. The aim of combining these two matrixes was to take advantage of each system's individual corrosion resistant properties, strength, adding long-lasting anticorrosion properties, increasing the degree of encapsulation and creating denser matrix. Furthermore, the fineness of hydrated magnesium phosphate particles is much higher than ordinary Portland cement particles. Due to this fineness, magnesium phosphate reacts much faster with water. Un-hydrated magnesium oxide particles are able of consuming extra water produced during geopolymerization process and produce magnesium hydroxide which could react with sulfuric acid and produce $MgSO_4$ and increase the pH. Combining magnesium phosphate matrix with fly ash also reduce the cost which is very favorable to sustainable development and environmental protection.

Different geopolymer mixes are prepared in section 4.4 and the best mix was chosen according to chemical stability and highest compressive and tensile strength properties. Then in section 4.5 different blended mixes of magnesium phosphate hydrate-geopolymer were prepared and evaluated according to chemical stability and tensile strength properties. SEM-EDS was used to

investigate the microstructure and composition of developed materials. Summary of the tests is shown in Table 4.12.

Table 4-12: Summary of the tests

Test	# Specimens	Testing Interval
Compressive strength	9 × 3	Age 14 days
Uniaxial tensile test	11 × 3	Age 7 days
SEM-EDS	30 points per sample	Age 14 days
Chemical stability	12	Every two weeks for four months

Then the best geopolymer and blended mixes were integrated with zinc-oxide particles and Zn-doped clay particles. Zn-doped clay particles preparation and properties are described in section 4.3. Leaching and chemical stability, tensile strength, bonding and shrinkage properties of final mixes were tested to evaluate the performance of the developed materials. Summary of the tests is shown in Table 4.13. Results show that geopolymer and Zn-doped coatings demonstrated significant improvements when compared with other coatings. Visual evidence confirms the better performance of these coatings over the defined period of observation.

Table 4-13: Summary of the tests

Test (Composite coatings)	**# Specimens**	**Testing Interval**
Bonding	6 × 3	Age 17 days
Uniaxial tensile test	5 × 3	Age 7 and 14 days
Toughness	5 × 3	Age 7 and 14 days
SEM-EDS	30 points per sample	Age 14 days
Chemical stability	6	Every two weeks for four months
Shrinkage	6 × 4	72 hours

Chapter 5: Evaluation of different coatings for protection of concrete against biogenic acid attack in sewage pipes

In this chapter, different types of coating materials including cement-based, geopolymer-based and multiphase composite are evaluated. Two different systems were considered to gain control over the release of zinc particles embedded in the coating matrix. The first mechanism was to keep the heavy metal molecule in 3D framework of geopolymer and magnesium phosphate. The second approach is to use sodium bentonite clay impregnated with zinc ions and functionalize it as an antimicrobial agent then mixed with different coating materials. As it was shown in Chapter 4, Zn-doped clay has acceptable mechanical properties and biocompatibility with the host coating material and can be integrated as a carrier loaded with the biocide into protective coatings. While there are studies of the antimicrobial characteristics of clay functionalized with heavy metals, the feasibility and properties of geopolymer-based and multiphase composite coatings integrated with zinc doped bentonite clay in accelerated bio-corrosion chamber has not been investigated.

Thirty arch-shaped mortar samples were cast to represent the top half of the concrete pipe and near the water level. Each set including 15 samples were coated and tested over the 6 months period. Prepared cement mortar samples, having a w/c of 0.5, were de-molded at 24 hours, and stored in curing room with 95% humidity and temperature (22 ±3°C) for 28 days.

Six corroded samples were also coated with developed coating materials and tested in the chamber to evaluate the performance of coating materials as a repair on corroded samples.

A combination of multiple evaluation tests and indicators were conducted to compare the relative performance of cement-based, geopolymer-based and blended composite-based coatings mixed with ZnO and Zn-doped clay particles after 6 months in corrosion chamber. The corrosion rate determined by measuring the reduction in flexural strength and evaluating the bond, pH variations and corrosion resistant properties of different coating materials. Also, the corrosion products were investigated by SEM.

5.1 Coating preparation

Three different sets of material were prepared; cement-based, geopolymer-based and blended composite-based coatings, details of the material properties are found in Chapter 4. Table 5.1 summarized the properties and challenges of each set of the coating material for sewage pipe application. Fly ash and zinc-doped bentonite clay were used as the precursor material and extra source of alumino-silicate in geopolymerization process. The alkali reactant solutions of sodium silicate-sodium hydroxide were used for alkalination of geopolymer. Details of the mix designs, test results and properties are provided in Chapter 4. A summary of the mix designs of different coatings is seen in Table 5.2.

Table 5-1: Advantages and disadvantages of different types of coating materials

Advantage	Coating material	challenge
Compatibility with the host material	Fiber reinforced Cement based coating **(CF)**	Porosity
Low cost		sustainability
Good bonding		Durability (corrosive material)
Good bond	Antibacterial fiber reinforced cement-based coating mixed with Zn particles **(CZF)**	Durability (corrosive material)
Compatibility with the host material		Short bio-resistance lifetime due to leaching
Low cost		Porosity
Antibacterial properties		Required Higher concentrations of antibacterial agent to have long term effect
		Contaminating surrounding environment
		Sustainability
Good bond, low cost	Antibacterial cement-based coating containing Zn-doped clay **(CCZF)**	Durability (corrosive material)
Compatibility with the host material		Sustainability
Slow released antibacterial properties		Mechanical properties (More clay should be used to get specific amount of Zn)
Good bond	Fiber reinforced Geopolymer coating **(GF)**	Porosity
Low cost		
More durable, high alkalinity		
Sustainable material		
Encapsulating properties	Antibacterial- Fiber reinforced Geopolymer mixed with ZnO **(GZF)**	Low Degree of encapsulation
Antibacterial properties		Porosity
More Durable, High alkalinity, good bond		
Sustainable material, Low cost		
High degree of encapsulation	Antibacterial- Fiber reinforced Geopolymer containing Zn-doped clay **(GCZF)**	Mechanical properties (More clay should be used to get specific amount of Zn)
Less corrosive, High alkalinity		Porosity
Good bond		Setting time
Slow released antibacterial properties		
Sustainable material		
Denser matrix	Multi-phase composite **(HM)**	Mechanical properties is unknown
Sustainable material		
Durability, good bond, self-healing properties		
Higher degree of encapsulation	Multi-phase composite containing Zn-doped clay **(HMCZ)**	Setting time
Denser matrix		Some mechanical properties is unknown
Durability, good bond, self-healing properties		
Slow released antibacterial properties		
Sustainable material		
Encapsulating properties	Multi-phase composite containing ZnO **(HM)**	Mechanical properties are unknown
Denser matrix, self-healing properties		
Durability, good bond		
Antibacterial properties		
Sustainable material		

Table 5-2: Mix design of different coating materials

	Tag	Water/binder	Zinc oxide/binder	Zinc-doped clay/binder	Sodium silicate/sodium hydroxide	MgO/PP
Reference-No coating	R	0.45	0	0	0	0
Cement-based coatings	CF	0.45	0	0	0	0
	CZF	0.45	0.14	0	0	0
	CCZF	0.45	0	0.5	0	0
Geopolymer-based coatings	GF	0.2	0	0	2.5	0
	GZF	0.2	0.14	0	2.5	0
	GCZF	0.2	0	0.5	2.5	0
Multiphase composite coatings	HM1	0.25	0.14	0	2.5	1.5
	HM1CZ	0.25	0	0.5	2.5	1.5
	HM1P	0.25	0.14	0	2.5	1.2
	HM1PCZ	0.25	0	0.5	2.5	1.2

Note: 0.1% Ply-Vinyl Alcohol (PVA) fiber is added to each mix design

5.2 Coating application

Arch-shaped mortar samples were cast to represent the top half of the concrete pipe and near the water level (Fig 5.1). Prepared cement mortar samples, having a w/c ratio of 0.5 were de-molded at 24 hours, and stored in curing room with 95% humidity and temperature (22 ±3°C) for 28 days. The average dry weights of the samples were 1.57 kg.

Figure 5-1: Casting arch-shaped mortar base for coatings

Different coating materials were applied on arch-shaped samples, see Table 5.2. Surface roughness plays an important role in the interfacial bond strength of coating materials. Therefore, before applying coating materials, arch-shaped samples were sand blasted to make sure that a good bond was developed afterwards. Performed sand blasting was very challenging and difficult due to the sample's special shape and achievement of even roughness along the samples. An industrial wet sandblasting kit was used from ATPRO Powerclean Equipment (398cc Honda GX390 4000 PSI BE). It consisted of sandblasting blue tank and plywood cover and an industrial floor lamp as could be seen in Figure 5.2.

Figure 5-2: Sandblasting system

Once the surface preparation process was completed, coatings were applied on samples (Figure 5.3). Then samples were covered with plastic tenting to avoid moisture loss for 24 hours. Samples were then placed in a closed container and sprayed with water twice daily for a duration of 14 days. The humidity inside the box was measured to be at 90% (±2%).

Poor drying conditions, over-brushing during the application, thickness of the coatings or the geometric shape of the samples caused small shrinkage induced surface cracks on some samples.

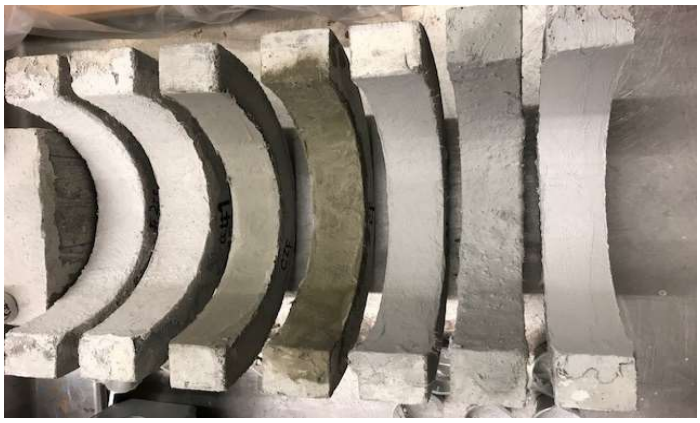

Figure 5-3: Application of different coatings on the surface of arch-shaped samples

5.3 Bacterial-induced corrosion experiment

The resistance of the zinc-doped coatings to biogenic corrosion caused by sulphur oxidizing bacteria was investigated by testing coated samples in the accelerated test chamber over the 6-month period. As described in Chapter 1, sulphate reducing bacteria (SRB) bacteria break down the organic matter and use sulfates present in wastewater and release sulfur ions. The sulfur ions released by bacteria react with dissolved hydrogen in the wastewater and form H_2S which gradually dissolves into the moist film that forms on the crown and walls of the sewer. Both CS and CSH (Calcium silicate hydrate) constituents of the concrete are able to react with H_2S and produce calcium sulfide (CaS) which is not stable in acidic solution and converts into calcium hydrogen sulfide ($Ca(HS)_2$) when H_2S is available. During the neutralization process, the pH of the concrete surfaces is reduced due to the carbonation and H_2S acidification and so the concrete surface changes to a more favorable environment for bacteria to grow on. Then, aerobic sulfur oxidizing bacteria (SOB) can inoculate on the concrete surface and use the diffused H_2S as a food source and oxidize sulfur compounds to sulfuric acid.

Generated sulfuric acid penetrates into the pores, reduces concrete alkalinity and dissolves calcium hydroxide. H_2SO_4 reacts with CH (calcium hydroxide) and CSH (Calcium silicate hydrate) to form gypsum, followed by reaction of gypsum with tri-calcium aluminate to form Ettringite. Corroded parts can be removed from the concrete wall by the flowing sewage during time.

In this study, a close-to-reality novel laboratory test method was designed for observing and measuring corrosion rate at different corrosion stages. Details of the designed accelerated test chamber are found in Chapter 2. Multiple stages of corrosion in actual concrete pipes and simulated conditions in the accelerated test chamber is summarized in Table 2.1 of Chapter 2.

For modeling bio-corrosion processes, two oxidizing-sulfur bacteria species, T. Thioparus (NSOB) and A. Thiooxidans (ASOB) strains were purchased from American type culture collection and cultivated according to ATCC medium 125 and 290S6. These microorganisms were kept in refrigerator at 4°C in a liquid medium. Test specimens were sprayed with Thiooxidans and Thioparus every 2 weeks for 6 months.

Excellent adhesion to the host material, acceptable mechanical strength after corrosion and high chemical and corrosion resistance of coating material are the most important factors that make the material suitable for pipeline applications. In this study, a combination of multiple evaluation tests and indicators are conducted to compare the relative performance of different coating materials after bio-corrosion. The corrosion rate determined by measuring the reduction in flexural strength and evaluating the corrosion resistant properties of different coating materials. Also, the corrosion products were investigated by SEM. During the test, the chamber's condition (pressure, Humidity, gases concentrations, sewage pH and temperature) were monitored continuously. Figure 5.4 shows how the specimens where positioned in the accelerated test chamber.

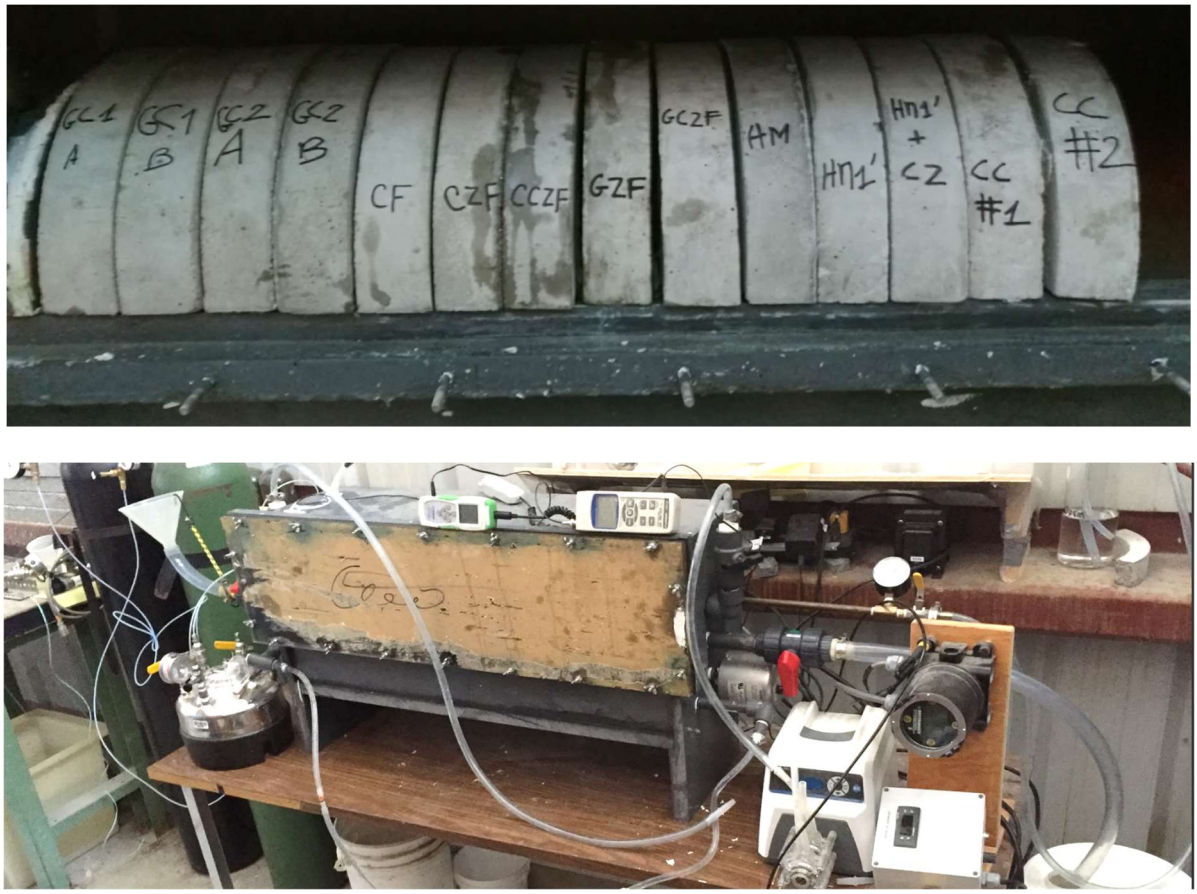

Figure 5-4: Position of the specimens in the designed accelerated test chamber

5.4 Surface pH measurements

The surface pH of samples was measured every two weeks for 6 months. A flat surface pH electrode (Extech 601100) is used to measure surface pH over time. For each measurement, the surface of the samples was wetted with about 1 ml of water. Five readings were made to determine the average value. Results are plotted in Fig 5.5.

At the beginning of the biocorrosion process (Figure 3.4), pH dropped to around 7-8. This happened while the samples were exposed to high gas concentration and biogenic acid to make the surface more favorable for bacterial growth. Afterwards the rate of pH variations slows down.

Initially the samples high pH and neutralization properties of coating compounds prevent the growth of bacteria. That's why the rate of pH variations up to 56 days is slower (Figure 3.4). Gradually, the neutralizing capacity of the samples is reduced, and the bacteria start to grow and reduces the pH faster on the surface. In addition, due to an increase in the porosity of the samples, pH drops quicker towards the end of the cycle. It was observed that the pH dropped between 120 to 180 days was much faster compare to rest if the bio-corrosion process. According to the results, the surface pH of cement-based coatings was reduced at a higher rate than geopolymer-based and multiphase composite coatings.

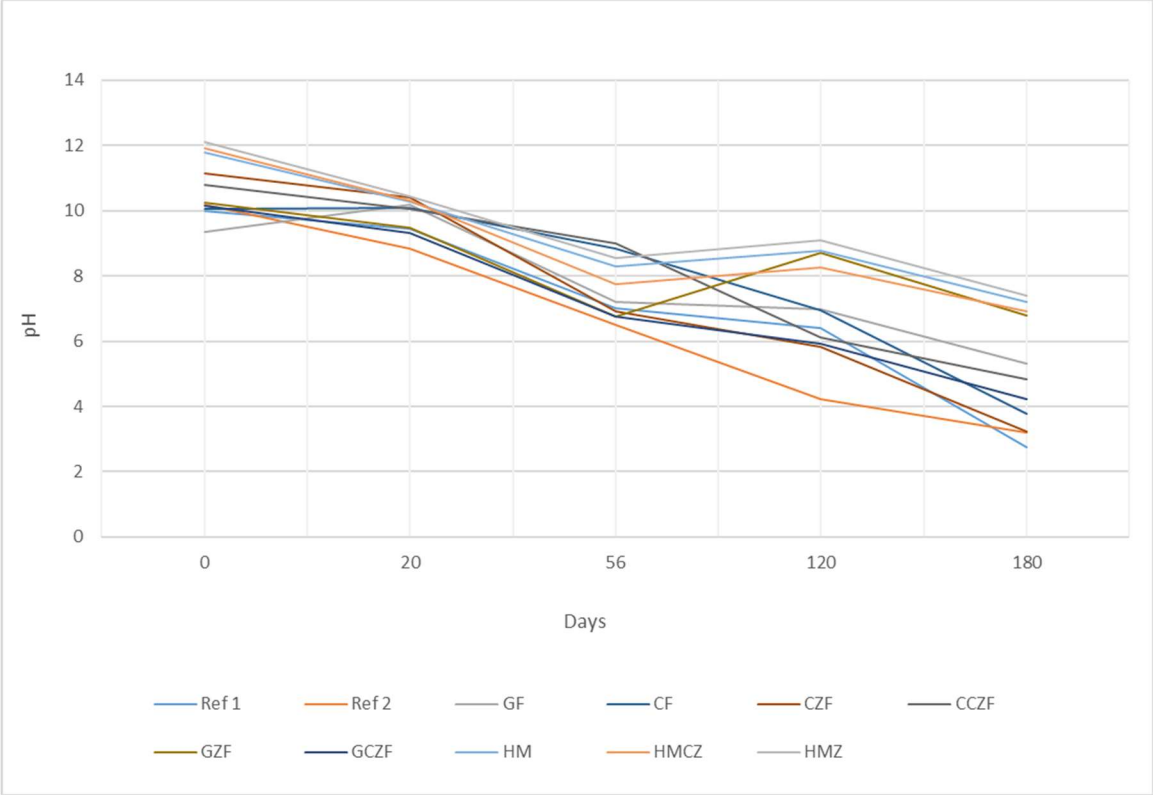

Figure 5-5: Sample's surface pH variations

As seen in Figure 5.5, surface pH of the blended samples was a little bit higher than other samples at the beginning and reduced to between 7 after 180 days. Geopolymers samples surface pH are also reduced to minimum 6 after 180 days. However, pH of cement-based samples reduced to around 3 at the end of the corrosion cycle. pH reduction in samples integrated with zinc particles

were less compare to other samples which shows Zn particles were successful in inhibiting the growth of bacteria and acid production. Also, Zn particles densify the matrix and inhibit acid penetration.

5.5 Flexural strength loss

After 180 days, resistance (capacity) of arch-shaped concrete samples coated with different materials were tested subjected to three-point bending.

As could be seen in Table 5.3 and Figure 5.6, uncoated samples show higher deflection during the corrosion process compare to coated samples. Corroded sample's average deflection increased by 51% after 180 days in chamber. According to the results the peak load decreased by 73% and the corresponding deflection increased by 25.5% after 180 days in corrosion chamber.

Table 5-3: Average ultimate strength and standard deviation of arch-shaped concrete samples coated with different materials after corrosion, CF: Cement mortar coating, CZF: Cement mortar coating mixed with ZnO, GZF: Geopolymer coating mixed with ZnO, GCZF: Geopolymer coating combined with Zn-doped clay particles, HMZ: composite coating mixed with ZnO, HMCZ: composite coating mixed with Zn-doped clay particles

Coating	**Ave. ultimate strength**	**σ**
Reference sample	4306.77	34
Uncoated sample	1120.65	81
CF	1438	54
CZF	1816	121
HMCZ	1710	32
HMZ	2108	43
GZF	2412	56
GCZF	2811	63

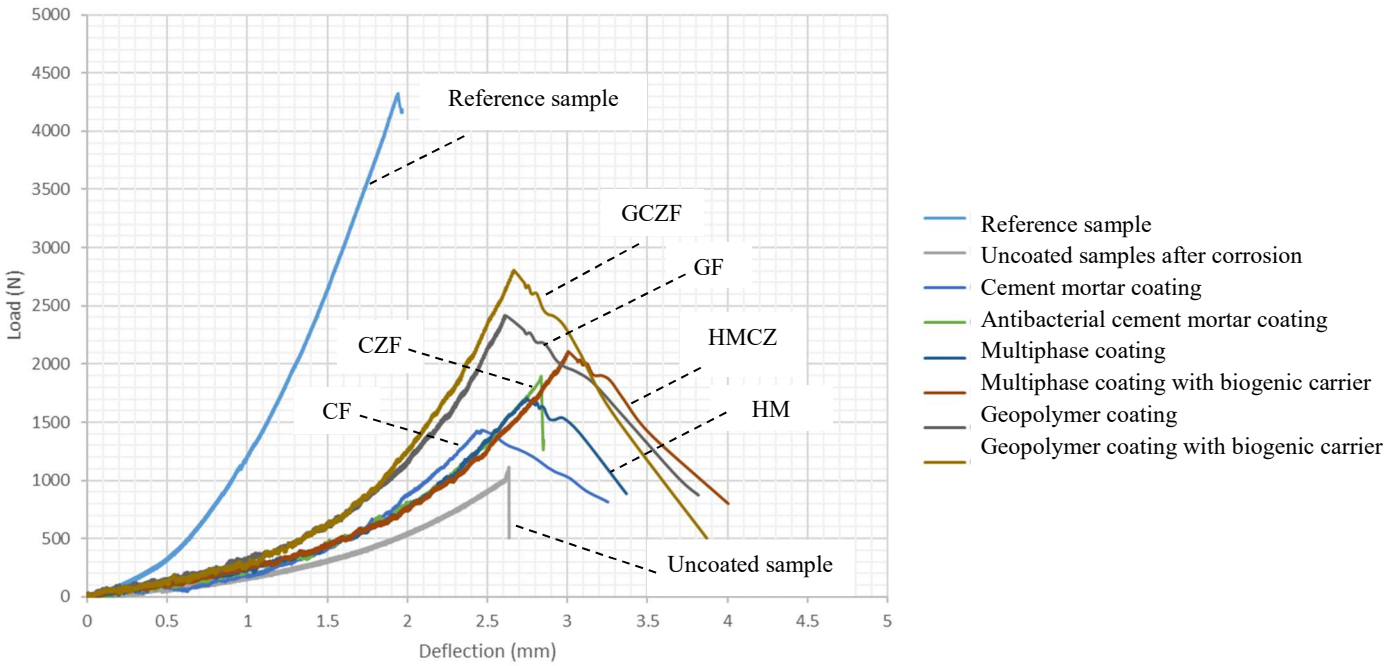

Figure 5-6: Load-deflection curves: effect of corrosion on the ultimate load bearing capacity of the samples

Not much change in remaining strength was observed between CF and CZF which means although the zinc particles were successful in keeping the pH higher and inhibiting bacterial growth on the surface, still hydrated cement particles corroded and detached from the surface.
However, for the samples coated with cement-based material, strength reduction was up to 52%. This means coating concrete pipes with cement mortar material slightly enhanced the resistance of the pipe towards corrosion. However, this would not last long since the material get corroded over time and disappears.

Overall much better performance was observed for geopolymer-based and multiphase composite coatings (MCC). Samples coated with MCC mixes and geopolymer-based coatings integrated with zinc particles lost strength up to around 35% which is less than uncoated samples or the samples coated with cement mortar. Ultimately, coatings were applied on uncoated corroded samples and tested under bending. Results of the flexural test displayed in Figure 5.7 showed that coating deteriorated pipe with the developed coating materials can restore samples strength between 30-60%. Uncoated samples strength after corrosion was around 1000 N, after coating the corroded sample the ultimate strength increased to around 3500 N for GCZF coating.

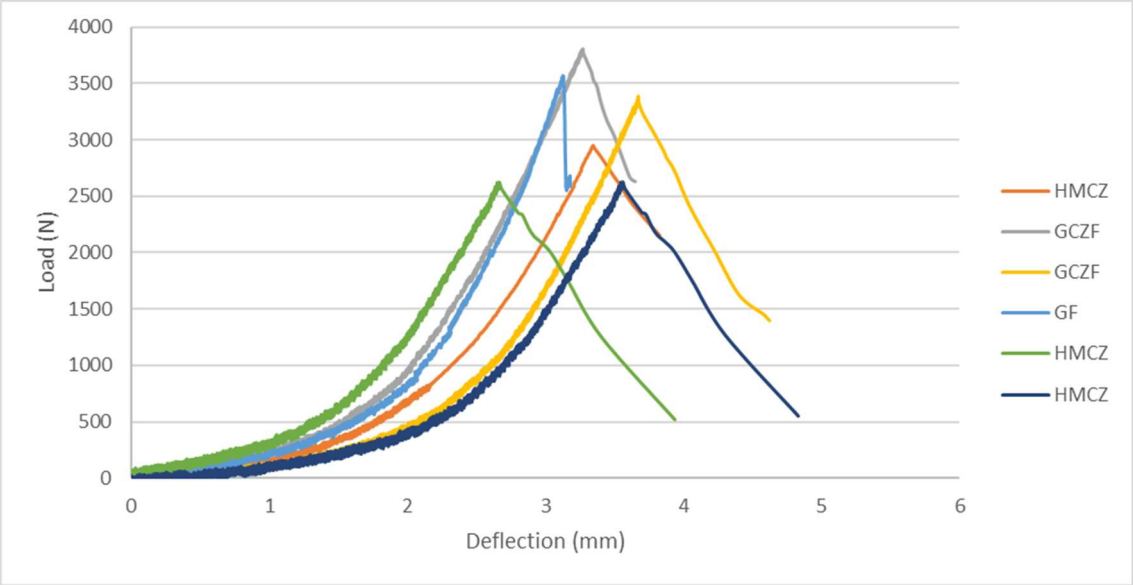

Figure 5-7: Ultimate load-bearing capacity of the corroded samples coated with multiphase composite coating

5.6 Surface morphology

Properties and microstructure of the coatings before and after corrosion were studied using scanning electron microscope (SEM), Figure 5.8, 5.9 and 5.11.

(a) CF-Before corrosion

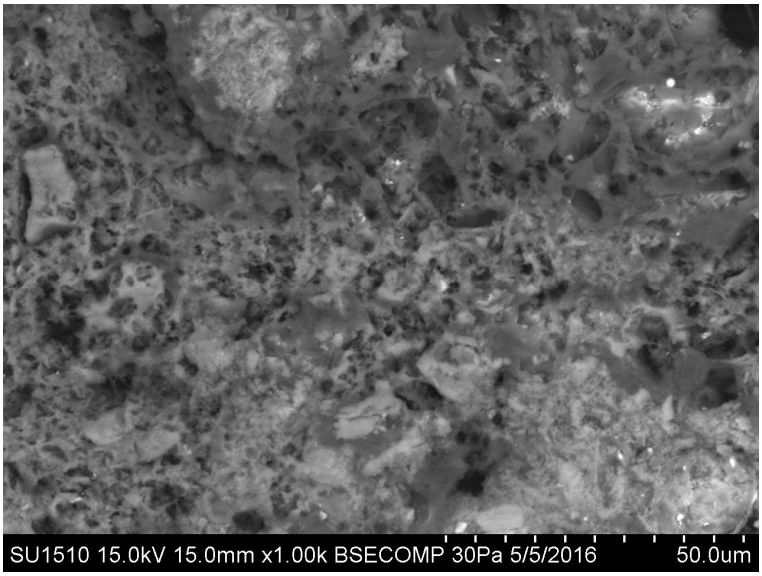

(b) CF-After corrosion

Figure 5-8: SEM images of CF coating before and after bio-corrosion process in this experiment

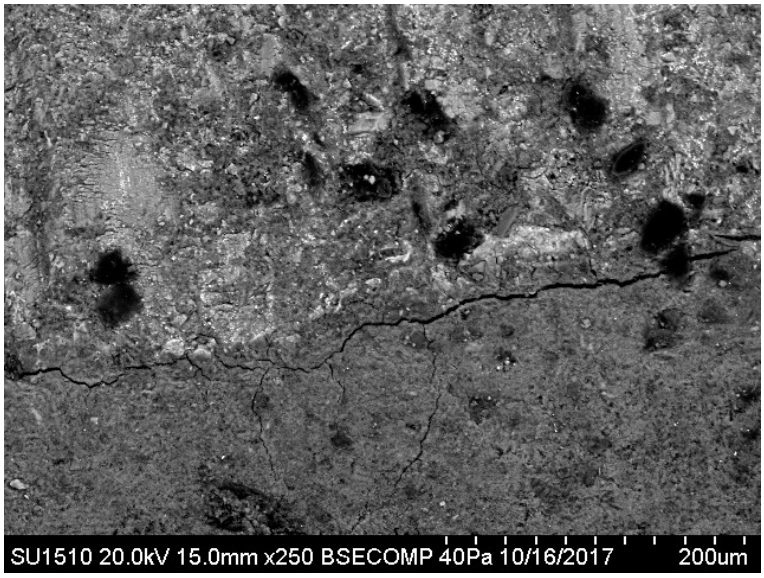

Figure 5-9: SEM image of interface between corroded and non-corroded parts in CZF coating

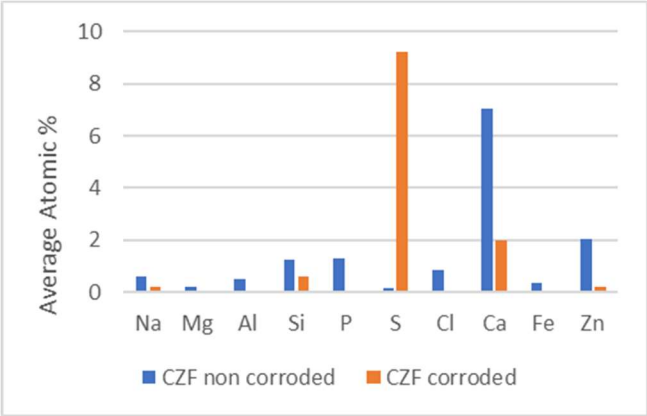

Figure 5-10: Comparison between the chemical composition of CZF before and after corrosion

As could be seen in Figure 5.8, cement mortar samples corroded severely. As it was described in chapter 2, biological activity and the reaction of diffused H_2S on sample's surface produce sulfuric acid. Creation of localized acidic conditions in pores and cracks cause dissolution of C_2S and C_3S. Sulfuric acid reaction with the CH and CSH constituents of the hydrated cement produce expansive products such as gypsum. So, dissolved and ionized calcium move easily through connected network of pores in the corroded cement matrix and leach out of the system. Leached calcium can react with calcium carbonate in the air above the sewage and form calcite (calcium carbonate). As

the pH value of the surface reduces due to carbonation and bacterial activity, calcite becomes soluble and leaves the matrix. Figure 5.10 indicates that S increase in corroded cement mortar samples compare to non-corroded samples. Zn and Ca completely leached out of the system after 6 months. There is a big crack and detachment between corroded parts and non-corroded parts in CZF samples, see Figure 5.9.

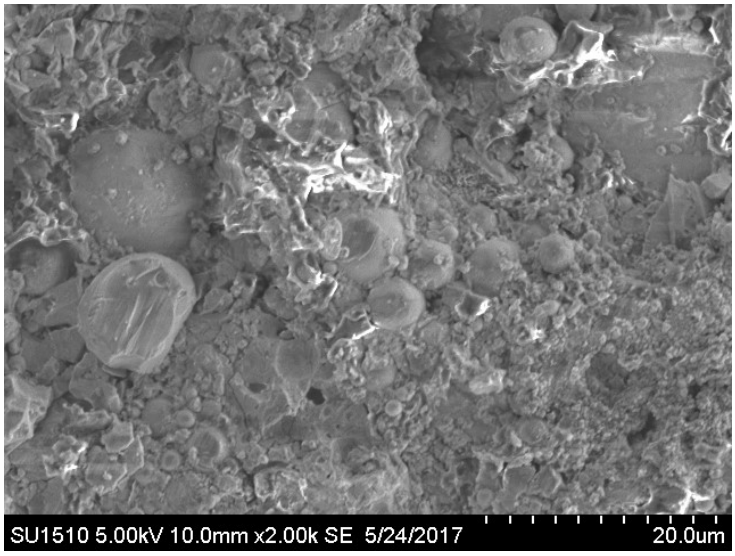

(a) GF- Before corrosion

(b) GF- After corrosion

Figure 5-11: SEM images of GF coating before and after biocorrosion process

According to Figure 5.12 and 5.13, although the microstructure of GZF changed slightly after biogenic acid attack, Zn particles did not leach out of the system much, see Figure 5.13. This suggests that antibacterial particles are encapsulated in geopolymer matrix successfully, but the amount of Si and Ca was reduced and S was increased in the matrix after corrosion which changed the surface microstructure.

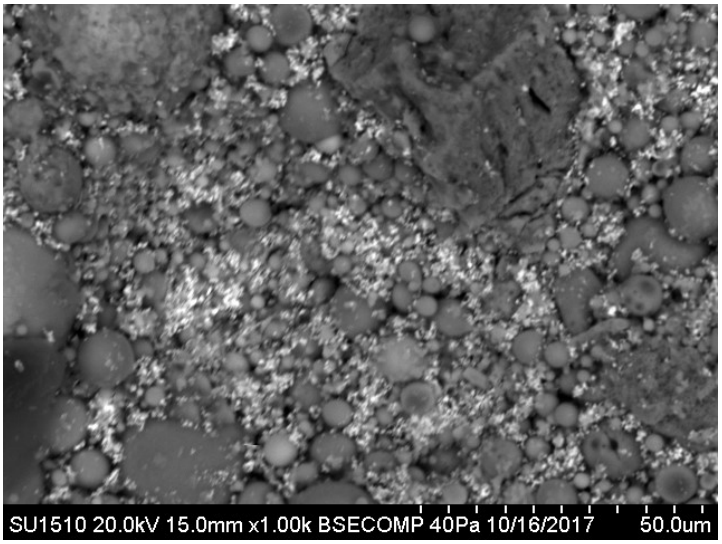

(a)GZF before corrosion

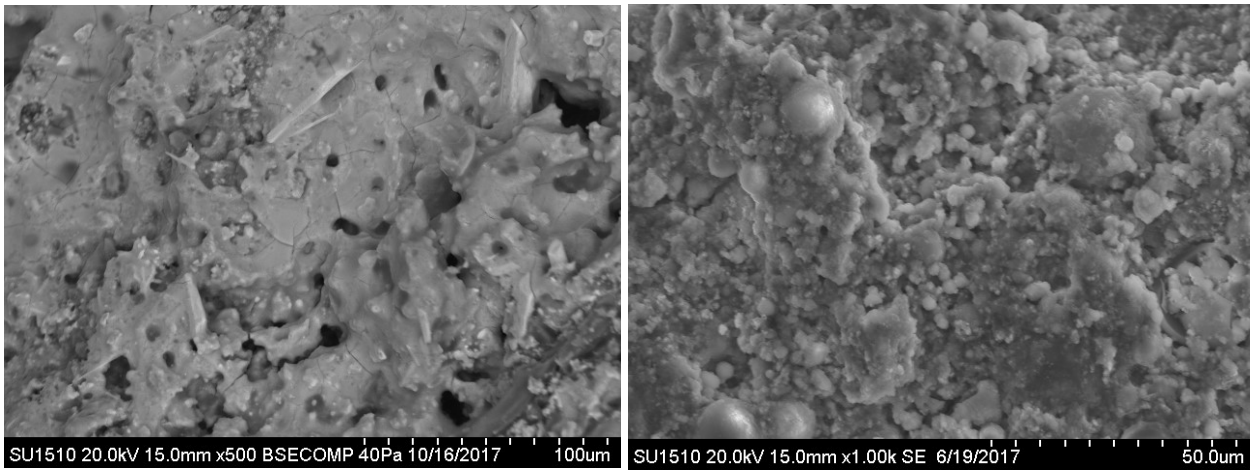

(b)GZF after corrosion

Figure 5-12: SEM images of GZF coating before and after biocorrosion process

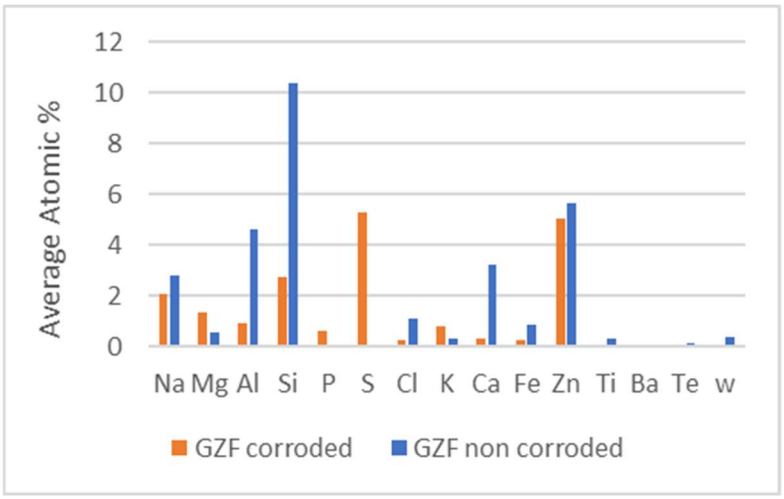

Figure 5-13: Comparison between the chemical composition of CZF before and after corrosion

According to Figure 5.14, HM microstructure was not compact after corrosion and the crystalline structure is affected by the biogenic acid attack. Unreacted fly ash particles acted as filler and strengthen the composite. By looking at the chemical composition of HM coating before and after corrosion, Figure 5.15, it could be concluded that the Zn particles were encapsulated in the system successfully. The amount of Zn particles in the coating before and after corrosion appears to be equal.

By comparing the encapsulation potential of geopolymer with MCC (multiphase composite coating) mix, it could be concluded that degree of encapsulation and immobilization of Zn particles in blended matrix was better when compared to geopolymer matrix. Also, the amount of leached Si in the MCC mix was lower compared to geopolymer mix after corrosion. However, Ca still leached and appears carbonated on the corroded surface. More microcracks were evident on the surface of the corroded HMZ compared to GZF.

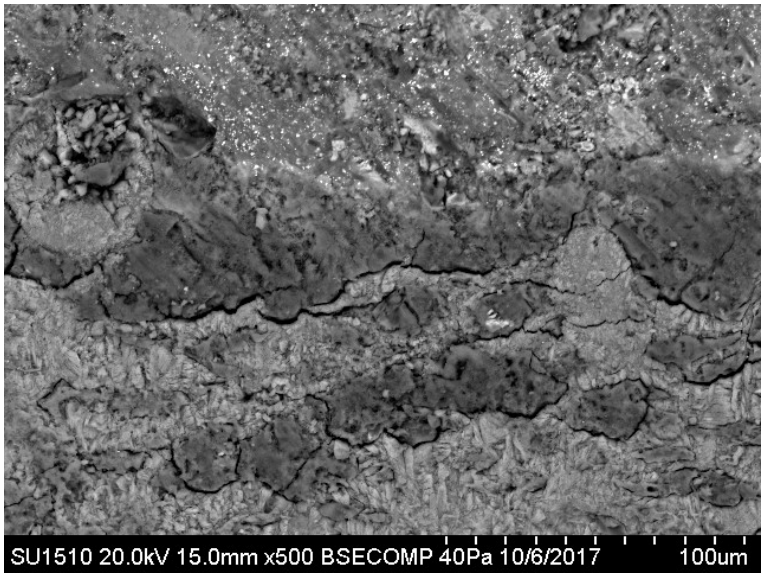

Figure 5-14: SEM image of interface between corroded and non-corroded parts in HMZ coating, Top: non-corroded part, Bottom: corroded part

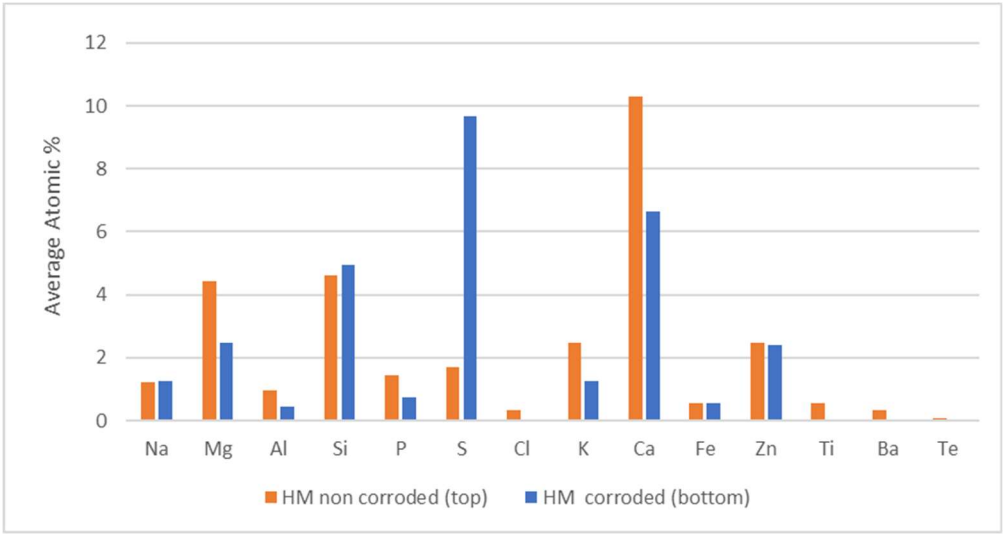

Figure 5-15: Comparison between the chemical composition of HMZ before and after corrosion

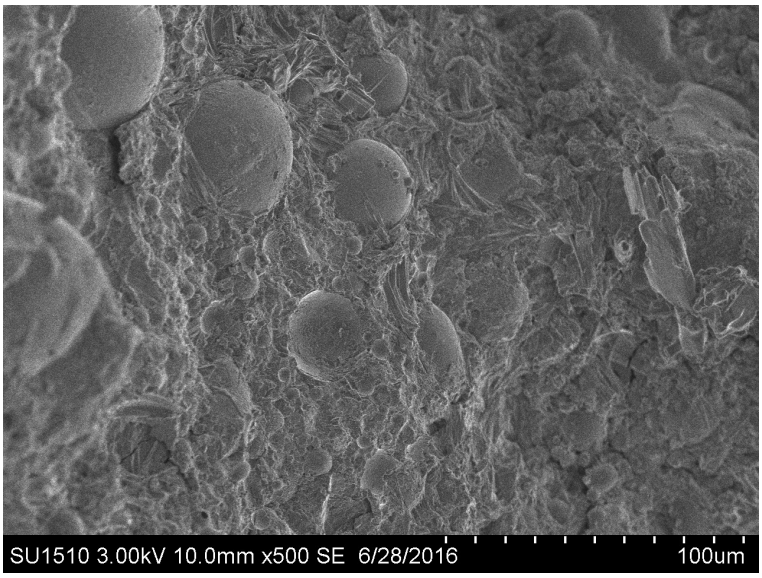

(a) HMCZ before corrosion

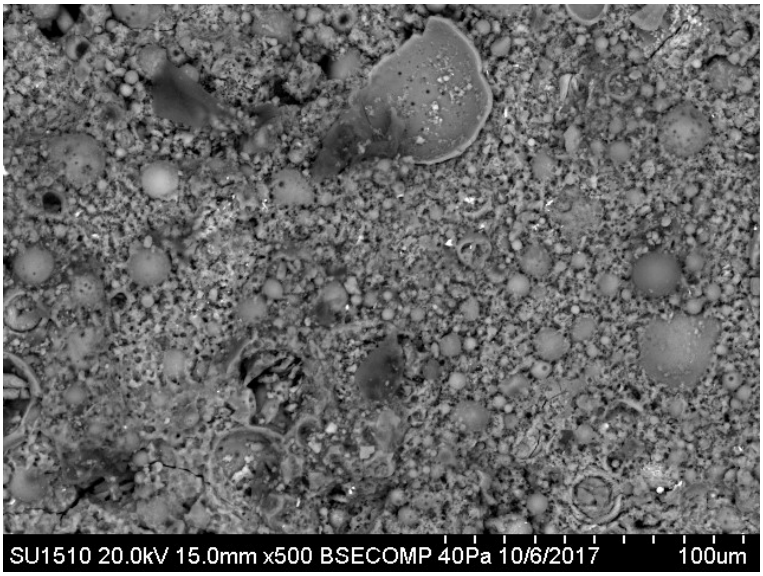

(b) HMCZ after corrosion

Figure 5-16: SEM images of HMCZ coating before and after biocorrosion process

By examining the microstructure of the multiphase composite HMCZ coating before corrosion, Figure 5.16 (a), it is clear that the amorphous geopolymer matrix appears strongly bonded together with crystalline hydrates of MgO. Also, aluminum phosphate gel is formed which is distributed in amorphous phase, coating the particles and glues particles to each other which made the

microstructure compact compared to the original geopolymer. However, Figure 5.16 (b) shows that the microstructure affected after corrosion. Although the porousity of the system increased after corrosion, Figure 5.17 indicates that Zn attached and entrapped in bentobite clay particles in the system perfectly. Also, the swelling properties of clay minerals has the blocking effect against the dissolved ions in the water inside the pores.

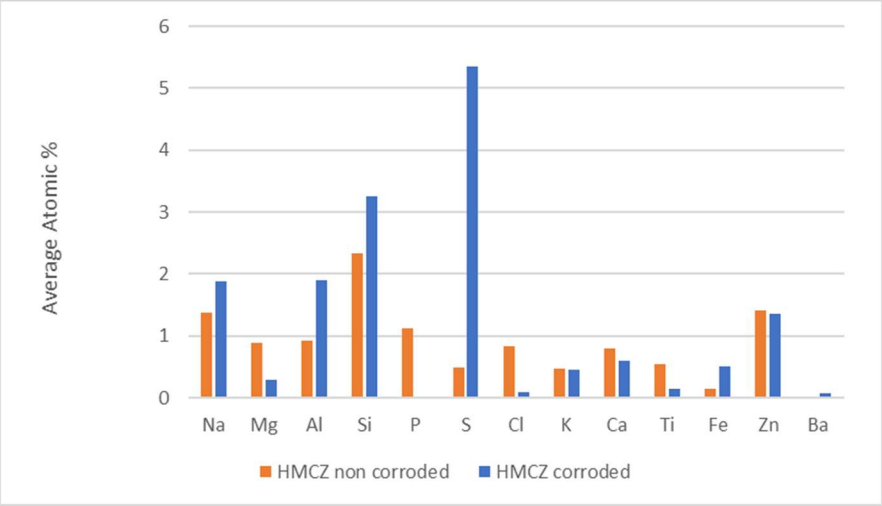

Figure 5-17: Comparison between the chemical composition of HMCZ before and after corrosion

5.7 Pull-off test

Pull-off testing was conducted following ASTM standard D7234-12 on corroded samples. Three to five samples were taken from each arch to obtain a value for bond strength. The purpose of the pull-off test is to verify if the coating surfaces still have sufficient strength to resist delamination. Uncertainties from the test included the amount of micro-cracking along the surface from flexural testing, and the curvature of the bonding surface.

Figure 5-18: Pull-off test set-up

With an average bond strength of 1.87 MPa and 1.92, the HMZ and HM corroded systems were able to display a good bond strength after accelerated bio-acid attack. Geopolymer-based samples performed at a pull-off strength of average 2.11 MPa, 2.29 MPa, and 2.78 MPa for GZF, GCZF and GF respectively. However, bond strength of CF, HMCZ and CZF and CCZF were below 1.2 after the bio-corrosion process.

Weak bond strength between cement mortar coatings and substrate showed that the acidic solutions penetrated the porous system and affected the bond beneath the coating. Overall, HMCZ showed promising results and properties, however the mixed designed should be optimized towards enhancing its bond with concrete substrate.

5.8 Discussion of the performance of different coating materials against biogenic acid attack

Different types of coating materials including cement-based, Geopolymer-based and multiphase composite were evaluated. Two different systems were considered to gain control over the release of zinc particles embedded in the coating matrix. The first mechanism was to keep the heavy metal molecule in 3D framework of geopolymer and magnesium phosphate. The second approach was to use sodium bentonite clay impregnated with zinc ions and functionalize it as an antimicrobial agent then mixed with different coating materials.

Thirty arch-shaped mortar samples were cast to represent the top half of the concrete pipe and near the water level. Samples were coated and tested in accelerated bio-corrosion chamber over the 6 months period. Six corroded samples were also coated with developed coating materials and tested in the chamber to evaluate the performance of coating materials as a repair on corroded samples.

A combination of multiple evaluation tests and indicators were conducted to compare the relative performance of cement-based, geopolymer-based and MCC composite coatings mixed with ZnO and Zn-doped clay particles after 6 months in corrosion chamber. The corrosion rate determined by measuring the reduction in flexural strength and evaluating the pH variations, bond and corrosion resistant properties of different coating materials. Also, the corrosion products were investigated by SEM. Table 5.4 shows the summary of the tests.

Table 5-4: Summary of the tests

Test	# Specimens	Testing Interval	Variations	CV
pH	24 × 5	Every 2 weeks for 6 months	12-3	10-35%
Flexural strength	24	---	35- 52%	---
SEM-EDS	18 × 3	Every 60 days for 6 months	---	---
Strength restoration	6	After 180 days	30-60%	---
Bond	9×3	After 180 days	1.2- 2.78 MPa	8-10%

Initially the high pH of samples and neutralization properties of coating compounds prevented the growth of bacteria. For this reason, the rate of pH variations up to 56 days is slower. Gradually, the neutralizing capacity of the samples was reduced, and the bacteria start to grow and lowers down the pH faster on the surface. In addition, due to an increase in the porosity of the samples, pH dropped quicker towards the end of the cycle. It was observed that the pH drop between 120 to 180 days was much faster compared to rest if the bio-corrosion process. According to the results, the surface pH of cement-based coatings reduced at a higher rate than geopolymer-based and multiphase composite coatings.

As could be seen in Figure 5.5, pH of the blended samples are a little bit higher than other samples at the beginning and reduced to between 7 after 180 days. Geopolymers samples pH are also reduced to minimum 6 after 180 days. However, pH of cement-based samples reduced to around 3 at the end of the corrosion cycle. pH reduction in samples integrated with zinc particles were less compared to other samples which shows Zn particles were successful in inhibiting the growth of bacteria and acid production.

Properties and microstructure of the coatings before and after corrosion were also studied using SEM-EDS. Results demonstrated cement mortar samples corroded severely. Creation of localized acidic conditions in pores and cracks cause dissolution of C_2S and C_3S. Sulfuric acid reaction with the CH and CSH constituents of the hydrated cement produce expansive products such as gypsum.

So, dissolved and ionized calcium move easily through the connected network of pores in corroded cement matrix and leach out of the system. Leached calcium can react with calcium carbonate in the air above the sewage and form calcite (calcium carbonate). As the pH value of the surface reduces due to carbonation and bacterial activity, calcite becomes soluble and leaves the matrix.

Unreacted fly ash particles acted as filler and strengthen the composite. By looking at the results of chemical composition of HM coating before and after corrosion, it could be concluded that the Zn particles encapsulated in the system successfully. The amount of Zn particles in the coating before and after corrosion is equal. By comparing the encapsulation potential of geopolymer with blended mix, it could be concluded that degree of encapsulation and immobilization of Zn particles in blended matrix has improved compare to geopolymer matrix. Also, the amount of leached Si in the blended mix was lower compare to geopolymer mix after corrosion.

It is clear that the amorphous geopolymer matrix can strongly bond together with crystalline hydrates of MgO in HMCZ matrix before corrosion. Also, aluminum phosphate gel is formed which is distributed in the amorphous phase, coating the particles and glues particles to each other which made the microstructure compact compared to the original geopolymer. Although the microstructure and porosity of the system changed slightly after corrosion, results indicate that Zn attached and entrapped in bentobite clay particles well. Also, the swelling properties of clay minerals have the blocking effect against the dissolved ions in the water inside the pores.

According to the results of the flexural strength test, uncoated samples show higher deflection during the corrosion process compare to coated samples. The average deflection of corroded samples increased by 51% after 180 days in the chamber. Results demonstrated the peak load decreased by 73% and the corresponding deflection increased by 25.5% after 180 days in corrosion chamber.

Not much change in remaining strength was observed between CF and CZF which means that although the zinc particles were successful in keeping the pH higher and inhibiting bacterial growth on the surface, hydrated cement particles still corroded and detached from the surface.

However, for the samples coated with cement-based material, strength reduction was up to 52%. This means coating concrete pipes with cement mortar material slightly enhances the resistance of the pipe towards corrosion. However, this will not last long since the material corrodes over time and disappears. Samples coated with multiphase composite coating (MCC) mixes and geopolymer-based coatings integrated with zinc particles lost strength up to around 35% which is less than uncoated samples or the samples coated with cement mortar.

Ultimately, coatings were applied on uncoated corroded samples and tested under bending. Results of the flexural test displayed in Figure 5.19 showed that coating deteriorated pipe with the developed coating materials can restore samples strength between 30-60%. Uncoated samples strength after corrosion was around 1000 N, after coating the corroded sample the ultimate strength increases to around 3500 N for GCZF coating.

Figure 5-19: Results of the flexural test (MCC: Multiphase composite coating)

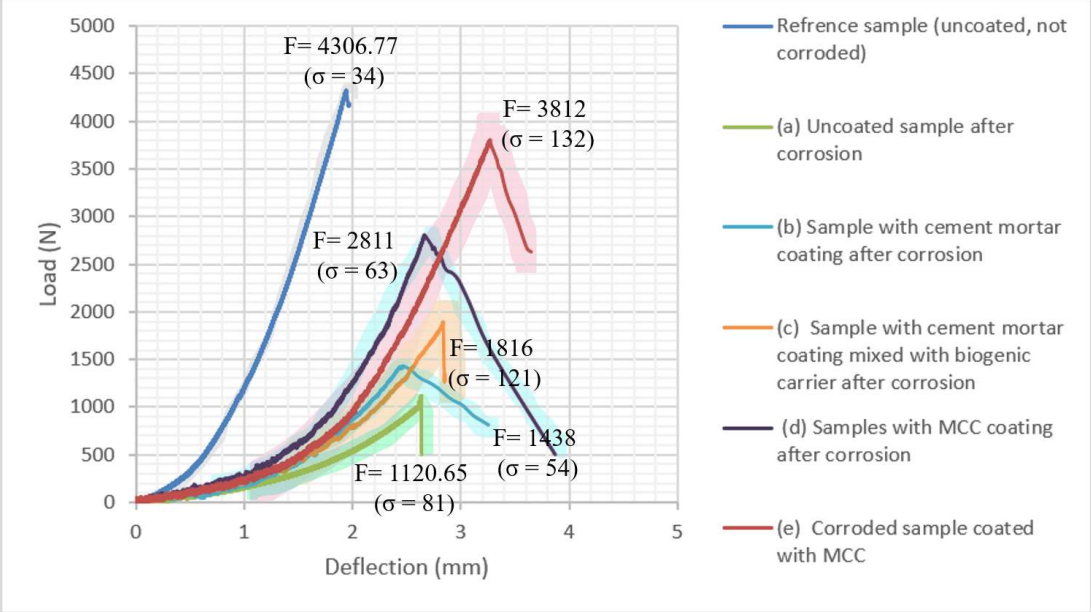

Load-deflection curves provided more insight about the strength of different coatings in real-life environments. Two variables must be further explored to understand the reason behind the strength gain, or loss. First, the developed geopolymer and multiphase composite coatings limit penetration

of biogenic sulfuric acid and inhibit bacterial growth and acid production as compared to the reference sample or cement mortar coatings, thus increasing flexural strength. Second, high bond strength and compatibility of the geopolymer and multiphase composite coatings with substrate increased strength through the properties of flexural strength and toughness, as well as, the addition of cross-sectional area.

The test results verified that zinc-doped clay and zinc oxide geopolymers performed well in regard to plastic shrinkage, bond strength and flexural strength. The main mechanism that zinc oxide and Zn-doped clay particles appear to have that influences concrete is their ability to inhibit bacterial growth and act as a filler to densify the matrix, which ultimately, decreases acid production and penetration. In addition, clay particles appear to bond with geopolymer structure. Also, the increased plastic shrinkage resistance of geopolymer and multiphase coatings limit ingress of harsh chemicals transported by wastewater, thus maintaining its bond with the concrete substrate.

Although adding ZnO or Zn-doped clay add antibacterial properties and creates a less permeable structure, this research has found to be harmful to compressive and flexural strength. Further testing may be required to confirm the mechanical properties.

A trend that the load-deflection curves also exhibits is the increase of flexural strength from the addition of zinc oxide which was observed in coatings including cement past coatings. This could also be explained by the fact that ZnO particles improves the pore structure.

Based on the results, developed antibacterial coatings can create a corrosion-resistant and effective physical/chemical barrier on concrete wastewater pipes that protects the concrete from bio-acid production and attack on the surface, as well as, ingress of aggressive bacteria. Moreover, coatings successfully immobilized antibacterial agents inside the matrix and increase bio-resistant lifetime and durability of the repair material. This leads to an increase in the service life of aged/corroded concrete pipelines. However, addition of ZnO particles or Zn-doped clay to the geopolymer-based coatings or blended mix of geopolymer magnesium phosphate showed patterns of decreasing bond

and mechanical properties which should be investigated further. Time limitations regarding testing in the corrosion chamber affected further testing for the purpose of this study.

Chapter 6: Conclusions, Recommendations and Future work

6.1 Significance of the experimental work

Carrying out an accelerated test in the laboratory is one of the most common ways of investigating the bio-corrosion resistance of different materials. In the accelerated tests, the degradation rate increased by means of higher concentrations of the aggressive medium, higher temperature and humidity, greater contact surfaces and alternate wetting drying cycles. In this study, a novel accelerated test chamber was designed and manufactured to simulate bio-corrosion in wastewater concrete pipes based on literature regarding similar steps and their advantages and disadvantages. Stages of the bio-corrosion in actual concrete pipe and simulated conditions in the accelerated test chamber are summarized in Chapter 2. Arch-shaped mortar samples were cast to represent the top half of the concrete pipe and near the water level. The microorganisms used throughout this study are sulfur-oxidizing bacteria species, T. Thioparus and A. Thiooxidans strains that were purchased from American type culture collection (ATCC).

Chapter 3 was a validation/test phase to estimate how well the designed accelerated test chamber is working. 15 Arch-shaped mortar samples were cast to represent the top half of the concrete pipe and near the water level and tested over the 6 months period. A combination of multiple evaluation tests and indicators were conducted to compare the relative performance of bio-deteriorated samples. The corrosion rate was determined by measuring pH, absorption and mass loss as well as the reduction in thickness and flexural strength which are the most important factors in durability and serviceability of concrete pipes. Also, the corrosion products were investigated by SEM.

Approximately 14% weight loss was observed in the samples at the end of the test. Similar to pH variation, in most of the specimens, the corrosion degree and so the weight loss was slower at the beginning. After around 100 days, small holes appeared on the surface and surface material was discolored. Results show that the absorption of the specimens increased by around 4% after 6 months in bio-corrosion chamber. It could be seen that the bio-corrosion process caused an average

thickness loss of around 2 mm and maximum thickness loss of around 4 mm on cement-mortar samples. The measurements with the laser scan were used to calculate surface roughness change after 180 days corrosion period. The average initial surface roughness of 0.82-0.93 mm increased after corrosion to 0.9737-1.43.

The resistance of arch-shaped cement mortar samples was also tested before and after corrosion subjected to three-point bending. According to the results the peak load decreased by 73% and the corresponding deflection increased by 25.5% after 180 days in corrosion chamber. The sharp drop in the flexural strength of the samples is related to higher porosity, mass loss and size reduction. Also, the reaction products are structurally weak and easily leached out of the hydrated matrix. The overall results of the experimental program described in Chapter 3 and growth curves suggest the improved accelerated test chamber design works.

Next step was to evaluate the performance of coating materials in the chamber. Two types of corrosion resistant coating materials with encapsulating properties were developed and evaluated in Chapter 4. The first material is Geopolymer and the second one is a blended mix of magnesium phosphate hydrates phase form in conjunction with geopolymer matrix. The aim of combining these two matrixes is to take advantage of each system's individual corrosion resistant properties, strength, adding long-lasting anticorrosion properties, increasing the degree of encapsulation and creating denser matrix. Furthermore, the fineness of hydrated magnesium phosphate particles is much higher than ordinary Portland cement particles. Due to this fineness, magnesium phosphate reacts much faster with water. Un-hydrated magnesium oxide particles are able of consuming extra water produced during geopolymerization process and produce magnesium hydroxide which could react with sulfuric acid and produce $MgSO_4$ and increase the pH. Combining magnesium phosphate matrix with fly ash also reduce the cost which is very favorable to sustainable development and environmental protection.

Two different methodologies were also considered to gain control over the release of heavy metals embedded in the coatings. First mechanism was to keep the heavy metal molecule (zinc oxide) in the 3D framework of the coating binders. Second approach is to use sodium bentonite clay

impregnated with zinc ions to functionalize it as an antimicrobial agent then combine it into the structure of the coating materials (blended geopolymer). Loaded clay particles have the potential to get incorporated as a secondary binding material and precursor in geopolymerization reaction. Results confirm that the addition of fly ash as a first source is necessary for geopolymerization in order to attain certain mechanical properties and strength. This is due to the layered-like structure of clay particles which cause low reactivity and low strength.

Leaching and chemical stability, tensile strength, bonding and shrinkage properties of final mixes were tested to evaluate the performance of the developed materials. Results show that geopolymer and Zn-doped coatings demonstrated significant improvements when compared with other coatings. Visual evidence confirms the better performance of these coatings over the defined period of observation.

Thirty arch-shaped mortar samples were cast and described in Chapter 5 to represent the top half of the concrete pipe and near the water level. Samples were coated with different coating materials and tested in accelerated bio-corrosion chamber over the 6 months period. 6 corroded samples were also coated with developed coating materials and tested in the chamber to evaluate the performance of coating materials as a repair on corroded samples. A combination of multiple evaluation tests and indicators were conducted to compare the relative performance of cement-based, geopolymer-based and blended composite-based coatings mixed with ZnO and Zn-doped clay particles after 6 months in corrosion chamber. The corrosion rate determined by measuring the reduction in flexural strength and evaluating the pH variations, bond and corrosion resistant properties of different coating materials. Also, the corrosion products were investigated by SEM.

The test results verified that zin-doped clay and zinc oxide geopolymers performed well in regard to plastic shrinkage, bond strength and flexural strength. The main mechanism that zinc oxide and Zn-doped clay particles have that influences concrete is their ability to inhibit bacterial growth and act as a filler to densify the matrix, which ultimately, decreases acid production and penetration. In addition, clay particles will bond with geopolymer structure. Also, the increased plastic

shrinkage resistance of geopolymer and multiphase coatings limit ingress of harsh chemicals transported by wastewater, thus maintaining its bond with the concrete substrate.
Although adding ZnO or Zn-doped clay add antibacterial properties and created a less permeable structure, this research has found to be harmful to compressive and flexural strength. Further testing may be required to confirm the mechanical properties. A trend that load-deflection curves also exhibits is the increase of flexural strength from the addition of zinc oxide which was observed in coatings including cement past coatings. This could also be explained with the fact that ZnO particles improves the pore structure.

Based on the results, developed antibacterial coatings can create a corrosion-resistant and effective physical/chemical barrier on concrete wastewater pipes that protects the concrete from bio-acid production and attack on the surface, as well as, ingress of aggressive bacteria. Moreover, coatings successfully immobilized antibacterial agents inside the matrix and increase bio-resistant lifetime and durability of the repair material. This leads to an increase in the service life of aged/corroded concrete pipelines. However, addition of ZnO particles or Zn-doped clay to the geopolymer-based coatings or blended mix of geopolymer magnesium phosphate showed patterns of decreasing bond and mechanical properties which should be investigated further.

The proposed methodology and the results add to a better understanding of the bio-corrosion process and provide quantitative information on the performance and effectiveness of different coating materials which is necessary in evaluating concrete pipe's serviceability and predicting the remaining service life of rehabilitated pipes.

6.2 Recommendations and future work

Based on results of the present study recommendations for future work include:

- An extensive research is needed to standardize evaluation methods and testing procedures related to resistance of concrete and coating materials to biogenic acid attack.

- Although microscopic methods such as SEM and EDS are successful in determining changes in the matrix after corrosion, advanced tests such as Nuclear Magnetic Resonance (MAS-NMR) spectroscopy is also required to evaluate the molecular properties and mechanism of corroded materials.

- Addition of water reducers, super-plasticizers, air entraining mixtures, latex polymers for increasing the physical properties of the developed coating can be considered in future work.

- Slant shear tests should be used to determine the interface strength between the repair materials and the concrete substrate.

- Self-healing properties of MgO particles should be tested and discuss further.

- More experimental testing and evaluation still needed to be done to stabilize the properties and optimize the amount of coating's ingredients.

- Using NDT methods to predict the strength gain of the repair material at early ages with ultrasonic wave propagation is recommended. Also, the possibility of using the method in-situ to determine the compressive strength of mortar paste repairs should be investigated. Ultrasonic pulse velocity (UPV) evaluation allows a contractor to determine the condition of the applied repair mortar in the field during the entire pipeline service life. Ultrasonic waves are also able to determine the rate of setting and hardening by the change in wave velocity as a function of time.

- The bond integrity of any repair material relies not only on bond strength but also on material compatibility, specifically dimensional compatibility. Further tests should be applied to check the ability of Zn-doped clay geopolymer and multiphase composite coatings to withstand volume changes without loss of bond and delamination and carry its share of the applied load without distress.

- The effect of loading on the corrosion process and their combined effect on serviceability, flexural deflection and residual loading capacity is also another important factor for which reports in current literature appear to be absent.

- Full scale field tests should be carried out to verify lab results

- Although the antibacterial properties of zinc oxide are generally acknowledged, a series of microbiological tests should be performed, and quantitative data should be collected on the developed coating's effect on bacterial growth.

- The effect of the source of zinc oxide and the amount of antibacterial used in the coating should be investigated further.

- To enhance the performance of the coating materials in tension different types of fibers and higher percentages should be examined

- Feasibility of the material for shotcreting applications should be investigated. The properties of the shotcrete including strength, toughness, shrinkage, durability (freeze-thaw and salt scaling) and permeability should be evaluated in detail. Also coating material requires high slump mix, both to allow for shotcrete application and also to ensure penetration of mixture into voids of corroded substrate.

- Increasing the rate of acceleration of the designed chamber by for example increasing the humidity or reducing sample's pH to lower amount at the beginning of the test

References

[1] [USEPA] U.S. Environmental Protection Agency. (2004). An examination of EPA risk assessment principles and practices. Washington DC: Office of the Science Advisor. PA 100/B-04/001.

[2] Aguzzi, C., Cerezo, P., Viseras, C., & Caramella, C. (2007). Use of clays as drug delivery systems: possibilities and limitations. Applied Clay Science, 36(1), 22-36.

[3] Ahmari, S., & Zhang, L. (2012). Production of eco-friendly bricks from copper mine tailings through geopolymerization. Construction and building materials, 29, 323-331.

[4] Al Bakri, A. M., Kamarudin, H., Bnhussain, M., Nizar, I. K., Rafiza, A. R., & Zarina, Y. (2012). The processing, characterization, and properties of fly ash based geopolymer concrete. Rev. Adv. Mater. Sci, 30, 90-97.

[5] Aldcroft, D., Jones, H., Turner, D., Edge, M., Robinson, J., & Seal, K. (2005). In U.S. Patent No. 6 9.,698 (Ed.), Particulate carrier for biocide formulations.

[6] Alexander, M. G., Bertron, A., & De Belie, N. (2013). Performance of cement-based materials in aggressive aqueous environments (Vol. 10), Springer.

[7] Alum, A., Rashid, A., Mobasher, B., & Abbaszadegan, M. (2008). Cement-based biocide coatings for controlling algal growth in water distribution canals Cement and Concrete Composites, 30(9), 839-847.

[8] Appendini, P., & Hotchkiss, J. H. (2002). Review of antimicrobial food packaging. Innovative Food Science & Emerging Technologies, 3(2), 113-126.

[9] Aydın, S., Yazıcı, H., Yiğiter, H., & Baradan, B. (2007). Sulfuric acid resistance of high-volume fly ash concrete. Building and environment, 42(2), 717-721.

[10] Bakharev, T. (2005). Resistance of geopolymer materials to acid attack. Cement and Concrete Research, 35(4), 658-670.

[11] Banthia, N., Yan, C., & Mindess, S. (1996). Restrained shrinkage cracking in fiber reinforced concrete: A novel test technique. Cement and Concrete Research, 26(1), 9-14.

[12] Berndt, M. L. (2011). Evaluation of coatings, mortars and mix design for protection of concrete against Sulphur-oxidising bacteria. Construction and Building Materials, 25(10), 3893-3902.

[13] Boon, A. G. (1995). Septicity in sewers: causes, consequences and containment. Water Science and Technology, 31(7), 237-253.

[14] Botterhuis, N. E., Sun, Q., Magusin, P. C., van Santen, R. A., & Sommerdijk, N. A. (2006). Hollow silica spheres with an ordered pore structure and their application in controlled release studies. Chemistry-a European Journal, 12(5), 1448-1456.

[15] Canadian Society of civil engineers, "Canadian infrastructure Report card: Informing the future", 2016.

[16] Chau, C., Hui, W., Ng, W., & Powell, G. (2012). Assessment of CO2 emissions reduction in high-rise concrete office buildings using different material use options. Resources, Conservation and Recycling, 61, 22-34.

[17] Davidovits, J. (2002). years of successes and failures in geopolymer applications. Market trends and potential breakthroughs. In Geopolymer 2002 Conference (Vol. 28, p. 29). Geopolymer Institute, Saint-Quentin France, Melbourne, Australia.

[18] De Belie, N., Monteny, J., Beeldens, A., Vincke, E., Van Gemert, D., & Verstraete, W. (2004). Experimental research and prediction of the effect of chemical and biogenic sulfuric acid on different types of commercially produced concrete sewer pipes. Cement and concrete research, 34(12), 2223-2236.

[19] Duxson, P., Fernández-Jiménez, A., Provis, J. L., Lukey, G. C., Palomo, A., & Deventer, J. S. J. (2007). Geopolymer technology: The current state of the art Journal of Materials Science, 42(9), 2917-2933.

[20] Edge, M., Allen, N. S., Turner, D., Robinson, J., & Seal, K. (2001). The enhanced performance of biocidal additives in paints and coatings Progress in Organic Coatings, 43(1-3), 10-17.

[21] Ehrich, S., Helard, L., Letourneux, R., Willocq, J., & Bock, E. (1999). Biogenic and chemical sulfuric acid corrosion of mortars. Journal of materials in civil engineering, 11(4), 340-344.

[22] Erich, S. J. F., Mendoza, S. M., Floor, W., Hermanns, S. P. M., Homan, W. J., & Adan, O. C. G. (2011). Decreased bio-inhibition of building materials due to transport of biocides. Heron, 56(3), 93.

[23] Fernández-Jiménez, A., Palomo, A., & Criado, M. (2005). Microstructure development of alkali-activated fly ash cement: a descriptive model. Cement and concrete research, 35(6), 1204-1209.

[24] Gajanan, S. K., Swaminathan, S., & Ahmad, A. (2007). Composition of polymer microcapsules of biocide for coating material (US Patent 20070053950 ed.)

[25] Gomez-Alvarez, V., Revetta, R. P., & Santo Domingo, J. W. (2012). Metagenome analyses of corroded concrete wastewater pipe biofilms reveal a complex microbial system. BMC microbiology, 12(1), 122.

[26] Graham, M. V., & Cady, N. C. (2014). Nano and microscale topographies for the prevention of bacterial surface fouling. Coatings, 4(1), 37-59.

[27] Gutiérrez-Padilla, M. G. D., Bielefeldt, A., Ovtchinnikov, S., Hernandez, M., & Silverstein, J. (2010). Biogenic sulfuric acid attack on different types of commercially produced concrete sewer pipes. Cement and Concrete Research, 40(2), 293-301.

[28] Hardjito, D., Wallah, S. E., Sumajouw, D. M., & Rangan, B. V. (2004). On the development of fly ash-based geopolymer concrete. Materials Journal, 101(6), 467-472.

[29] Hewayde, Esam (2005) "The impact of coatings on biological generation of sulfides in wastewater concrete pipes," Department of Chemical and Biochemical Engineering, Canada.

[30] Hormann, K., Hofmann, F., & Schmidt, M. (1997). Stability of concrete against biogenic sulfuric acid corrosion, a new method for determination. InProceedings of the 10th international congress on the chemistry of cement, Gothenburg.

[31] Hudon, E., Mirza, S., & Frigon, D. (2010). Biodeterioration of concrete sewer pipes: state of the art and research needs. Journal of Pipeline Systems Engineering and Practice, 2(2), 42-52

[32] Ikeda, M., Otsuki, N., Nishida, T., & Minagawa, H. (2004). Influence of type of cement on Ca leaching from concrete using experimental acceleration method. In Proceedings of the 29th Conference on Our World in Concrete & Structures, Singapore (pp. 25-26).

[33] Islander, R. L., Devinny, J. S., Mansfeld, F., Postyn, A., & Shih, H. (1991). Microbial ecology of crown corrosion in sewers. Journal of Environmental Engineering, 117(6), 751-770.

[34] Jämsä, S., Mahlberg, R., Holopainen, U., Ropponen, J., Savolainen, A., & Ritschkoff, A. C. (2012). Slow release of a biocidal agent from polymeric microcapsules for preventing biodeterioration. Progress in Organic Coatings, 76, 269-276.

[35] Jiang, G., Keller, J., & Bond, P. L. (2014). Determining the long-term effects of H2S concentration, relative humidity and air temperature on concrete sewer corrosion. Water research, 65, 157-169. Guide to Concrete Repair, 2nd Ed. U.S. Department of the Interior.

[36] Jiang, G., Zhou, M., Chiu, T. H., Sun, X., Keller, J., & Bond, P. L. (2016). Wastewater-enhanced microbial corrosion of concrete sewers. Environmental Science & Technology, 50(15), 8084-8092.

[37] Khale, D., & Chaudhary, R. (2007). Mechanism of geopolymerization and factors influencing its development: a review. Journal of Materials Science, 42(3), 729-746.

[38] Kosmatka, S. H., Kerkhoff, B., & Panarese, W. C. (2011). Design and control of concrete mixtures. Portland Cement Assoc.

[39] Kriven, W. M. (2010). Inorganic polysialates or'geopolymers'. American Ceramic Society Bulletin, 89(4), 31-34.

[40] Liew, Y. M., Heah, C. Y., & Kamarudin, H. (2016). Structure and properties of clay-based geopolymer cements: A review. Progress in Materials Science, 83, 595-629.

[41] Liu, Z., & Kleiner, Y. (2013). State of the art review of inspection technologies for condition assessment of water pipes. Measurement, 46(1), 1-15.

[42] Lvov, Y. M., Shchukin, D. G., Mohwald, H., & Price, R. R. (2008). Halloysite clay nanotubes for controlled release of protective agents. ACS Nano, 2(5), 814-820.

[43] Maeda, T., Negishi, A., Nogami, Y., & Sugio, T. (1996). Nickel inhibition of the growth of a sulfur-oxidizing bacterium isolated from corroded concrete. Bioscience, biotechnology, and biochemistry, 60(4), 626-629.

[44] Magniont, C., Coutand, M., Bertron, A., Cameleyre, X., Lafforgue, C., Beaufort, S., & Escadeillas, G. (2011). A new test method to assess the bacterial deterioration of cementitious materials. Cement and Concrete Research, 41(4), 429-438.

[45] Mahmoodian, M., & Alani, A. M. (2013). Multi-failure mode assessment of buried concrete pipes subjected to time-dependent deterioration, using system reliability analysis. Journal of failure analysis and prevention, 13(5), 634-642.

[46] Manjunath, G., & Giridhar, C. (2011). Compressive strength development in ambient cured geo-polymer mortar. International journal of earth sciences and engineering, 4(6), 830-834.

[47] Metcalf, E. (2003). Inc., Wastewater Engineering, Treatment and Reuse

[48] Milde, K., Sand, W., Wolff, W., & Bock, E. (1983). Thiobacilli of the corroded concrete walls of the Hamburg sewer system. Microbiology, 129(5), 1327-1333.

[49] Minaoikova, M., & Škvara, F. (2006). Fixation of heavy metals in geopolymeric materials based on brown coal fly ash. Ceramics− Silikáty, 50(4), 200-207.

[50] Mirza, S. (2006). Durability and sustainability of infrastructure—A state-of-the-art report. Canadian Journal of Civil Engineering, 33(6), 639-649.

[51] Monteny, J., Vincke, E., Beeldens, A., De Belie, N., Taerwe, L., Van Gemert, D., & Verstraete, W. (2000). Chemical, microbiological, and in-situ test methods for biogenic sulfuric acid corrosion of concrete. Cement and Concrete Research, 30(4), 623-634.

[52] Montes, C., & Allouche, E. N. (2012). Evaluation of the potential of geopolymer mortar in the rehabilitation of buried infrastructure. Structure and Infrastructure Engineering, 8(1), 89-98.

[53] Mori, T., Nonaka, T., Tazaki, K., Koga, M., Hikosaka, Y., & Noda, S. (1992). Interactions of nutrients, moisture and pH on microbial corrosion of concrete sewer pipes. Water research, 26(1), 29-37.

[54] Negishi, A., Muraoka, T., Maeda, T., Takeuchi, F., Kanao, T., Kamimura, K., & Sugio, T. (2005). Growth inhibition by tungsten in the sulfur-oxidizing bacterium Acidithiobacillus Thiooxidans. Bioscience, biotechnology, and biochemistry,69(11), 2073-2080.

[55] Nielsen, A. H., Hvitved-Jacobsen, T., & Vollertsen, J. (2005). Kinetics and stoichiometry of sulfide oxidation by sewer biofilms. Water Research, 39(17), 4119-4125.

[56] Noeiaghaei, T., Mukherjee, A., Dhami, N., & Chae, S. R. (2017). Biogenic deterioration of concrete and its mitigation technologies. Construction and Building Materials, 149, 575-586.

[57] Nydén, B. M., Nordsstierna, L. O., Bernad, E. M., & Abdalla, A. M. A. A. (2010). U.S. Patent Application No. 12/800,292.

[58] O'Connell, M., McNally, C., & Richardson, M. G. (2010). Biochemical attack on concrete in wastewater applications: A state of the art review. Cement and Concrete Composites, 32(7), 479-485.

[59] Pangdaeng, S., Phoo-ngernkham, T., Sata, V., & Chindaprasirt, P. (2014). Influence of curing conditions on properties of high calcium fly ash geopolymer containing Portland cement as additive. Materials & Design, 53, 269-274.

[60] Pomeroy R. D. (1976) The Problem of Hydrogen Sulfide in Sewers, Clay Pipe Development Ass. Ltd, London.

[61] Raijiwala, D. B., & Patil, H. S. (2010). Geopolymer concrete A green concrete. In Chemical, Biological and Environmental Engineering (ICBEE), 2010 2nd International Conference on (pp. 202-206). IEEE.

[62] Rattanasak, U., Pankhet, K., & Chindaprasirt, P. (2011). Effect of chemical admixtures on properties of high-calcium fly ash geopolymer. International Journal of Minerals, Metallurgy, and Materials, 18(3), 364-369.

[63] Richardson, B. A. (1988). Control of microbial growths on stone and concrete. Biodeterioration 7, 101-106.

[64] Ryu, G. S., Lee, Y. B., Koh, K. T., & Chung, Y. S. (2013). The mechanical properties of fly ash-based geopolymer concrete with alkaline activators. Construction and Building Materials, 47, 409-418.

[65] Salwiczek, M., Qu, Y., Gardiner, J., Strugnell, R. A., Lithgow, T., McLean, K. M., & Thissen, H. (2014). Emerging rules for effective antimicrobial coatings. Trends in biotechnology, 32(2), 82-90.

[66] Sanchez-Silva, M., & Rosowsky, D. V. (2008). Biodeterioration of construction materials: state of the art and future challenges. Journal of Materials in Civil Engineering, 20(5), 352-365.

[67] Sand, W., Dumas, T., & Marcdargent, S. (1994). Accelerated biogenic sulfuric-acid corrosion test for evaluating the performance of calcium-aluminate based concrete in sewage applications,12(32), 234-234.

[68] Santo Domingo, J. W., Revetta, R. P., Iker, B., Gomez-Alvarez, V., Garcia, J., Sullivan, J., & Weast, J. (2011). Molecular survey of concrete sewer biofilm microbial communities. Biofouling, 27(9), 993-1001.

[69] Satoh, H., Odagiri, M., Ito, T., & Okabe, S. (2009). Microbial community structures and in-situ sulfate-reducing and sulfur-oxidizing activities in biofilms developed on mortar specimens in a corroded sewer system. Water research, 43(18), 4729-4739.

[70] Scarfato, P., Di Maio, L., Fariello, M. L., Russo, P., & Incarnato, L. (2012). Preparation and evaluation of polymer/clay nanocomposite surface treatments for concrete durability enhancement. Cement and Concrete Composites, 34(3), 297-305.

[71] Scarfato, P., Russo, P., & Acierno, D. (2011). Preparation, characterization, and release behavior of nanocomposite microparticles based on polystyrene and different layered silicates. Journal of Applied Polymer Science, 122(6), 3694-3700.

[72] Shi, C., Jiménez, A. F., & Palomo, A. (2011). New cements for the 21st century: The pursuit of an alternative to Portland cement, Cement and Concrete Research, 41(7), 750-763.

[73] Song, X. J., Marosszeky, M., Brungs, M., & Chang, Z. T. (2005). Response of geopolymer concrete to sulphuric acid attack. In Proceedings of World Congress Geopolymer, 157-160.

[74] Sørensen, G., Nielsen, A. L., Pedersen, M. M., Poulsen, S., Nissen, H., Poulsen, M., & Nygaard, S. D. (2010). Controlled release of biocide from silica microparticles in wood paint. Progress in Organic Coatings, 68(4), 299-306.

[75] Tazawa, E. I., Morinaga, T., & Kawai, K. (1994). Deterioration of concrete derived from metabolites of microorganisms. Special Publication, 145, 1087-1098.

[76] Terzano, R., Spagnuolo, M., Medici, L., Vekemans, B., Vincze, L., Janssens, K., & Ruggiero, P. (2005). Copper stabilization by zeolite synthesis in polluted soils treated with coal fly ash. Environmental science & technology, 39(16), 6280-6287.

[77] United States. Environmental Protection Agency. (1980). Duette mine construction and operation NPDES permit: Environmental impact statement

[78] Upadhyaya, J. K., Biswas, N., & Tam, E. (2014). A review of infrastructure challenges: assessing stormwater system sustainability. Canadian Journal of Civil Engineering, 41(6), 483-492.

[79] US Engineering and Research Center, "Bureau of reclamation Concrete Laboratory, fifty years," 1981.

[80] Van Jaarsveld, J. G. S., Van Deventer, J. S. J., & Lorenzen, L. (1997). The potential use of geopolymeric materials to immobilize toxic metals: Part I. Theory and applications. Minerals Engineering, 10(7), 659-669.

[81] van Jaarsveld, J., & Van Deventer, J. S. J. (1999). Effect of the alkali metal activator on the properties of fly ash-based geopolymers. Industrial & Engineering Chemistry Research, 38(10), 3932-3941.

[82] Vincke, E., Verstichel, S., Monteny, J., & Verstraete, W. (1999). A new test procedure for biogenic sulfuric acid corrosion of concrete. Biodegradation, 10(6), 421-428.

[83] Vollertsen, J., Nielsen, A. H., Jensen, H. S., Wium-Andersen, T., & Hvitved-Jacobsen, T. (2008). Corrosion of concrete sewers—the kinetics of hydrogen sulfide oxidation. Science of the Total Environment, 394(1), 162-170.

[84] Waijarean, N., Asavapisit, S., & Sombatsompop, K. (2014). Strength and microstructure of water treatment residue-based geopolymers containing heavy metals. Construction and Building Materials, 50, 486-491.

[85] Wallah, S., & Rangan, B. V. (2006). Low-calcium fly ash-based geopolymer concrete: long-term properties.

[86] Wang, M. R., Jia, D. C., He, P. G., & Zhou, Y. (2011). Microstructural and mechanical characterization of fly ash cenosphere/metakaolin-based geopolymeric composites. Ceramics International, 37(5), 1661-1666.

[87] Wang, S., Li, L., & Zhu, Z. H. (2007). Solid-state conversion of fly ash to effective adsorbents for Cu removal from wastewater. Journal of hazardous materials, 139(2), 254-259.

[88] Wei, S., Jiang, Z., Liu, H., Zhou, D., & Sanchez-Silva, M. (2013). Microbiologically induced deterioration of concrete: a review. Brazilian Journal of Microbiology, 44(4), 1001-1007.

[89] Wells, T., & Melchers, R. E. (2015). Modelling concrete deterioration in sewers using theory and field observations. Cement and Concrete Research, 77, 82-96.

[90] Wells, T., Melchers, R., & Bond, P. (2009). Factors involved in the long-term corrosion of concrete sewers. 49th Annual Conference of the Australasian Corrosion Association: Corrosion and Prevention, 345-356.

[91] Whitekettle, W. K., Tafel, G. J., & Zhao, Q. (2010). U.S. Patent No. 7,824,557. Washington, DC: U.S. Patent and Trademark Office.

[92] Wilson, M. A., Carter, M. A., & Hoff, W. D. (1999). British standard and RILEM water absorption tests: A critical evaluation. Materials and Structures, 32(8), 571-578.

[93] Xie, N., Bell, J., & Kriven, W. M. (2010). Fabrication of structural leucite glass–ceramics from potassium-based geopolymer precursors. Journal of the American Ceramic Society, 93(9), 2644-2649.

[94] Xu, J. Z., Zhou, Y. L., Chang, Q., & Qu, H. Q. (2006). Study on the factors of affecting the immobilization of heavy metals in fly ash-based geopolymers. Materials letters, 60(6), 820-822.

[95] Yip, C. K., Lukey, G. C., Provis, J. L., & van Deventer, J. S. (2008). Effect of calcium silicate sources on geopolymerisation. Cement and Concrete Research, 38(4), 554-564.

[96] Yongsiri, C., Vollertsen, J., Rasmussen, M., & Hvitved–Jacobsen, T. (2004). Air–water transfer of hydrogen sulfide: an approach for application in sewer networks. Water Environment Research, 76(1), 81-88.

[97] Yousefi, A., Allahverdi, A., & Hejazi, P. (2014). Accelerated biodegradation of cured cement paste by Thiobacillus species under simulation condition. International Biodeterioration & Biodegradation, 86, 317-326.

[98] Yousefi, A., Hejazi, P., & Allahverdi, A. (2013). Evaluation of effective strategies for cultivation of Acidithiobacillus Thiooxidans as cement-degrading bacteria. Iranian Journal of Chemical Engineering, 10(2).

[99] Yuan, H., Dangla, P., Chatellier, P., & Chaussadent, T. (2015). Degradation modeling of concrete submitted to biogenic acid attack. Cement and Concrete Research, 70, 29-38.

[100] Yunfen, H., Wenjuan, Z., & Hongbo, L. (2008). Properties of fly ash-based geopolymers concrete [J]. Journal of Beijing University of Civil Engineering and Architecture, 1, 003.

[101] Zhao, J. Q., Kuraoka, S., Baker, T. H. W., Gu, P., Masson, J. F., Boudreau, S., & Brousseau, R. J. (1998). Durability and performance of gravity pipes: a state-of-the-art literature review.

Appendix A

Flow Cytometry results, A. Thiooxidans

Thiooxidans, Sample #1, pH=4.556, Day 1, #cells in 50µL sample: 8584, 11565, 13306

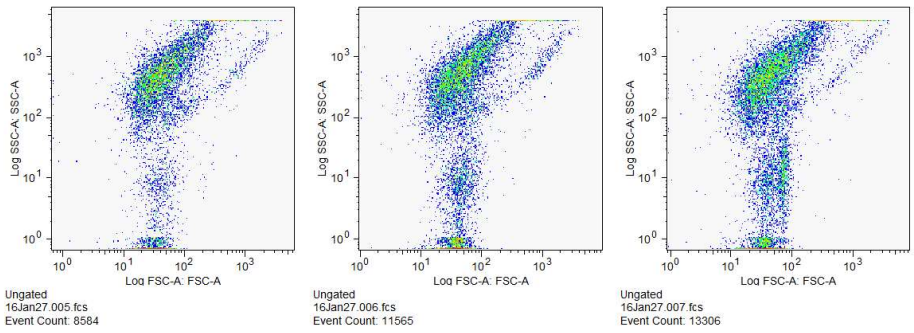

Thiooxidans, Sample #2, pH=3.867, 23 hr, #cells in 50µL sample: 13707, 15212, 19350

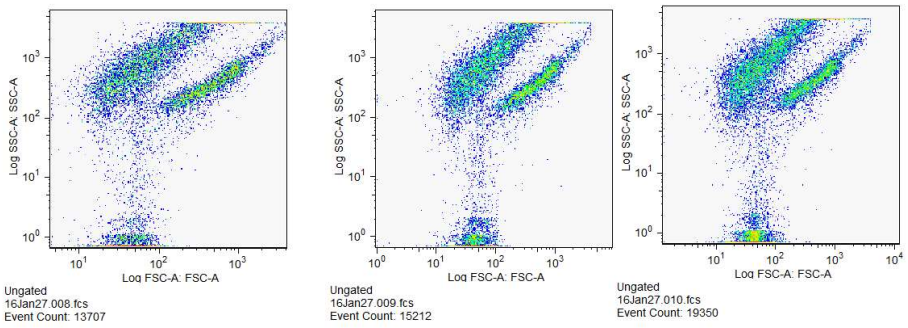

Thiooxidans, Sample #3, pH=3.955, 27 hr, #cells in 50µL sample: 13624, 16230, 18804

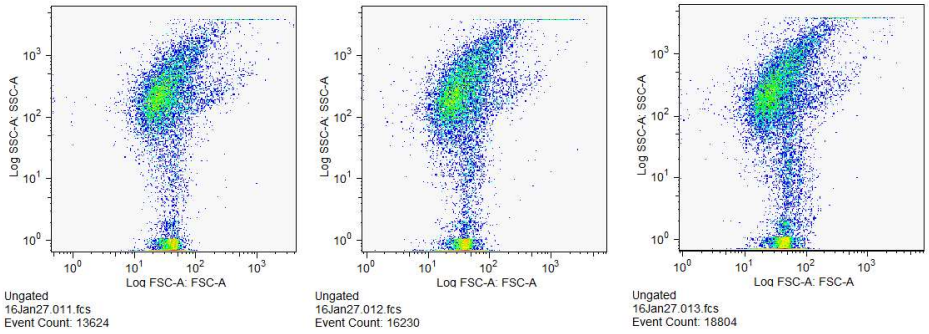

Thiooxidans, Sample #4, pH=3.883, 35.5 hr, #cells in 50µL sample: 21465, 14087, 11700

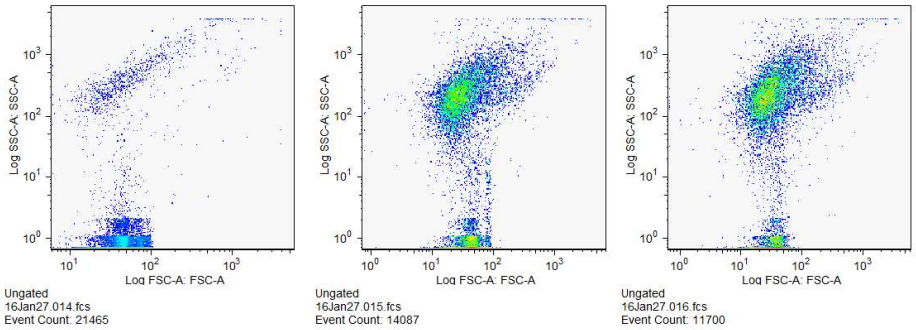

Thiooxidans, Sample #5, pH=3.26, 64 hr, #cells in 50µL sample: 38590, 43237, 51934

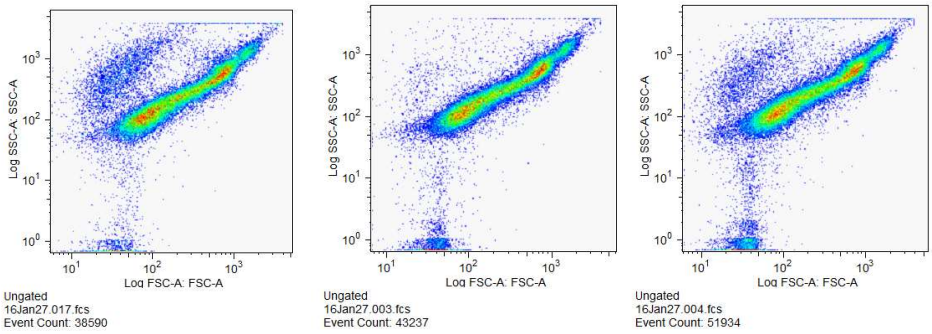

Thiooxidans, Sample #6, pH=2.663, 82 hr, #cells in 50µL sample: 38650

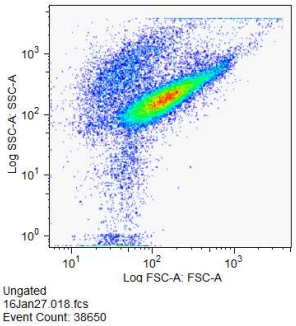

Thiooxidans, Sample #7, pH=1.92, 160 hr, #cells in 50µL sample: 23145, 22109, 21979

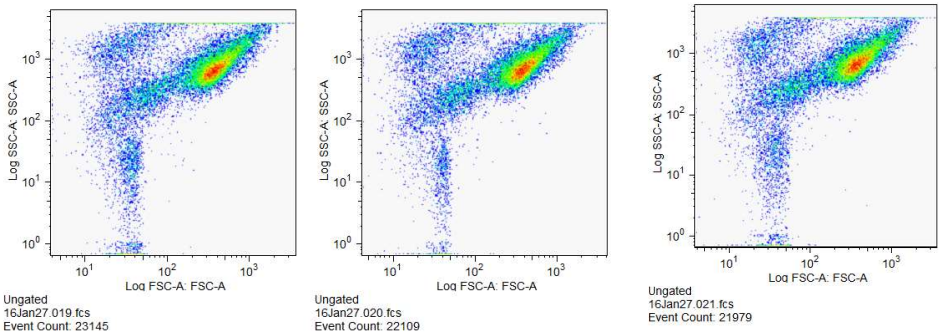

Thiooxidans, Sample #8, pH=1.869, 178 hr, #cells in 50µL sample: 27876

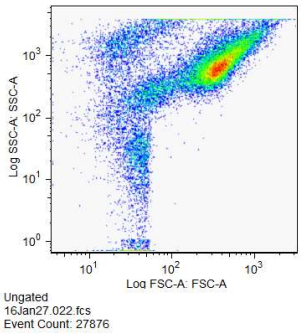

Thiooxidans, Sample #9, pH=1.834, 204.5 hr, #cells in 50µL sample: 27512

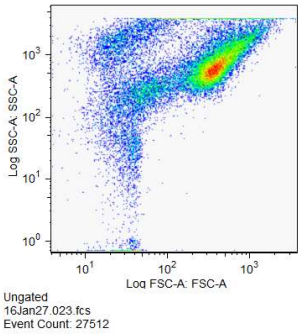

Thiooxidans, Sample #10, pH=1.599, 348.5 hr, #cells in 50µL sample: 47173

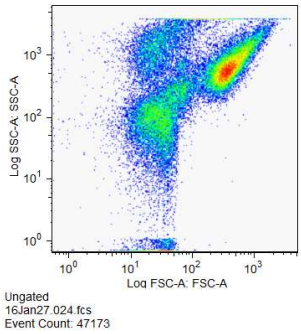

Flow Cytometry results, Thioparus:

Thioparus Media (Blank), S6

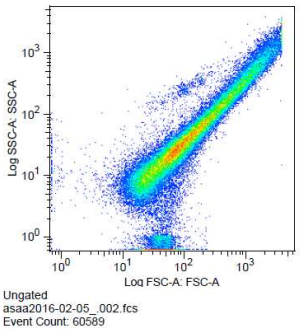

Thioparus, Sample P1, pH=5.978, Day 2, #cells in 50µL sample: 305541

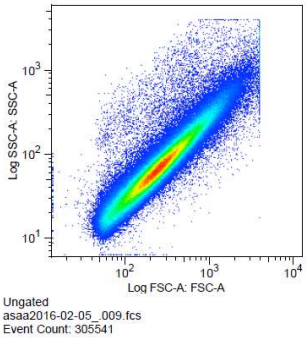

Thioparus, Sample #2, pH=4.339, Day 9, #cells in 50µL sample: 72534

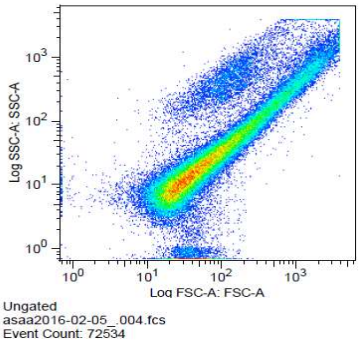

Thioparus, Sample #3, pH=3.85, Day 12, #cells in 50µL sample: 63481

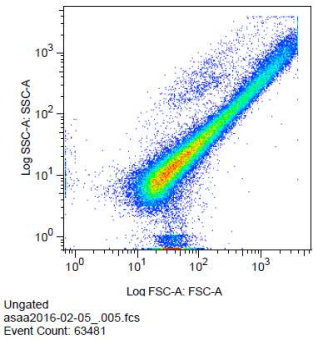

Thioparus, Sample #4, pH=3.915, Day 13, #cells in 50µL sample: 62273

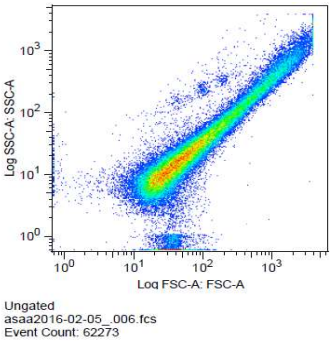

Thioparus, Sample #5, pH=3.75, Day 14, #cells in 50µL sample: 15186